Methods of Accurate ^{106}Ru and ^{125}I Eye Plaque Dosimetry Using Radiochromic Film in a Solid

Water "Eye" Phantom and a Small Silicon Diode in a Water Tank

Samuel Trichter

Submitted in partial fulfillment of the requirements for the degree of

Doctor of Public Health

Environmental Health Sciences

Mailman School of Public Health

COLUMBIA UNIVERSITY

2019

Abstract

Methods of Accurate ^{106}Ru and ^{125}I Eye Plaque Dosimetry Using Radiochromic Film in a Solid Water "Eye" Phantom and a Small Silicon Diode in a Water Tank

Samuel Trichter

Purpose: The use of ^{106}Ru eye plaques for the treatment of intraocular malignancies has produced inconsistent clinical outcomes and has even resulted in treatment failures. I hypothesized that inconsistent clinical results were attributable to high uncertainties in ^{106}Ru eye plaque dosimetry. Furthermore, I hypothesized that more accurate methods for assessing radiation dose from eye plaques would lead to more reliable treatment planning and therefore better overall clinical outcomes.

Methods: A Solid Water "eye" phantom with several novel features was developed for radiochromic film eye plaque dosimetry. Films perpendicular to the central axis of the eye plaques were sandwiched between inserts in the phantom. Small holes in the inserts enabled the film to be marked with respect to the eye plaques, assuring exact geometrical co-registration. In cooperation with the manufacturer, special thin radiochromic films were developed and utilized to permit dosimetric measurements almost at the eye plaque surface. Precise film punches were developed for the purpose of cutting films with diameters as small as 8.5 mm and making cutouts in films without damaging the cut edges. Findings from a secondary dosimetry system, utilizing a small silicon diode in a water tank, were compared to film data. In addition to testing the new dosimetry methods with ^{106}Ru eye plaques, which utilize high energy (MeV) β emissions, this approach was also applied to ^{125}I containing eye plaques, which due to their inherently lower energy (keV) γ emission spectrum, raised additional dosimetric complications. In the latter case dosimetry, films and the diode were calibrated for absolute dosimetry using calibrated ^{125}I seeds in Solid Water and

water, respectively, applying the TG-43 formalism. A novel calibration method of radiochromic film for low-energy photon dosimetry was introduced. Monte Carlo simulations were used to convert the results measured in Solid Water to liquid water, and to compare measured and simulated dosimetric results.

Results: Dosimetric characterization of both [106]Ru eye plaques and a novel concept ^{125}I eye plaque are described. Furthermore, dosimetry of a 20 mm [125]I Collaborative Ocular Melanoma Study (COMS) eye plaque validated the presumed substantial dose reduction resulting from its gold alloy backing and seed carrier insert predicted by Monte Carlo simulations. Dose distributions measured with radiochromic film were in good agreement with diode measurements and Monte Carlo simulations. Replicate film results were reproducible from 0.9% to 5.5%. As little as 4% non-uniformities in planar dose rates were easily detected using [106]Ru eye plaques. The novel ^{125}I eye plaques had uniform dose distributions. Dosimetric characterization of the 20 mm COMS plaque demonstrated that the plaque's dose rate was 15% lower than that predicted by homogenous TG-43 calculations. Lastly, Monte Carlo simulations indicated dose conversion factors between water and film in Solid Water compared to water and Solid Water alone differed by as much as 16.8%. Change in the calcium content of Solid Water from 2.3% to 1.7% resulted in a 3.3% calculated difference in dose to film and in an 8.7% difference in dose to Solid Water.

Conclusions: Precise and reproducible [106]Ru and ^{125}I eye plaque dosimetry was achieved utilizing radiochromic film in a water equivalent phantom and a small semiconductor diode in water. Co-registration of eye plaques and films permitted not only precise treatment planning calculations along the central axis of the plaque, but also made it possible to account for dosimetric non-uniformities using 2D or 3D methodologies. A calibrated ^{125}I seed enabled calibration of the film and the diode for absolute dosimetry of ^{125}I containing eye plaques. Dose measurements on the

inner surface of the plaques provided precise assessment of the scleral dose, its homogeneity, and of the active area of the plaques for coverage determination. Monte Carlo simulations facilitated conversion of doses measured in various media to liquid water.

Table of Contents

List of Tables and Figures

3. Eye plaque dosimetry results and discussion.

1. Introduction/Literature Review.

Intraocular malignancies, although infrequent, may cause loss of vision and can be life threatening[1]. The two main kinds of primary intraocular tumors are choroidal melanomas and retinoblastomas, with approximately 2500 new choroidal melanoma cases and 250 new retinoblastoma cases diagnosed annually in the U.S[2]. Historically, treatment consisted of enucleation of the eye; however, retinoblastoma, an early childhood cancer, affects both eyes in approximately one third of patients[2]. Since Stallard[3, 4] first used temporarily-applied episcleral eye plaques made of ^{60}Co foil, radiation therapy for intraocular tumors has become a viable alternative to enucleation. A large number of studies[5-29] show that eye plaques provide good local control and survival rates similar to or better than enucleation, but with the distinct advantages of eye preservation and, in many cases, satisfactory vision outcomes.

As the names indicate, choroidal melanomas originate in the choroid, while retinoblastomas start off in the retina. Intraocular tumors are therefore more commonly located on the posterior aspect of the eye. The eye plaque is designed in the form of a cap that is surgically positioned over the base of the tumor as shown in Figure 1.

Each eye plaque has suture lugs or eyelets that allow it to be sutured to the sclera. To assure adequate coverage of various tumor geometries, eye plaques are available in diverse sizes and shapes. Some eye plaques feature cutout notches for protection of the macula and optic nerve when the tumor is located in their proximity or avoidance of iris irradiation when treating ciliary body melanomas[30]. Once an eye plaque of an appropriate size and shape to cover the tumor and provide for a margin is selected, it is inserted during a surgical procedure that involves precise positioning over the tumor base. After the prescribed dose is delivered over the course of several days, the plaque is removed from the patient's eye in a manner similar to the insertion procedure.
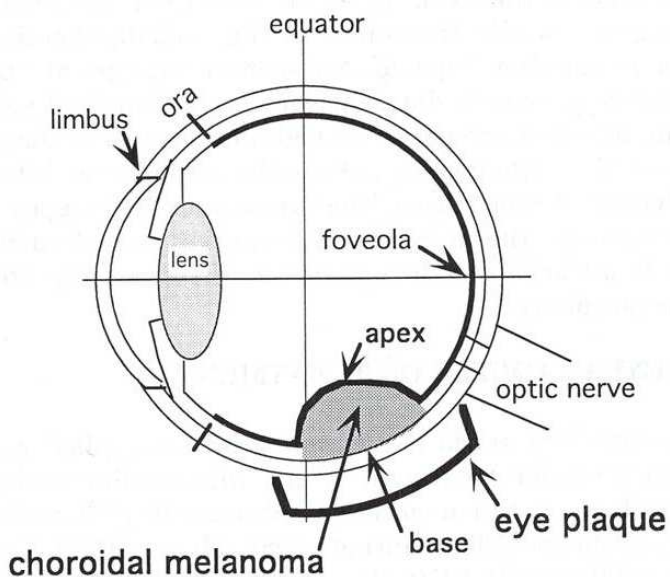
Figure 1. Schematic drawing of an eye showing the main anatomical structures and a melanoma originating in the choroid. An eye plaque is placed on the sclera over the tumor base. [Courtesy of Chiu-Tsao, S.-T.[31] (Figure 2, p. 454).]

Since the introduction of the first eye plaques using ^{60}Co foil by Stallard in 1961[3, 4], a range of mechanical designs and isotopes have been used. Table 1 below lists the major isotopes that have been or are presently in use:

Isotope	Type of Radiation and Average Energy	Half-life
^{60}Co	1.25 MeV photons	5.26 years
^{192}Ir	~0.38 MeV photons	73.83 days
^{198}Au	0.412 MeV photons	2.7 days
^{125}I	28.0 keV (27-35 keV) photons	59.43 days
^{103}Pd	20.7 keV (20-23 keV) photons	17 days
^{90}Sr/^{90}Y	Beta emitter, 2.2801 MeV maximum energy, 0.9336 MeV average energy. The maximum and mean energy are of ^{90}Y.	10523 days
^{106}Ru/^{106}Rh	Beta emitter, 3.541 MeV maximum energy, 1.41 MeV average energy. The maximum and mean energy are of ^{106}Rh.	373.59 days

Table 1. Isotopes that have been or are currently used for eye plaque radiation therapy. The average energies are nominal values assuming typical encapsulation of the sources.

While a number of authors have reported the use of ^{60}Co[14, 18, 32-34] or ^{192}Ir[14, 35] eye plaques, both have major disadvantages. Because of their relatively high photon energy (and thus deep penetration), achieving dose conformity over the small distances associated with ocular tumors presents a challenge, in addition to the unavoidable radiation protection issues. By contrast, the depth-dose distribution of ^{125}I is similar to those of ^{60}Co and ^{192}Ir within the first 15 mm, but attenuates rapidly beyond this depth[35-37]. Reducing the dose from ^{60}Co by 50% requires a 12 mm lead shield, while only 0.5 mm of gold decreases the dose from ^{125}I to less than 0.1%[37]. This effectively protects the structures posterior and lateral to the plaque, and prevents the medical team from receiving an unnecessary dose. Therefore, ^{125}I has become the radionuclide of choice for the Collaborative Ocular Melanoma Study (COMS), a large international controlled study initiated in 1986 and supported by the National Eye Institute[37]. Since this selection was made, ^{125}I has been the most widely used isotope for eye plaques in the U.S. The design of the COMS study eye plaques has been standardized[37, 38], and has become the most widely used eye plaque geometry in the U.S. as well as the geometry of choice in many institutions outside the U.S. Their design has been described in detail[31, 39, 40].

In Europe, eye plaque therapy has primarily utilized ^{106}Ru eye plaques since their invention by Dr. Lommatzsch in 1964[5, 6]. A beta-emitter with a maximum energy of 3.541 MeV and a half-life of 373.59 days[41], ^{106}Ru/^{106}Rh provides more conformal dose distributions than ^{125}I due to its rapid dose fall-off and offers better protection to critical structures of the eye, but is limited to tumors not higher than 5 mm[6, 7]. Treating larger tumors with ^{106}Ru eye plaques would result either in underdosing the tumor, or in an unacceptably high scleral dose and unacceptably long treatment time. All ^{106}Ru eye plaques are manufactured by Eckert & Ziegler BEBIG GmbH, Berlin, Germany. This company took over the former East German entity that had manufactured the

plaques since their invention. [106]Ru eye plaques have never been widely used in the U.S., likely because they were originally manufactured in the German Democratic Republic, and meanwhile the U.S. adopted the COMS plaques. The COMS plaques have no tumor height restriction, a limitation on the use of [106]Ru eye plaques when dose delivery to the apex of the tumor is judged to be optimal and is prescribed accordingly. In Europe, ophthalmologists often follow a different prescription philosophy that prioritizes delivery of a proper dose to the tumor base over tumor apex dose, thereby eliminating the 5 mm limitation on tumor height (private communication). Moreover, [106]Ru eye plaques had to be commissioned dosimetrically, and were plagued by erroneous dosimetric data and non-uniform dose distributions, which are subjects of this work and described in the published article[42]. It should also be noted that between 2007 and 2011, the manufacturer of [106]Ru eye plaques, stopped deliveries to the U.S. for business reasons (private communication). Furthermore, while the user can control the dose rate of COMS plaques by ordering seeds of appropriate strength, thereby enabling insertion and removal of the eye plaques at convenient times, the dose rate of [106]Ru eye plaques is a given on the specific dates of the procedures, causing operating rooms scheduling issues (private communication).

In the COMS study, which dealt with choroidal melanomas, the choice of optimal treatment decision between enucleation or radiation therapy was concerned with preservation of vision or cosmetic appearance as well as with patient survival[8, 9, 43]. It was hypothesized that enucleation may disseminate micrometastasis and thus result in metastatic disease, a situation presumably avoided with radiation therapy[43]. Therefore, the main question for the COMS study ophthalmologists was which treatment is superior in terms of extending the patient's life[43]. The outcome of the COMS study[8, 9], which was published in 2001-2002, found "the absence of a clinically or statistically significant difference in survival for patients randomly assigned to

4

enucleation versus brachytherapy" and that local treatment failures after plaque therapy were "relatively infrequent events." Confirmed mortality rates from metastatic melanoma at 5 years were 9% after plaque therapy and 11% after enucleation[8]. In the case of [106]Ru, Seregard[11] re-analyzed results of plaque therapy for melanoma from 5 trials. He reported a 6% melanoma mortality rate at 5 years and concluded that the survival rate appears higher after plaque therapy than after enucleation. For retinoblastoma it was shown[16, 19, 44] that eye plaque therapy provides a rate of local control as high as 89% at 52 months of follow-up.

1.1. COMS eye plaques.

COMS plaques consist of a 0.5 mm thick gold alloy (Modulay) backing and a silicone insert with 5 mm long x 1.25 mm deep grooves for the loading of standard brachytherapy seeds, which are approximately 4.5 mm long x 0.8 mm in diameter. The gold alloy backing serves as a holder for the silicone seed carrier insert, and has 6 tabs with suture holes, but its main purpose is radiation shielding. The rounded metal backing is surrounded by a cylindrical part called the "lip" that is designed to protect such sensitive structures as the optic nerve, optic disk, and macula. The seed carrier insert is made of medical grade silicone rubber (Silastic). The radius of its internal curvature is 12.3 mm conforming to 24.6 mm, which is considered the "average" diameter of an eye. It has fixed locations for the seeds, and it assures that all seeds are at 1 mm distance from the outer scleral surface. The 1 mm distance is required in order to minimize "hot spots" in the scleral layer[31], and was originally intended to achieve a dose distribution approximating that of the commercially available pre-COMS ^{60}Co plaques[37].

A number of alternative plaque designs employing ^{125}I brachytherapy seeds have been in use since the 1980s[35, 36, 44-51]. Some designs also utilize [103]Pd brachytherapy seeds[20, 26, 51], even though the first experiments with [103]Pd seeds used the COMS design[52]. Calculations for the use of [103]Pd in a

COMS plaque design are described by Chiu-Tsao et al[40], but it is not clear if this configuration was ever used clinically, except as reported by Finger[52].

There are, however, a number of problems related to the use of COMS eye plaques. The COMS plaques are 2.75 mm thick[39], causing patient discomfort. Dosimetrically, the COMS plaques have localized hot and cold spots, since they are assembled from separate brachytherapy seeds. The ^{125}I seeds in COMS plaques are arranged in a standard geometry. The dosimetry of the seeds is assumed to be described by the TG-43 formalism[53]. Treatment planning calculations assume the point source model for the seeds, and assume that the seeds are surrounded by homogenous liquid water. The latter assumption ignores the effects of the gold alloy backing, the Silastic insert, inter-seed attenuation, eye-air interface, and other possible factors that could affect the low energy photon scatter[54]. Several authors have attempted to calculate and/or measure these effects[55-58], but they either measured the effect of a plaque loaded with a single seed[55-57] or focused on the effects outside the shielding lip[58]. These works suggest a dose reduction in the range of 10% or more at 1 cm from the seed along the central axis of the plaque as compared to homogenous water. Recent assessments and Monte Carlo simulations[54, 59, 60] including fully loaded plaques found that the delivered dose is substantially lower than the accepted point source model in homogenous liquid water. Some of these measurements and calculations were done in full scatter phantoms and some were made in phantoms mimicking the human head with an eye to air interface. Phantom selection affected the results. Monte Carlo simulations by Thomson et al[54] in a full scatter phantom found a 14% dose reduction 1 cm from the inner sclera along the central axis of the plaque for a 20 mm COMS plaque fully loaded with ^{125}I seeds. Our measurements of a fully loaded 20 mm COMS plaque performed using radiochromic film in the Solid Water "eye" phantom placed into a full scatter phantom confirmed the Monte Carlo results by Thomson et al[54] and the corrected Plaque

Simulator results, the only commercially available eye plaques treatment planning software. These are presented in this work and were also reported at an Annual Meeting of the American Association of Physicists in Medicine (AAPM)[61], earning the Best in Physics award. These measurements were done at the request of Dr. Chiu-Tsao, Chair of the AAPM's Task Group 129[40], who was impressed by our earlier dosimetry of ^{106}Ru eye plaques and wanted to experimentally confirm the Monte Carlo simulations of ^{125}I COMS eye plaques by other groups, as well as to test the dosimetric corrections by the author of Plaque Simulator[59, 62-64]. These measurements were necessary because Monte Carlo simulations can be trusted only if verified by experiment. Unlike earlier reports[55-58], for the first time, this work presents a complete experimental characterization of a fully loaded COMS plaque.

1.2. ^{106}Ru eye plaques.

The ^{106}Ru eye plaques are made of pure silver (Ag 99.99%) with a total thickness of 1 mm. The shape is a spherical cap with an inner radius of 12 to 14 mm, which conforms to the typical human eye[65]. The radioactive material, ^{106}Ru/ ^{106}Rh in the form of a thin film, is electrolytically deposited on 0.2 mm-thick silver foil that is encapsulated between a 0.1 mm silver window on the concave (facing the eye) side and the silver backing that stops approximately 95% of the beta-radiation posterior to the plaque[41].

Since ^{106}Ru eye plaques are made of a continuous layer of encapsulated radioactive material, all treatment planning calculations are based on actually measured dosimetric data for each eye plaque. These data are provided by the manufacturer in the form of absolute dose rate measured as a function of depth (distance from the inner concave surface of the plaque along its central axis). The manufacturer also provides a surface map of dose rates relative to that on the central axis at a specified number of points, measured on concentric circles around the central axis 1 mm from the

plaque's surface. Prior to 2002, dosimetric data was provided by BEBIG for only 4 points along the central axis and 9 surface points on a circle for small plaques or 17 surface points on 2 circles for the larger plaques (see an example of a small plaque certificate in Appendix 2). The surface points were and still are measured 1 mm from the plaque's inner surface. The cylindrical (see below) detector long axis is parallel to the central axis of the plaque, which means that it is perpendicular to the plaque's surface only on the central axis of the plaque and is angled relative to the surface at all other points (personal observation during a visit to the plaques manufacturer BEBIG). Therefore, these measurements are of questionable value. At that time the dosimetric data had a stated uncertainty of ±30% (k=2). The manufacturer data were acquired with a cylindrical plastic scintillator (2 mm height by 2 mm diameter) with the absolute absorbed dose rate calibration based on the primary standard of the national laboratory of the former German Democratic Republic. The large detector lacked the necessary resolution needed to measure the rapidly changing dose distributions of the small concave plaques with dose gradients as large as 30%/mm. A number of authors[66-74] have attempted to reduce this uncertainty and to perform quality assurance of the plaques. The findings included dose rate disagreements between -37% to +74% with the manufacturer's data[72] and non-uniform dose distributions with off-axis hot and cold spots. These results are discussed in more detail in our published article[42]. Our own measurements using radiochromic film in our specially designed Solid Water "eye" phantom and with a small semiconductor diode in a water tank found that dose rates provided by the manufacturer were 1.55 – 2.11 times lower than our findings, with off-axis hot spots of up to 23%[42, 75-77]. The diameter of the mechanically smallest (CCX type) plaque is 11.6 mm, and its internal height is just 1.3 mm. Due to its small size this plaque is ideally suited for the treatment of retinoblastoma in small children as young as one week old. The CCX plaques are notoriously

difficult to measure due to their small size and therefore, until recently, except for our published data of the CCX 41 plaque[78], there was no published dosimetric data for these plaques[79]. Our data[78] was used by Hermida-López[79] for comparison with his Monte Carlo simulations. Our published article[42] and this work include additional data on CCX plaques. Hermida-López recently published his measurements of two CCX plaques as well[80].

Prior to the 2002 NIST (U.S. National Institute of Standards and Technology, Gaithersburg, MD) calibration, CCX plaques had the highest dosimetric discrepancy between BEBIG's dosimetry and the improved dosimetry done by NIST[81]. The central axis dose rate disagreements were assumed to result from the large size of the plastic scintillator detector employed by BEBIG, as well as its calibration for absolute beta dosimetry. The non-uniform dose distributions were attributed to the non-uniform distribution of the radioactive isotope under the surface of the plaque. In May of 2002, BEBIG sent a letter to its customers[81] informing them that the company had started using a smaller plastic scintillator (1.0 mm diameter and 0.5 mm height) calibrated by the NIST, which reduced the uncertainty to ±20% (k=2). They also started providing dosimetric data at 11 points along the central axis and 33 off-axis surface points (see an example of a small post-2002 plaque certificate in Appendix 3). In the same letter[81], BEBIG provided conversion factors from the old ASMW (standardization office of the former German Democratic Republic) dosimetry to the NIST calibrated dosimetry, which are in close agreement with our results for the plaques measured in this work[42]. BEBIG also improved their manufacturing processes, resulting in more uniform dose distributions. The improvements in accuracy of the dosimetric measurements and the better uniformity of the dose distributions were verified by our independent measurements[42, 82, 83].

^{106}Ru eye plaques provide a convenient and good alternative to COMS ^{125}I plaques in treating small intra-ocular malignancies. They are substantially thinner than the COMS plaques (1 mm vs.

2.75 mm), and are much better tolerated by patients, do not require assembly, can be reused, and offer more conformal dose distributions than ^{125}I eye plaques due to a more rapid dose fall-off. A recent publication[84] reported findings of a FMEA (failure mode and effects analysis) of the COMS plaque process in accordance with the TG-100 AAPM report[85]. The publication[84] found that the COMS plaques technique consists of 12 major processes, 121 sub-processes and 188 potential failure modes, starting with the diagnosis and ending with the treatment. At least 50 of the 188 potential failure modes are a consequence of the fact that COMS plaques are assembled from individual seeds; these failure modes are eliminated by the use of ^{106}Ru eye plaques.

There are also, however, a number of problems related to ^{106}Ru eye plaques. The local control rate in radiation therapy strongly depends on the delivery of a certain minimal dose to the tumor, while the overall clinical result in terms of preserving vision or the eye (for cosmetic reasons) – is a function of keeping the doses to critical structures of the eye at an acceptable level. Messmer *et al*[86] report that a decrease in external beam radiation dose used for the primary treatment of retinoblastoma from 50 Gy to 40 Gy increased local failures observed within 26 months after radiation therapy from 22% to 49%. Hermann *et al*[87] compare the outcomes of various studies and conclude that for melanomas treated with ^{106}Ru plaques, there is no significant difference in treatment outcome when the apical dose (the usual prescription point in the treatment of ophthalmic tumors) is increased from 100 Gy to 160 Gy. The authors[87] suggest defining a system that can characterize the dose distribution in the tumor as a basis for comparison among studies, because it seems that the apical and basal doses alone are insufficient for this purpose. But Hermann *et al*[87] overlooked the possibility that the various studies use either incorrect or incomparable dosimetric data. We hypothesize that the very large uncertainties associated with the manufacturer's dosimetry can explain the discrepancy between various published studies.

An additional source of failures of [106]Ru plaques is insufficient coverage close to the rim of the plaque. Taccini *et al*[71] found a dose rate decrease to less than 40% of the uniform value in the region 1 mm from the rim of the plaque, which is farther from the rim than expected based on BEBIG's earlier specifications of a 0.60 mm – 0.75 mm inactive area for most of the plaques. BEBIG's most recent specification[30] defines an inactive border 0.75 mm from the rim for most of the plaques. Our work[42] confirms that for one of the measured CCX eye plaques the uniform coverage ended 1.25 mm from the rim vs. the expected 0.75 mm. This insufficient coverage close to the rim of the plaques may explain findings by Barker *et al*[88] of higher than anticipated numbers of tumor recurrences when using [106]Ru eye plaques. Barker *et al*[88] suggested adding 3 mm wide margins to the tumor size when selecting a plaque in order to achieve sufficient tumor coverage. Another dosimetric issue of importance concerning [106]Ru plaques are dose distributions in plaques with cutouts. The manufacturer provides a standard set of measured data which includes the dose rate on the central axis and the relative surface dose rates measured at 33 points at a distance 1.0 mm from the inner concave surface. These data, however, neither show nor suggest that the dose on the central axis is not the highest dose in the planes perpendicular to the central axis (see an example of a plaque certificate with a cutout in Appendix 4). These plaques apparently contain substantial hot areas shifted with respect to the central axis, as seen from our measurements of a CIA plaque with a cutout presented in this work and in the published article[42]. Since the dose is prescribed along the central axis of the plaque, the off-axis hot area overdoses a part of the eye. This must be made known to the prescribing physician and taken into account whenever relevant. Recent published guidelines from AAPM and GEC-ESTRO state that [106]Ru plaques must be commissioned dosimetrically by a medical physicist prior to clinical use[89]. This requirement is in line with the requirements of the AAPM's TG-40 Report[90], which includes acceptance and quality

assurance requirements of brachytherapy sources. At present, there are no ^{106}Ru primary calibration standards in the U.S. and most other countries, and therefore there is no ADCL (Accredited Dosimetry Calibration Laboratory) calibration available and commercial tools or instruments for the acceptance and commissioning of ^{106}Ru eye plaques are unavailable. This deficiency is addressed by the findings in this thesis.

The thesis evaluated dosimetrically 8 different ^{106}Ru eye plaques belonging to CCX, CCA and CIA types.

Absolute dose values can be measured in a precise way by a qualified medical physicist during the commissioning of the eye plaque using methods described herein as well as other techniques[41]. However, the dose non-uniformity, including the region close to the rim of the plaque, can hardly be accounted for by current one-dimensional treatment planning techniques. This can result either in the underdosing of the tumor or the overdosing of adjacent healthy eye tissue, contributing to treatment complications and side effects. Our published article[42] describes a two-dimensional treatment planning technique, developed at Memorial Sloan-Kettering Cancer Center (MSKCC) with our participation - that uses the eye plaques dosimetric data measured in this work and that can account for dose non-uniformities of the actual plaques.

1.3. Novel ^{125}I eye plaque.

To overcome the above limitations and technical difficulties associated with ^{125}I and ^{106}Ru eye plaques, Implant Sciences Corporation of Wakefield, MA developed a prototype novel ^{125}I eye plaque design using ion implantation techniques. In contrast to ^{125}I plaques assembled from brachytherapy seeds, the novel design creates a continuous layer of ^{125}I in a glass substrate within the plaque. The plaques are approximately 1 mm thick (similar to ^{106}Ru plaques). It was hypothesized that the ion implantation technique could create a plaque with very uniform ^{125}I

density, which would result in highly uniform dose distributions without the hot or cold spots typical of plaques assembled from brachytherapy seeds or the dosimetric non-uniformities seen in ^{106}Ru eye plaques. Since ^{125}I isotope is utilized, the plaque would not be limited to treating tumors with apical heights of 5 mm or less. However, these plaques would have to be commissioned dosimetrically by measurements, like ^{106}Ru eye plaques. Dosimetry of ^{125}I photons introduced additional challenges addressed by this thesis.

The ion implantation technique and equipment used in this project were developed by Implant Sciences Corporation in order to manufacture ^{125}I brachytherapy seeds. Accelerated ^{124}Xe ions bombard a silicon dioxide (quartz) target, penetrating its surface. To manufacture an eye plaque, the target, which is a segment of a hollow sphere of quartz, is moved uniformly through the ion beam. The expected result is a relatively uniform slightly subsurface distribution of ^{124}Xe ions. The quartz substrate is then encapsulated in a thin layer of titanium (100 μm – 200 μm) and activated by neutron irradiation in a nuclear reactor, creating a relatively uniform, slightly subsurface distribution of ^{125}I. The activated plaque would be attached to a gold backing with suture eyelets similarly to COMS plaques. After using the plaque on a patient, the decayed plaque could be re-activated in a nuclear reactor and reused for other patients, since only a small fraction of ^{124}Xe would become ^{125}I during each activation. The re-activation of used plaques could potentially reduce costs, allowing the company and hospitals to keep sufficient numbers of plaques on hand given the substantially shorter 59.43 days[53] half-life of ^{125}I as compared to the 373.59 days[41] half-life of ^{106}Ru.

Implant Sciences Corporation has additionally proposed the creation of a special collimator insert covering the inner (concave) surface of the plaque. This collimator would be custom manufactured for each patient using a 3D conformal treatment plan based on 3D imaging information of the

diseased eye, enabling simultaneous delivery of radiation from multiple directions, similar to non-coplanar external beam radiation treatments. The collimator would be made of gold in the shape of a 0.13 mm thick spherical cap with groups of 0.1 mm diameter holes spaced 0.13 mm apart in a hexagonal array. Each group would correspond to a "radiation beam", such that all beams would result in a 3D conformal dose distribution covering the tumor and sparing the critical structures of the eye. The collimator would precisely fit the inner concave surface of the eye plaque. This approach will likely reduce the number of complications and toxicities of eye plaque brachytherapy reported by many authors[5, 6,12-15, 17, 20, 22, 25-27, 45, 91-95], which may result in loss of vision and enucleations.

This work reports dosimetric measurements performed on two 16 mm diameter prototype ^{125}I eye plaques made by Implant Sciences Corporation using radiochromic film in our Solid Water "eye" phantom and a small semiconductor diode in a water tank, based on methodology that was successfully applied by the author for accurate beta dosimetry of ^{106}Ru eye plaques.

The first prototype was not a final design eye plaque, but was used in order to study the feasibility of achieving dose uniformity as well as a clinically useful dose rate in the range of 60 cGy/hour – 105 cGy/hour at the tumor apex as recommended by the American Brachytherapy Society[96]. The second prototype was a fully assembled eye plaque, which, except for suture lugs, included all parts of the final product including a prototype collimator. We report full dosimetric characterization of the second prototype eye plaque using radiochromic film in our Solid Water "eye" phantom without the collimator and a comparison of the measured results with Monte Carlo simulations. We further report testing the feasibility of the collimator, studying possible dose non-uniformity resulting from the collimator design, as well as the clinical usefulness of the resulting dose rate, since the collimator would significantly attenuate the dose rate of the eye plaque.

Dosimetry of the novel[125]I plaques presented further challenges, since radiochromic films have always had strong energy dependence at low photon energies[97-100]. This energy dependence has improved starting with the new EBT film[101, 102]. The strong energy dependence of the older types of film that use the GAFCHROMIC film emulsion and the lesser dependence of the newer types that use the EBT emulsion have been shown by Monte Carlo simulations[103], but this remains an unresolved issue. It appears that the energy dependence at the low photon energies strongly depends on certain chemicals in the active layer and is film batch dependent[104, 105]. Therefore, the low energy of the ^{125}I eye plaque photons made it impossible to use high energy linac or ^{60}Co beams for radiochromic film calibration purposes, as was done for [106]Ru eye plaque measurements. Consequently, calibration of films for measurements at ^{125}I energy requires a source of the same energy. A unique film calibration method using a ^{125}I seed in our Solid Water "eye" phantom was developed in this work. Measurements at low photon energies required placements of the phantoms for eye plaque dosimetry or seed calibration into an appropriate scatter phantom, since the contribution of photon scatter to the absorbed dose could be as high as 38%[106]. The dosimetry of the novel ^{125}I eye plaque was also done using a semiconductor diode. While semiconductor diodes were used for absolute dosimetry of [106]Ru eye plaques[42, 67], to the best of our knowledge diodes were previously used only for relative dosimetry of ^{125}I brachytherapy seeds[107-109] and ^{125}I eye plaques[110]. In this work the semiconductor diode was calibrated for absolute dosimetry of ^{125}I using a calibrated ^{125}I brachytherapy seed.

1.4. Radiochromic film.

Radiochromic film is the main tool used for eye plaque dosimetry in this work. Radiochromic film is a color monochrome film that, produces an image as a result of irradiation, without any kind of chemical or non-chemical (for example thermal) processing and is almost insensitive to visible

light[111, 112]. All radiochromic films used in this work were GAFCHROMIC™ films developed, manufactured and provided by International Specialty Products (ISP, Wayne, NJ). In 2011 ISP was acquired by Ashland (Covington, KY). Currently, they are the sole manufacturer of radiochromic film in the sensitivity range reasonable for use in the field of medical dosimetry.

In 1998, the AAPM Task Group 55 (TG-55)[98] published recommendations for film dosimetry using radiochromic film[98]. Many new types of film, however, have been developed since 1998. In addition, conventional radiographic film is no longer being manufactured and its use has been replaced by radiochromic film and/or digital devices. A review co-authored by the author updated the status of radiochromic film, covering all film types up to and including EBT film released in 2004[113]. Since then, as part of ongoing research and development, ISP changed technology and moved to EBT2 and then EBT3 films. The AAPM therefore formed a new Task Group 235 for the purpose of updating the original TG-55[98]. The author is a member of TG-235, and certain results of this work are included and cited in the TG-235 report, which is currently undergoing final review prior to publication[114].

A few important features of radiochromic film:

• The film is sensitive to polarization of the readout light source. Therefore, directions of cutting and scanning should be strictly controlled. This variation can be as large as 80%[115] depending on the film scanner used. Rotating the film by 90 degrees can result in variation of 30% in measured optical density using our Epson 1680 scanner.

• The pre-EBT types of radiochromic film, such as MD-55-2, were inherently non-uniform[116, 117]. The non-uniformity was mainly caused by thickness variation of the sensitive layer of the film and was about 4% in the direction of coating vs. 15% in the perpendicular direction. The direction of coating was marked by the manufacturer on each sheet of film. The sheet size of

MD-55-2 film was only 12.5 cm x 12.5 cm (5" x 5"). In accordance with our method of managing film non-uniformity, all sheets of film belonging to a specific production lot were cut into 3 cm-wide strips in the direction of coating using a precise office paper cutter, keeping track of each strip's position on the sheet (for example ─ first strip from the left). Films used for measurements of a particular eye plaque would always belong to the same strip, continuing from sheet to sheet. This produces sub-film lots with an inherent non-uniformity in the 4% range, rather than the possible 15% if films were randomly cut from any location on the sheet. We applied this technique for dosimetric measurements of CCX 41 and CCX 55 eye plaques using MD-55-2 film, as well as the first prototype of the novel ^{125}I eye plaque using XR-T film.

Starting with EBT film the production processes achieved greater control over the thickness of the active layer, substantially improving the uniformity of the film. The later EBT2 and EBT3 films employ a different chemistry and coating technology, and include a blue dye component in the active layer that, is almost insensitive to radiation. This makes it possible to further account for thickness variation of the active layer, thereby improving film dosimetry precision by applying multi-channel dosimetry techniques[118].

• The other major deficiency of pre-EBT radiochromic film was its low sensitivity. Due to the low sensitivity the dosimetric characterization of a ^{106}Ru eye plaque could take over a month, comprising a significant part of the source's one year useful life. The extended exposure times can also potentially affect the measurement uncertainty due to possible dose rate effects[119].

• Radiochromic film has inherent post-exposure growth of optical density which we found was 16% in the first hour after irradiation, but substantially lower after a few hours. Therefore, the eye plaque and calibration films must be scanned at the same time interval after irradiation.

Despite the issues detailed above, radiochromic film is almost an ideal dosimeter for eye plaque dosimetry as well as any other dosimetric application in radiation therapy due to its near tissue equivalency (except for XR-T film) and sub-millimeter spatial resolution. On the other hand, due to the noted sensitivity to polarization, inherent non-uniformity, post-exposure growth, and some additional environmental dependencies, such as temperature and humidity, absolute dosimetry using radiochromic film requires following a rather strict protocol, as described in the literature[73, 98, 111-113, 116, 117, 119-122], learned through trial-and-error and additionally refined in the process of this work.

While working on dosimetry of [106]Ru eye plaques the author proposed to the manufacturer of the film the idea of developing a new type of radiochromic film that would provide substantially higher sensitivity and uniformity than the present films. Increasing the sensitivity by about 15 times (which would require about 200 cGy for an optical density of 0.5) and significantly improving the uniformity would result in a film that can replace radiographic film in many mainstream applications such as IMRT and linac QA, which have much larger markets than brachytherapy dosimetry, providing the company with an incentive to invest in the project. To accomplish this objective, the manufacturer would also have to supply film in large sheets (at least 8 in x 10 in vs. the then current 5 in x 5 in) and bring the price of the film into a range comparable with radiographic film (from $50 for a 5" x 5" sheet to $10 for an 8" x 10" sheet). After rigorous marketing studies with participation of the author, the manufacturer agreed to proceed with development of a new type of radiochromic film, which was commercially released in 2004 under the name EBT film. In the course of the development of the new film the author was the first to test samples of the new batches, and to uncover new problems. One key discovery was the finding of significant non-uniformity, which was not expected. The investigation of the possible causes

led to the discovery of a very strong dependence of the new active component on environmental humidity. Eventually, this was significantly improved by changes to the film chemistry and to the packaging of the films, which to this day are packaged with paper sheets interlaced between the sheets of film. While the moisture effect on film non-uniformity was substantially improved, environmental moisture in the film still had a strong effect on dosimetry results. The author further investigated this issue and worked out a solution involving cutting the film at least 24 hours prior to irradiation, enabling its moisture content to equilibrate with the environment[42, 113]. As the author found, the moisture did not actually affect the dose measured by the film, but instead affected the scanned optical density up to 10% in the absence of a 24 hour period to equilibrate with the environment. Our recommendation was not only suggested in Soares *et al*[113], but was also incorporated into the forthcoming TG-235[114]. Another problem identified by the author was the lateral scanner artifact, later studied by many researchers[115, 123-129]. Some of our early EBT experience was presented at an AAPM annual meeting[130]. Following the development of EBT film, the author of this work was the first to test prototype EBT2 films, and first to test and use special unlaminated EBT1, EBT2 and EBT3 films.

    1.5. Monte Carlo simulations.

Dosimetric results in radiation therapy are usually reported in terms of dose to water[53, 131], while dosimetric measurements are frequently done in "water equivalent" solid phantoms that enable precise measurement setups, such as the eye plaque dosimetry reported in this work. Several authors have reported that Monte Carlo simulations are a good tool for conversion between dose to media and dose to water[132-135]. All film dosimetry in this work was done in Gammex 457 Solid Water™ (Gammex, Middleton, WI, Sun Nuclear Corporation) water-equivalent plastic. Meigooni *et al*[135] report that there are two main types of Solid Water with either a 2.3% or 1.7% calcium

content. This difference can affect the conversion factors for ^{125}I by as much as 5%. A sample of Solid Water used in this work was sent to a chemical laboratory for calcium content testing. We initiated additional Monte Carlo simulations in order to study conversion between dose to film in Solid Water and dose to liquid water, since Meigooni *et al*[135] did not examine film in Solid Water, but only reported Solid Water conversions to liquid water. We report Monte Carlo derived conversion factors from Solid Water to liquid water for ^{125}I dosimetry and their dependence on radiochromic film type, as well as on the calcium content of Solid Water.

2. Materials and Methods.

2.1 Eye plaques.

2.1.1 ^{106}Ru eye plaques.

Eight different ^{106}Ru eye plaques belonging to three types (CCX, CCA and CIA) were dosimetrically characterized in this work. Front and back views of several ^{106}Ru eye plaques are shown in Figure 2. The CIA plaque in Figure 2 has a cutout in order to position it in the vicinity of the iris[30]. A typical cross section of a ^{106}Ru plaque is shown in Figure 3, and all 16 types of ^{106}Ru eye plaques manufactured by Eckert & Ziegler BEBIG are shown in Figure 4.

The plaques are made of pure silver (Ag 99.99) with a total thickness of 1 mm. The shape is a section of a hemisphere with an inner radius of 12 to 14 mm, which conforms to the typical human eye dimension[65]. Each eye plaque has several suture lugs used to suture it to the sclera.

The radioactive material, ^{106}Ru /^{106}Rh in the form of a thin, electrolytically deposited layer on a 0.2 mm thick silver foil is encapsulated between a 0.1 mm silver window on the concave (facing the eye) side, and 0.7 mm thick silver backing which stops approximately 95% of the beta-radiation posterior to the plaque as reported by BEBIG and given in ISO International Standard 21439:2009[41].

Figure 2. Front and back views of a CCA, CIA, and CCX eye plaques. These are "dummy" plaques, which are an exact silver replica of the appropriate plaque, but without the radioactive layer. They can be distinguished from the real plaque by the hole through the plaque and missing serial number.
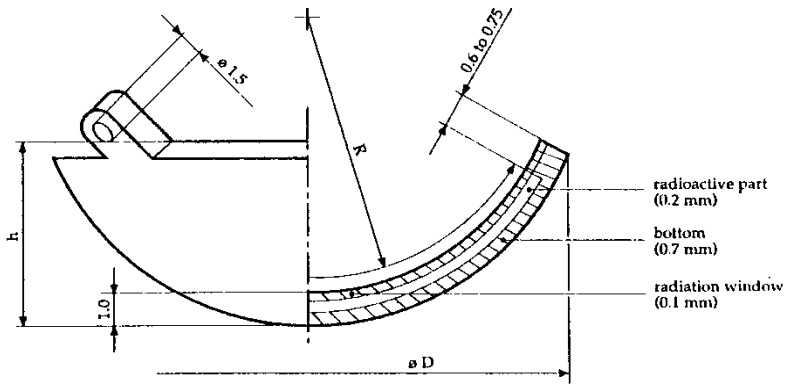
Figure 3. Cross section of a [106]Ru eye plaque (reprinted from an eye plaque data sheet by permission from Eckert & Ziegler BEBIG).
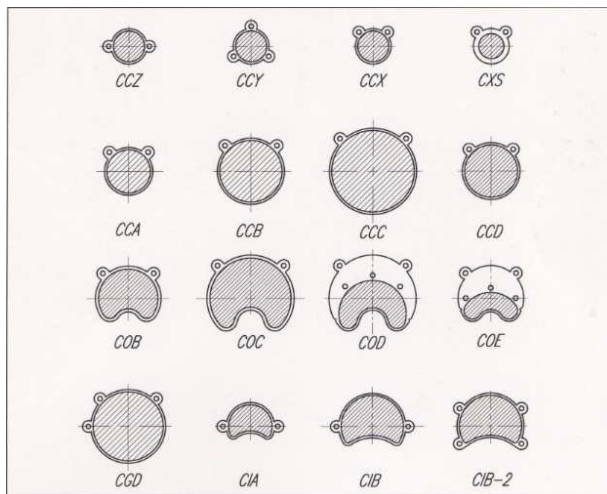
Figure 4. All 16 types of [106]Ru eye plaques manufactured by Eckert & Ziegler BEBIG (reprinted from User Manual: Ru-106 Eye Applicators Rev. 12[30] by permission from Eckert & Ziegler BEBIG).

The [106]Ru /[106]Rh mother-daughter system emits beta-radiation with a maximum energy of 3.541 MeV, as well as 20% 0.512 MeV, 10% 0.622 MeV, 1.6% 1.05 MeV, 0.4% 1.13 MeV, and 0.2% 1.55 MeV gamma radiation per decay[41]. Bremsstrahlung produced by interactions of the beta

particles with the source material is also emitted[41]. The half-life of the parent isotope is 373.59 days[41].

The first plaque characterized was CCX 36. The dosimetric measurements of this plaque were done using the NIST phantom provided to us by Dr. Soares (NIST) and shown in Figure 14. The remaining seven plaques: CCX 41, CCX 55, CCX 104, CCX 129, CCX 219, CCA 892, and CIA 156 were characterized using a Solid Water "eye" phantom designed in the course of this work (the number after the plaque type is the serial number of the plaque). The CCX plaques have a diameter of 11.6 mm and internal height of 1.3 mm and are mechanically the smallest plaques manufactured by BEBIG. They were of special interest at Memorial Sloan-Kettering Cancer Center for treatment of retinoblastoma in small children and therefore 6 out of the 8 plaques belong to this type. CCA has a diameter of 15.3 mm and internal height of 2.3 mm. CIA has the same dimensions as CCA, but has a cutout for treatment of ciliary body melanoma[30].

2.1.2 COMS plaques.

The design of COMS plaques was standardized for the COMS study[37, 38].

All COMS plaques in the U.S. and originally for worldwide use are manufactured by Trachsel Dental Studio, Inc. in Rochester, MN. Chiu-Tsao[31] describes the design of the standard COMS plaques, which have been made in 5 diameters of 12 mm, 14 mm, 16 mm, 18 mm, and 20 mm. Chiu-Tsao[31] also provides the exact seed arrangement for every plaque and the material composition of the gold backing. An unpublished document by Kline[136] provided by Trachsel as a data sheet/user manual describes exact details of the design, drawings and material compositions including plaques with cutouts. Later publications by Chiu-Tsao et al[39, 40] add two additional diameters of eye plaques to the original five – 10 mm and 22 mm, which were not included in the study, but eventually were made available by Trachsel.

A typical design of a COMS ^{125}I eye plaque is shown in Figure 5 below, while its components are shown in Figure 6.

L.   Seed arrangement in the silastic seed carrier insert and the gold plaque design. (a) Top view and (b) side view of a 14 mm COMS standard plaque.
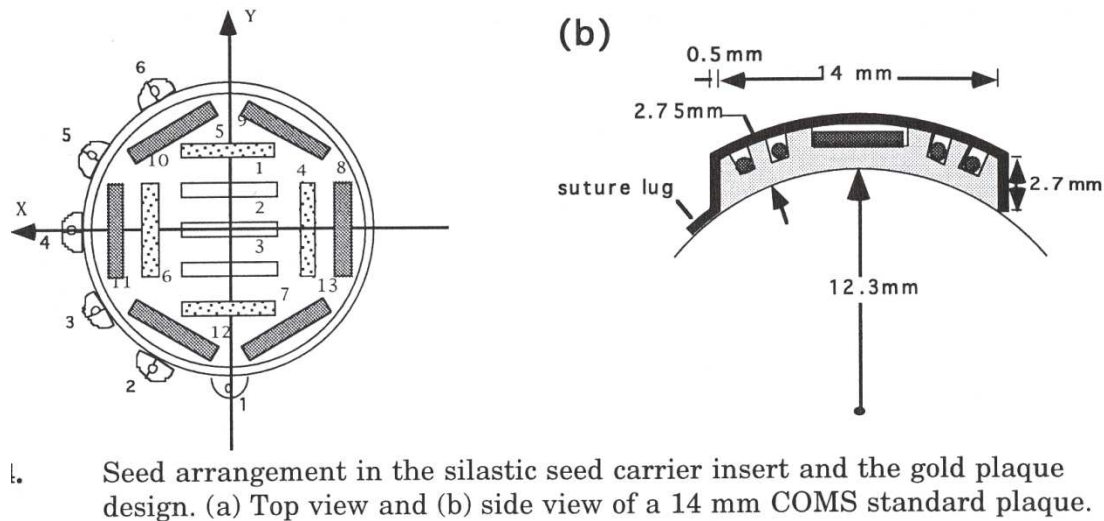
Figure 5. Cooperative Ocular Melanoma Study plaque design (reprinted from Chiu-Tsao[39]).

The gold alloy backing is made of an approximately 0.5 mm thick alloy with a trade name Modulay, which consists by weight of 77% gold, 14% silver, 8% copper, and 1% palladium[39, 40, 136]. The alloy was selected for its biological inertness, ease of fabrication and shielding properties[136]. The gold alloy backing holds the Silastic seed carrier insert, which is glued to its internal concave surface. The backing serves as a radiation shield and stops approximately 99% of the radiation[37]. A cylindrical part called the "lip" surrounds the rounded backing. The "lip" is designed to protect sensitive structures as the optic nerve, the optic disk, and macula. The "lip" has six lugs with suture holes enabling suturing the plaque to the sclera. The seed carrier insert is made of medical grade silicone rubber called Silastic (Dow Corning Corporation, Midland, MI) bio-medical grade elastomer MDX4-4210[40, 136].

24
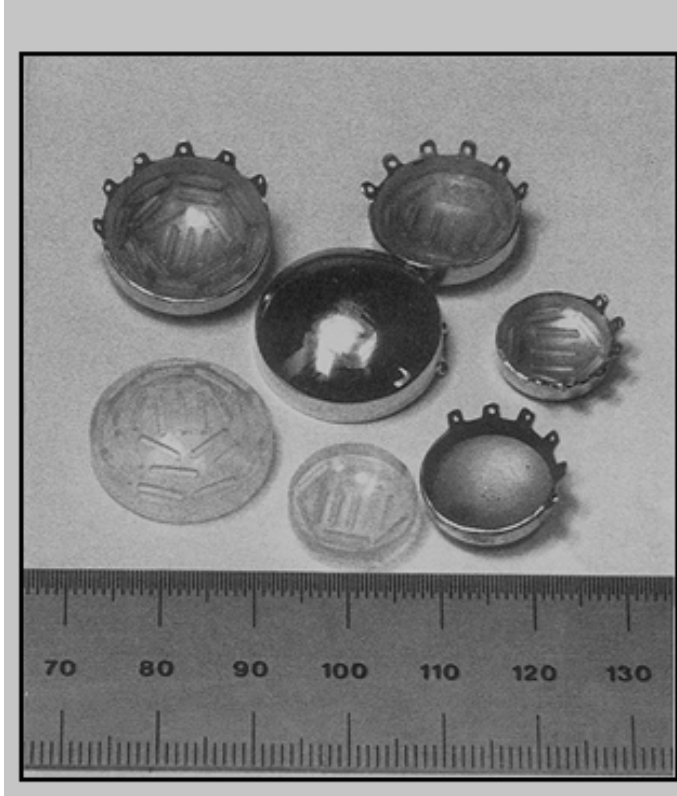
Figure 6. COMS plaques: gold backings, silastic inserts, assembled plaques without seeds.

The radius of the seed carrier's internal curvature is 12.3 mm conforming to 24.6 mm, the "average" diameter of the human eye. It has fixed locations for the seeds, and it assures that all seeds are at 1 mm distance from the outer scleral surface. AAPM's TG-129[40] provides the seed locations for all seven COMS plaques shown in Figure 7 and a table of seed coordinates for each plaque. The seed coordinates can be used in standard treatment planning systems, like Pinnacle (Phillips North America Corporation, Andover, MA) and Eclipse BrachyVision (Varian Medical Systems, Inc., Palo Alto, CA) in conjunction with TG-43[53, 137], enabling treatment planning calculations of COMS eye plaques. Unfortunately, these widely used approaches do not correct for the combined dose reduction effects of the gold alloy backing, Silastic seed carrier and other plaque construction details described by Thomson *et al*[54] and studied in this work.
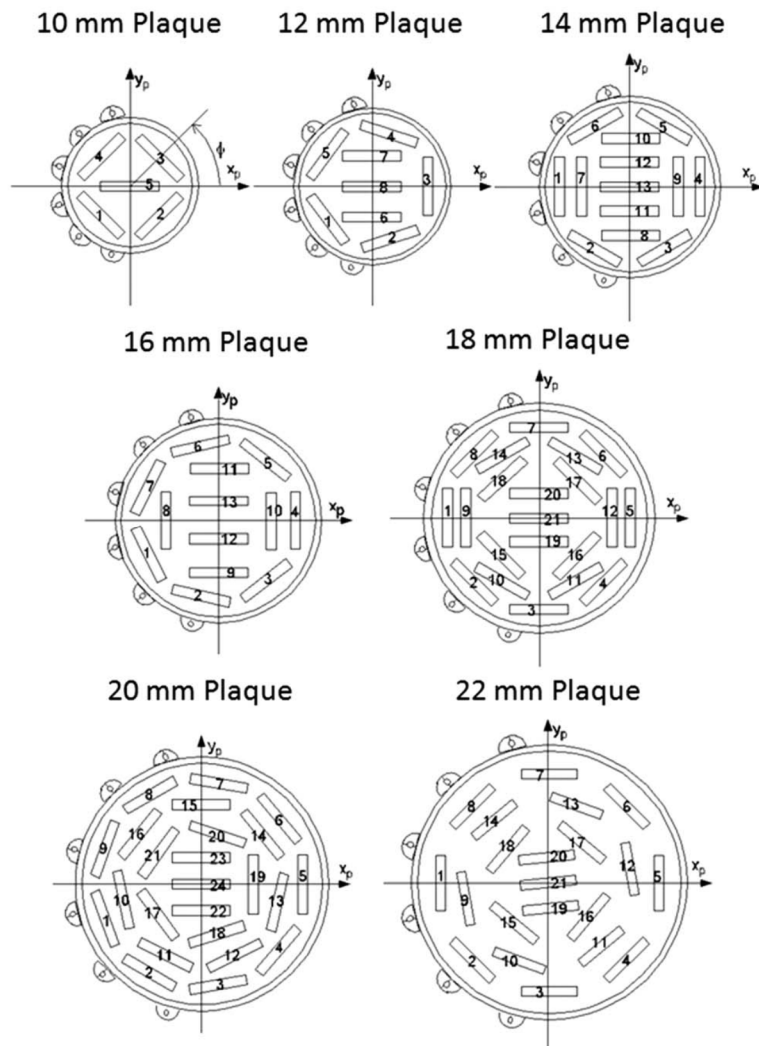
Figure 7. Seed diagrams for 10 mm – 22 mm COMS plaques viewed from the internal (concave) aspect of the seed carrier insert (reprinted from Chiu-Tsao *et al*[40]).

The 20 mm COMS plaque studied in this work was assembled from standard Modulay backing and Silastic seed carrier (Trachsel Dental Studio, Inc. Rochester, MN) used for treatment of patients at Memorial Sloan-Kettering Cancer Center (MSKCC). One complication in building the phantom parts was the discovery that the Modulay backing was not perfectly round with its diameter varying from 20.66 mm to 21.20 mm, so we used the average of several measurements around the plaque of 20.80 mm. Also, its thickness varied between 0.48 mm and 0.51 mm, as one

could probably expect from a product manufactured by a dental workshop. A picture of the concave side of the fully loaded 20 mm plaque is shown in Figure 8.

Figure 8. Picture of the fully loaded 20 mm COMS eye plaque dosimetrically characterized in this work. The Oncura 6711 seeds are visible through the silicone seed carrier. The ruler in the picture is a Starrett (L.S. Starrett Company, Athol, MA) metric ruler, with 0.5 mm smallest division.

The plaque was loaded with 24 Oncura Model 6711 ^{125}I seeds with air kerma strength 6.75 U/seed on the reference date (apparent activity 8.57 mCi/seed) provided for this work by Oncura, Inc. (Arlington Heights, IL). The seeds were requested to have air kerma strengths within 1% of each other. The reported average of the batch was 6.7517 U with 0.0211 U standard deviation. The highest deviation of a single seed from the average was 0.60%. After receipt of the seeds they were calibrated using an HDR 1000 Plus S/N A990685 well chamber with the seed insert calibrated by the University of Wisconsin ADCL for the 6711 seed with a calibration coefficient 0.2376 U/pA and the Standard Imaging Max 4000 S/N E041325 ADCL calibrated electrometer with calibration coefficient 1.000. The calibration results had an average of 6.7023 U, with standard deviation of 0.0267 U on the same reference date as that specified by the manufacturer. The calibrated average differed only -0.73% from the reported average air kerma strength of the batch, which is excellent agreement. The highest deviation of a single seed calibrated by us from the batch average was 0.8%. The manufacturer's air kerma strength was used for further calculations.

2.1.3 Novel ^{125}I eye plaque and collimator.

The drawings of the cross-sections and bottom views of the two 16 mm diameter prototype eye plaques are shown in Figures 9 and 10. The main part of both prototypes is a quartz substrate in the shape of a spherical cap, with a layer of ^{124}Xe ions implanted at the inner surface. For the first prototype, created in phase I of the project and shown in Figure 9, a 0.5 mm pure gold (Au 99.99) backing conforming to the spherical cap was attached to the rear side of the quartz substrate and both were encapsulated in a polymer enclosure prior to activation. The second prototype, shown in Figure 10, was created for phase II of the project. For the second prototype, the 0.3 mm thick quartz substrate with the layer of implanted ^{124}Xe ions was encapsulated in a 0.125 mm thick enclosure of titanium prior to activation.

For the second prototype, the radius of curvature of the concave surface of the eye plaque attached to the sclera was 12.2 mm, similar to the 12.3 mm of the COMS plaques[31].
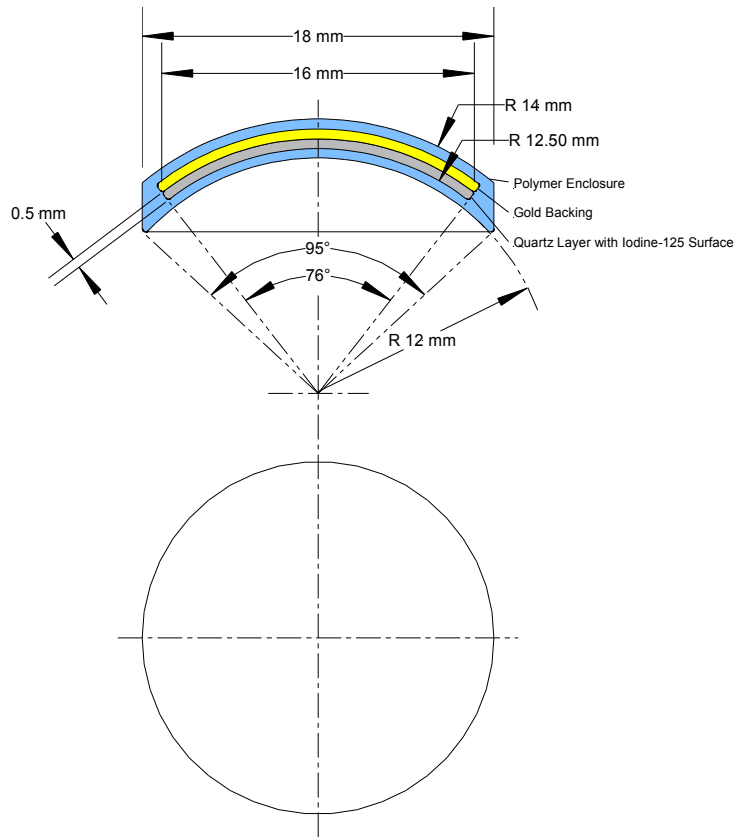
Figure 9. Cross section and bottom view (looking from the concave surface of the plaque) of the first prototype plaque.

An exploded view of the quartz substrate and the parts of the titanium encapsulation of the second prototype are shown in Figure 11. Pictures of the parts of the second prototype and the encapsulated eye plaque are shown in Figure 12.

After activation, a 0.5 mm pure gold (Au 99.99) backing was attached to the plaque. The gold backing in the shape of a spherical cap was continued as a cylinder, called the "lip" in COMS

plaques[31], but has no attached suture lugs. The outer diameter of the lip was 18.5 mm and its height was 0.5 mm. The main role of the lip is to shield normal structures of the eye adjacent to the plaque as defined in the COMS protocol.
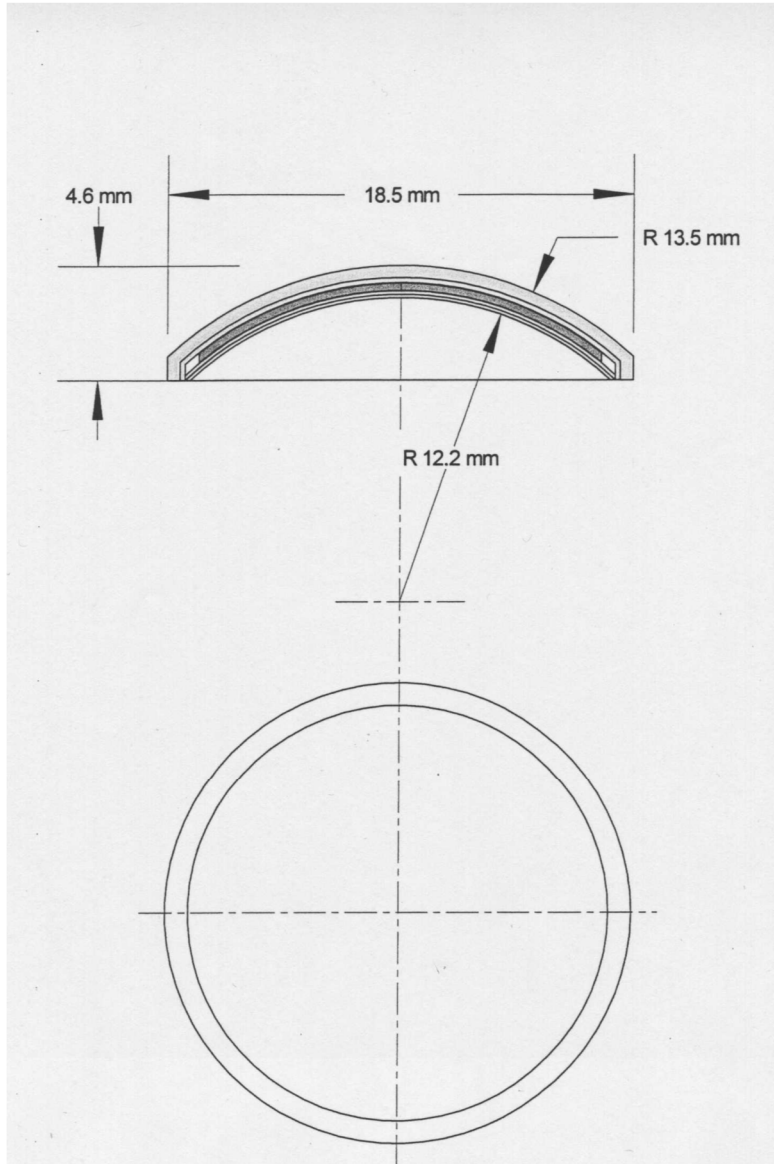
Figure 10. Cross section and bottom view (looking from the concave surface of the plaque) of the second prototype plaque.

The apparent activities of the first and second prototype eye plaques were estimated from exposure measurements by Implant Sciences as 103 mCi and 14.7 mCi respectively.
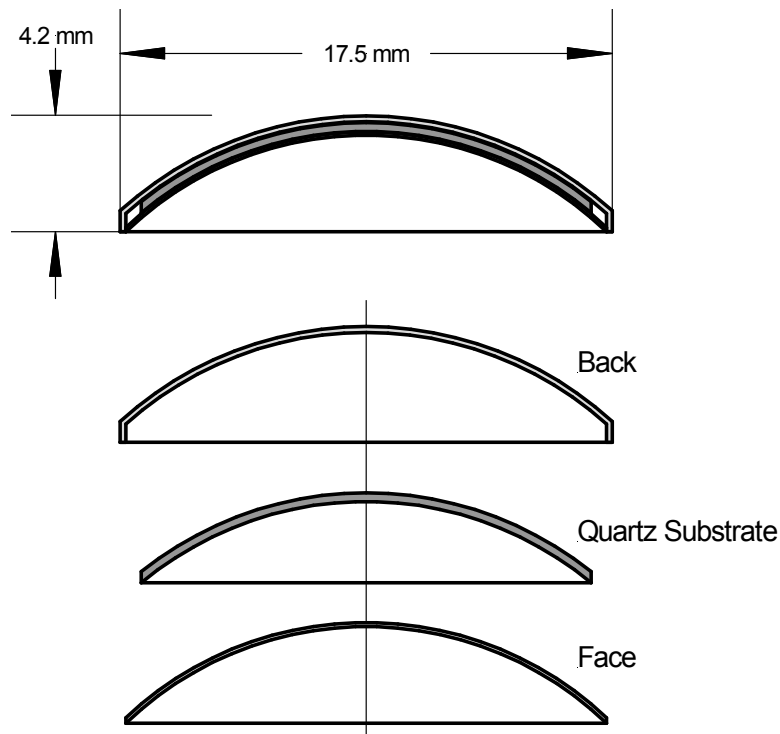
Figure 11. An exploded view of the second prototype plaque's encapsulation without the gold backing.

Figure 12. Second prototype quartz substrate before implantation (left) and after implantation with titanium encapsulation components (center), and after encapsulation in titanium (right).

The collimator was fabricated from 0.13 mm thick pure gold (Au 99.99) in a form of a spherical cap and had a radius of curvature of 12.2 mm in order to conform to the concave surface of the eye plaque. The prototype collimator tested in this work is shown in Figure 13.
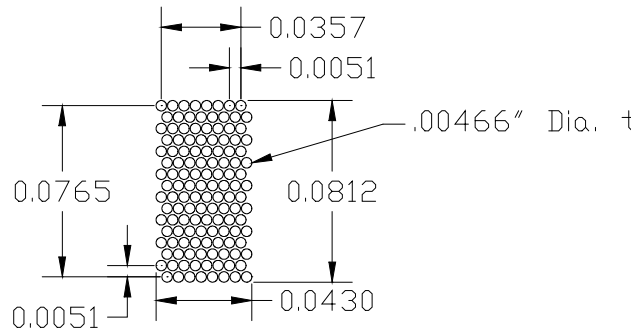
Figure 13. Special collimator configuration. Collimator holes of 0.1 mm diameter are spaced 0.13 mm apart in a hexagonal array. Dimensions in the drawing are in inches, since it was a production drawing.

The tested collimator consisted of a 2.0 mm x 1.09 mm area around the central axis of the plaque which had 128 0.1 mm diameter holes separated by 0.13 mm in a hexagonal array.

2.2 Solid Water "eye" phantom.

Our first eye plaque dosimetry experiment consisted of measurements performed on CCX 36 [106]Ru eye plaque using both radiochromic film in a water-equivalent solid phantom and a small semiconductor diode in a water tank.

The radiochromic film measurements were done using a NIST-manufactured set of phantoms made of WT1 (RMI 457 Solid Water™) water-equivalent plastic (we are indebted to Dr. C. Soares for making his phantom available to us). The phantom, shown in Figure 14 below, is the same

phantom used for radiochromic film [106]Ru eye plaque dosimetry at NIST described by Soares *et al*[73] and has been used by NIST to provide dosimetric calibration to BEBIG from 2002 until 2012.
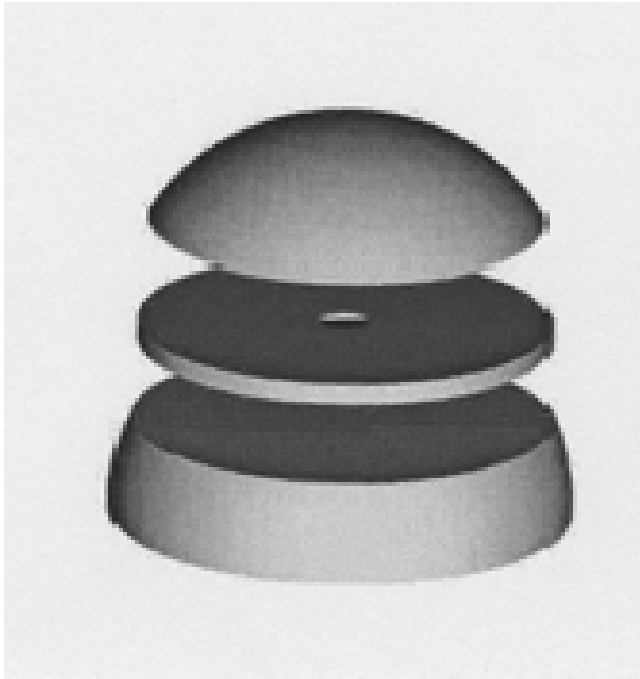
Figure 14. One set of the NIST Solid Water phantoms for [106]Ru eye plaque dosimetry.

The phantom consisted of nine sets consisting of an upper spherical section each having a radius of curvature of 12mm, corresponding to the inner radius of BEBIG's eye plaques and matching bottom parts. Each pair (set) enabled placement of a film in a plane perpendicular to the central axis of the plaque at a specified distance from the plaque's inner surface varying between 0.5 mm and 10.0 mm, sandwiching it between the upper and bottom parts. The upper and bottom part of each set together with the film formed a hemisphere of a radius of 12 mm. The eye plaque was placed on the top of the upper section, and the thickness of the upper section defined the distance of the top surface of the film from the eye plaque. The phantom enabled TLD measurements as well. Figure 14 shows a holder disk for round TLDs.

Using the NIST phantom the author learned that radiochromic film in a Solid Water phantom is a

reproducible high resolution technique which has the potential of measuring accurate dose distributions needed for precise treatment planning and delivery.

On the other hand, the NIST phantom had several limitations for the purpose of our work. Placing the eye plaque on top of the phantom in a reproducible way without moving the parts of the phantom and the film was a real challenge. Even with the help of a specially designed jig this task was very complicated. An additional limitation of this measurement setup was complete lack of co-registration between the film and the eye plaque. This caused difficulties in identification of the positions of detected non-uniformities, and was an obstacle for two-dimensional (other than the measurement plane) or three-dimensional reconstruction of dose distributions. Another problem of these phantoms was their limitation to dosimetry of ^{106}Ru plaques. They could not be used for ^{125}I plaques because of their BEBIG tailored geometry, and because ^{125}I measurements require a scatter phantom. While ^{106}Ru eye plaques dosimetry was the original aim of this work, we considered from the early days working on dosimetric challenges of ^{125}I eye plaques. Therefore a phantom was designed in this work and described in detail in the published article[42] which is part of this dissertation. This phantom enables:

- Performing measurements on eye plaques using ^{106}Ru as well as ^{125}I or any other radionuclide or combination of radionuclides.

- Precise reproducible positioning of the eye plaques with respect to the films, which can be kept in place intact for the duration of measurements for as long as weeks.

- Co-registration between the plaques and films which enables reconstruction of 2D dose distributions at selected planes or 3D dose distributions from a set of films irradiated at planes perpendicular to the central axis of the eye plaque.

Figure 15 and Figure 16 below are pictures of the actual phantom and its parts assembled for measurements of CCX 55 eye plaque, as well as of an exposed MD55-2 radiochromic film. CCX 55 was the first eye plaque measured in this phantom.
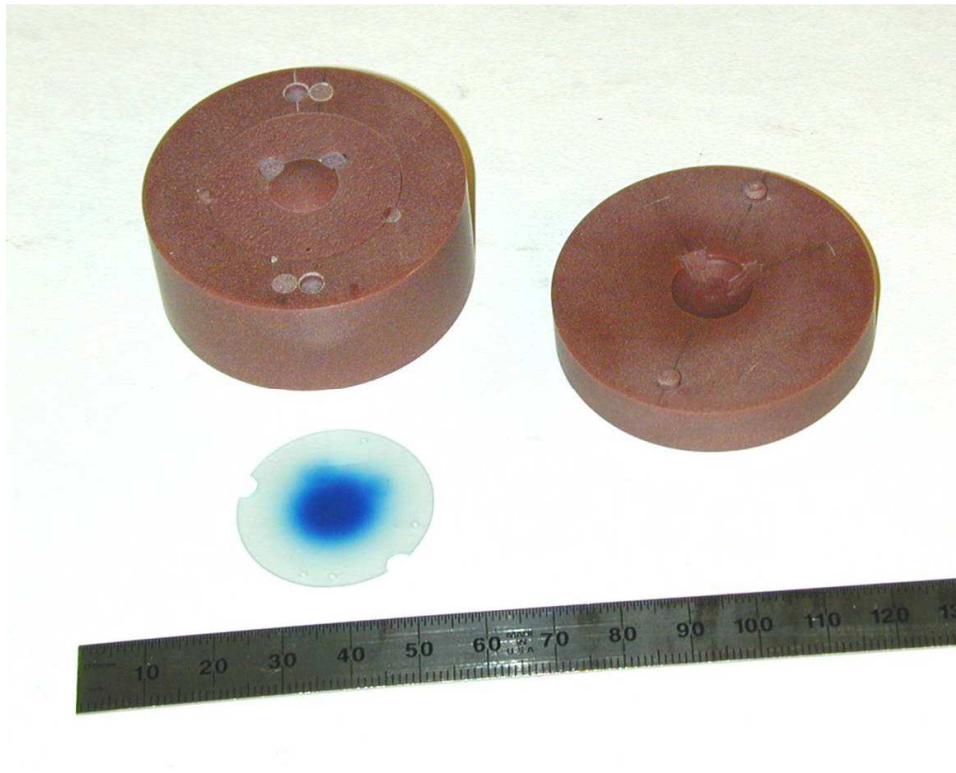
Figure 15. Picture of the "eye" phantom assembled for a CCX 55 plaque measurement with a MD-55-2 film exposed by this plaque.

Figure 16. Parts of the "eye" phantom configured for a CCX plaque.

Figures 17 and 18 below show an assembly drawing of the "eye" phantom with a [106]Ru eye plaque and of the assembled "eye" phantom with a [106]Ru eye plaque. Both were not included in the published article[42] for brevity. In both figures all parts except for the eye plaque are made of Solid Water, different shades and colors are used in order to visualize the different parts. Obviously, the parts of the phantom which come in contact with the eye plaque have to be designed and manufactured for each kind and model of eye plaque in order to assure its precise tight fit to the phantom.
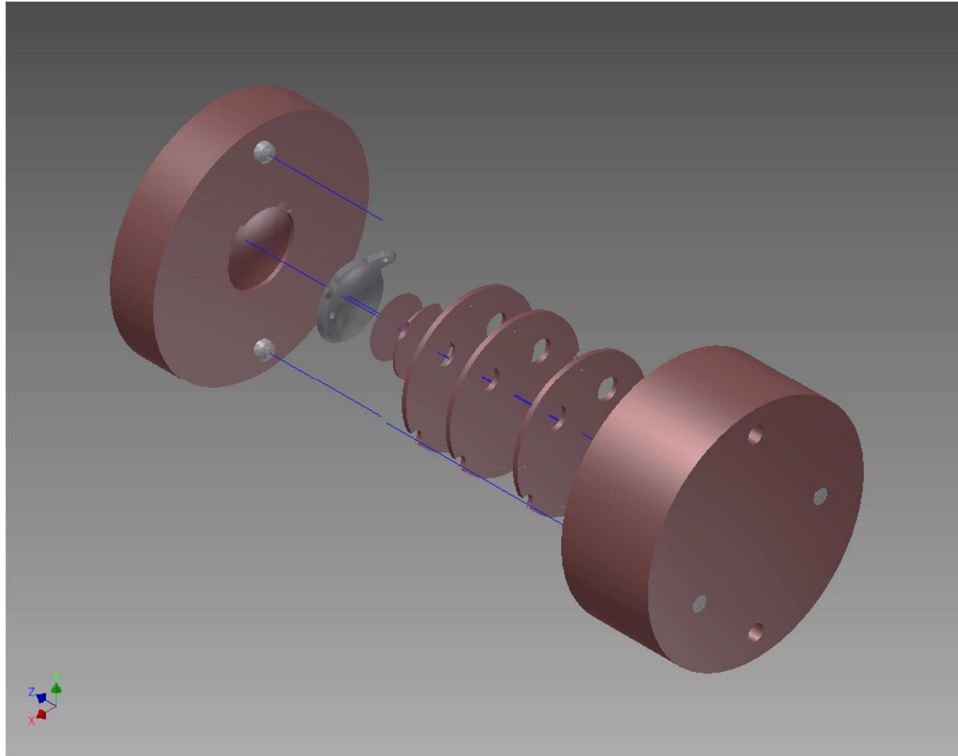
Figure 17. Assembly drawing of the "eye" phantom with a ^{106}Ru eye plaque.
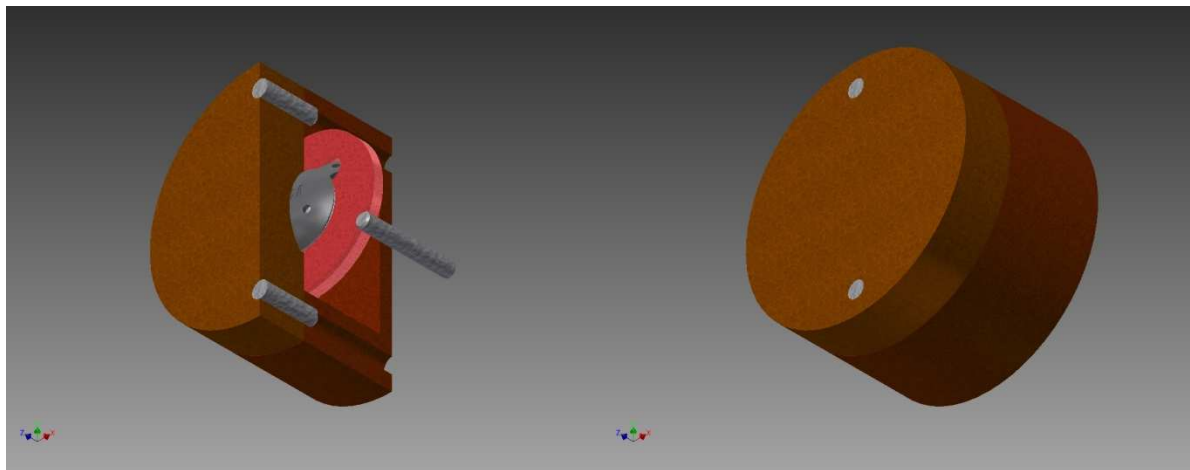
Figure 18. Drawing of the assembled "eye" phantom with a ^{106}Ru eye plaque.

There are a few important points which were not mentioned in the paper[42], again for brevity. When the plaque is placed on top of the spherical part of the phantom, its lower border, for example the "lip" of a COMS plaque should not be in contact with the flat surface of the upper phantom insert which holds the spherical part, but should be above it, even by a small fraction of a mm, which can be inspected visually. Apparently the plaques have mechanical tolerances, and if the "lip" is a little longer this may create an air pocket between the inner concave surface of the plaque and the top of the spherical part of the phantom. In this case the dosimetric results will be wrong. This happened to us with a set of measurements of a ^{106}Ru eye plaque. Some of the phantom parts had to be re-done and the measurements repeated. The other lesson was learned with larger plaques, like the 20 mm COMS plaque. Since we tried to perform measurements every mm starting with the inner concave surface of the plaque, there were a number of measurement planes inside the plaque. Creation of a single set of inserts enabling one to put films in, let's say, four planes inside the plaque, even one film at a time, would create a very unstable construction. Therefore, the solution was to have a number of sets for the measurements inside the plaque, similar to the sets in the NIST phantom shown in Figure 14. For example, the 20 mm COMS plaque required four such sets. Obviously the eye plaque would still be held in place since its suture lugs would fit into the holes in the phantom. The small round films, which fit inside the plaque cannot be marked using a needle, like the larger films, which was very important for controlling the orientation of the films (to minimize polarization effects during film readout) and for co-registration of the films and the plaques. Therefore the reference orientation of these films was marked using a thin permanent marker prior to punching them from the page of film and then these films were positioned in the phantom making sure that the reference orientation matched the direction of the

large films; this direction serves as one of the coordinate axes in the scanning and analysis process (the Y axis).

The phantom parts for measurements on the second prototype of the novel ^{125}I eye plaque together with the second prototype are shown in Figure 19.

The phantom drawings for dosimetry of ^{106}Ru eye plaques are part of the published article[42], while the drawings for the dosimetry of the 20 mm COMS plaque are shown in Figures 20 and 21 below. The phantom and its parts configured for the 20 mm COMS eye plaque measurements are shown in Figure 22, while the assembled phantom with the 20 mm COMS plaque and the phantom cover, which was created as an imprint of the backing of the eye plaque, conforming to it and holding the eye plaque in place, are shown in Figure 23.

For ^{125}I measurements the "eye" phantom has to be inserted into a scatter phantom which would model the irradiation conditions with a high degree of accuracy. Dosimetry of ^{106}Ru does not require a scatter phantom due to the short range of the beta particles and relatively small photon component. As explained in the published article[42] the latter statement was tested irradiating ^{106}Ru eye plaque films with and without a scatter phantom; there was no measurable difference. On the other hand even for ^{106}Ru measurements we placed the "eye" phantom with the eye plaque and film into a 50 mm diameter cylindrical hole at the center of a 30 cm x 30 cm x 3 cm Solid Water slab which was on top of a 30 cm x 30 cm x 5 cm Solid Water slab and covered by another 30 cm x 30 cm x 5 cm Solid Water slab in order to create full backscatter, and a stable measurement environment, so if the film was trying to curve, it would not be able to push the phantom open or otherwise affect the measurement.
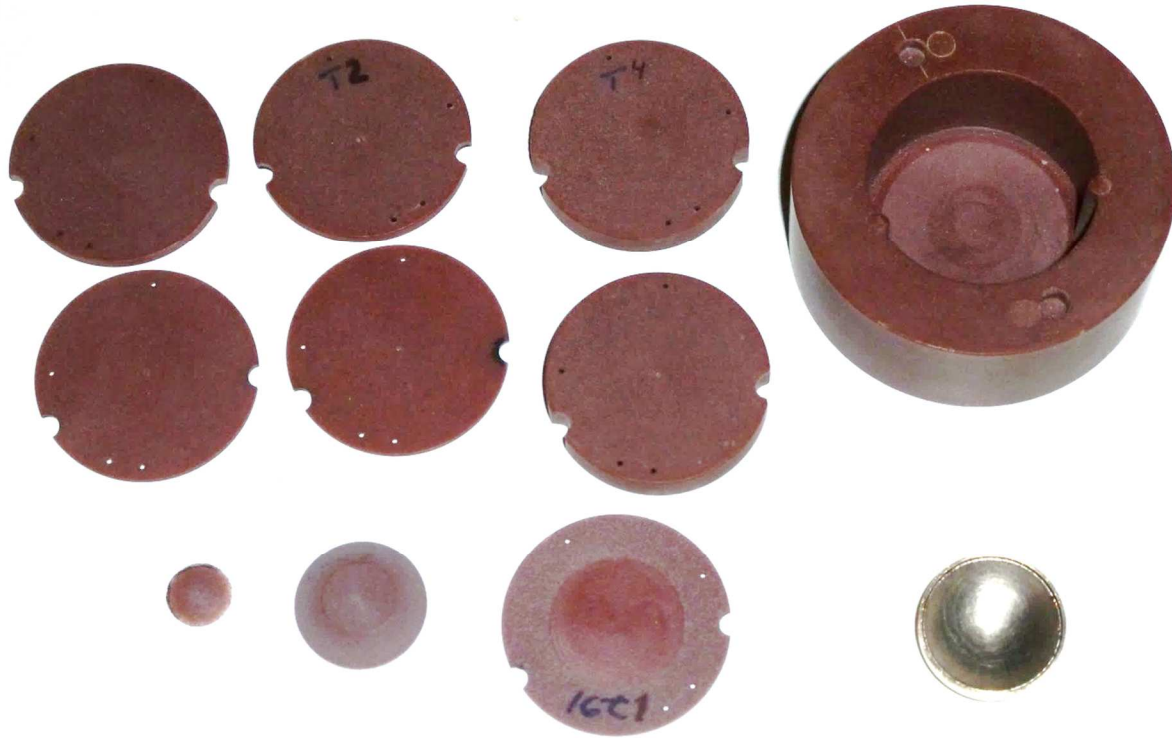
Figure 19. Picture of the top view of the phantom body and its various inserts for measurements of the second prototype of the novel ^{125}I eye plaque. The top view of the concave side of the second prototype eye plaque is at the bottom right.

The measurements of the first prototype of the novel ^{125}I eye plaque were done in a "head" phantom mimicking scatter conditions when irradiating a patient's eye, i.e., having an eye-air interface similar to the "eye-head" phantom used by Chiu-Tsao *et al*[56]. The 3 cm thick Solid Water slab with the phantom and eye plaque was placed on top of a 0.5 cm thick 30 cm x 30 cm Solid Water slab held in the air by two Styrofoam blocks at its sides and covered by additional 15 cm thickness of 30 cm x 30 cm Solid Water slabs. This created scatter conditions similar to a realistic

scenario of eye plaque treatment, having scatter from the patient head and lack of scatter due to an eye-air interface. In this measurement setup the eye plaque was placed at the posterior aspect of the eye approximately 2.5 cm from the eye-air interface.

Measurements of the second prototype of the novel ^{125}I eye plaque were done in a full scatter 30cm x 30cm x 30 cm Solid Water cube created by placing the 3 cm thick slab with the phantom on top of 13.5 cm thickness of Solid Water slabs and covering it with 13.5 cm thickness of Solid Water slabs in order to compare the results with Monte Carlo simulations by Implant Sciences.

The same full scatter phantom was used for dosimetric characterization of the 20 mm COMS eye plaque in order to test the BrachyDose Monte Carlo simulations by Thomson *et al*[54] and Plaque Simulator calculations. Calibration of radiochromic film for ^{125}I eye dosimetry using a calibrated ^{125}I eye seed was also done in the same 30 cm x 30 cm x 30 cm Solid Water cube.
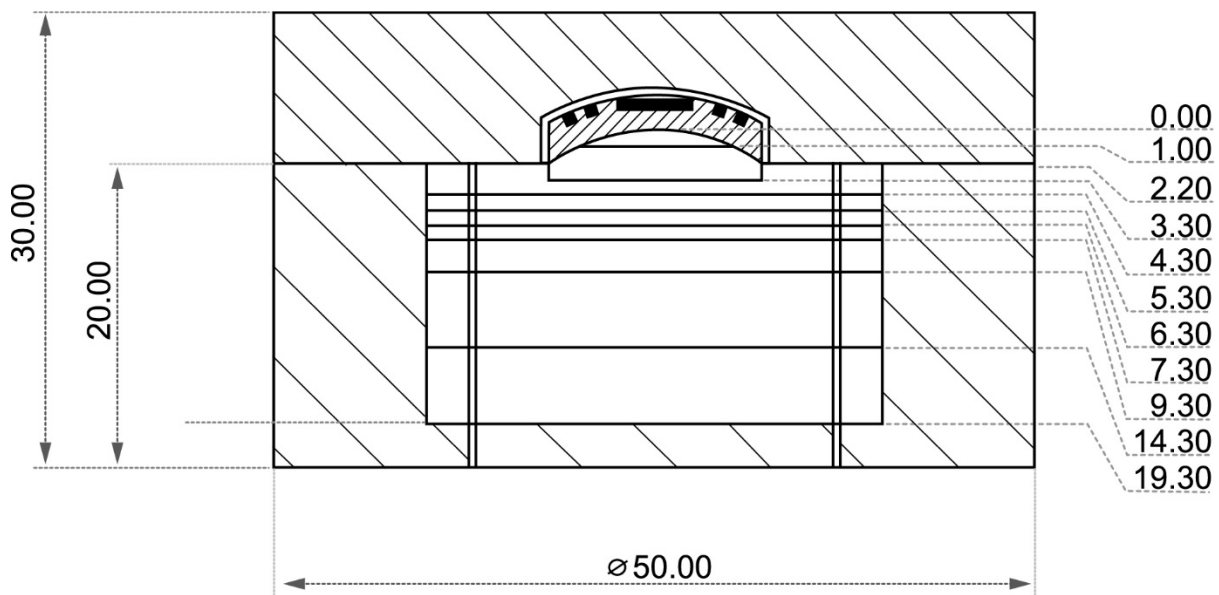
Figure 20. Cross section of the Solid Water "eye" phantom shown with the 20 mm COMS eye plaque (all dimensions in mm).
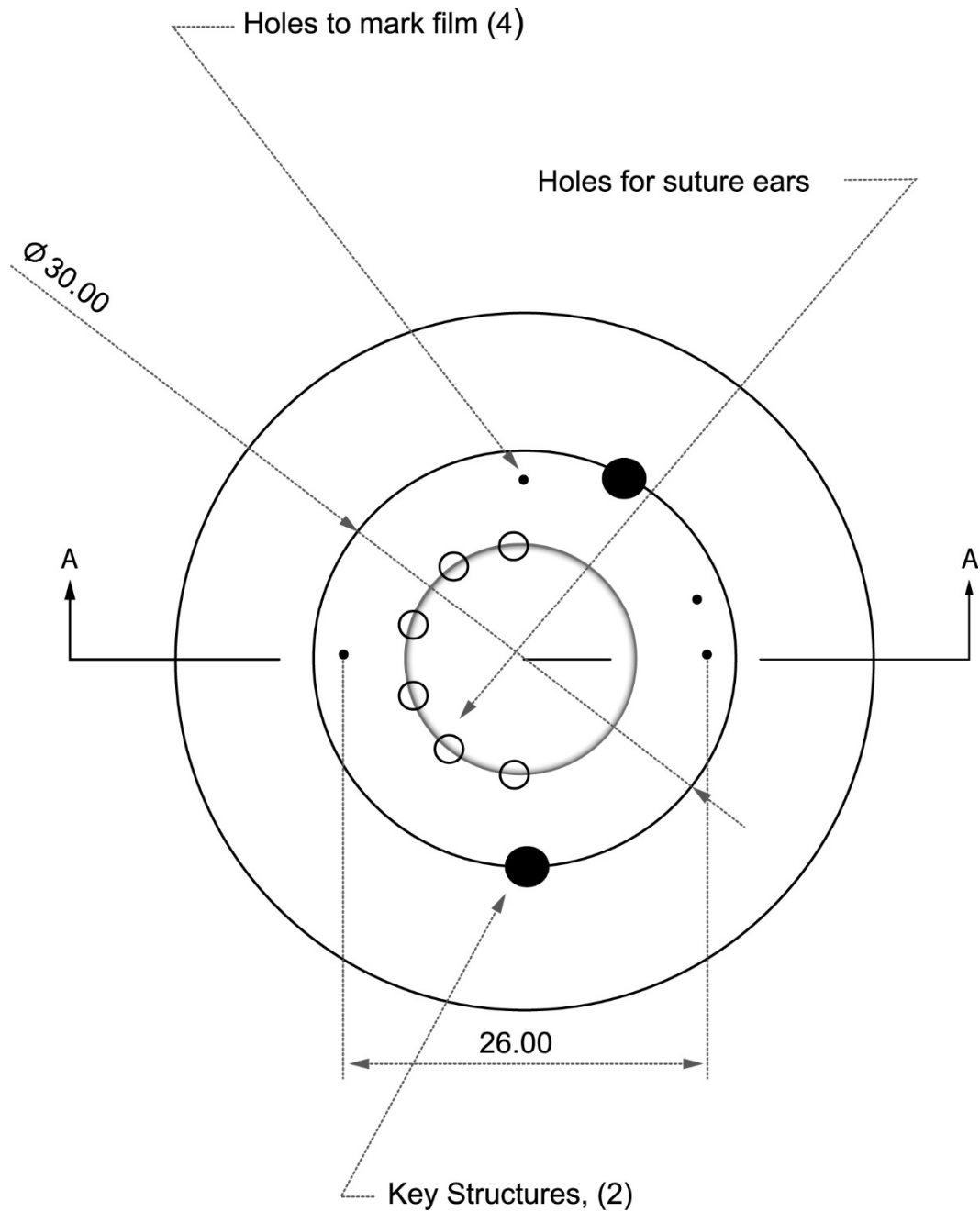
Figure 21. Top view of an insert of the "eye" phantom with the 20 mm COMS eye plaque, inserted into the phantom, showing the key structures (Solid Water pins), and holes for marking the films (all dimensions in mm). The key structures are solid black for visibility. A – A marks the cross-section shown in Figure 20.

Figure 22. Solid Water "eye" phantom with its various inserts for measurements of the 20 mm COMS plaque with the fully loaded 20 mm COMS plaque at the bottom left corner.
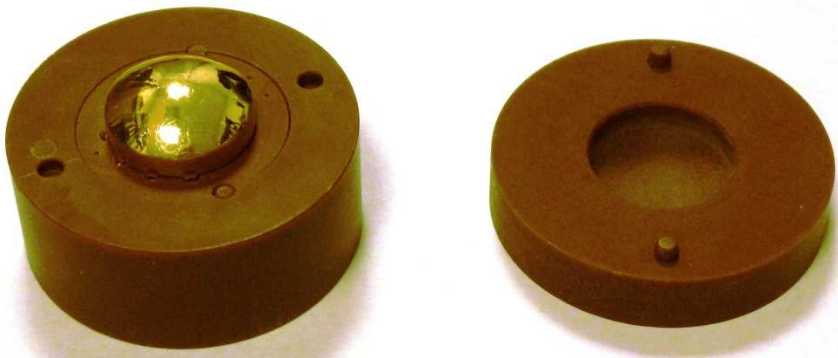
Figure 23. Solid Water "eye" phantom with the fully loaded 20 mm COMS plaque assembled for measurement and the upper part of the phantom with the imprint of the plaque.

The Solid Water slabs used for building the phantom and subsequently all its parts, as well as the 3 cm thick Solid Water slab with the cylindrical 50 mm hole were originally purchased as non-certified Solid Water and their exact material composition was not known. In preparation for Monte Carlo simulations there was a need to know the material composition of the two slabs. The author asked the company Gammex (Middleton, WI, Sun Nuclear Corporation) for help. The company was able to locate the information by the serial numbers of the slabs, as presented in Table 2 below:

	3.0 cm slab with 5.0 cm hole	Phantom and its parts
	Batch 992 (s/n 457 9992 4)	Batch 11218 (s/n 457 11218 2)
Hydrogen (H)	8.402	8.399
Oxygen (O)	18.340	18.312
Carbon (C)	68.970	69.017
Nitrogen (N)	1.978	1.962
Calcium (Ca)	2.31	2.31
Chlorine (Cl)	0.0 ?	0.0 ?
Density g/cm^3	1.0412	1.0477

Table 2. Elemental composition of the two Solid Water slabs used for creation of the "eye" phantom and measurement setup as percent by weight by element. The chlorine content was not reported, but since it is usually reported as only 0.1%, it was assumed to be 0.0%.

The densities of the slabs in Table 2 were calculated by us shortly after their purchase weighing each slab using a precise Mettler (Mettler Toledo, Columbus, OH) scale, which we calibrated using standard weights and measuring its dimensions using Starrett rulers and calipers.

A potential problem with the elemental composition of Solid Water is described in the published article[42]. There are two kinds of Solid Water, which differ in the calcium content, either 2.3% or 1.7%, which results in substantial dosimetric differences when used for low photon energy dosimetry[135]. We were personally warned by Dr. Williamson, the Editor-in-Chief of Medical

Physics, that the company may report the wrong calcium content, which happened to him when conducting an experiment described by Patel *et al*[138] and suggested that we should perform a chemical analysis of the phantom. Therefore a sample of the phantom was sent for chemical analysis to Analytical Answers, Inc. (Woburn, MA), the same laboratory used by Patel *et al*[138]. The result of gravimetric ashing and scanning electron microscopy/energy dispersive X-ray spectroscopy revealed calcium content of $2.32 \pm 0.06\%$ consistent with the manufacturer's report. All our other Solid Water material was purchased as certified Solid Water with 2.3% calcium content as well.

2.3 Radiochromic film.

At the beginning of this work there were available two types of GAFCHROMIC film: HD-810 and MD-55-2. The MD-55-2 type used for dosimetry of the CCX 36 eye plaque required a dose of about 30 Gy in order to achieve an optical density of about 0.5, which can be reasonably used for extraction of dosimetric data. A 30 Gy dose to the film required irradiation times between a day and a week, depending on the film distance from the plaque, for dosimetric characterization of a standard activity ^{106}Ru eye plaque. The HD-810 film type was not considered for this project since it required a 100 Gy dose for the same optical density which would result in considerably longer irradiation times. Therefore MD-55-2 film was used for dosimetric characterization of the CCX 36, CCX 41 and CCX 55 ^{106}Ru eye plaques. The CCX 36 eye plaque was characterized using MD-55-2 Lot #37350. CCX 41 and CCX 55 eye plaques were characterized using MD-55-2 film Lot # I1215.

Two new types of film were under development when this work started and were tested when they became available: HS and XR-T. The HS film was supposed to be somewhat more sensitive, but otherwise similar to MD-55-2 film. Upon testing of HS film Lot # 30263-1-C1, its sensitivity was

not found to be a significant improvement over the MD-55-2 Lot #I1215 already in use, as can be seen in Figure 24, since even the sensitivity of the film batches could be quite different and it seems that MD-55-2 Lot # I1215 was on the better sensitivity end. Therefore HS film was not used in this work. Figure 24 compares optical densities calculated from pixel values as OD = log (I/I$_0$) of films irradiated on a ^{60}Co machine in identical conditions scanned on an Argus II scanner with a red acetate filter[120].
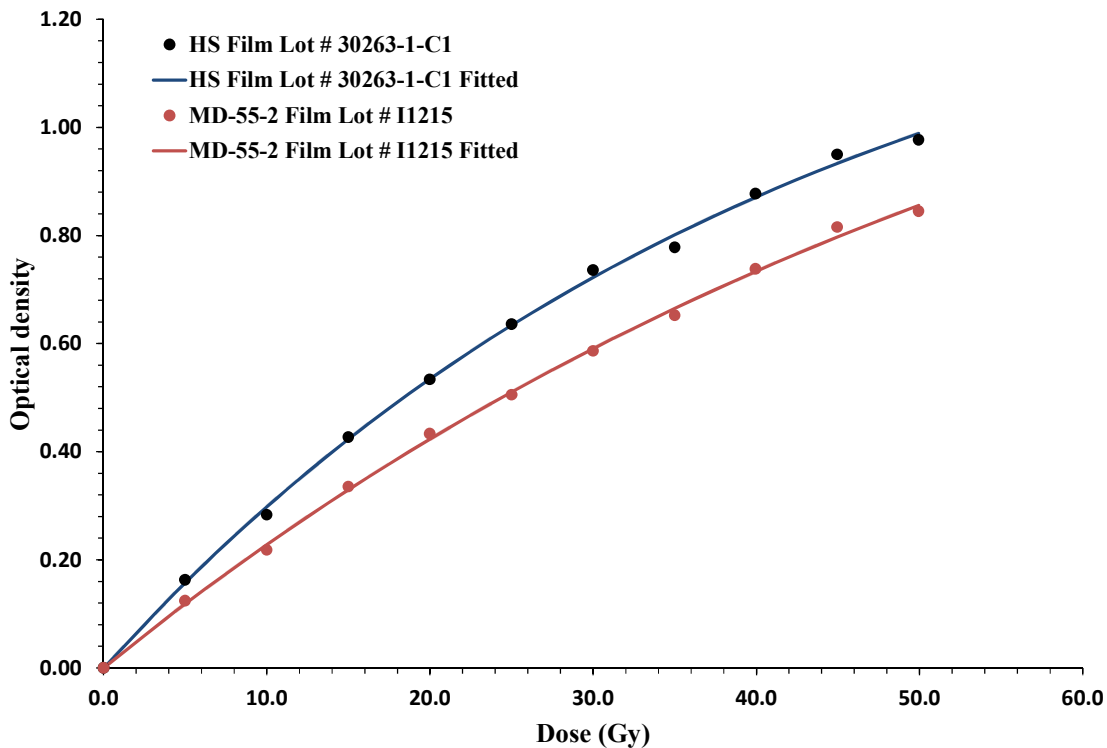
Figure 24. Comparison of optical densities of experimental HS film Lot #30263-1-C1 and MD-55-2 film Lot #I1215.

The XR-T film was 12 times more sensitive than MD-55-2 for ^{125}I energy photons[100]. The XR-T film had additional high Z components (Br, Cs), in order to increase its sensitivity to low energy photons, but made this film not tissue equivalent and similar to silver-halide radiographic film. XR-T film Lot # K02b28XRT was used for dosimetry of the first prototype of the novel ^{125}I eye

plaque, producing excellent results. The first development of our novel calibration technique for low energy photons described in the film calibration section was done with this film.

While the general construction, elemental composition and other features of the XR-T film were described by Soares *et al*[113], the particular lot used in this work had a 27 μm thick active layer with the following elemental composition (percentage by mass): H-6.9, C-46.6, N-8.6, O-14.8, Br-8.7, Cs-14.4, resulting in an effective Z = 26.6, as compared to effective Z = 6.27 for the standard GAFCHROMIC emulsion[113].

Since the old GAFCHROMIC emulsion films were inherently non-uniform, the technique of creating more uniform sub-film lots discussed in section 1.4 of the Introduction was applied for dosimetric measurements of CCX 41, and CCX 55 eye plaques using MD-55-2 film and of the first prototype of the novel ^{125}I eye plaque using XR-T film, as well as for testing of the HS film.

The new EBT2 and EBT3 films are much more uniform than older film types and have the blue dye component, which enables doing multi-channel dosimetry[118], which was tested in this work. Dosimetric measurements of only one eye plaque, CCX 219, were done using EBT3 film and we did not see any difference in applying single-channel dosimetry vs. multi-channel dosimetry, but this definitely matters in measurements using large radiation fields and films, like IMRT QA[118]. Starting with EBT1 film, we randomized the eye plaques' films and calibration films vs. their original position on the film sheet in order to avoid non-uniform coating trends.

The new EBT film Lot #34141 2x2IL was immediately used for dosimetry of ^{106}Ru eye plaques CCX 104, CIA 156, and CCA 892.

EBT film Lot #34351-05 was used for dosimetry of the second prototype of the novel ^{125}I eye plaque. The EBT emulsion's sensitivity is similar to the sensitivity of the XR-T film, but without adding high Z components, thus maintaining near tissue equivalency[113]. The EBT emulsion films

are designed to be much more uniform than the former GAFCHROMIC emulsion films, which was verified by our own measurements and published by others[139]. Therefore no special selection of parts of the film sheets was implemented when cutting films for measurements as was done for pre-EBT films.

The cross section of the composition of the new EBT film is shown in Figure 25 below, as well as in Figure 4a of the included published article[42].

clear polyester - 97 microns

active layer - 17 microns

surface layer - 6 microns

active layer - 17 microns

clear polyester - 97 microns
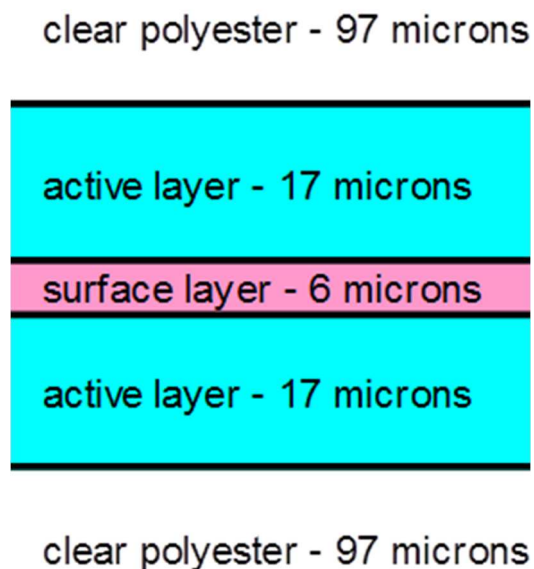
Figure 25. Cross section of GAFCHROMIC EBT film.

Since the film's sensitivity goal was 200 cGy (a typical patient dose in radiation therapy) in order to make it usable for IMRT QA, the film had to be a double emulsion film, having two active layers protected by clear polyester on both sides. The total thickness of the film was 0.20 - 0.25 mm as measured for different production batches using a micrometer vs. expected nominal 0.234 mm. The thickness variation between different production batches points toward sensitivity

variation of different production batches as was the case of pre-EBT films. The thickness of EBT film is similar to the thickness of the MD-55-2 film used by the author previously. Therefore, while the new film became of significant value for this work, the thickness continued to be a limiting factor of this film from becoming an "ideal" dosimeter for eye plaque dosimetry. The thickness limitation is very important for beta dosimetry with dose gradients of ~30%/mm, in the proximity of the concave surface of the plaque, where the dose gradient is highest. This thickness and design make the EBT film very rigid. It was impossible to bend it to a small radius of curvature in order to measure the dose close to the surface of an eye plaque. Therefore, the surface dose, which is the dose to the outer sclera, could not be reliably measured, which is important when there is a limitation on the maximum scleral dose which can be delivered or a requirement to deliver a minimal scleral dose as prescription dose. No other dosimeter can measure the dose rate closer than about 0.5 - 1.0 mm from the surface of the plaque due to geometrical and mechanical limitations of the smallest detectors (TLD's, plastic scintillators, semiconductor diodes)[41]. For [106]Ru eye plaques the surface dose reported by the manufacturer is extrapolated from plastic scintillator measurements the closest of which was about 0.6 mm from the surface (this was later improved to 0.48 mm). In the Introduction it was noted that [106]Ru eye plaques can have substantial dose non-uniformities which result from non-uniform distribution of radioactive material in the active layer. These non-uniformities cause dosimetrically hot or cold spots on the sclera. This is another reason to measure accurately the surface dose. Surface dose measurements would also provide precise information about the dose fall-off at the edge of the plaques enabling selection of appropriate plaque sizes for tumor coverage. Similar considerations apply to the novel ^{125}I eye plaques of designs similar to [106]Ru plaques studied in this work. Even COMS plaques which are based on TG-43[53] dosimetry have large dosimetric uncertainties, since TG-43 parameters are not

well defined in the near field and the near field effects of the Silastic insert and gold alloy backing are not well established, as already discussed. Therefore, International Specialty Products created per our request a special thin GAFCHROMIC film, named EBT1, which consists of a single layer of the film shown in Figure 25 (shown in Figure 4b of the published article[42]) and shown in Figure 26 below. In this film the active layer is covered just by 3 microns of protective coating on one side. This film permits nearly direct contact of the film with the eye plaque surface for surface dose measurements and is sufficiently flexible for this purpose. The sensitivity of the film is half of the double emulsion film, but still satisfactory for eye plaque dosimetry (~400 cGy for optical density of 0.5).

surface layer - 3 microns

active layer - 17 microns

clear polyester - 97 microns
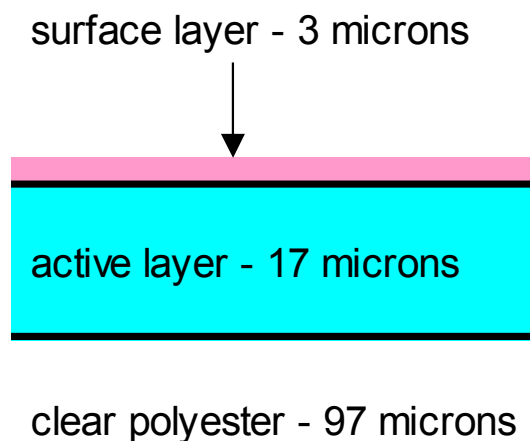
Figure 26. Cross section of special thin GAFCHROMIC EBT1 film.

EBT1 film Lot #35314-4H was used in this work for dosimetric characterization of CCX 129 ^{106}Ru eye plaque, and of the 20 mm fully loaded COMS plaque.

Following the development of special thin EBT1 film, ISP developed for this work special thin EBT2 film, Lot #040309-1B, which was used for ^{125}I film calibration experiments. Its active layer is covered only by a 4 micron surface layer and its structure is shown schematically in Figure 27.

The shift from EBT film to EBT2 and then EBT3 film happened when ISP changed the film technology from EBT film to the next generations. The author of this thesis was testing the newest types of film and received special batches of thin films manufactured specifically for this thesis. The newest film, EBT3, is shown schematically in Figure 28. It uses an improved coating technique resulting in more uniform film than EBT2. EBT3 film was used for Monte Carlo comparison with EBT film when studying the dose differences in Solid Water with different calcium content. EBT3 film was used for the Monte Carlo comparison, since its structure with clear polyester layers on both sides of the film was similar to the structure of EBT film used for the novel ^{125}I eye plaque project for which Monte Carlo simulations were done. Regular EBT3 film was not used for actual measurements in this work, since at this point we used only special thin unlaminated films.

surface layer - 4 microns

active layer - 35 microns

clear polyester - 175 microns
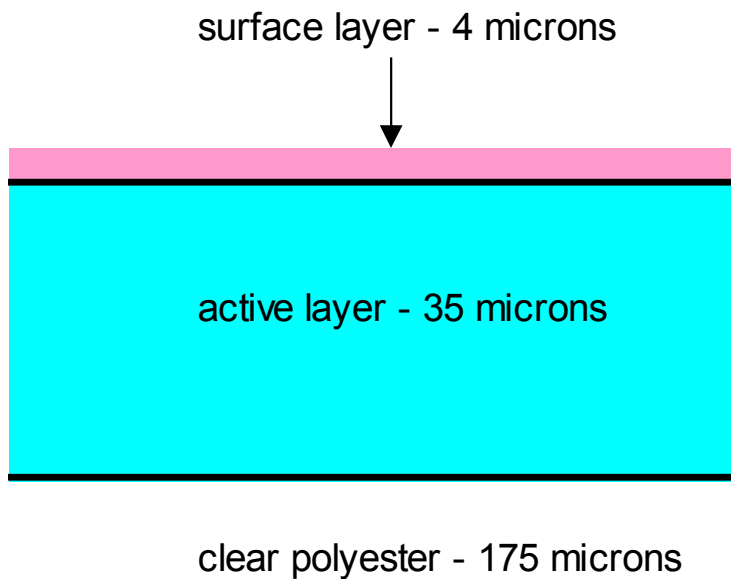
Figure 27. Structure of special thin GAFCHROMIC EBT2 film.

clear polyester - 125 microns

active layer - 28 microns
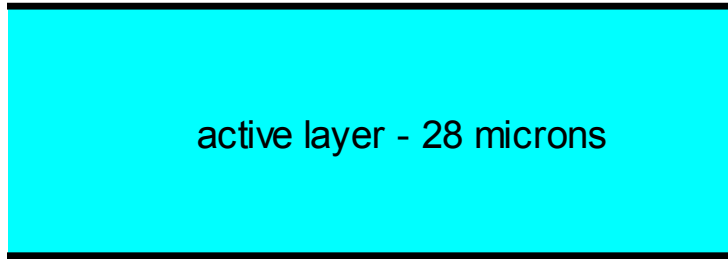
clear polyester - 125 microns

Figure 28. Structure of GAFCHROMIC EBT3 film.

Based on our recommendations and results, Ashland currently delivers commercially unlaminated EBT3 film, which consists of a 125 μm thick clear polyester substrate and a 14 μm thick active layer without any protective coating as shown in Figure 29 and Figure 4c of the published article[42]. Unlaminated EBT3 film Lot #02171601 was used for dosimetry of [106]Ru CCX 219 eye plaque.

active layer - 14 microns
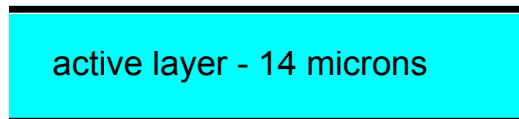
clear polyester - 125 microns

Figure 29. Structure of unlaminated GAFCHROMIC EBT3 film.

2.4 Preparation of films in the appropriate sizes and shapes and some film handling aspects.

The eye plaque dosimetry technique presented in this work requires precise cutting of round films with diameters as small as 8.5 mm and thin 3 mm wide strips, which could be placed on the concave surface of the eye plaques. The cutting had to be done without creating rough damaged edges resulting in air gaps between the films and parts of the phantom and without separation of layers of the films, which would make all or large part of the film unusable. Radiochromic films have between two and seven layers, which can easily separate during cutting[113]. MD-55-2 film is a double active layer film, consisting of a total of 7 layers; XR-T film is a single active layer film, consisting of a total of three layers; EBT film, as shown in Figure 25 has two active layers for a total of five layers, and EBT3 film has again a single active layer for a total of three layers, as shown in Figure 28. Even the thin unlaminated films have at least two layers. Since the films are sensitive to scanner light polarization, the direction of cutting and subsequent scanning has to be strictly observed. First, the sheets of films are cut into strips, preserving and marking the proper directionality, using an office paper cutter, which damages approximately 5 mm of film from the cutting edge. Therefore the strips are cut accordingly wider to enable creation of round films with appropriate diameters. Initially round films were punched from these strips using a set of round punches created especially for this purpose by MSKCC's Instrument Shop using a press or just a hammer for the smallest punches. Since these punches still left rough edges and caused separation of layers, they created a set of special punches using precise instrument cutting dies custom made by Dayton Lamina Corporation (Dayton, OH). A picture of the set of punches is shown in Figure 5 of the published article[42]. The set includes seven round cutting dies enabling punching round films with diameters of 0.335" (~8.5 mm), 0.413" (~10.5 mm), 0.492" (12.5 mm), 0.551" (~14.0 mm), 0.590" (~15.0 mm), 0.630" (~16.0 mm), and 0.689" (~17.5 mm). In addition the set includes

a 30 mm diameter cutting die with two semi-circle cutouts as shown in the drawing in Figure 30, which is the main film size of the "eye" phantom. The cutouts are needed to accommodate the key structures of the phantom. Later a cutting die for punching 3 mm wide 30 mm long film strips which could be attached to the concave inner surface of the plaques was added to the set and is shown in Figure 31.
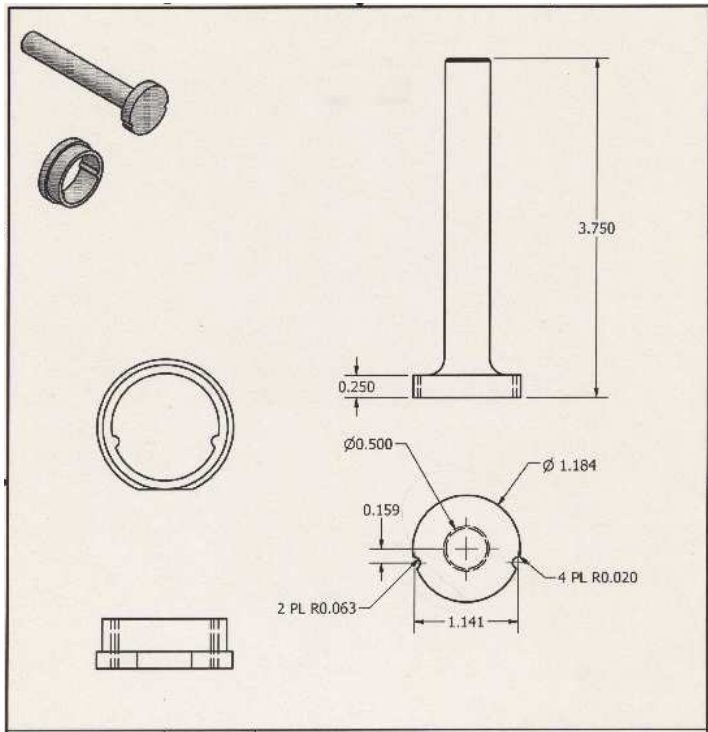
Figure 30. Cutting die and matrix for 30 mm diameter films. All dimensions in inches.

In order to use these cutting dies, a special punching device is shown in Figure 5 of the published article[42] and assembled in Figure 32. Its cross section showing the design details is shown in Figure 33. The cutting dies resulting from this custom fabrication cut films without any damage, leaving clean flat edges without ridges (which occur even when using a laser cutter) and no separation of layers.
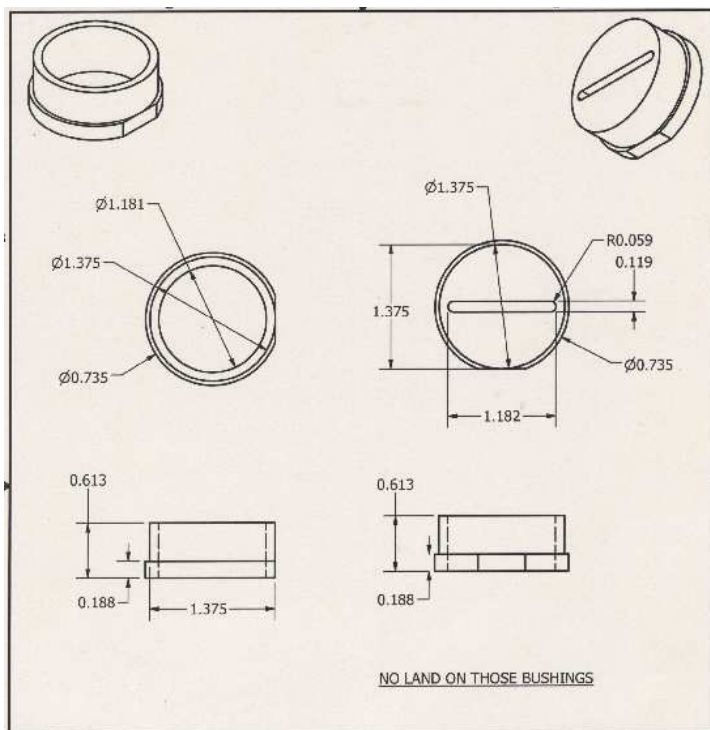
Figure 31. Cutting die and matrix for 3 mm wide 30 mm long film strips. All dimensions in inches.

Starting with EBT film, the sheet of film, usually 8" x 10", is cut into sufficiently wide strips in the standard direction decided in our protocol, which is the portrait orientation, using a high quality office cutter with a roller knife. In order to observe this direction and control the strips position on the sheet, the film sheet is attached to a piece of graph paper, cut along the lines of the graph paper in the portrait orientation and the number of the strip is written with a marker pen at the upper left corner (our convention). Then the strips are either cut by the same paper cutter into rectangular films (usually 2.0 cm x 2.0 cm) for calibration purposes or used for punching round or other shaped films, marking at the upper left corner of each rectangular piece the coordinate of the piece on the sheet in the form of the row#-column#. Then each calibration or punched film is kept in a separate light-tight envelope which has the two-digit number of the film. Starting with EBT films, the film uniformity was greatly improved and there was no need to create sub-batches along the direction

55

of coating, as the author did for MD-55-2 films. Some degree of non-uniformity, however, remained. Therefore, whether the films are used for calibration or eye plaque dosimetry purposes, starting with EBT1 film, the films were randomized with the respect to their position on the film page using the random number generator function of Microsoft Excel, eliminating the possibility of following any possible coating non-uniform trend on the film sheets.

Figure 32. Assembled film cutting die punching device.

When punching the 30 mm diameter films with cutouts the strip has to be properly held in the punching device. The cutouts sufficiently define the direction in the phantom, which is then marked by needle marks, as described in the description of the phantom design[42]. The 3 mm wide

strips are always punched in the long direction of the strip using the attached graph paper. When it comes to punching the smaller round films without cutouts, the proper direction is marked on the film piece to be punched in two locations along the diameter coinciding with the portrait orientation of the page, prior to punching. In addition these marks are used for matching the film position and orientation with the eye plaque during the measurement process.

Handling tips for radiochromic film have been described in detail[113]. The issue of moisture content and equilibration with the environment was discussed in the Introduction. Thus, films used for calibration and eye plaque measurements were pre-cut usually several days prior to irradiation, at least 24 hours, corresponding to 48 or more hours prior to scanning.
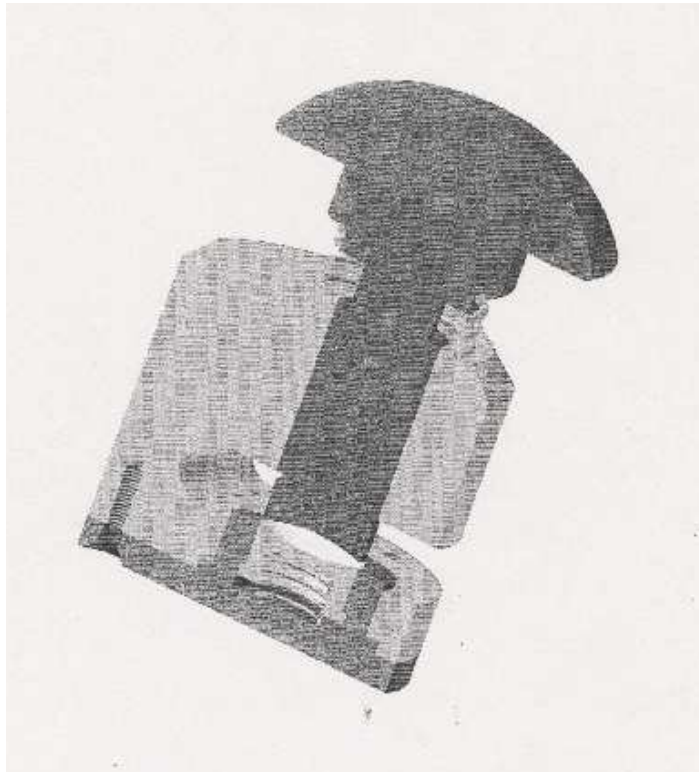
Figure 33. Cross section of the film cutting die punching device.

2.5 Film scanning.

All films used in this work were read-out using one of three CCD scanners. All scanning was done in transmission mode of the scanners. Initially, an AGFA ARCUS II flatbed scanner (Agfa-Gevaert N. V., Mortsel, Belgium) was used. The scanning was done at 85 micron resolution with a red acetate filter[120] and RIT113 Film Dosimetry software (Radiological Imaging Technology, Inc., Colorado Springs, CO). When this scanner became unavailable, a Vidar VXR 16 Dosimetry Pro 16 bit film scanner (Vidar Systems Corporation, Herndon, VA) was used. The scanning was done at 89 micron resolution with films placed into clear plastic sheet protectors together with a red acetate filter for XR-T film and with a yellow acetate filter (as recommended by the manufacturer of the film) for EBT film. The same RIT software was used for scanning. The third reader, with which most of the work was done was an Epson Expression 1680 flatbed scanner (Seiko Epson Corporation, Nagano, Japan) using EPSON Scan software in 48 bit RGB mode with all filters and image enhancements de-activated, followed by extraction of the red channel. The films were mostly scanned at resolutions of 254 dpi (100 microns pixel size) or 512 dpi (50 microns pixel size). The red channel provides optimal response for GAFCHROMIC film[113], but since the RIT software was limited to monochrome (16 bit) scanning, we had to use the red acetate filter for MD-55-2 film[120]. The yellow acetate filter was utilized for EBT film in order to maximize film response with the Vidar scanner. The calibration curves of MD-55-2 film Lot #I1215 scanned using the ARCUS II scanner with and without the red acetate filter are shown in Figure 34.

 Scanned images were saved as TIFF files for further processing. Our standard scanning protocol, which was started using the Epson 1680 scanner, always included a preview scan in

order to equilibrate the film temperature with the scanner temperature followed by the measurement scan or two, if we used different resolutions.
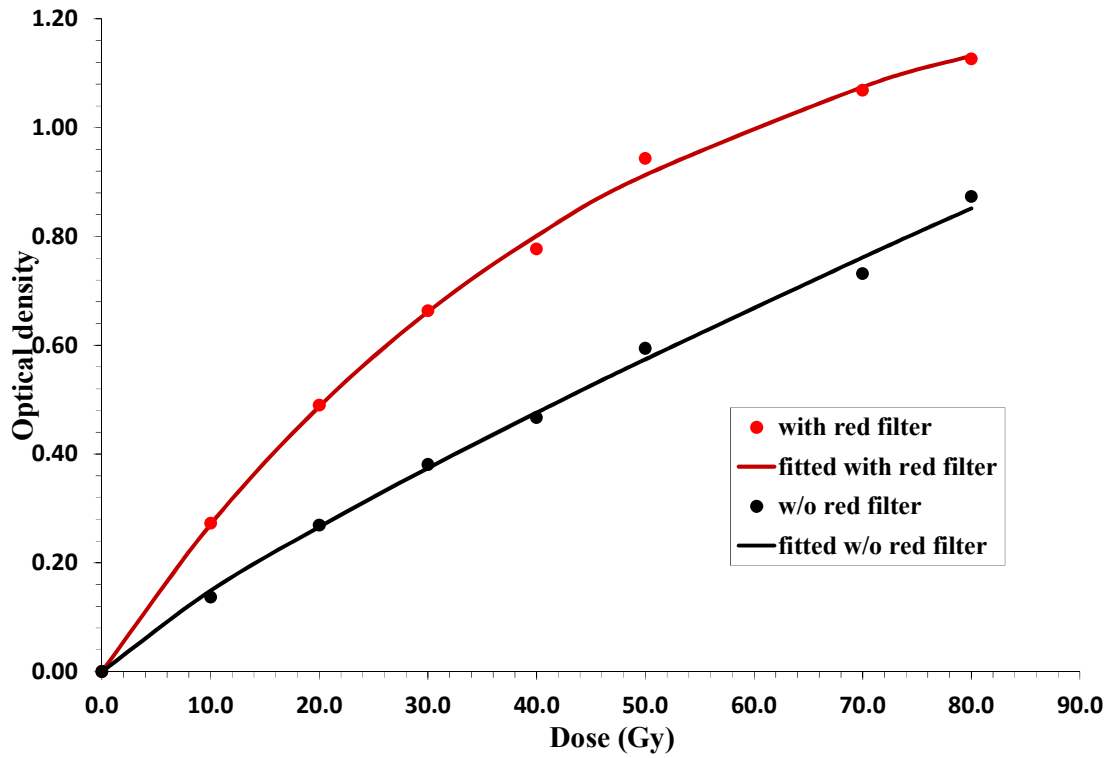
Figure 34. MD-55-2 film Lot# I1215 calibration curve scanned with and without the red acetate filter.

Since there were discussions in the literature (for example Lynch *et al*[115]) about the effect of scanner temperature and scanner stability on the dosimetry results, we tested possible effects on our scanning protocol for a period of time, scanning standard optical density tablets provided by the manufacturer of the film together with films, but did not see any measurable effect.

2.6 Calibration of film for absolute dosimetry.

    2.6.1 Calibration of radiochromic film for absolute [106]Ru dosimetry.

The published article includes a description of film calibration for [106]Ru eye plaque dosimetry less

charts of the calibration curves and their fitting with analytical functions, which were not shown

for brevity. The calibration curve of MD-55-2 Lot #I1215 is shown in Figure 24. For dosimetry

use it was fitted with an analytical function. Calibration curves of thin EBT1 film Lot#35314-4H

and unlaminated EBT3 film Lot #02171601 are shown in Figure 35. Both calibration curves in the

form of pixel values vs. dose were fitted with analytical functions suggested by the curve fitting

program CurveExpert Professional software by Daniel G. Hyams, Madison, AL. The EBT1 curve

was fitted with a function:

$$pixel\ value = \frac{a * b + c * dose^d}{b + dose^d}$$

The unlaminated EBT3 curve was fitted with a function:

$$pixel\ value = \frac{a + b * dose}{1 + c * dose + d * dose^2}$$

where a, b, c and d are fit parameters, which use the same letters, but have different values and

units for each function.

60
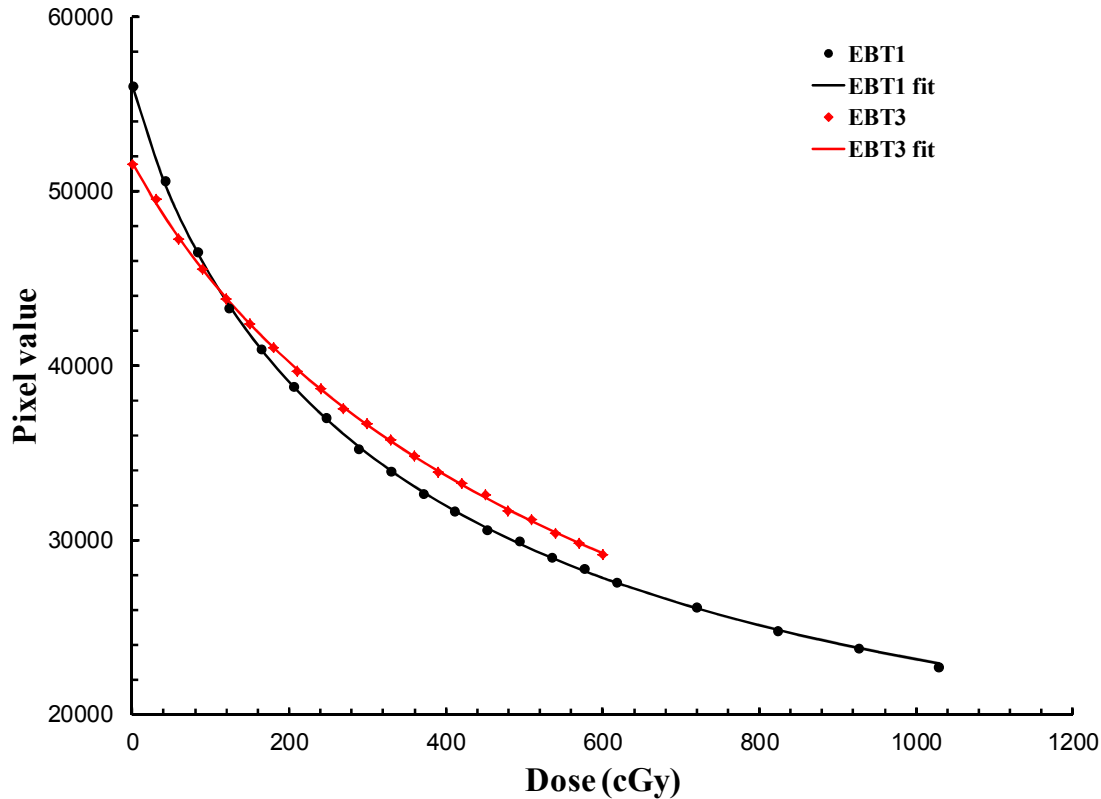
Figure 35. Calibration curves of EBT1 film Lot #35314-4H used for dosimetry of CCX 129 plaque and unlaminated EBT3 film Lot # 02171601used for dosimetry of CCX 219 plaque.

2.6.2   Calibration of radiochromic film for absolute ^{125}I eye plaque dosimetry.

Generally, old GAFCHROMIC films under-responded at low photon energies, which include those of the ^{125}I source studied in this work. The exception is XR-T film, which over-responded at these energies, similar to silver halide radiographic film[100, 113]. EBT film was found to have minimal energy dependence[101, 113] at ^{125}I energies, but this could still depend on the particular lot used. Of some concern is that earlier reports noted possible dose rate dependence of GAFCHROMIC films[119] or "temporal history mismatch", when used for low dose-rate brachytherapy dosimetry[140]. Therefore both, XR-T Lot #K02b28XRT and EBT Lot #34351-05 films were calibrated for absolute dosimetry of the novel ^{125}I plaques using calibrated [125]I I-Plant

61

model 3500 brachytherapy seeds (Implant Sciences Corporation). Special thin EBT1 Lot #35314-4H and special thin unlaminated EBT2 Lot #040309-1B films were calibrated using a calibrated Model 6711 ^{125}I seed (Oncura, Inc., Arlington Heights, IL), thus eliminating both the energy and dose rate dependence of the response, but still potentially vulnerable to possible "temporal history mismatch".

This work developed a novel calibration technique for absolute ^{125}I dosimetry, which creates a calibration curve from a single irradiated film, rather than the usual irradiation of a large number of films to single doses[141]. This approach improved the uncertainty of reading the optical density pertaining to a single dose on a film irradiated by a seed. Unlike using large uniform fields for film calibration on a linac, in the case of calibration using a brachytherapy seed, the single dose is understood as the point dose on the film at the shortest distance from the seed center, usually at the center of the film. Technically, this should be a single pixel, but the optical density of a single pixel is affected by image noise and film non-uniformity and, considering mechanical uncertainties, it is even hard to decide which single pixel to use, as can be seen from a profile of pixel values through the center of a film (Figure 38). The calibration seed is placed into an opening at the center of the top surface of a specially designed phantom insert (Figure 36). The insert with the seed is placed as the top insert of the cylindrical body of the "eye" phantom filled with Solid Water inserts and a film is placed between the inserts under the seed at a specified distance from the seed center. The distance of the film from the seed should be more than 5 mm, since closer than 5 mm the TG-43[53] dose is not well defined. The phantom with the seed and film is covered with a special flat top cover (without an impression for an eye plaque) and placed in the middle of a full scatter 30 cm x 30 cm x 30 cm Solid Water phantom for the required irradiation time. The latter is estimated using the TG-43 formalism[53] in order to deliver a sufficiently high dose to the

center of the film, which would cover the dose range expected in the eye plaque measurements. A single film is irradiated under the described conditions. The irradiated film and an unexposed film are scanned according to the data analysis protocol of the particular experiment, including scanner model (calibration films and eye plaque films have to be scanned on the same scanner), scanning time delay after end of exposure, and orientation on the scanner. The unexposed film is needed in order to provide the "0" dose background of the film.
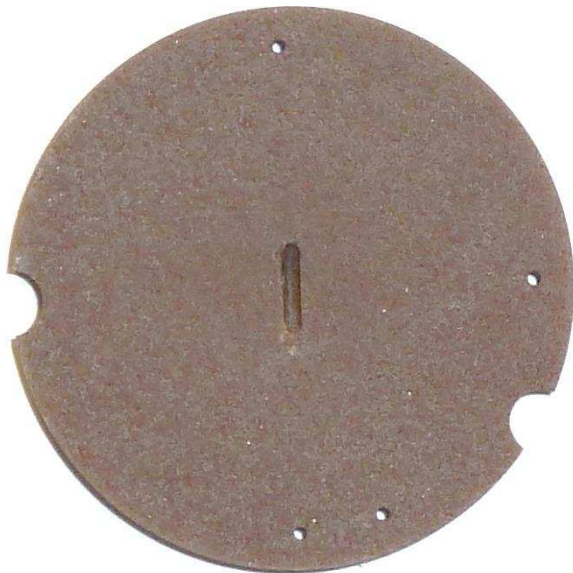
Figure 36. Seed calibration insert of the Solid Water "eye" phantom.

The seed axis and a perpendicular axis passing through the center of the seed are marked on the film prior to irradiation using a thin needle through the holes in the insert. A typical irradiated film and an unexposed film are shown in Figure 37. Since the special thin EBT1 films tend to curl on the scanner, they were lightly taped in order to ensure good contact and avoid Newton's rings.

63

The next step was to extract from the film data a profile of pixel values vs. coordinate on the film centered exactly under the center of the seed in the direction perpendicular to the seed axis. This was done using Contour, MSKCC's film dosimetry program, utilized for all film analysis.
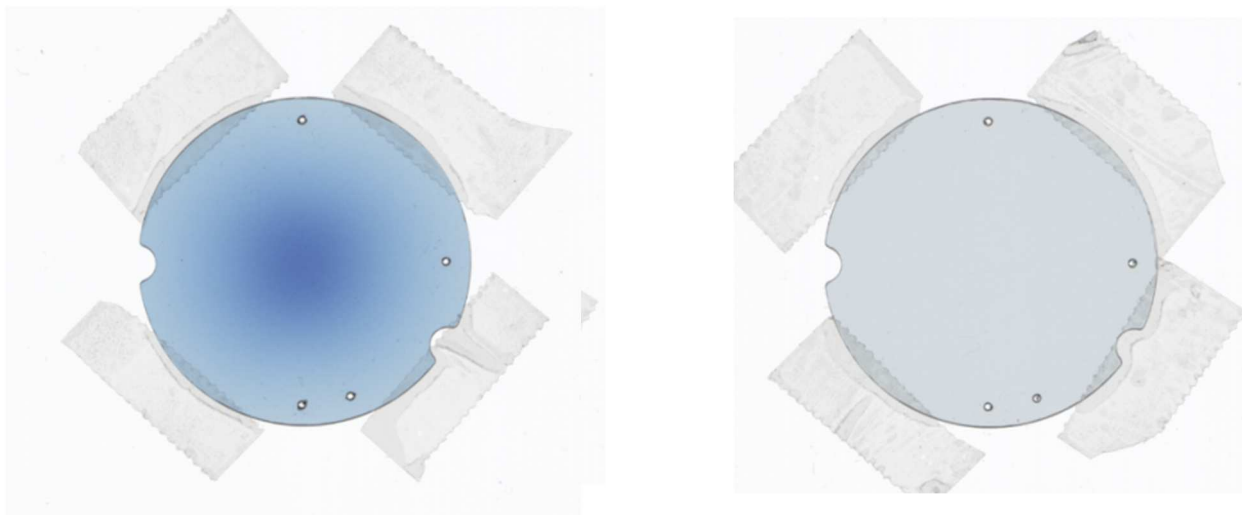
Figure 37. On the left special thin EBT1 Lot #35314-4H film 6-1 irradiated by a calibrated ^{125}I seed, on the right unexposed film 4-1 from the same Lot.

Films were scanned at resolutions of 89 − 100 μm, resulting in profiles consisting of many data points. These profiles were slightly shifted, usually about one pixel, in order to make them symmetrical vs. the seed center, similar to what is done with water tank profiles of a linear accelerator, in order to exclude possible mechanical setup uncertainties. The profiles were than mirrored and averaged in order to improve noisy data and exclude possible film non-uniformity. A typical raw profile, consisting of 200 points extracted from film data prior to centering and symmetrization is shown in Figure 38.

The expected dose on the film at each point of the profile is calculated using the line approximation of the TG-43 formalism[53], while the distance of the points of the profile on the film from the seed center is derived using a simple geometrical calculation. Use of a central profile perpendicular to the seed axis eliminated the need to account for the 2D anisotropy function $F(r, \theta)$. Substituting the distance from the film center with dose gives a curve providing the dependence of pixel values on the film on dose, which is the calibration curve of the film at the given irradiation and scanning conditions.
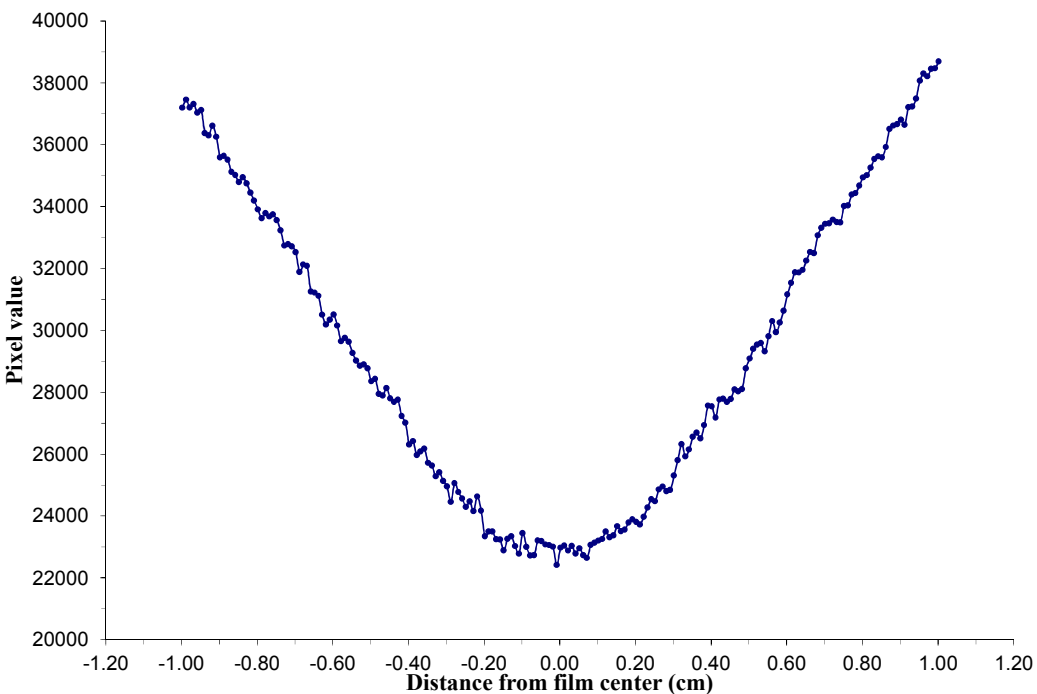
Figure 38. Raw pixel value profile vs. distance from film center along a line perpendicular to the direction of the calibration seed axis at the seed center for film 6-1 of EBT1 Lot #35314-4H shown in Figure 37.

The resultant calibration curves were further fitted with analytical functions for use in the film dosimetry process. A set of Microsoft Excel spreadsheets keeping all the data and performing the necessary calculations was developed in this work.

The film calibration process described above produces a very fine-resolution calibration curve which would be equivalent to irradiation of a very large number of films to single doses, for example at least 100 for the case shown in Figure 38.

We then compared the calibration technique described here to a calibration curve derived from irradiating many films and using the center dose point only, and found them equivalent, except that this technique is more efficient and provides a much higher resolution. In some cases, one film does not cover the full dose range needed for the experiment, due to geometrical limitations of the "eye" phantom. In such cases, it is possible to irradiate a second film to a different dose such that both films cover the expected dose range and then combine the two calibration curves into one, a technique originally developed by Soares and McLaughlin[142]. Calibration curves for special thin EBT1 Lot #35314-4H and special thin unlaminated EBT2 Lot #040309-1B films created using the described technique are shown in Figure 39. Both curves were fitted with 5th order polynomials. The EBT1 calibration curve was created and used for dosimetry of fully loaded 20 mm COMS plaque, while the unlaminated EBT2 curve was created for testing purposes of the EBT2 film and of the calibration method. The surprising finding was that unexpectedly the shape of the curves is virtually identical, despite the fact that EBT2 film belongs to a chemically and technologically different generation of films. The average point by point ratio of the EBT1 fitted curve to the EBT2 fitted curve is 1.14 with a standard deviation of 0.01. The particular EBT2 Lot is just more sensitive than the particular EBT1 Lot. Another surprise finding was observed when we compared the calibration curves of the EBT1 Lot #35314-4H calibrated using the calibrated ^{125}I seed as shown in Figure 39 with the calibration curve of the same film Lot calibrated using 6 MeV linear accelerator electrons for ^{106}Ru dosimetry of the CCX 129 eye plaque shown in Figure 35. The comparison is shown in Figure 40. Instead of the expected near energy independence of the EBT

family[101, 113], we found that this EBT1 Lot has strong energy dependence at least at low photon energies and it actually under-responds at these energies.
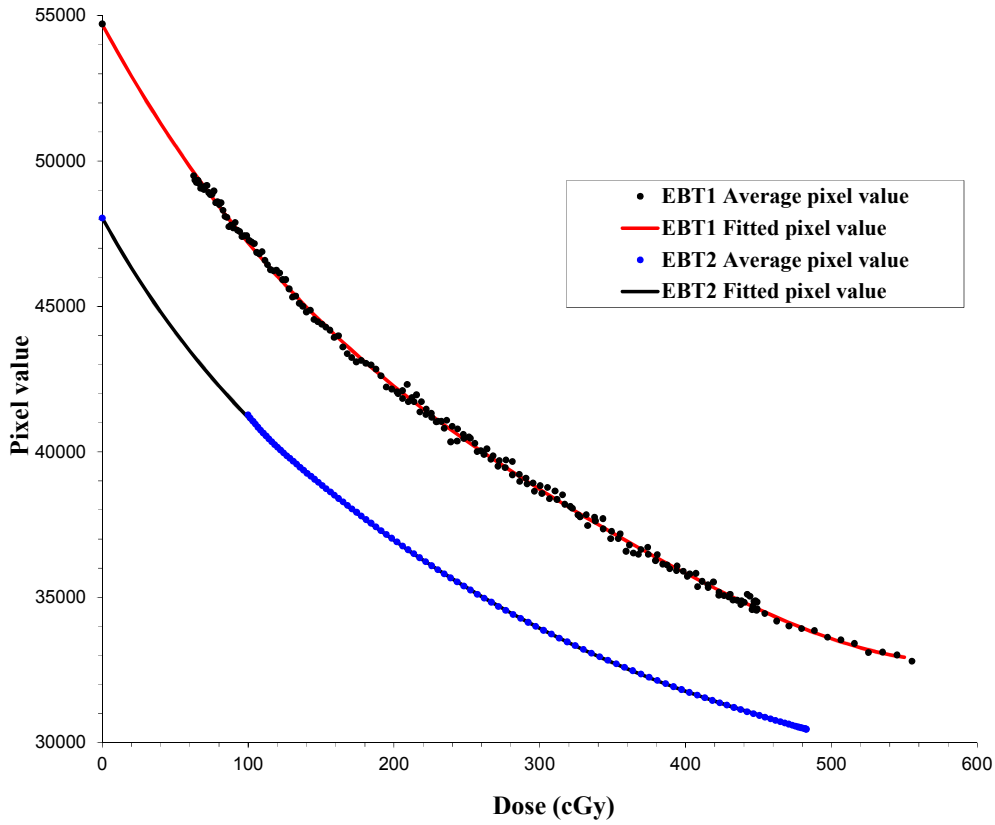
Figure 39. Calibration curves of special thin EBT1 film Lot #35314-4H and special thin unlaminated EBT2 film Lot #040309-1B using a calibrated ^{125}I seed.
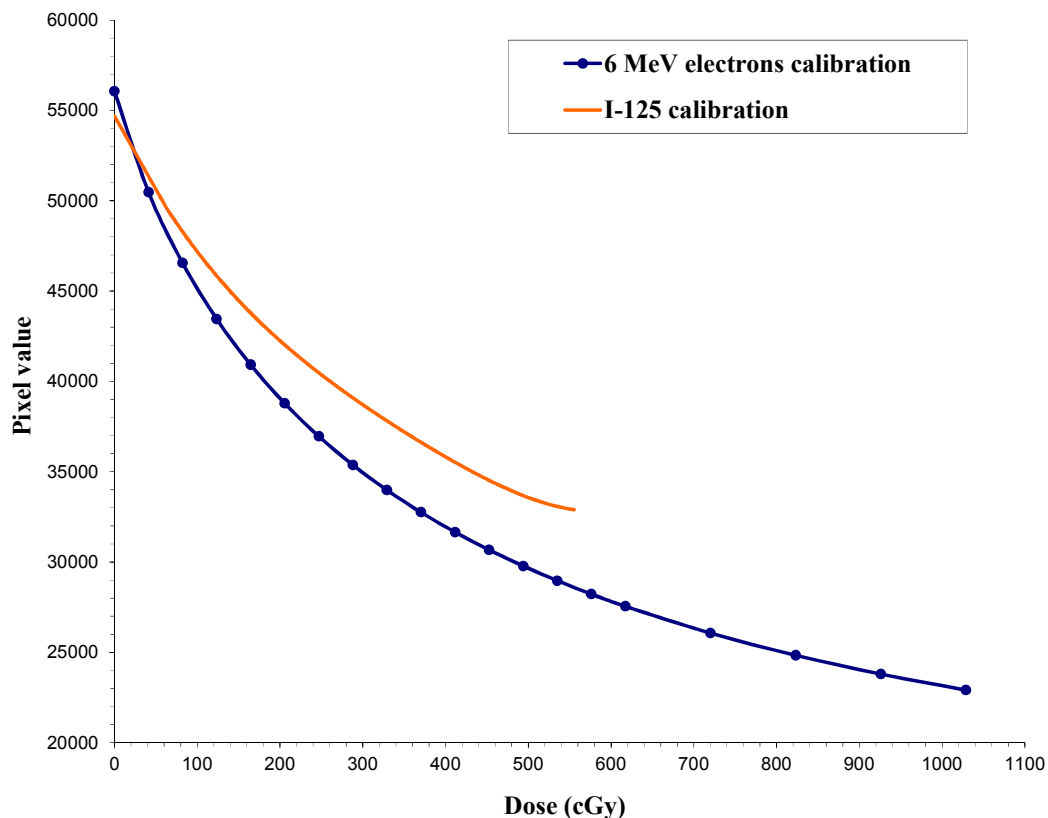
Figure 40. Calibration curves of special thin EBT1 film Lot #35314-4H using a calibrated ^{125}I seed and 6 MeV electrons.

The calibration of the XR-T film Lot #K02b28XRT used for the film dosimetry of the first prototype eye plaque was done using a calibrated [125]I I-Plant model 3500 brachytherapy seed. The film was placed at a depth of 5.73 mm under the seed (distance between the center of the seed's long axis and the center of the film's active layer) in the geometry described above in a full scatter 30 cm x 30 cm x 30 cm Solid Water phantom. The film was irradiated for almost 20 days (475 hours 21 minutes) in order to achieve a sufficient dose, since the calibrated seed had air kerma strength of only 1.3285 U at the beginning of the irradiation. Due to the very long irradiation time

the film was scanned 7 days after the end of the irradiation in order to be at a stable post-exposure optical density, minimizing or avoiding possible "temporal history mismatch"[140]. The film was scanned using the Vidar VXR 16 Dosimetry Pro 16 bit film scanner at 89 µm resolution. The scanning was done using RIT film dosimetry software. Since the Vidar scanner moves the film through a fluorescent light source/CCD combination, the small film was placed into a clear sheet protector prior to scanning together with a red acetate filter. The film was scanned at the center of the scanner in order to minimize potential film-scanner positional effects. In addition, the marked axis of the film was made to coincide with the direction of scanning in order to preserve the film orientation for consistent film directionality. The scanned film data were analyzed using MSKCC's film dosimetry Contour program. The expected dose at the depth of the center of the active layer of the film was calculated using the line source approximation of the TG-43 formalism[53]. The seed data set was taken from Duggan and Johnson[143], since our measurements of the first prototype eye plaque predated the publication of the consensus data set for the [125]I I-Plant model 3500 brachytherapy seed.

The calibration of the EBT film used for the film dosimetry of the second prototype eye plaque was again done using a calibrated [125]I I-Plant model 3500 brachytherapy seed. The film was placed at a depth of 6.71 mm under the seed, in the geometry described above in a full scatter 30 cm x 30 cm x 30 cm Solid Water phantom. 6.71 mm is the distance between the center of the seed's long axis and the center of the film, which in this case does not coincide with a center of an active layer, since EBT film has two active layers, as shown in Figure 25. The calibrated seed had an air kerma strength of 5.604 U at the beginning of the irradiation. The film was irradiated for 24.175 hours so that the TG-43[53] calculated dose expected at the film center was 313.9 cGy, this time using the published consensus data set[137]. The irradiated film and an unexposed film were scanned 24 hours

after exposure using the Epson Expression 1680 flatbed scanner in 48 bit color followed by the extraction of the red channel instead of using a red filter, since the scan was done in a color mode. The analysis of the films was done using MSKCC's film dosimetry Contour program. For scanning on the Epson scanner the films were placed at the center of the scanner bed, in order to avoid scanner induced light scatter non-uniformity, with the film axis oriented in the portrait direction of the scanner in order to preserve the film orientation.

As mentioned above, calibration of films for the fully loaded 20 mm COMS plaque experiment was done using our novel technique, but still irradiating many films in order to better study different aspects of the approach. This was possible since we received a very strong seed, with 27.45 U air kerma strength, which kept irradiation times reasonably short. For calibration of EBT1 film Lot #35314-4H, the films were placed 5.6315 mm under the seed (5.62 mm phantom thickness + 0.0115 mm film thickness to the middle of the active layer). Eleven films were irradiated to doses 50.75 cGy – 1,430.96 cGy at the film center. Irradiation times varied from ~41 minutes to almost 18 hours. For calibration of EBT2 film Lot #040309-1B, the films were placed 5.6415 mm under the seed (5.62 mm phantom thickness + 0.0215 mm film thickness to the middle of the active layer). Eight films were irradiated to doses 71.51 cGy – 1,112.71 cGy at the film center and irradiation times varied between ~2 and ~25 hours. As above, all irradiations were done in a full scatter 30 cm x 30 cm x 30 cm Solid Water phantom. Prior to irradiations all films were randomized as to their positions on the respective film sheets using MS Excel's random number generator. All films, including unexposed films, were scanned 24 hours after the end of the irradiation using the Epson 1680 Expression scanner in 48 bit color followed by the extraction of the red channel. The films were placed at the center of the scanner bed orienting the original portrait orientation of the film page in the long direction of scanning (portrait orientation of the

scanner) as per our usual scanning protocol. The scanned data were analyzed using MSKCC's Contour film dosimetry program.

2.7 Eye plaque dosimetry and data analysis.

Details of this subject are fully described in the published article[42], which is attached to the end of this thesis as Appendix 1. Films were irradiated one at a time, in order to deliver approximately the same dose to each film, which would produce the desirable optical density of about 0.5 in the high dose area of the film. For MD-55-2, this dose was about 30 Gy, for XR-T film it was about 5 Gy, for EBT film, about 200 cGy, and for thin special EBT1 film and unlaminated EBT2 film it was about 400 cGy.

The MD-55-2 films were scanned 48 hours after irradiation, while the XR-T films were scanned 7 days after irradiation, due to extremely long irradiation of the calibration film as a very weak calibration seed was utilized. All other films were scanned 24 hours after the end of irradiation in order to let the polymerization process stabilize and have all films scanned at the same level of post-exposure growth[98]. If the calibration films were scanned 24 hours after irradiation, then the eye plaque films were scanned after 24 hours as well. Both calibration and eye plaque films were always placed at the center of the scanner bed lightly attached to it using adhesive tape at the edges of the film in order to avoid Newton's ring artifacts. Films were scanned in the same orientation, usually portrait with respect to the original sheet of film. In general, CCD scanners suffer from a lateral response artifact[123, 124] resulting in decreased pixel values (increased measured optical density) toward the lateral edges of the scanner bed. However, since the films used in this work were small and always positioned at the same location at the center of the scanner, reader bed positioning corrections were not required[113]. Special attention was given to the temporal stability of the scanners, monitored by periodic scanning of reference optical density tablets.

Film scanning produces a point-by-point, high resolution 2D optical density map of the irradiated film. Applying the calibration curve to each pixel of the optical density map converts the latter into a 2D dose distribution. Since each film was exposed at different dates and times, the 2D dose distributions were converted to dose rate distributions at a certain reference date and time, using the exposure dates and times, and decay constants of the radionuclide in question. The film analysis was always done using MSKCC's Contour software package, which was customized in order to accommodate the requirements of this work. The ability to use scanned films in the form of TIFF files and circular regions of interest were added to the software.

2.8 Silicon diode dosimetry of the novel ^{125}I eye plaque.

The use of the silicon diode as a secondary dosimeter for ^{106}Ru eye plaques was described in detail in the published article[42]. The same p-type silicon diode, the Scanditronix Stereotactic Field Detector (SFD) model DEB050 (Scanditronix Medical AB, Uppsala, Sweden, currently IBA Dosimetry GmbH, Schwarzenbruck, Germany) in a Scanditronix RFA200 water tank was used for dosimetry of the first prototype novel ^{125}I eye plaque. Unfortunately, after just two films and diode measurements, this plaque developed a radioactive leak and the experiments were discontinued. This diode detector has a 60 μm typical effective thickness of the measurement volume with a 0.6 mm ± 0.1 mm detector diameter, and a distance of 0.61 mm ± 0.15 mm displacement of the effective measurement point from the front surface of the detector. Externally, the detector is a 4.0 mm diameter cylinder which was oriented along the central axis of the eye plaque. The closest measurement point of the diode was 0.87 mm from the inner surface of the plaques due to the concave shape of the plaques and the 4.0 mm diameter of the diode both of which limited how close the diode can come to the surface of the plaque. The eye plaque was attached using Dow Corning High Vacuum grease (Dow Corning Corporation, Midland, MI) to the cap of the Solid

Water "eye" phantom placed upside down, and the cap was attached using the same grease to a Lucite base positioned at the bottom of the water tank. The cap was used for this purpose since it had a customized imprint of the particular eye plaque. A special Lucite centering jig was created to assure that the diode was precisely centered on the central axis of the eye plaque and was not displaced laterally from the axis. The arrangement is shown in Figure 6 of the published article[42]. After setup, the Lucite jig was removed for measurements. The water tank's mechanism and software were used to position and drive the diode detector. For eye plaque measurements, the center of the plaque's inner concave surface was covered by only 35 mm of water in order to create a water/air interface similar to the Solid Water/air interface created when the "eye" phantom was inserted into the "head" phantom for film measurements. For the first prototype of the novel ^{125}I eye plaque, depth dose measurements were performed every 0.5 mm from 0.87 to 26.87 mm from the inner surface of the plaque. For absolute depth dose measurements, the detector was connected to a Memorial Sloan-Kettering Cancer Center ADCL calibrated in-house built electrometer model 821 and two readings were taken at each point: each integrated for 60 seconds. Then the results of both measurements were averaged.

For ^{125}I novel eye plaque measurements the diode was calibrated for absolute dosimetry in the same Scanditronix RFA200 water tank with the same MSKCC's in-house built electrometer model 821 using the same calibrated ^{125}I I-Plant model 3500 brachytherapy seed, which was used later for XR-T Lot # K02b28XRT film calibration, in a setup similar to the eye plaque setup. At the time of the calibration the air kerma strength of the seed was 1.6229 U. The seed was attached to a Solid Water disk using Dow Corning High Vacuum grease, and the latter was attached using the same grease to the Lucite base positioned at the bottom of the water tank. The seed was located at an approximately 13 cm depth of water at 22°C during measurements, the same temperature as

during eye plaque measurements. The diode was first brought in contact with the seed and then retracted to a distance of 5.01 mm between the seed long axis and the effective measurement point of the diode using the mechanism of the RFA200 water tank, where a set of four readings was recorded for 1, 2, 3, and 4 min. Then the diode was retracted to two more distances from the seed, 5.51 mm and 6.01 mm, and the measurements were repeated. The expected dose at the diode was calculated using the line source approximation of the TG-43 formalism[53], while the seed data set was taken from Duggan and Johnson[143] as described for the XR-T film calibration. The diode calibration taken as the average dose rate per reading at the three distances was 1270.57 cGy/hour-reading with a standard deviation of 34.70 cGy/hour-reading at the appropriate reference date. The diode results were in good agreement with film dosimetry results, even though per the manufacturer's specifications the diode was rated for energies above 1 MeV, and silicon semiconductor diodes have been used in the past only for relative dosimetry of ^{125}I seeds[107-109] and for relative dosimetry of ^{125}I eye plaques[110]. The mean spectral energy of ^{125}I is virtually unchanged with distance from the source in water[106, 144] and the relative absorbed-dose energy response correction for ^{125}I sources measured with a silicon detector is constant with the distance from the source[144], which qualifies the silicon diode for relative dose measurements along the central axis of the eye plaques, and, if properly calibrated, for absolute dose measurements as used in this work. Measurements off the central axis would require testing the diode's angular response at these energies, which was not done, but still profiles across the plaque in three planes perpendicular to the central axis of the plaque at distances 6.2 mm, 7.9 mm, and 15.6 mm from the center of the inner surface were obtained by scanning in the same water tank setup. For the scans the diode detector was connected to the water tank electrometer which was not calibrated for absolute dosimetry, therefore the scanning results are considered relative.

2.9 Monte Carlo simulations of the novel ^{125}I eye plaque dosimetry.

Implant Sciences Corporation performed numerous Monte Carlo simulations of the concept for the novel eye plaque; we compared in this work the expected dosimetry of the second prototype eye plaque calculated by Monte Carlo with the results of our absolute film dosimetry. Moreover, it should be noted that all our film calibrations, whether for ^{106}Ru eye plaques, using ^{60}Co machines or linear accelerators, or for ^{125}I eye plaques, using calibrated ^{125}I seeds, are done in Solid Water phantoms. The doses ascribed to pixel values of the calibration films are known in terms of dose to liquid water, since the ^{60}Co machines, linear accelerators and ^{125}I seeds are calibrated in terms of dose to liquid water using either TG-51[145] (TG-21[146] before that) or TG-43[53]. The eye plaque film dosimetry is done in Solid Water, even though the dose of interest in radiation therapy is dose to liquid water. Conversion of the absorbed dose measured in Solid Water to absorbed dose in liquid water may require additional corrections usually done by Monte Carlo[132-135]. Of special interest is the work by Meigooni *et al*[135] which found that certain batches of Solid Water may have 1.7% calcium content, while other batches may have 2.3% calcium content, and depending on the calcium content of the Solid Water, the Monte Carlo calculated dose conversion factors from Solid Water to liquid water may vary by as much as 5% for ^{125}I. We performed analysis of our Solid Water and found that all our Solid Water has 2.3% calcium content as discussed in our published article[42]. Unfortunately, published works[132-135] deal only with differences between absorbed dose in solid water equivalent materials and liquid water, but do not analyze the film dosimetry process, which has a calibration component and a measurement component. Also, the calibration is done to the film in the solid medium, but not to the solid medium itself, and the eye plaque measurements are again reading dose to film in the solid medium, not dose to the solid medium. I hypothesized that since film calibrations and film dosimetry measurements both are done in Solid Water, while

the calibration dose data is known in liquid water, the results of the film dosimetry are doses in liquid water without the need for additional corrections. This hypothesis was rigorously tested utilizing the second prototype of the novel ^{125}I eye plaque using Monte Carlo simulations by Dr. Munro, the inventor of the novel ^{125}I eye plaque. He extensively used Monte Carlo simulations in the invention process. Therefore, the eye plaque and calibration seed modeling were already in place as per specifications provided by Implant Sciences Corporation. The author has supplied our phantom and film geometrical drawings and elemental compositions to be used as input data, based on specifications provided by Gammex, Inc. and International Specialty Products respectively. The author defined the required simulations and analyzed the Monte Carlo results. We already had film calibration and dosimetric results of the second prototype eye plaque done using film in Solid Water with the film calibrated using seed dosimetric data in liquid water. Therefore, the I-Plant model 3500 calibration seed data was converted using Monte Carlo to data in Solid Water, instead of liquid water. Then we created new film calibration curves in terms of doses to film in Solid Water. Then all eye plaque measurements were re-calculated using these calibration curves and the result was eye plaque data in terms of dose to film in Solid Water. Then the eye plaque results were converted using Monte Carlo to doses in liquid water needed for comparison with our original uncorrected results in order to test the hypothesis.

The materials and methods employed by Dr. Munro in this analysis were similar to those employed in the Monte Carlo analysis of the Model 3500 seed[147]. Radiation transport calculations were performed on a Windows™ (Microsoft Corporation, Redmond, WA) based personal computer running the MCNP5 Monte Carlo computer code[148] (Los Alamos National Laboratory, Los Alamos, NM). The software was used to simulate coupled photon and electron transport through material using the MCPLIB04 photo-atomic cross-section tables provided with the MCNP5 code.

These cross section tables are derived from the EPDL97 dataset[149], and offer superior representation of low energy photoelectric interactions in low Z materials relative to previous EPDL datasets[150-152]. Simulations were performed in water, Solid Water, and radiochromic film computer models with a total of 5×10^8 source photon (SP) histories processed for each simulation.

Photon Energy (keV)	Abundance
27.202	0.396
27.472	0.731
30.944	0.0674
30.955	0.130
31.704	0.0375
35.493	0.0668
Total:	1.4287

Table 3. [125]I source photons used in the Monte Carlo model. Source photons with energies less than 5 keV, and source electrons, were ignored due to their relatively low yields and negligible chance of penetrating the titanium capsule.

The ^{125}I photon spectrum was characterized as 6 photons with energies and abundances obtained from the Brookhaven National Laboratory web site[153] and which emanate isotropically from positions within the active, ion implanted, layer of the seed core or plaque substrate. The ^{125}I photon spectrum used in this investigation is listed in Table 3.

 A complete description of the Monte Carlo methodology used is provided by Medich et al[154]. The uncertainty in the overall results is estimated to be less than 3%, largely due to uncertainties in cross section values, using methodology described by Medich et al[155].

2.9.1 Seed calibration geometry.

The ^{125}I I-Plant model 3500 brachytherapy seed used for the EBT film calibration was modeled in liquid water. The dose rate in terms of cGy/hour-U was calculated along straight lines perpendicular to the seed long axis in the center planes of each active layer at the expected position of the calibration film in the Solid Water phantom (i.e., the film plane parallel to the seed plane at a distance 6.71 mm between the mid-plane of the active layers and the center of the seed long axis). Along these straight lines are the profiles used to create the calibration curve of the film, described in the film calibration section. A cross section of EBT film shown in Figure 25 of the Radiochromic film section can help one to understand the geometry.

The dose rate used for all calculations was the average between the dose rates to the upper active layer of the film and the lower active layer of the film, while the mid-plane of the film was used for all coordinates on the film. The next step was to replace the liquid water with the Solid Water phantom in the seed calibration geometry described in the film calibration section 2.6.2, and to repeat the Monte Carlo simulations. The ratio of the dose rate to film in Solid Water to the dose rate to film in liquid water was first averaged between equidistant points from the center of the film, then fitted with a 5th degree polynomial using CurveExpert Professional software (Daniel G.

Hyams, Madison, AL) and used to multiply each point of the calibration curve created as described in the film calibration section 2.6.2, resulting in a calibration curve for dose to film in Solid Water. Re-evaluation of films measured with the second prototype eye plaque was done using the latter calibration curve, resulting in doses to film in Solid Water, which were later converted to doses to liquid water using Monte Carlo simulations as explained in next section. In order to better understand the order of magnitude and importance of this correction, we tested if results would differ if the film was replaced by Solid Water, *i.e.,* how important it is to model the actual film used as opposed to just using a ratio of dose to Solid Water to dose to liquid water. The Solid Water used in this work contains 2.3% calcium, but we also tested the dose to Solid Water with 1.7% calcium content, both of which were discussed by Meigooni *et al*[135].

2.9.2 Eye plaque geometry.

The second prototype eye plaque was first modeled in liquid water and then in Solid Water, in the "eye" phantom inserted into the full scatter 30 cm x 30 cm x 30 cm phantom, as described in the Solid Water "eye" phantom section. The dose rates in cGy/hour-mCi were calculated on the central axis of the plaque (axis perpendicular to the center of the inner concave surface of the plaque, which is facing the eye) every 0.25 mm, starting 0.25 mm from the surface of the plaque to 12.50 mm from the surface of the plaque. For the depth dose rate simulations in Solid Water, an EBT film was modeled at each location, thus the dose rate to film in Solid Water was calculated. At each depth the dose rates were averaged over a circular area with a radius of 0.5 mm. A similar circular area was used to evaluate the doses at the centers of the irradiated films in the Contour program. The dose rates in liquid water normalized to 3 mm from the plaque's inner surface were used for comparison with the depth dose rates measured on films. The ratio of the central axis dose

rates to film in Solid Water to the dose rates to liquid water was used to convert the dose rates measured on the central axis of the films from doses to film in Solid Water to doses to liquid water. Then, dose rates were calculated in liquid water for each film position perpendicular to the central axis of the plaque in terms of dose rates to circular annuli with radii increasing by 0.1 mm, starting with a 0.05 mm circle, the next annulus between radii 0.05 mm and 0.15 mm, and so on until the radius of the actual film for small films which fitted inside the eye plaque or the radius 12.95 mm for the large films below the eye plaque was reached. Then the simulations were repeated for films modeled in Solid Water at the same locations. The ratios of dose rates to film in Solid Water to dose rates to liquid water were used to convert the dose rates measured in Solid Water to dose rates in liquid water. We did not convert the full 2D dose map derived from the planar films in Solid water to 2D dose maps in liquid water, but rather converted selected profiles in the films. If the results were to be used for treatment planning, a full conversion of the film data to liquid water would be possible using this method.

3. Eye plaque dosimetry results and discussion.

    3.1 [106]Ru eye plaques.

The accurate dosimetry methods, techniques and results as applied to [106]Ru eye plaques are described in the published article[42] which is attached as Appendix 1. Partial results of [106]Ru eye plaques dosimetry were also presented at a number of national and international meetings[75-77, 82, 83] and the author contributed his accumulated experience as a co-author of the ISO International Standard 21439:2009: Clinical Dosimetry – Beta Radiation Sources for Brachytherapy[41].

In addition to published [106]Ru eye plaque findings, below are results of interest not shown in the published article[42]. Eight different [106]Ru eye plaques belonging to three types (CCX, CCA and CIA) were dosimetrically characterized in this thesis. The first plaque characterized in this work

was CCX 36. The dosimetric measurements of this plaque were done using the NIST phantom provided to us by Dr. Soares and shown in Figure 14. Working on the dosimetric characterization of this eye plaque started our learning curve in dealing with radiochromic film dosimetry, which included film handling, scanning and calibration protocols developed in this work and published in its process[42, 113]. The remaining six plaques: CCX 41, CCX 55, CCX 104, CCX 129, CCX 219, CCA 892, and CIA 156 were characterized using the Solid Water "eye" phantom designed in the course of this work.

The measurements of the CCX 36 eye plaque were done using GAFCHROMIC MD-55-2 film belonging to Lot #37350, irradiating one film at a time to an approximate dose of 30 Gy at the center of the film. Eight films were irradiated at distances ranging from 0.70 mm to 10.14 mm from the middle of the film to the inner surface of the plaque. Films at depths 2.62 mm and 3.21 mm were repeated to test the reproducibility and the results were within 1.30% and 12.0% of each other, respectively. These measurements were done before we established the technique of cutting the batch of film into more uniform sub-batches, described in section 1.4 of the Introduction. The films were calibrated using a ^{60}Co teletherapy machine as recommended for electron dosimetry by TG-55[98]. The dose rate measured along the central axis of the CCX 36 plaque is shown in Figure 41. The film results were fitted using a Gaussian Model analytical fit using CurveExpert Professional:

$$\text{Dose rate} = a * \text{EXP} - \frac{(\text{Distance} - b)^2}{2 * c^2}$$

where a, b, and c are fit parameters.
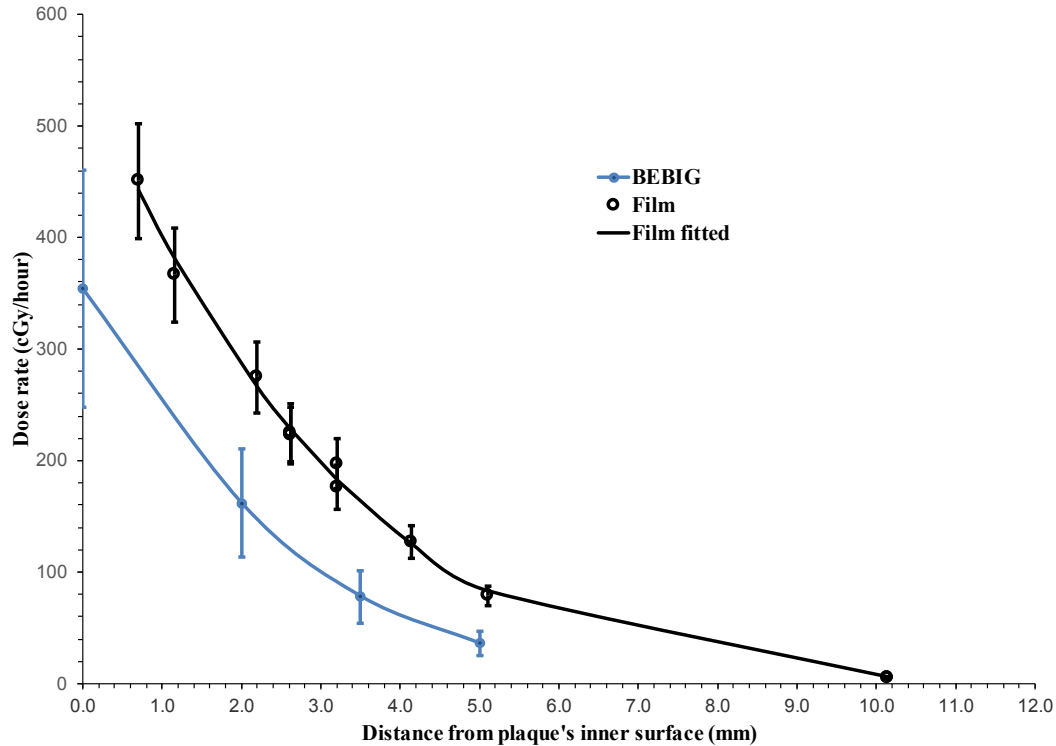
Figure 41. Dose rate measured along the central axis of the CCX 36 plaque along with a fitted analytical curve and the data provided by BEBIG.

The BEBIG uncertainty reflected in the error bars was the stated ±30% (k=2), while our measurement uncertainty for this type film was 11.5% (k=2), somewhat larger than the 8.6% (k=2) uncertainty determined for later EBT types of film[42]. The increase in uncertainty reflected a 4% film non-uniformity in the uncertainty calculation vs. 1.5% for EBT type films. The measured dose rate was substantially higher than the dose rate provided by BEBIG, as discussed in the Introduction section and in the published article[42], which shows in Figure 7 the results of CCX 55 eye plaque measured using film and a semiconductor diode, as well as a comparison of our measurements with NIST results shown in Table 1. A planar dose distribution of the CCX 36 plaque is shown in Figure 42. There is a 16.6% hot spot centered approximately 3.5 mm from the center of the film.
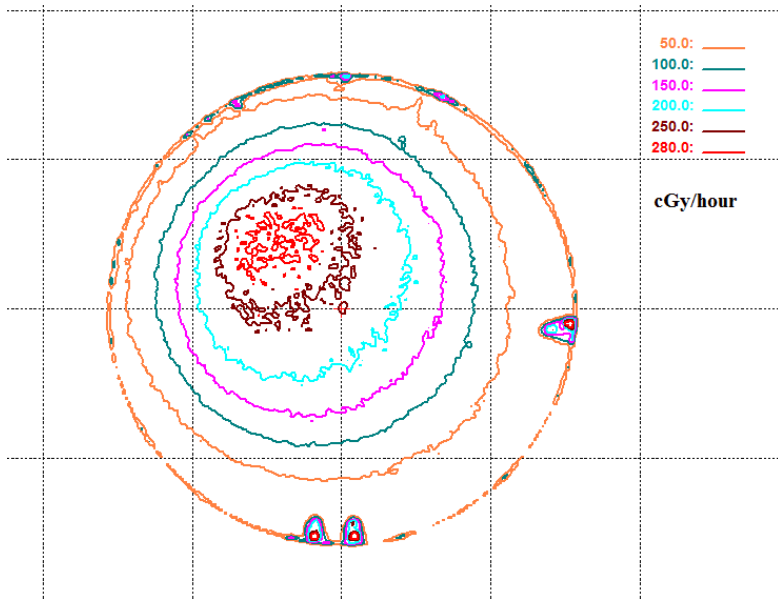
Figure 42. Dose rate in a plane perpendicular to the central axis of the CCX 36 plaque at depth 3.21 mm from the plaque. View from the plaque. 0.5 cm between grid lines.
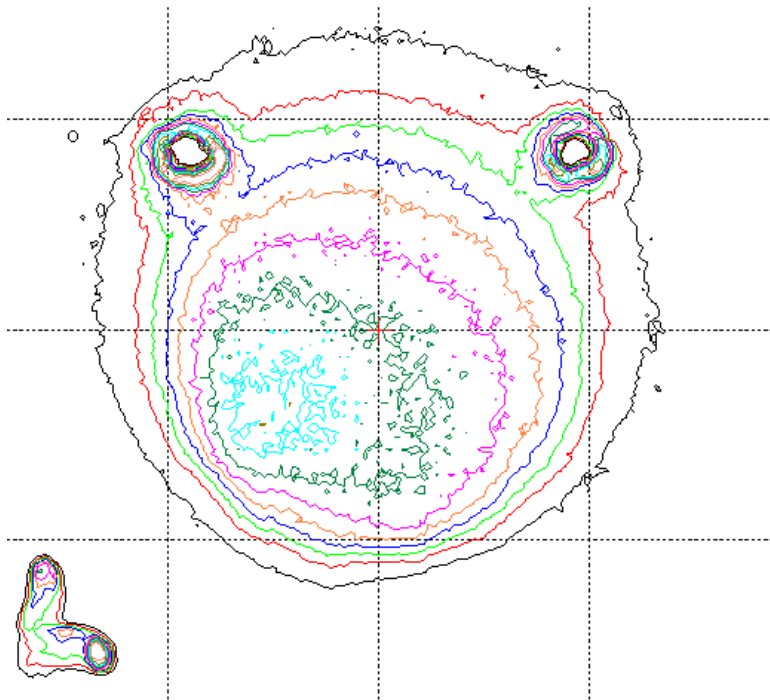
Figure 43. Setup image of the CCX 36 eye plaque. View from the plaque. 0.5 cm between grid lines.

During measurements in the NIST phantom it was found that it is very difficult to control the film rotation vs. the eye plaque, since the phantom had no co-registration features. The marks on the film seen in Figure 42 were helpful for controlling the film's direction of polarization for proper scanning purposes, but not co-registration with the eye plaque. Therefore a setup image of the plaque obtained by simply placing it on film and allowing it to irradiate the film for some time is shown in Figure 43. Even though this image shows isodose lines, these have no dosimetric meaning, except to show the approximate location of the dosimetric non-uniformity vs. the plaque's suture lugs.

Of special interest is the CCX 41 plaque which was only briefly mentioned in the published article[42]. This plaque was delivered by BEBIG to Dr. Soares at NIST in order to calibrate BEBIG's dosimetry. The calibration process started with NIST calibrating the eye plaque twice using calibrated HD-810 GAFCHROMIC film and the NIST phantom shown in Figure 14, as well as two calibrated scintillation detectors. The films and the plastic scintillation detectors were calibrated using the same calibrated $^{90}Sr/^{90}Y$ ophthalmic applicator. The results of the four sets of measurements were fitted with an analytical function and the whole process and results were detailed in the NIST Calibration Report[156]. Then NIST was supposed to return the eye plaque to BEBIG with the Calibration Report[156] and BEBIG was supposed to use the eye plaque as their standard for calibration of their plastic scintillators used for dosimetry in the production of eye plaques. In this particular case we borrowed the eye plaque after the NIST calibration prior to its return to BEBIG by NIST and performed a full set of film measurements in our "eye" plaque phantom using MD-55-2 film belonging to Lot #I1215. Sheets 2 and 3 of the lot were cut into 3 cm wide strips in order to use more uniform film in accordance with our previously described technique and the strip marked as 2 from both sheets was used. The film was calibrated using

84

MSKCC's ^{60}Co teletherapy machine. The full set of dose distributions of our measurements is shown in Figures 44a – 44h below. This is the only full set of measurement results shown in this dissertation, done in order to present a full set of film results.
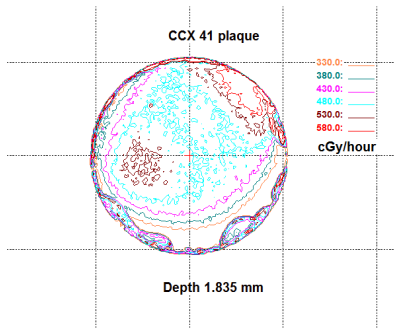
Figure 44a. Dose rate in a plane perpendicular to the central axis of the CCX 41 plaque at depth 1.835 mm from the plaque. View from the plaque. 0.5 cm between grid lines.
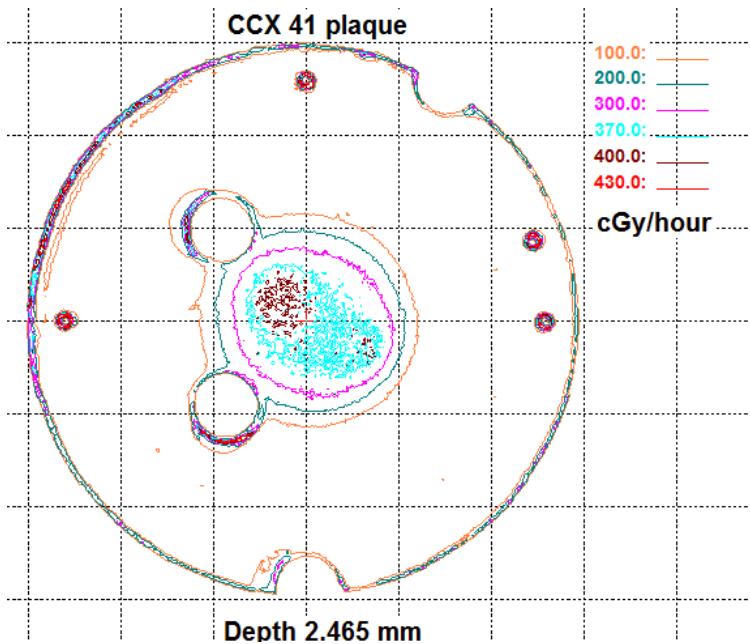
Figure 44b. Dose rate in a plane perpendicular to the central axis of the CCX 41 plaque at depth 2.465 mm from the plaque. View from the plaque. 0.5 cm between grid lines.
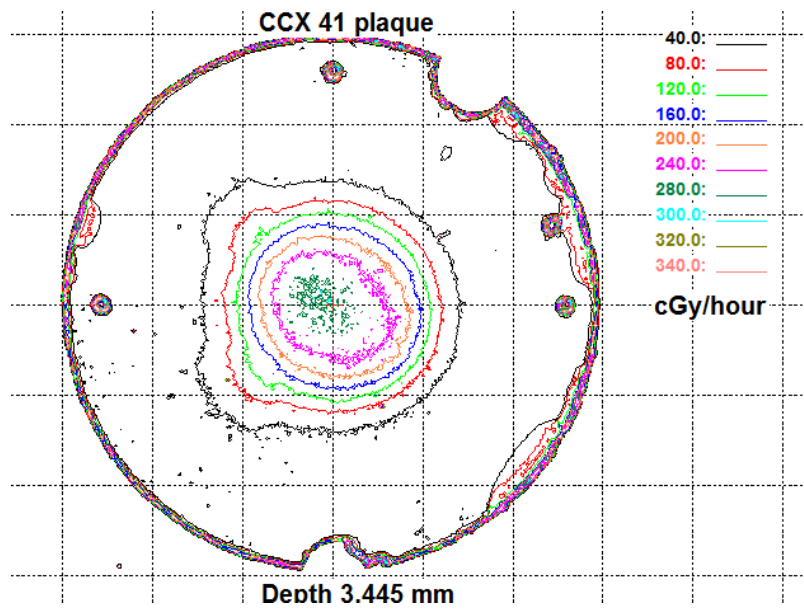
Figure 44c. Dose rate in a plane perpendicular to the central axis of the CCX 41 plaque at depth 3.445 mm from the plaque. View from the plaque. 0.5 cm between grid lines.
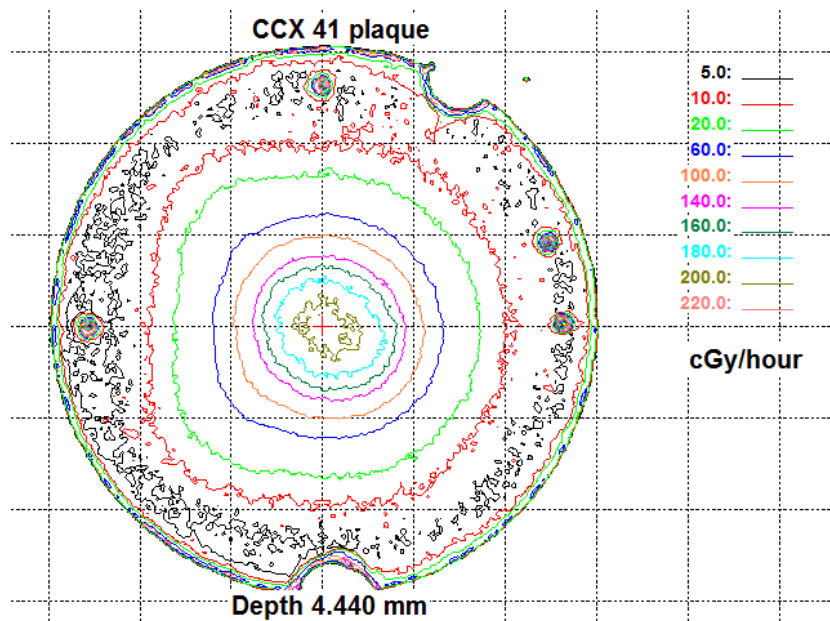
Figure 44d. Dose rate in a plane perpendicular to the central axis of the CCX 41 plaque at depth 4.440 mm from the plaque. View from the plaque. 0.5 cm between grid lines.
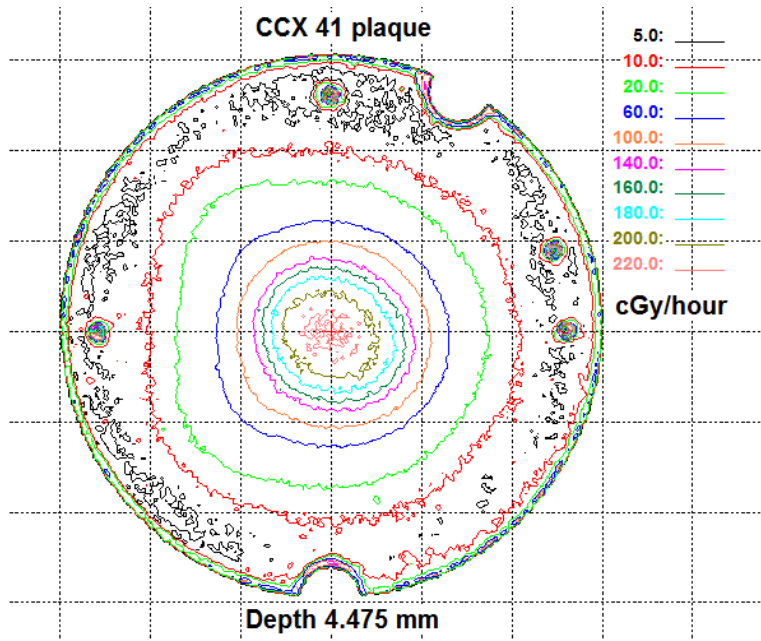
Figure 44e. Dose rate in a plane perpendicular to the central axis of the CCX 41 plaque at depth 4.475 mm from the plaque. View from the plaque. 0.5 cm between grid lines.
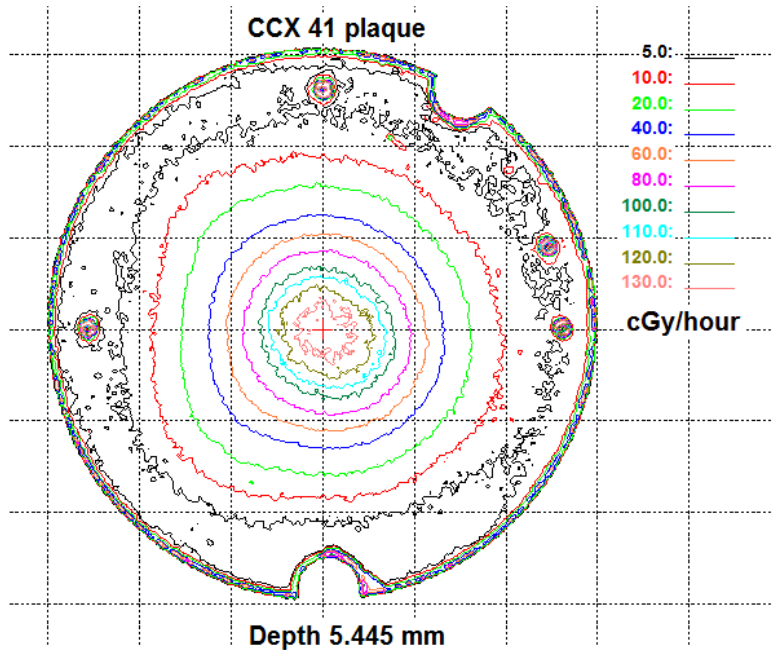
Figure 44f. Dose rate in a plane perpendicular to the central axis of the CCX 41 plaque at depth 5.445 mm from the plaque. View from the plaque. 0.5 cm between grid lines.
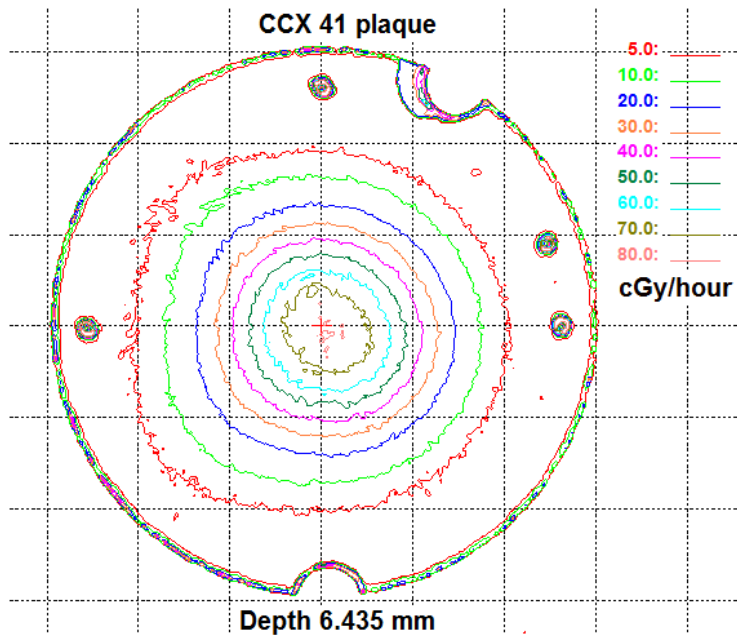
Figure 44g. Dose rate in a plane perpendicular to the central axis of the CCX 41 plaque at depth 6.435 mm from the plaque. View from the plaque. 0.5 cm between grid lines.
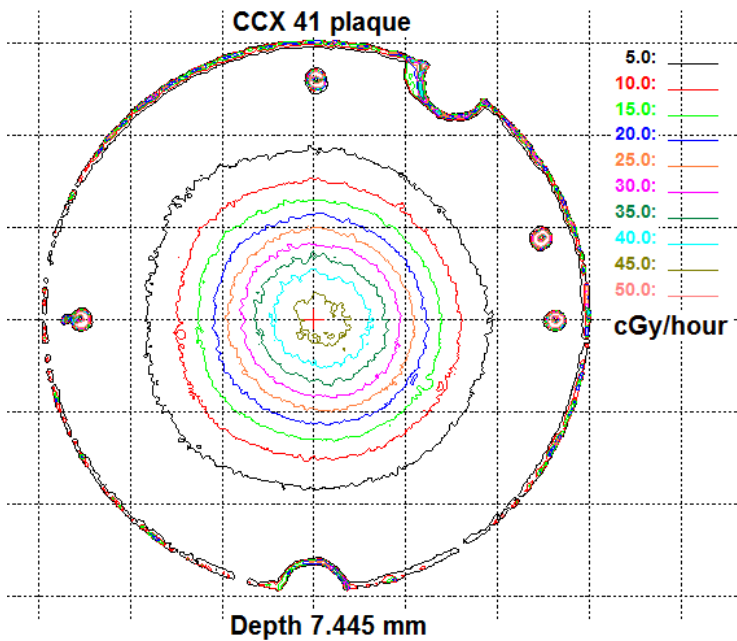
Figure 44h. Dose rate in a plane perpendicular to the central axis of the CCX 41 plaque at depth 7.445 mm from the plaque. View from the plaque. 0.5 cm between grid lines.

The agreement between repeat films is within 5.3%. The dose rate measured along the central axis of the plaque along with the fitted curve of the NIST measurements[156] is shown in Figure 45.
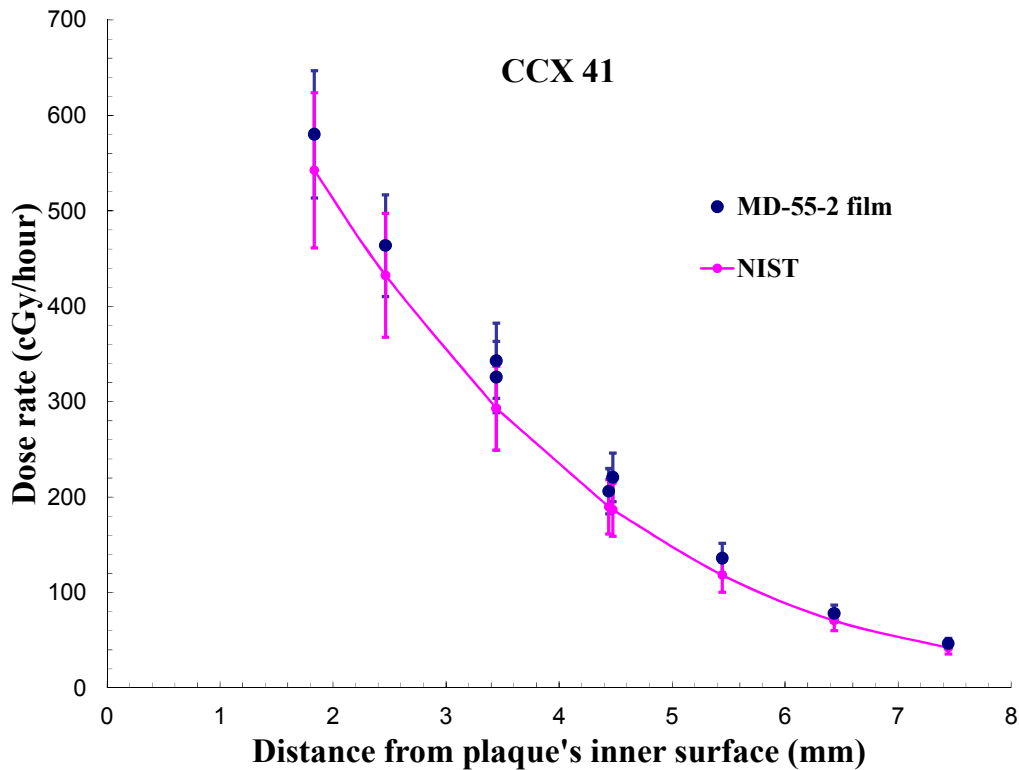
Figure 45. Dose rate measured along the central axis of the CCX 41 plaque compared to the NIST Calibration Report fitted curve[156].

Cross comparisons of this kind are the gold standard of dosimetric measurements and are performed on a routine basis between NIST, national standard laboratories of other countries and accredited dosimetry calibration laboratories in the U.S. Our results agreed to within 8% with the NIST report, which is good agreement for this kind of measurement[73] and within accepted combined uncertainties (k=1) for radiochromic dosimetry of ophthalmic brachytherapy sources[41, 113]. The combined expanded uncertainty of the NIST measurement is 15% (k=2)[156] and the estimated combined expanded uncertainty of our measurement is 11.5% (k=2) using MD-55-2 film. Moreover, the results of these measurements and the NIST results were used by Dr. Kirov

from Memorial Sloan-Kettering Cancer Center as the "gold standard" for testing his liquid scintillation method. This project resulted in a meeting presentation and publication[78, 157], which included our results. Since this was the only published data on CCX plaques dosimetry until recently, it was used by Hermida-López for comparison with his Monte Carlo simulations of ^{106}Ru eye plaques[79].

A 2D treatment planning program enabling one to account for dosimetric non-uniformities of ^{106}Ru eye plaques, which can result in hot and cold spots in the treated eye, was developed at MSKCC using the film measured data, and is briefly described in the published article[42]. The program calculates for any depth and lateral distance from the central axis minimum and maximum doses in the form of isodose lines as shown in Figure 46.
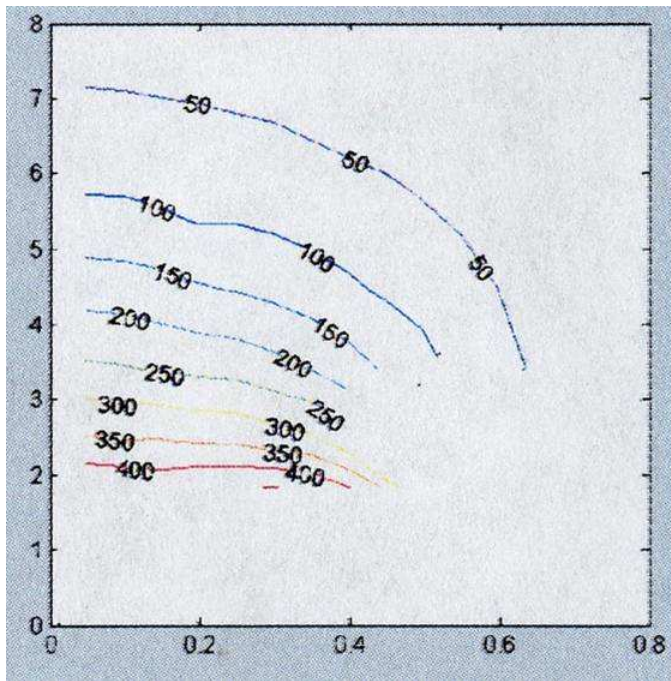
Figure 46. Minimum isodose lines in cGy/hour of a ^{106}Ru eye plaque calculated from film measurements. The vertical axis is distance along the central axis of the plaque in mm; the horizontal axis is lateral distance from the central axis in cm.

These isodose lines then can be superimposed on the ultrasound image of the tumor as shown in Figure 47 enabling one to account for overdosing critical structures by the maximum doses or underdosing the tumor in case of cold spots.
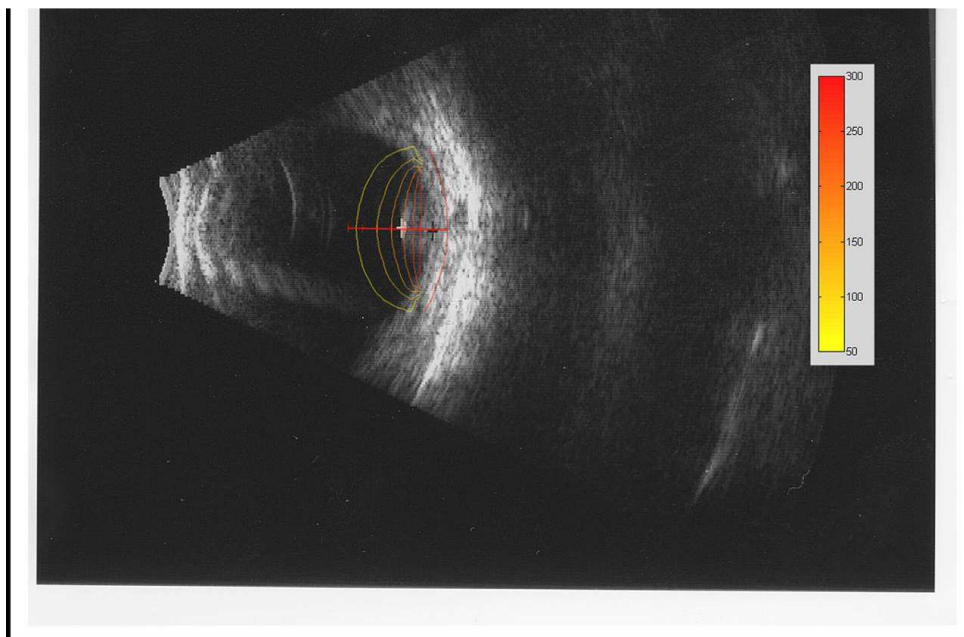
Figure 47. Minimum isodose lines of a ^{106}Ru eye plaque superimposed on an ultrasound image of an ophthalmic tumor.

3.2 Novel ^{125}I eye plaque and collimator.

3.2.1 First prototype eye plaque.

The film dosimetry of the first prototype eye plaque was done using XR-T film Lot # K02b28XRT as detailed in the Radiochromic film section 2.3, using the head phantom setup described in the Solid Water "eye" phantom section 2.2. Two films were irradiated at distances 2.9 mm and 10.79 mm from the inner surface of the plaque. Unfortunately the work on the first prototype had to be

stopped after these two films, since we discovered a minor degree of radioactive contamination that was traced to encapsulation problems. Each film was scanned 7 days after the end of irradiation using the Vidar VXR 16 Dosimetry Pro 16 bit film scanner at 89µm resolution, driven by RIT film dosimetry software. The films were scanned in clear sheet protectors together with a red acetate filter exactly like the calibration film as described in sections 2.5 and 2.6.2.

The dose rate distribution measured using a film perpendicular to the central axis of the plaque at the distance 10.79 mm from its inner surface is shown in Figure 48. The dose rate along the central axis of the plaque measured using the Scanditronix stereotactic diode in a water tank, as described in section 2.8, together with a fitted analytical curve and superimposed film results, are shown in Figure 49. The results in both figures were decayed to the same reference date.
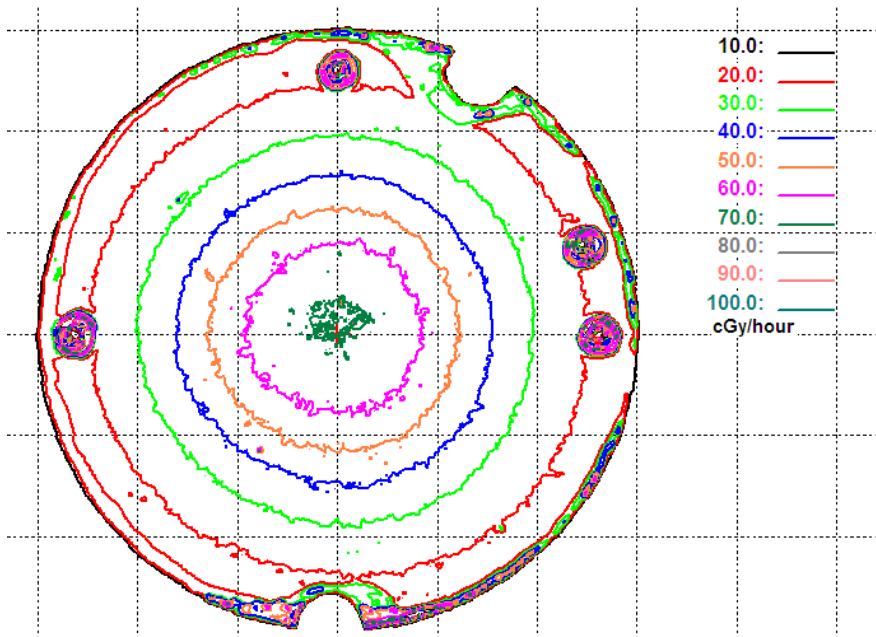
Figure 48. Dose rate distribution at the distance 10.79 mm from the inner surface of the first prototype plaque. View from the plaque. 0.5 cm grid.
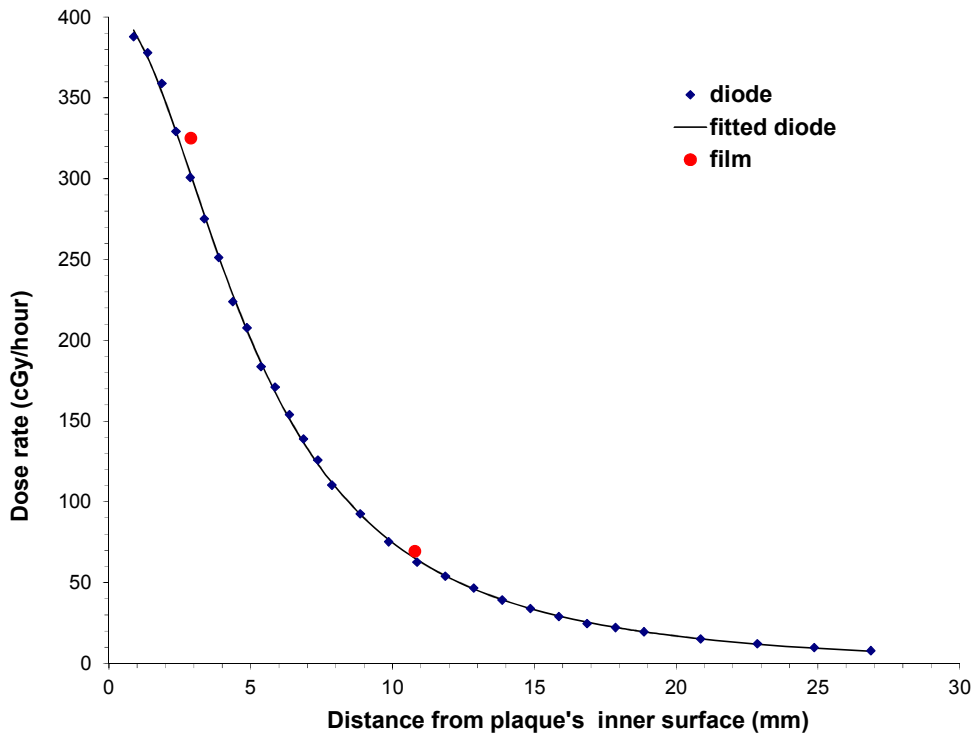
Figure 49. Dose rate on the central axis of the first prototype plaque measured using the Scanditronix stereotactic diode along with a fitted analytical curve and both film measurements.

The curve was fitted using CurveExpert Professional software by a rational function

$$Dose\ rate = \frac{a + b * x}{1 + c * x + d * x^2}$$

where a, b, c, and d are the fit parameters and x is the distance from the inner surface of the plaque along the central axis. The fitted function provides the dose rate at any point along the central axis of the plaque. The dose rate at the center of the 2.90 mm film was found to be 7.7% higher than the dose rate measured at the same distance using the Scanditronix stereotactic diode in the water tank, while the dose rate at the center of the 10.79 mm film was found to be 6.5% higher than the respective diode dose rate. This is well within our uncertainty of 14.6% (k=2) for ^{125}I eye plaque

radiochromic film dosimetry and is within the accepted combined uncertainties (k=1) for radiochromic film dosimetry of ophthalmic and low energy photon brachytherapy sources[41, 113]. It should be noted that the results of the semiconductor diode calibrated using a calibrated ^{125}I brachytherapy seed were in good agreement with film dosimetry results, even though, per the diode manufacturer's specifications, it is rated for energies above 1 MeV.

Water tank scans across the plaque in a plane including its central axis using the Scanditronix stereotactic diode at three different distances from the plaque's inner surface are shown in Figure 50. The distances were measured along the central axis of the plaque. These scans were done using the uncalibrated electrometer of the water tank and therefore are considered relative only.
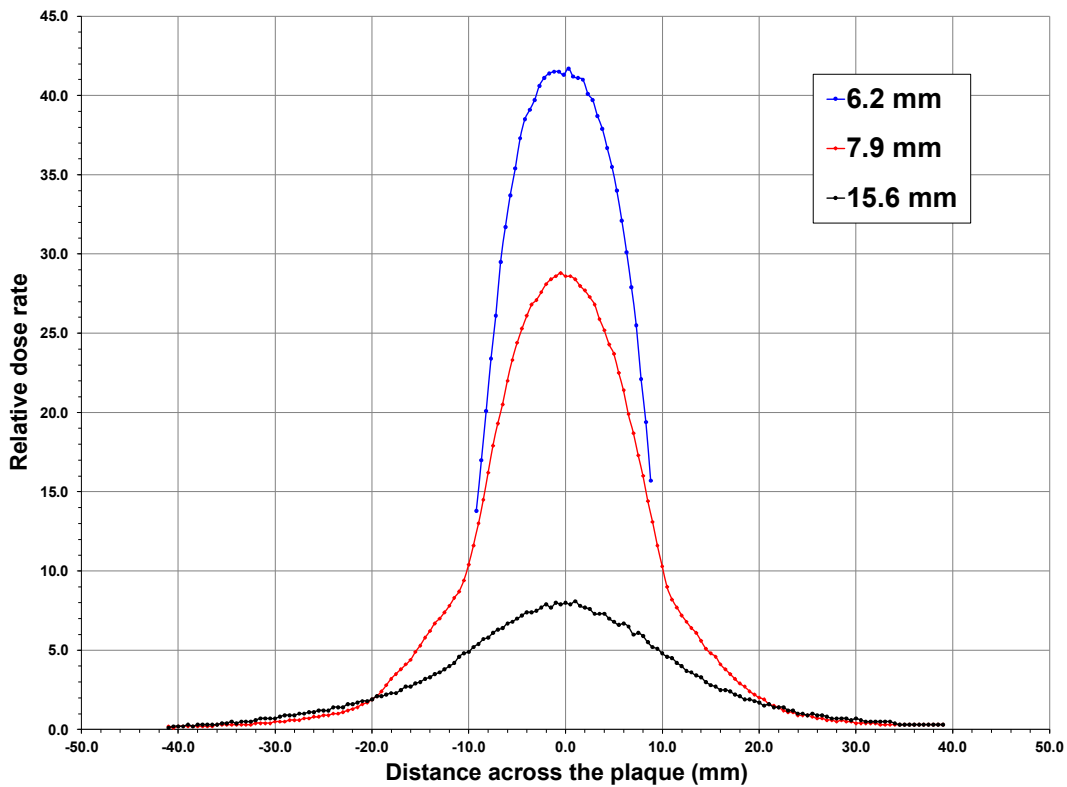
Figure 50. Water tank scans across the plaque at three different distances from the inner surface of the plaque.

The results of the film dosimetry for both films, as can be seen in the film shown in Figure 48, as well as the water tank scans shown in Figure 50, demonstrate highly symmetrical dose distributions around the central axis and do not exhibit any hot or cold spots.

The dose rate on the central axis 6.0 mm from the plaque's inner surface (5.0 mm from the inner sclera, which is the standard COMS prescription point for tumors not higher than 5.0 mm) is 163.2 cGy/hour. The dose rates recommended by the American Brachytherapy Society are $60 - 105$ cGy/hour at the tumor apex[96]. In the first prototype eye plaque, these dose rates are achieved for tumors with apical heights of 7 - 10 mm and thus, the dose rates are clinically relevant. Changing the activity of the manufactured plaque would enable customization of the dose rate to the apical height of the tumor to be treated.

3.2.2 Second prototype eye plaque.

Film dosimetry of the second prototype eye plaque was done using EBT film Lot # 34351-05 as described in the Radiochromic film section 2.3 using the full scatter phantom setup described in the Solid Water "eye" phantom section 2.2. Films were irradiated without the collimator in 9 planes perpendicular to the central axis of the plaque at distances ranging from 0.96 to 12.33 mm from the inner surface of the plaque. In addition, four films with the collimator were irradiated at distances 0.24, 1.09, 2.83, and 5.48 mm from the inner surface of the plaque. The film at the distance 0.24 mm was a curved film attached to the surface of the collimator. All films were scanned 24 hours after the end of the irradiation using the Epson Expression 1680 flatbed scanner in 48 bit color mode, followed by the extraction of the red channel. A portion of the films were scanned again 48 hours after the end of the irradiation in order to access post-exposure growth during the second 24 hours after irradiation. As usual a number of films were exposed at the same

depth in order to access measurement reproducibility. Dosimetric results of the replicate films were within 0.9% of each other, which is indicative of the uncertainty of the measurements.

Film analysis was done using MSKCC's film dosimetry Contour program. First, all scanned films were converted from pixel values to dose to liquid water using the uncorrected calibration curve created by irradiating the calibration film in Solid Water, but using the seed TG 43[53] data, which provides dose to liquid water. Then, the films without the collimator were converted again from pixel values to dose to film in Solid Water using the Monte Carlo corrected calibration curve as described in the Seed calibration geometry sub-section 2.9.1 of the Monte Carlo simulations of the novel ^{125}I eye plaque dosimetry section 2.9. The latter results were converted again using Monte Carlo conversion factors from dose to film in Solid Water to dose to liquid water, which were deemed the correct results of the eye plaque dosimetry. The results with the uncorrected calibration curve were compared to the Monte Carlo corrected results in order to assess the level of precision added by the Monte Carlo correction, or the uncertainty introduced by lack of correction. The films with the collimator were not corrected using Monte Carlo, *i.e.*, the second prototype eye plaque was not modeled in Monte Carlo with the collimator for this dosimetric analysis. The role of the films with the collimator was limited to assessment of the existence of hot and cold spots due to the collimator and to assessment of the effect of the collimator on dose rate.

A typical example of a dose rate distribution measured using film is shown in Figure 51. The film was located 5.35 mm from the inner surface of the plaque. A horizontal profile across the center of the film in Figure 51 is shown in Figure 52. The profile is shown in three versions, as described above: 1) uncorrected dose rate to water (measurement done in Solid Water, but calibration done using TG-43[53] parameters in liquid water), 2) dose rate to film in Solid Water, and 3) dose rate to film in Solid Water converted to dose rate in liquid water using Monte Carlo simulations.

96
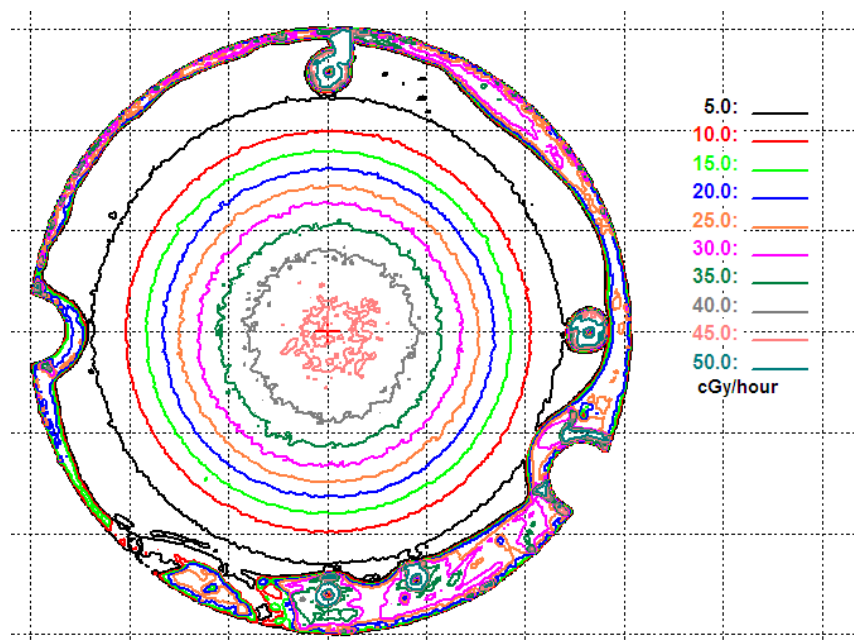
Figure 51. Dose rate distribution at distance 5.35 mm from the inner surface of the plaque. View from the plaque. 0.5 cm between grid lines.

It is clearly seen from the profiles in Figure 52, as well as from the planar films, such as the one shown in Figure 51, that the second prototype eye plaque has a radially isotropic dose distribution without hot and cold spots, similar to that exhibited by the first prototype eye plaque. It is possible to conclude from both prototypes that the eye plaque manufacturing process results in eye plaques with uniform distribution of ^{125}I.

The dose rate along the central axis of the plaque measured using radiochromic film (uncorrected results) along with the Monte Carlo simulated dose rate in liquid water along the central axis are shown in Figure 53. Both curves were normalized at 3.0 mm from the inner surface, since the Monte Carlo simulation does not provide the absolute dose rate of the eye plaque. For the normalization purpose the film CAX dose rate was fitted with an analytical curve (not shown in

Figure 53). It can be seen that the dose rate measured using film is in good agreement with the Monte Carlo simulation.
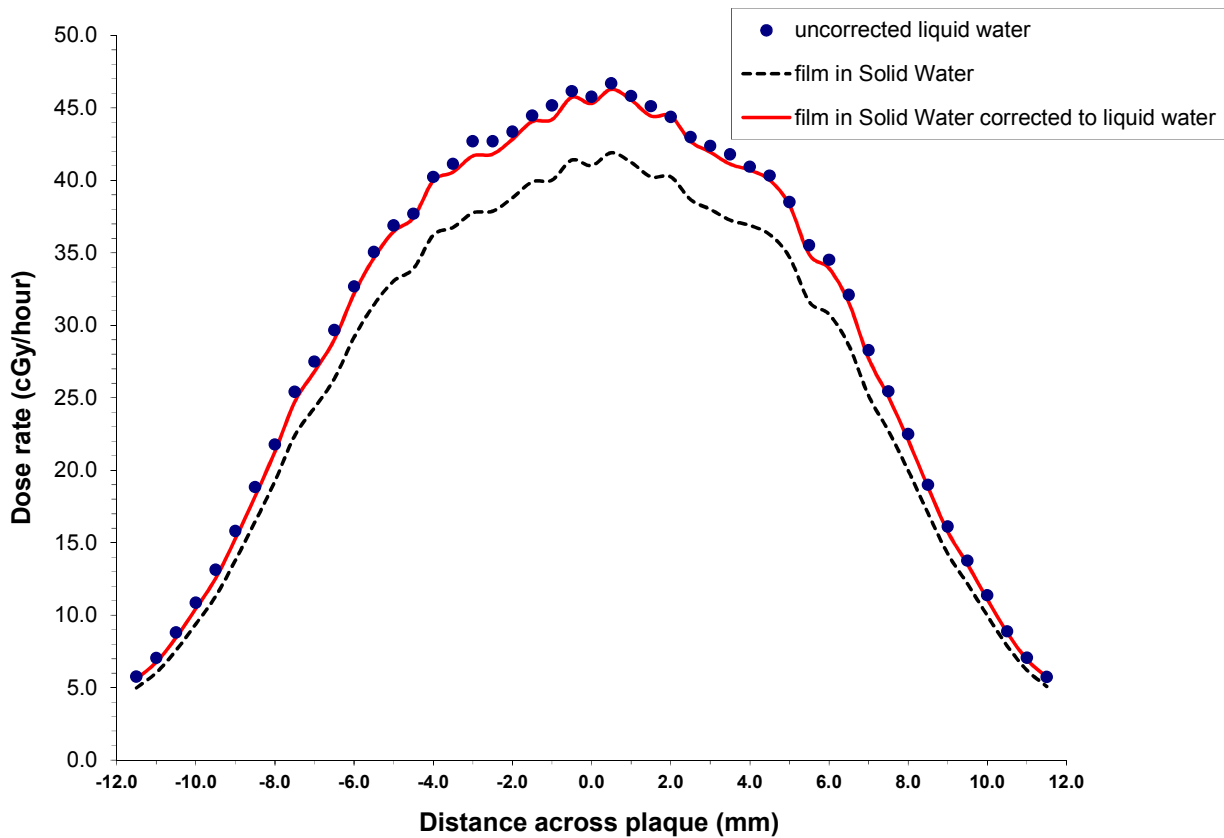
Figure 52. Three versions of a horizontal profile through the central axis of the film at a distance 5.35 mm from the inner surface of the plaque: 1) uncorrected dose rate to water (measurement done in Solid Water, but calibration done using TG-43[53] seed parameters in liquid water), 2) dose rate to film in Solid Water, and 3) dose rate to film in Solid Water converted to dose rate in liquid water using corrections determined from Monte Carlo simulations.
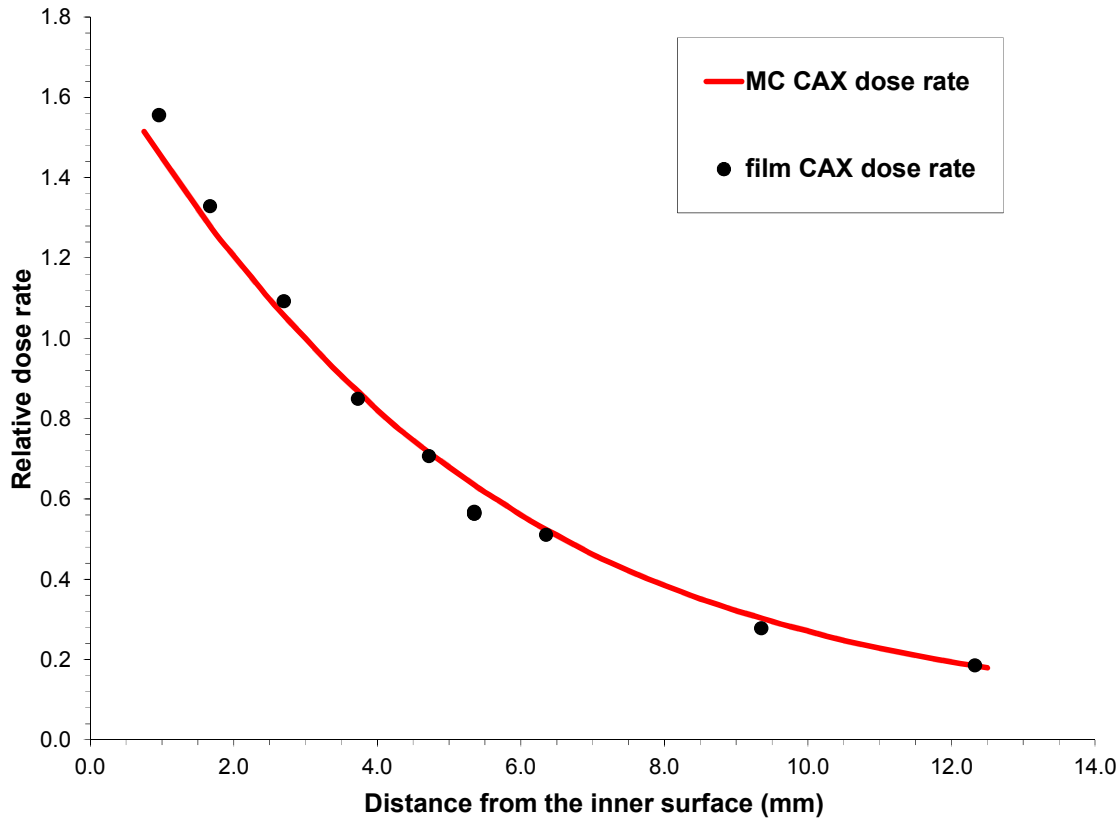
Figure 53. Relative dose rate on the central axis (CAX) of the second prototype plaque measured using radiochromic film along with the Monte Carlo simulated relative dose rate. Both curves are normalized at a distance 3.0 mm from the inner surface of the plaque.

Figure 54 depicts the uncorrected absolute dose rate to liquid water along the central axis of the plaque measured using radiochromic film (measurement done in Solid Water, but calibration done using TG-43[53] parameters for liquid water) together with the superimposed dose rate to film in Solid Water converted to dose rate in liquid water along with a fitted analytical curve of the dose rate to film in Solid Water converted to dose rate in liquid water. The curve has been fitted using a reciprocal quadratic function

$$Dose\ rate = \frac{1}{a + b * x + c * x^2}$$

where a, b, and c are fit parameters and x is the distance from the inner surface of the plaque along the central axis. The fitted function enables one to calculate the dose rate at any point along the central axis of the plaque.
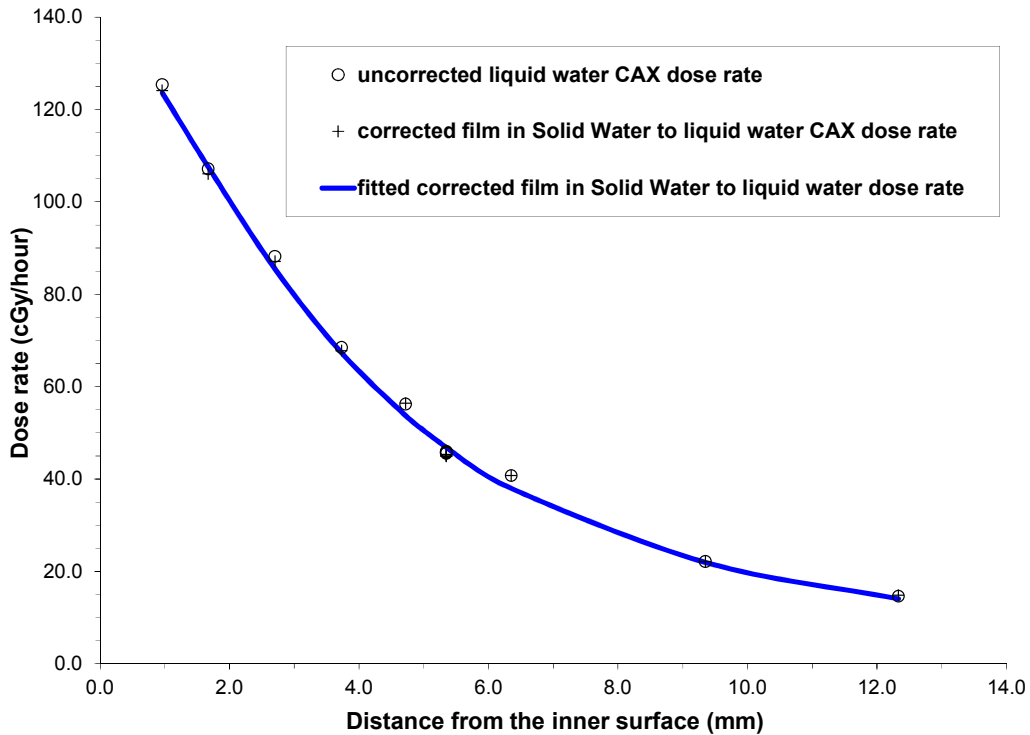
Figure 54. Uncorrected absolute dose rate on the central axis of the plaque with superimposed dose rate to film in Solid Water converted to dose rate in liquid water along with a fitted analytical curve of the dose rate to film in Solid Water converted to dose rate to in liquid water.

The results shown in Figures 52 and 54 indicate, at least for EBT film in Solid Water 2.3 (Solid Water with 2.3% calcium content), the uncorrected method (all calibrations and measurements done in Solid Water using TG-43[53] parameters in liquid water for calibration) produces very similar results to the same measurements corrected and converted using Monte Carlo simulations. The actual ratio between the results varies between 0.989 and 1.024 (average 1.0075 ± 0.0096 std. dev.). These differences are well within the uncertainties of the measurements and Monte Carlo

simulations employed. This finding supports the hypothesis presented in section 2.9, at least for this particular case, namely that when calibrations and measurements are done in the same kind of Solid Water phantoms, while using calibration doses defined in liquid water, the final result is dose in liquid water. This conclusion, however, should be tested for each phantom/film combination. The dose rate on the central axis 6.0 mm from the plaque's inner surface (5.0 mm from the inner sclera) is 40.8 cGy/hour. It should be noted although this value is below the clinical dose rate range recommended by the American Brachytherapy Society[96], the activity of the second prototype was four times weaker than of the first prototype at the time of dosimetric measurements.

Partial results of the dosimetric analysis of the second prototype of the novel ^{125}I eye plaque were presented at an annual meeting of the American Association of Physicists in Medicine[158].

3.2.3 Monte Carlo corrections.

The dose rates of the calibration ^{125}I I-Plant model 3500 seed in terms of cGy/hour-U to liquid water, and to EBT film in Solid Water, calculated using Monte Carlo are shown in Figure 55. The dose rates are calculated in the midplane of the film or in liquid water at the coordinate where the midplane of the film would be, along a profile crossing the center of the seed perpendicular to the seed long axis. The ratio of the dose rates shown in Figure 55 averaged between the "left" and "right" sides of the seed along with a curve fitted using a 5th degree polynomial is shown in Figure 56. The fitted ratio was used to multiply each point of the uncorrected calibration curve as explained in section 2.9.1 and obtain a film calibration curve of dose to EBT film in Solid Water. The eye plaque results obtained using this corrected calibration curve were converted to dose in liquid water using Monte Carlo as explained in section 2.9.2 and one such profile is shown in Figure 52. These calculations and conversions were done for all films at all measurement depths. The uncorrected and corrected results comparison on the central axis is shown in Figure 54.
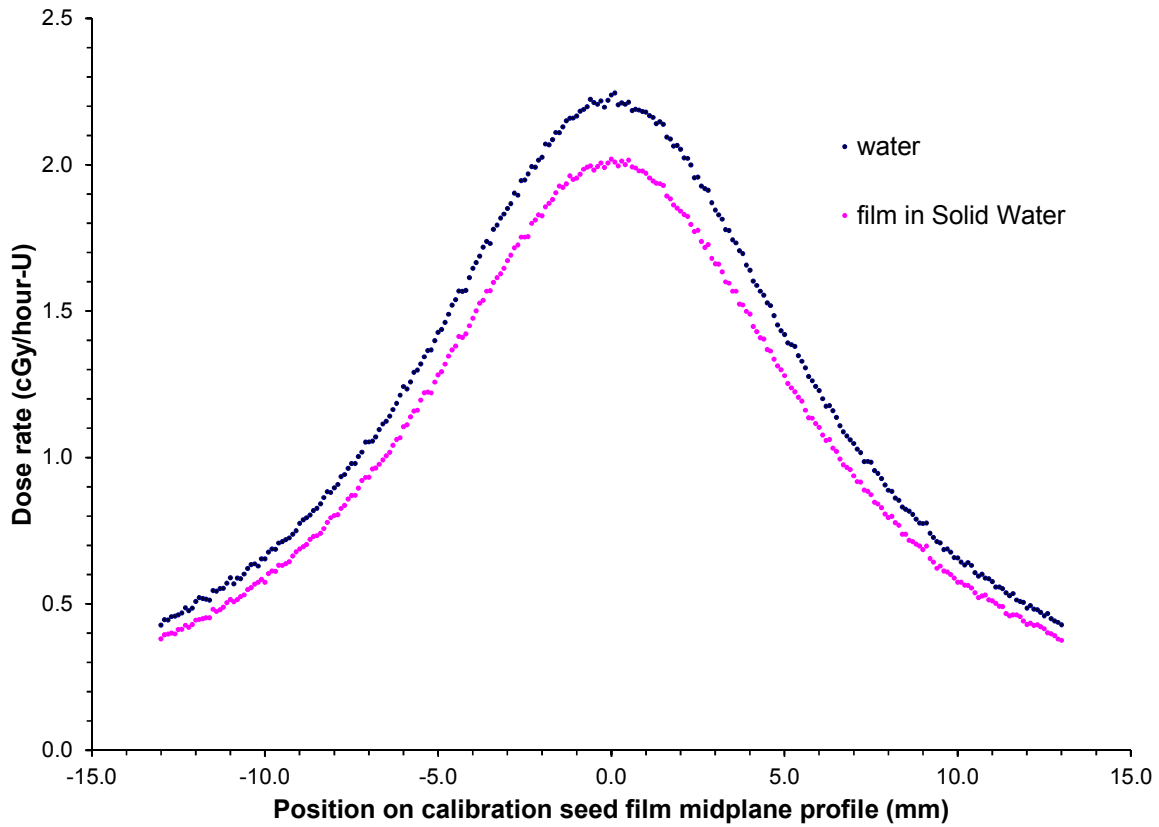
Figure 55. Dose rate along a profile perpendicular to the calibration seed long axis crossing the seed center in the midplane of EBT calibration film in Solid Water, and the dose rate in liquid water along the same profile.
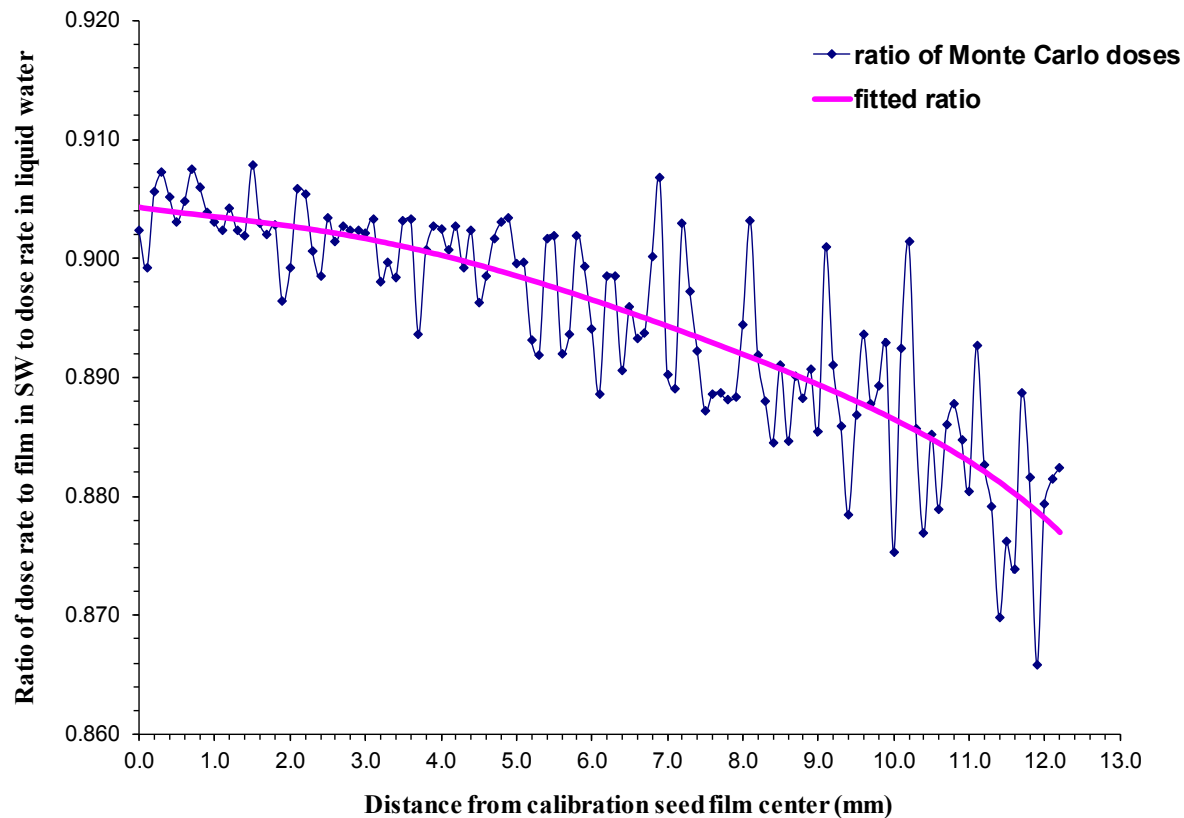
Figure 56. Ratio of dose rate to EBT film in Solid Water to dose rate in liquid water together with an analytical fit.

In order to better understand the behavior of the Monte Carlo corrections, the seed geometry was modeled in two types of Solid Water with and without film at the calibration film depth of 6.71 mm. The elemental composition of both types of Solid Water is given in Table 4 and of both types of film in Table 5. The Solid Water used in this work has 2.3% calcium content and is similar to what Meigooni *et al*[135] called Solid Water 2.3. We used our exact composition and called it the same name. The Solid Water with 1.7% calcium content used for our Monte Carlo simulations has the exact composition of the Solid Water 1.7 cited by Meigooni *et al*[135]. The elemental compositions of the active layers of EBT and EBT3 film and of the clear polyester which is part of the films were provided by the manufacturer of the films.

Element	Solid Water1.7 Wt %	Solid Water2.3 Wt %
Hydrogen	8.2%	8.4%
Carbon	68.0%	69.0%
Nitrogen	2.4%	2.0%
Oxygen	19.6%	18.3%
Chlorine	0.1%	0.0%
Calcium	1.7%	2.3%
Density of the Solid Water	1.036	1.044

Table 4. Elemental composition and densities of Solid Water 2.3 and Solid Water 1.7 used for Monte Carlo modeling in this work.

Element	EBT film active layer Wt %	EBT3 film active layer Wt %	Clear Polyester Wt %
Hydrogen (H)	9.4	8.64	4.20
Lithium (Li)	0.8	0.63	
Carbon (C)	57.4	49.91	62.50
Nitrogen (N)	13.2	0.64	
Oxygen (O)	16.4	32.27	33.30
Sodium (Na)		0.35	
Aluminum (Al)		6.55	
Sulfur (S)		0.49	
Chlorine (Cl)	2.8	0.54	
Total	100	100	100

Table 5. Elemental composition of the main parts of EBT and EBT3 films.

Lateral distance from film center (mm)	Ratio of dose rate to EBT film in Solid Water 2.3 to dose rate to liquid water	Ratio of dose rate to Solid Water 2.3 to dose rate to liquid water	Ratio of dose rate to EBT film in Solid Water 1.7 to dose rate to liquid water	Ratio of dose rate to Solid Water 1.7 to dose rate to liquid water
0.0	0.907	1.039	0.923	0.941
1.0	0.905	1.037	0.923	0.941
2.0	0.903	1.034	0.923	0.942
3.0	0.901	1.032	0.923	0.942
4.0	0.899	1.030	0.924	0.942
5.0	0.897	1.027	0.924	0.943
6.0	0,895	1.025	0.924	0.943
7.0	0.893	1.022	0.925	0.943
8.0	0.891	1.020	0.925	0.944
9.0	0.889	1.018	0.925	0.944
10.0	0.887	1.015	0.925	0.944
11.0	0.885	1.013	0.926	0.945
12.0	0.883	1.010	0.926	0.945
Average ratio	0.895	1.025	0.924	0.943

Table 6. Ratios of dose rate to EBT film in two types of Solid Water to dose rate in liquid water, and ratios of dose rates in two types of Solid Water at film's location, but without the film to dose rate in liquid water.

Lateral distance from film center (mm)	Ratio of dose rate to EBT3 film in Solid Water 2.3 to dose rate to liquid water	Ratio of dose rate to Solid Water 2.3 to dose rate to liquid water	Ratio of dose rate to EBT3 film in Solid Water 1.7 to dose rate to liquid water	Ratio of dose rate to Solid Water 1.7 to dose rate to liquid water
0.0	1.077	1.039	1.097	0.941
1.0	1.076	1.037	1.098	0.941
2.0	1.074	1.034	1.099	0.942
3.0	1.072	1.032	1.100	0.942
4.0	1.071	1.030	1.100	0.942
5.0	1.069	1.027	1.101	0.943
6.0	1.067	1.025	1.102	0.943
7.0	1.065	1.022	1.103	0.943
8.0	1.064	1.020	1.103	0.944
9.0	1.062	1.018	1.104	0.944
10.0	1.060	1.015	1.105	0.944
11.0	1.059	1.013	1.106	0.945
12.0	1.057	1.010	1.106	0.945
Average ratio	1.067	1.025	1.102	0.943

Table 7. Ratios of dose rate to EBT3 film in two types of Solid Water to dose rate in liquid water, and ratios of dose rates in two types of Solid Water at film's location, but without the film to dose rate in liquid water.

The results of the Monte Carlo simulations for all four conditions for EBT film – ratios of dose rates to film in Solid Water to dose rates in liquid water, and dose rates in Solid Water at the location of the film, but without film, to dose rates in liquid water are given in Table 6, while the same ratios for EBT3 film are given in Table 7.

It can be seen that both the calcium content and the film composition strongly influence the results. In the case of Solid Water 2.3 the ratio decreases by 2.7% when moving from the central axis to the 12.0 mm lateral distance with EBT film, and decreases by 2.8% without the film. This result can be considered constant within the uncertainties with and without film, but the ratio itself with film is on average 12.7% lower than without film. In the case of Solid Water 1.7, the ratio increases by 0.4% with and without EBT film, again constant within the uncertainties. The ratio itself with film is, however, on average 2.0% lower than without film. In both cases, the ratio with film is lower than the ratio without, and notably much lower when using Solid Water 2.3, which seems to be the prevalent type delivered by the manufacturer. For EBT3 film in the case of Solid Water 2.3 the ratio decreases by 1.9% when moving from the central axis to the 12.0 mm lateral distance with EBT3 film and decreases by 2.8% without the film. While this finding can be considered constant within the uncertainties with and without film, the ratio itself with film is on the average 4.1% higher than without film. In the case of Solid Water 1.7, the ratio increases by 0.8% with film and by 0.4% without film, again almost constant within the uncertainties, but the ratio itself with film is on the average 16.8% higher than without film. Therefore it is very important to have the exact elemental composition of the Solid Water used for low-energy photon dosimetry, as well as to model the geometry with the film used. The literature concerning Monte Carlo derived differences between solid media and liquid water[132-135], already noted in the Introduction focused only on dose differences between these two types of media, but did not look into dose to the

dosimeter used in solid media and its conversion to dose to liquid water, which is film in our case. Dose to the film can be as much as 16.8% different then dose to the solid media without film. The large difference between the EBT and EBT3 films ratios could possibly be explained by the difference between the mass energy absorption coefficients (μ_{en}/ρ) vs. liquid water shown in Figure 57, which were calculated using the mass energy absorption coefficients of the elements[159]. The μ_{en}/ρ for EBT3 film is always larger than liquid water, while for EBT film it is always smaller.
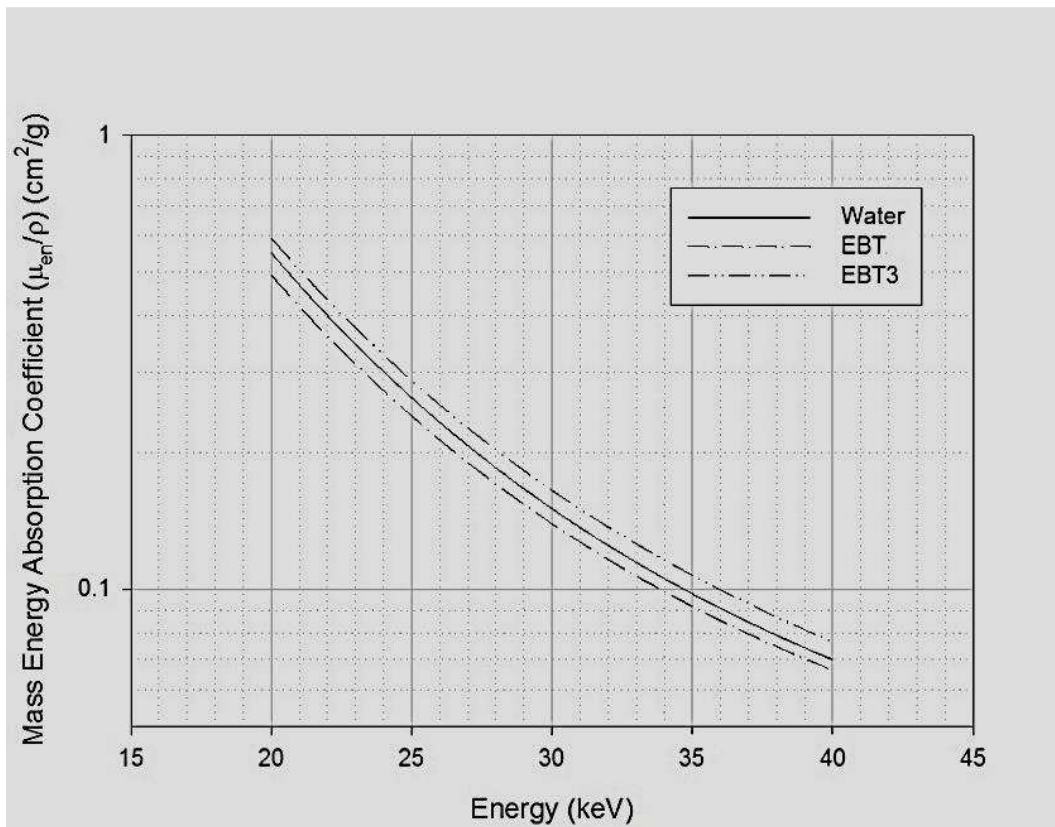
Figure 57. Mass absorption coefficients of water, EBT and EBT3 films.

In order to convert the eye plaque results from dose to EBT film in Solid Water to dose in liquid water for measurements on the central axis, a Monte Carlo simulation was performed both in liquid

water and in EBT film in Solid Water. Calculations were made at 0.25 mm intervals along the central axis of the plaque and at each of the 9 planar films, as explained in the Eye plaque geometry sub-section 2.9.2 of Monte Carlo simulations of the novel ^{125}I plaque dosimetry section 2.9.

The ratio of dose to liquid water to dose to EBT film in Solid Water along the central axis of the plaque has been fitted with a linear fit: y=a+bx, using CurveExpert Professional software, where y is the ratio, and x is the coordinate along the central axis of the plaque, a and b are the fit parameters. This ratio increases with depth from 1.092 at 0.25 mm depth to 1.122 at 12.5 mm depth for a total change of 3.0%. It was used to convert the film measurements from dose to EBT film in Solid Water to dose to liquid water. The uncorrected and corrected results for the measured dose rate along the central axis are shown in Figure 54 and were already discussed.

The off-axis ratios of dose to liquid water to dose to EBT films in Solid Water for 5 out of the 9 film planes are shown in Figure 58.

These off-axis ratios were used to convert profiles across films from dose rate to EBT film in Solid Water to dose rates to liquid water. One such example is shown in Figure 52. Again, the uncorrected and corrected results are in very close agreement, even despite clear trends seen in Figure 58. In the example shown in Figure 52 at the depth 5.35 mm, the average ratio between uncorrected and corrected profiles is 1.018 with a standard deviation of 0.011. It seems that these trends just offset the conversion trends introduced by the film calibration curve, when converting the measured results to dose to EBT film in Solid Water. And, as already said, it can be concluded that at least for EBT film in Solid Water 2.3, the uncorrected method (all calibrations and measurements done in Solid Water using TG-43[53] parameters for liquid water for calibration) produces very similar results to the same measurements corrected and converted using Monte Carlo simulations.
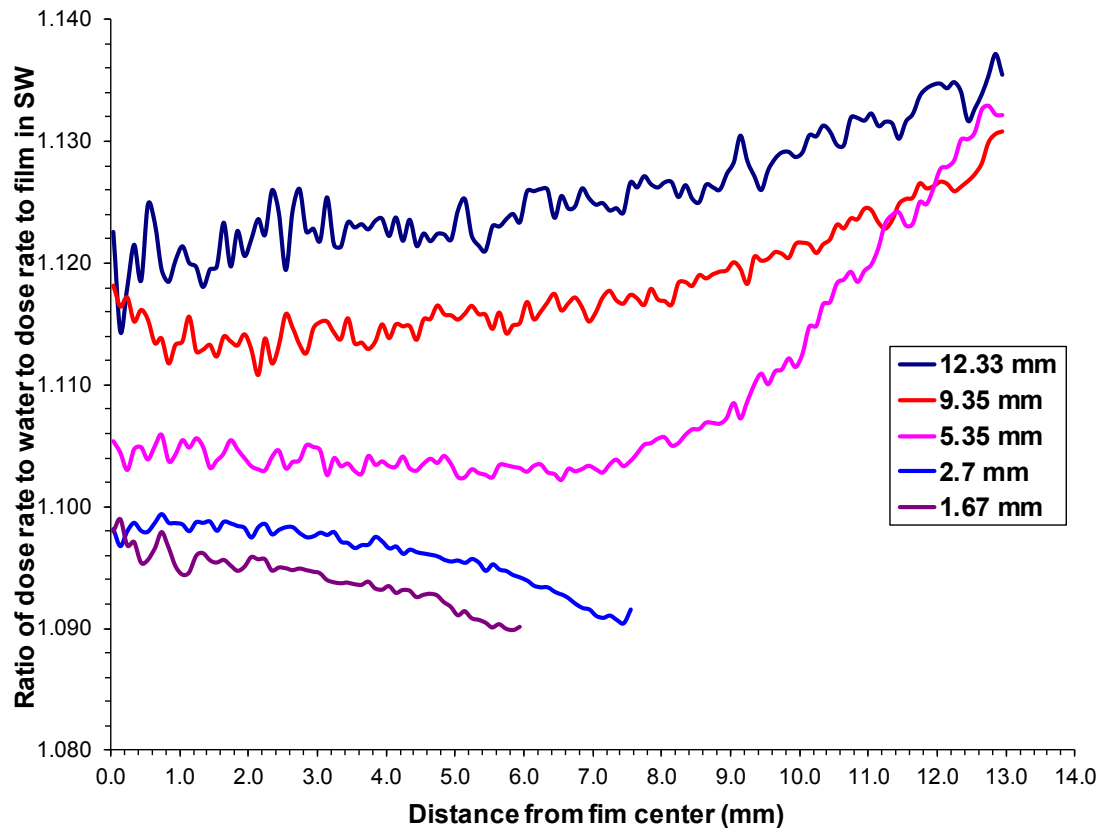
Figure 58. Off-axis ratios of dose rate to liquid water to dose rate to EBT films in Solid Water at 5 planar films perpendicular to the central axis of the plaque at different distances from the inner surface of the plaque.

3.2.4 Collimator dosimetry.

The dose rate distributions produced by the collimator described in the Novel ^{125}I eye plaque and collimator section 2.1.3 at distances 0.24 mm (surface of the plaque), 1.09 mm (inner sclera), and 2.83 mm, are shown in Figures 59, 60, and 61. The dose rate at 5.48 mm from the plaque was too weak to display.
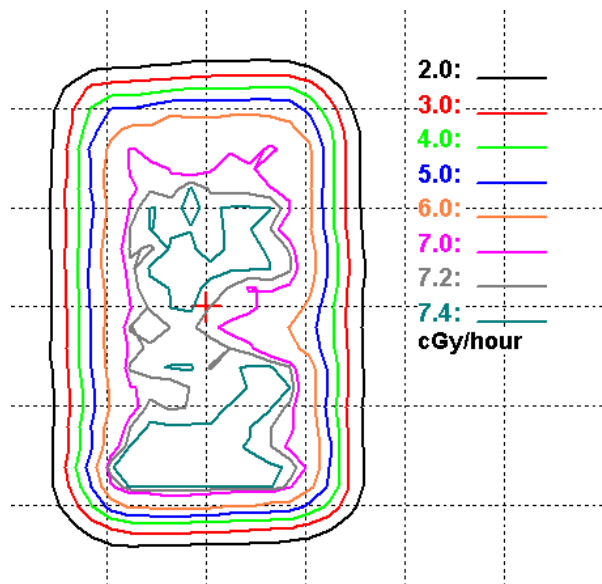
Figure 59. Dose rate distribution at the distance 0.24 mm from the inner surface of the plaque. The film is attached to the curved surface of the collimator. View from the plaque. 0.5 mm grid. Dose rate at CAX 7.28 cGy/hour.
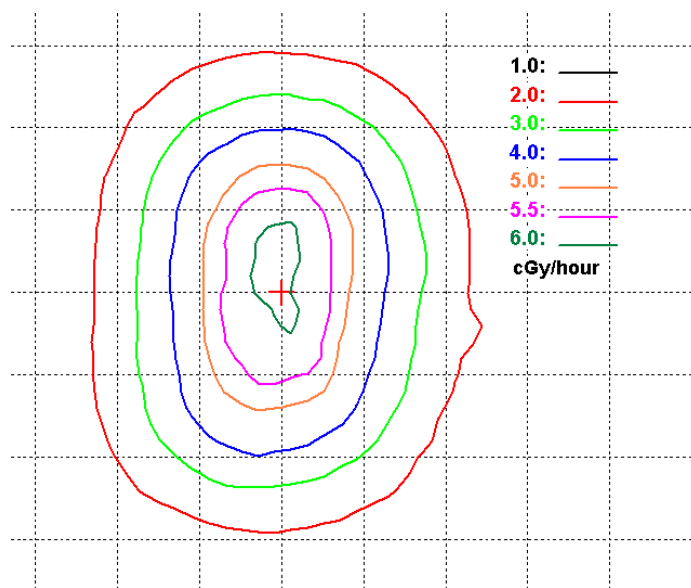
Figure 60. Dose rate distribution at the distance 1.09 mm from the inner surface of the plaque. View from the plaque. 0.5 mm grid. Dose rate at CAX 6.0 cGy/hour.
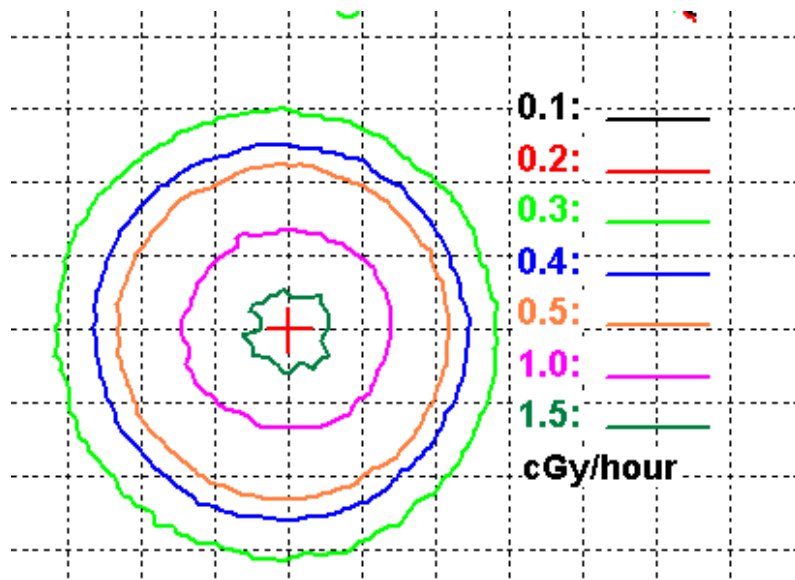
Figure 61. Dose rate distribution at the distance 2.83 mm from the inner surface of the plaque. View from the plaque. 1.0 mm grid. Dose rate at CAX 1.5 cGy/hour.

Vertical profiles through the central axis of the films shown in Figures 59, 60, and 61 are shown in Figure 62. It can be seen from the dose rate distributions and profiles, especially the profile at the level of the inner sclera, that the collimator does not produce hot and cold spots. The collimated dose rate at 1.09 mm is 20.1 times weaker, and at 2.83 mm is 55.3 times weaker, than un-collimated dose rates, since only a very small area of the eye plaque contributes to the collimated dose rate. The total area of the 128 holes was about 1 mm^2 vs. 276 mm^2 total inner surface of the plaque. Further from the plaque's surface the contribution of the total inner surface to the uncollimated dose rate is much larger, hence the much stronger attenuation 2.83 mm from the plaque as compared to 1.09 mm.

A 3D treatment plan would consist of a number of collimated fields, and the plaque could have much higher activity than the second prototype, but this could still produce insufficient dose rates,

especially for larger tumors. The divergence of the collimated fields seen in Figures 59 - 62 needs

further investigation, as it could become a limiting factor in creation of clinical treatment plans.
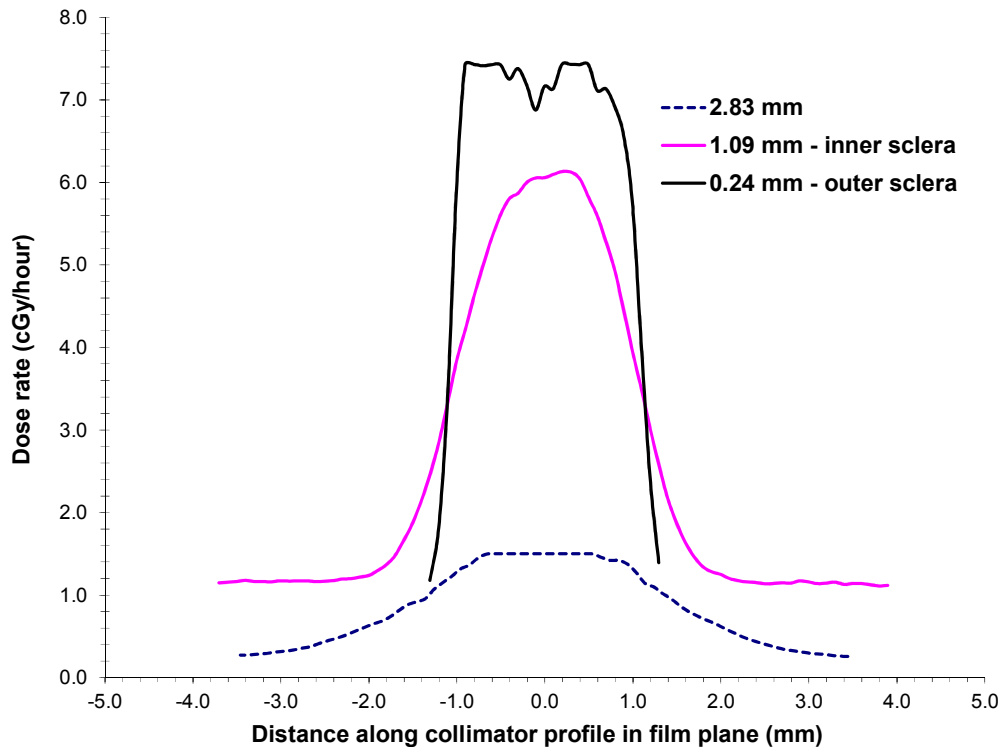
Figure 62. Vertical profiles through the central axis of the 0.24 mm, 1.09 mm, and 2.83 mm films.

3.3 Fully loaded 20 mm COMS plaque.

Film dosimetry was done at 16 planes perpendicular to the central axis of the plaque at distances

ranging from 0.0115 mm to 19.10 mm from the inner surface of the plaque, corresponding to the

distance to the outer sclera, using the special thin EBT1 film Lot 35314-4H in the Solid Water

"eye" phantom placed at the center of a 30 cm x 30 cm x 30 cm full scatter phantom. A calibrated

Model 6711 ^{125}I seed (Oncura, Inc., Arlington Heights, IL) and the TG-43[53] formalism were used

for film calibration. All results are presented in terms of dose rate per unit air kerma strength per

seed. Results of duplicate films agreed to within 5.5%.

The comparison between the measured dose rate on the central axis of the plaque and the dose rate calculated using BrachyDose Monte Carlo calculations[54] using the assumption of heterogeneous geometry, which includes the Silastic insert and the gold alloy (Modulay) backing, is shown in Figure 63. The measured curve was obtained using uncorrected film data, which are based on film calibration in Solid Water with TG-43[53] parameters for liquid water. In the case of 2.3% calcium Solid Water combined with EBT film, the uncorrected results are in close agreement with Monte Carlo corrected results, well within measurement and Monte Carlo uncertainties, as was shown in the case of the novel ^{125}I eye plaque discussed in sub-section 3.2.2. Therefore, Monte Carlo corrections were not needed. Measured depth dose on the central axis agrees well with the results of Monte Carlo calculations. The point by point average ratio of the fitted measurements curve to the Monte Carlo fitted curve is 0.971 ± 0.027 std. dev. These results validate the BrachyDose Monte Carlo simulations concerning the dose reduction effect of the plaque's backing and insert[54]. As per the BrachyDose Monte Carlo results presented in TG-129[40], the plaque's dose rate on the central axis is on the average about 15% lower than predicted by homogenous TG-43[53] calculations (average ratio between heterogeneous to homogenous calculation is 0.853 ± 0.017 std. dev.). Uncorrected (homogenous) and corrected (heterogeneous) central axis dose rates calculated using the Plaque Simulator software are presented in Figure 63 as well. It can be seen that the corrected dose rate is in good agreement with the BrachyDose Monte Carlo and the measurements of this work.

A dose rate distribution 7.34 mm from the inner surface of the plaque is presented in Figure 64. It is possible to see that it is radially isotropic and uniform. The effect of the six suture lugs on the 14 cGy/hour/U isodose line is clearly visible.
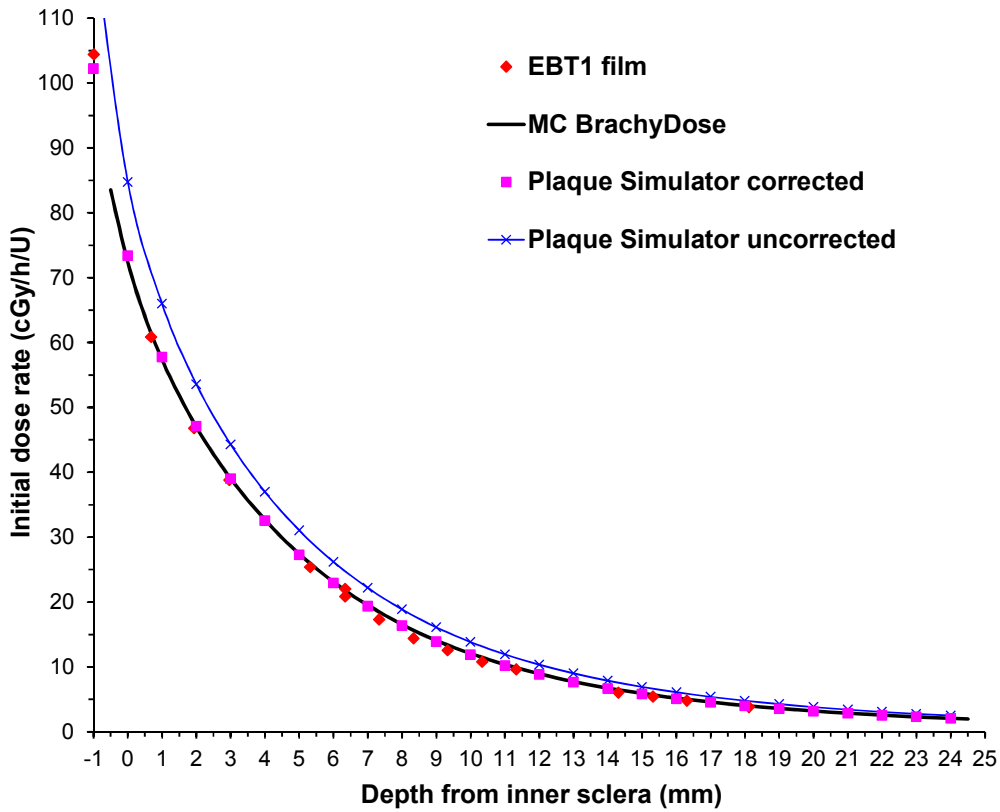
Figure 63. Comparison of dose rate at the central axis of the plaque measured using film, BrachyDose Monte Carlo calculations, as well as Plaque Simulator corrected and uncorrected calculations.
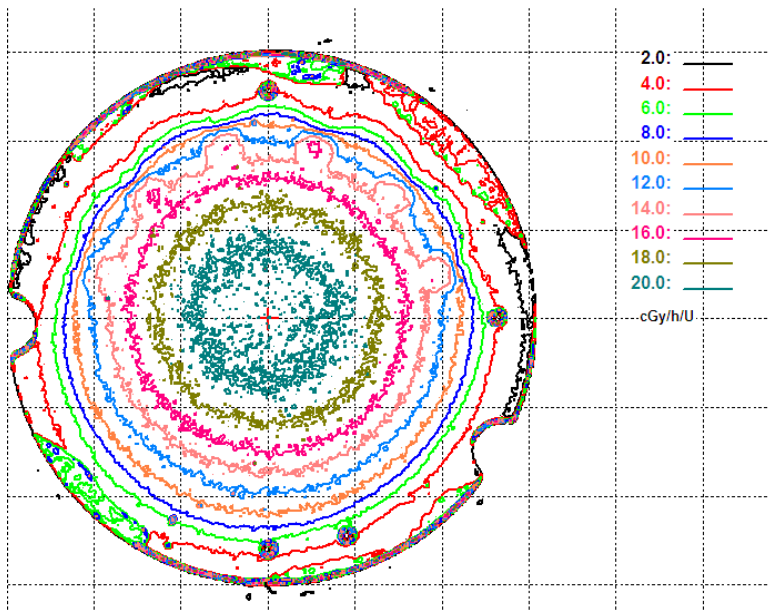
Figure 64. Dose rate distribution at the distance 7.34 mm from the inner surface of the plaque. View from the plaque. 0.5 cm between grid lines.

4. Uncertainties.

The complete analysis of uncertainties of [106]Ru eye plaque dosimetry is part of the published article[42]. Analysis of ^{125}I plaque dosimetry using radiochromic film is presented in Tables 8 and 9 below. The main difference between [106]Ru eye plaque dosimetry and ^{125}I eye plaque dosimetry using radiochromic film is the radiation source used for film calibration. While film calibration using a Linac beam results in a combined uncertainty of 2.9%, the same calibration using a calibrated ^{125}I seed results in a combined uncertainty of 6.6% due to high uncertainty in the air kerma strength of the calibration seed and in the TG-43[53] parameters. This difference in film calibration uncertainty results in 14.6% combined expanded (k=2) uncertainty for ^{125}I plaque dosimetry as compared to 8.6% combined expanded (k=2) uncertainty for [106]Ru eye plaque dosimetry using radiochromic film.

Component of uncertainty	Uncertainty %	Type
Uncertainty in a single film response from Table 2[42]	2.3%	A and B
Uncertainty in calibration seed air kerma strength	1.8%	B
Uncertainty in TG-43[53] parameters of the calibration seed	5.4%	B
Uncertainty in fitting parameters of the calibration curve	1.5%	B
Combined standard uncertainty for film calibration	6.6%	

Table 8. Estimated uncertainties in film calibration using a ^{125}I calibration seed.

Component of uncertainty	Uncertainty %	Type
Uncertainty in a single film response from Table 2[42]	2.3%	A and B
Uncertainty in film calibration from Table 8	6.6%	A and B
Film non-uniformity	1.5%	A
Uncertainty in measurement depth	1.6%	A and B
Uncertainty in irradiation time	0.1%	A
Combined uncertainty	7.3%	
Combined, expanded (k=2) uncertainty	14.6%	

Table 9. Estimated uncertainties in ^{125}I eye plaque dosimetry using radiochromic film.

5. Conclusions.

Radiochromic film in a Solid Water phantom is a convenient, accurate, and reproducible dosimeter for ^{106}Ru and low energy photon eye plaque dosimetry. The new special single layer films enable direct dose measurements on the inner surface of the plaques, providing precise assessment of the scleral dose, its uniformity, and of the active area of the plaques for coverage

determination. Cutting, preparation and handling of radiochromic films play an important role in precise absolute film dosimetry.

The Scanditronix stereotactic diode is a precise reproducible dosimeter for eye plaque dosimetry, and can be used for either ^{106}Ru or ^{125}I absolute dosimetry. This thesis, for the first time, presents its use for absolute ^{125}I dosimetry.

A calibrated ^{125}I seed and the TG-43[53] formalism can be used for calibrating radiochromic film and the Scanditronix stereotactic diode for absolute dosimetry.

The ion-implantation technique developed by Implant Sciences Corporation can be used to manufacture dosimetrically reproducible 1 mm thick ^{125}I eye plaques featuring uniform and symmetrical dose distributions without hot and cold spots. The dose rate of the Implant Sciences Corporation's eye plaques is clinically relevant in accordance with the criteria of the American Brachytherapy Society[96]. The dosimetric results measured by film dosimetry and the semiconductor diode were in good agreement with each other and with Monte Carlo simulations of the same plaque.

The collimator designed for the novel ^{125}I eye plaque produces sufficiently uniform dose distributions in terms of hot and cold spots. The collimator concept should be further investigated since it is not clear if a reasonable number of collimated fields in combination with higher activity of the eye plaques can produce clinically viable dose rates. The effect of the divergence of the collimated beams on the possible treatment plan, however, is unclear. Lack of high resolution 3D imaging of ophthalmic tumors is an additional obstacle.

This work validates the BrachyDose Monte Carlo simulations[54] concerning the dose reduction effect by the plaque's backing and the Silastic insert of COMS plaques. Clinical

implications of the dose rate reduction effect should be well understood prior to attempting to change well established treatment protocols.

Monte Carlo simulations were successfully used for converting the dose rates measured using radiochromic film in Solid Water to those in liquid water. It was found that for the combination of film and Solid Water used in this work, the uncorrected method (all calibrations and measurements done in Solid Water using TG-43[53] parameters for liquid water for calibration) produced very similar results to the same measurements corrected and converted using Monte Carlo simulations. The differences between the two methods are small when considering the uncertainties involved in the film dosimetry process, as well as in the Monte Carlo simulations. This conclusion has to be carefully checked for each combination of film and Solid Water, since the conversion factors can significantly differ between Solid Water 2.3 and Solid Water 1.7, as well as between different types of film. The data in this thesis indicates, when calculating the conversion factors between results in Solid and liquid water, it is insufficient to convert the dose between the different media, the film has to be modeled in Solid Water as well, since the difference in conversion factors with and without film was found to be as high as 16.8% for the particular combinations tested.

The measured data provide a full 3D dosimetric characterization of the eye plaques, accounting for all heterogeneities used in their design, as well as dose non-uniformities, and can be directly used by applicable 2D or 3D treatment planning programs for treatment of patients, enabling delivery of correct doses and protection of critical structures.

Each Ru-106 eye plaque must undergo accurate dosimetric commissioning and acceptance prior to its clinical use. Because of the history of conflicting dosimetric results, it is important to clarify the source of the dosimetry used in the prescription protocol.

Despite improved quality and dosimetry by BEBIG or recent advances in COMS plaques dosimetry, it is the ultimate responsibility of the medical physicist and physician to accept and commission the eye plaques for clinical use and decide what values to use for treatment delivery.

6. Future directions.

Production and standardization of the "eye" phantom and film punches would enable medical physicists to use these tools for commissioning and acceptance of eye plaques. Even if accredited dosimetry calibration laboratories will offer eye plaque calibration services, there will be institutions which will prefer doing their own acceptance and commissioning of eye plaques. Plastic scintillator systems for eye plaque dosimetry are not commercially available and not simple to build and calibrate.

Regarding the novel ^{125}I eye plaque project, the author discussed with its inventor Dr. Munro the possibility of re-activating the second prototype in a nuclear reactor and repeating its dosimetric measurements to test the hypothesis that these plaques can be re-activated and re-used. It would also be interesting to further test the collimator idea using the new thin unlaminated films.

Recently, BEBIG created their own line of COMS plaques for customers outside of the U.S. Based on examination of two plaques of 16 mm and 20 mm diameters, these appear to be fabricated with a much higher quality than Trachsel's plaques utilized in this work. BEBIG makes only the five classic COMS plaques with diameters 12 mm, 14 mm, 16 mm, 18 mm, and 20 mm per the exact geometrical COMS specifications. However, the gold alloy backing has a different material composition than Modulay, consisting of 86% gold, 11.5% platinum, and the remaining 2.5% composed of zinc, iron, rhodium, and indium. The seed carrier insert is made from an unspecified biocompatible silicon. It is not clear if BEBIG's COMS eye plaques result in the same

dose reduction as Trachsel's COMS plaques, given the different material compositions. Therefore, it would be important to test dosimetrically the BEBIG manufactured COMS plaques.

If 3D imaging such as, high resolution CT, MRI and 3D ultrasound, becomes available for use in eye plaque treatments, treatment planning using dosimetric data acquired in the commissioning process of eye plaques may become a reality.

7. Appendix 1.

The accurate dosimetry methods, techniques and results as applied to [106]Ru eye plaques are described in the published article[42] below. The references in the article have double numbering; the numbers as they appear in the journal are shown in red, while the numbers shown in black are the running reference numbers of this dissertation.

15 Years of [106]Ru Eye Plaque Dosimetry at Memorial Sloan-Kettering Cancer Center and Weill Cornell Medical Center Using Radiochromic Film in a Solid Water Phantom

Samuel Trichter, Department of Radiation Oncology, New York - Presbyterian Hospital, Weill Cornell Medical Center, New York, NY 10065, email sat9014@nyp.org

Christopher G. Soares, Duluth, MN 55805

Marco Zaider, Department of Medical Physics, Memorial Sloan-Kettering Cancer Center, New York, NY 10065.

J. Keith DeWyngaert, Department of Radiation Oncology, New York - Presbyterian Hospital, Weill Cornell Medical Center, New York, NY 10065.

Larry A. DeWerd, Department of Medical Physics, School of Medicine and Public Health, University of Wisconsin-Madison, Madison, WI 53705

Norman J. Kleiman, Department of Environmental Health Sciences, Mailman School of Public Health, Columbia University, New York, NY 10032

Abstract

Purpose: ^{106}Ru eye plaques are widely used for treatment of intraocular malignancies, providing a good alternative to enucleation. Due to past dosimetric uncertainties, we routinely perform our own hospital-based acceptance testing and commissioning of ^{106}Ru eye plaques using radiochromic film as recommended by ISO standard 21439:2009 "Clinical dosimetry-beta radiation sources for brachytherapy". A Solid Water "eye" phantom with several novel features and related tools were developed for accurate radiochromic film dosimetry of eye plaques.

Methods: The phantom enables full 3D dosimetric characterization of eye plaques. Films perpendicular to the central axis of the eye plaques are sandwiched between inserts in the phantom. Small holes in the phantom inserts enable marking the films with respect to the eye plaques, assuring exact geometrical co-registration. Special thin unlaminated radiochromic films were utilized, enabling dosimetric measurements virtually at the surface of the eye plaques. Precise film punches were developed in order to cut films with diameters as small as 8.5 mm and make cutouts in films without damaging the cut edges. The dosimetry method was validated using a silicon diode in a water tank and cross-calibrating one CCX type plaque with the U.S. National Institute of Standards and Technology (NIST).

Results: Full dosimetric characterization of three CCX type and partial characterization of a CIA type ^{106}Ru eye plaques is presented. Replicate film results were reproducible to within 4% - 5%. Even 4% non-uniformities in planar dose rates were easily detected. While the quality of post 2002 plaques has substantially improved, the central axis dose rates were found 6% - 11.4% lower than the manufacturer's data for two CCX plaques. The active area of one of the post 2002 plaques ends 1.25 mm from the rim vs. expected 0.75 mm. Dosimetric hot spots were found near the rim of another of the post 2002 plaques. Comparison with recent Monte Carlo calculations of ^{106}Ru

plaques by Hermida-López, Med. Phys. 40 (10), 2013 found good agreement along the central axis, but some lateral differences were found possibly due to construction variations of actual plaques.

Conclusions: Accurate and precise ^{106}Ru eye plaque dosimetry was achieved utilizing radiochromic film in the phantom introduced here. Co-registration of eye plaques and films permits not only precise treatment planning calculations along the central axis of the plaque, but also accounts for dosimetric non-uniformities using 2D or 3D methodologies. Dose measurements on the inner surface of the plaques provide precise assessment of the scleral dose, its homogeneity, and the active area of the plaques for coverage determination. With proper film calibration and irradiation geometry the technique can also be used for dosimetry of ^{125}I eye plaques.

Key words: eye plaques, radiochromic film, film dosimetry, brachytherapy dosimetry, ^{106}Ru

1. Introduction

Intraocular malignancies, although infrequent, are life threatening and may cause loss of vision. The two main kinds of primary intraocular tumors are choroidal melanomas and retinoblastomas, with approximately 2,500 new choroidal melanoma cases and 250 new retinoblastoma cases diagnosed annually in the U.S[12]. Historically the treatment consisted of enucleation of the eye, however with the advent by Stallard[23] in 1961 of temporarily-applied episcleral eye plaques made of ^{60}Co foil, radiation therapy for intraocular tumors has become a viable alternative to enucleation. Eye plaques provide good local control and survival rates similar or better than enucleation, and in many cases preserve vision[3-66, 8, 9, 11].

A range of mechanical designs and isotopes have been used for eye plaques since their invention, but currently the majority of eye plaques employ either ^{125}I in the Collaborative Ocular Melanoma Study (COMS) design described by Chiu-Tsao[7,831, 39] or beta emitting ^{106}Ru eye plaques

introduced by Lommatzsch in 1964[97] and manufactured by Eckert & Ziegler BEBIG GmbH, Berlin, Germany. The COMS plaques are most commonly used in the U.S., while ^{106}Ru eye plaques are the most popular in Europe. COMS plaques are assembled from ^{125}I brachytherapy seeds, have localized hot spots and are 2.75 mm thick[839], causing patient discomfort. ^{106}Ru eye plaques are made of pure silver (Ag 99.99%) in the shape of a section of a hemisphere with an inner radius of 12 to 14 mm, which conforms to a typical human eye. They have a continuous layer of encapsulated radioactive material and are just 1 mm thick, offering greater patient comfort. A 0.2 mm thick silver foil with a thin film of electrolytically deposited radioactive material is encapsulated between a 0.1 mm thick silver foil window and 0.7 mm thick silver backing, which absorbs approximately 95% of the beta radiation posterior to the plaque as reported by BEBIG and given in ISO International Standard 21439:2009[1041].

As a beta emitter, ^{106}Ru/^{106}Rh provides better protection to critical parts of the eye due to a more rapid dose fall-off. On the other hand, this feature limits ^{106}Ru eye plaques to treatment of tumors with apical heights no higher than 5 mm. The sharper dose gradients, however, require precise treatment planning based on accurate dosimetric information. Due to the design of ^{106}Ru eye plaques they can be commissioned for use only by dosimetric measurements and are prone to dosimetric non-uniformities due to potential thickness variations of the radioactive layer and silver window. BEBIG, the manufacturer of the eye plaques, provides absolute central axis dose rate and relative surface dose rate normalized to the central axis measured using a plastic scintillator dosimetry system. Prior to May 1, 2002, BEBIG provided these measured dosimetric data for each eye plaque with a stated uncertainty of ±30% (k=2) using a scintillator with a diameter of 2.0 mm and height of 2.0 mm calibrated using ASMW standard of the former German Democratic Republic. Dosimetric results were delivered for only 4 points on the central axis and 9 surface dose

points on a circle for small plaques or 17 surface dose points on two concentric circles for the large plaques. Attempts by medical physicists to further reduce this uncertainty and to perform quality assurance measurements reported dose rate disagreements between -37% and +74% from the data supplied by the manufacturer for 8 out of 14 tested applicators[11][72] using a plastic scintillator system as well as up to -110% found in our measurements[12][75] using radiochromic film in a Solid Water phantom as reported in this work. Non-uniform dose distributions with off-axis hot and cold spots were reported using TLDs[13,14][66,68] and radiochromic film dosimetry in a Solid Water phantom[12,15][73,75]. A variety of methods were employed for ^{106}Ru eye plaque dosimetry, including but not limited to TLDs[13,14][66,68], p-type silicon diode[16][67], extrapolation chamber[15,17][73,160], plastic scintilators[11,15,18][69,72,73], radiochromic film dosimetry[12,15,19,20][71,73,75,78], BANG gel[21][161] and liquid scintillator[20][78]. Soares *et al*[15][73] did a cross comparison of eight measurement methods using planar and concave applicators. Due to the high dosimetric uncertainties ^{106}Ru eye plaques prescription protocols did vary widely from institution to institution. This observation may explain why a comparison of various studies reported, that the "optimal apical and scleral doses have not yet been found"[22][87].

Starting May of 2002 BEBIG introduced a small plastic scintillation detector with a diameter of 1.0 mm and height of 0.5 mm calibrated by the U.S. National Institute of Standards and Technology (NIST), which improved the uncertainty to ±20% (k=2)[23][81]. BEBIG published conversion factors from the old ASMW dosimetry to the new NIST calibrated dosimetry[23][81] in form of ratios between the two techniques. For the smaller plaques like the CCX type presented in this work the ratios were as high as 2.06, since dosimetry of these small plaques has proved notoriously difficult. Dosimetric data was provided for 11 central axis points and 33 surface points. At the same time BEBIG introduced improved manufacturing processes, but a recent

publication[24162] however still reported source non-uniformities of 13 – 20%. Following the 2002 NIST calibration ^{106}Ru eye plaque dosimetry was extensively reviewed by ICRU 72[25121], Netherlands Report on Beta Dosimetry[26163] and ISO Standard 21439:2009[1041]. The latter standard while not excluding other methods, selected as recommended methods for beta dosimetry radiochromic film, plastic scintillators, silicon diodes and TLDs. Measurements by Kaulich *et al*[2774] using plastic scintillators, Heilemann *et al*[24162], as well as our measurements presented in this work using radiochromic film demonstrated substantial improvement by the manufacturer of the eye plaques post 2002 NIST calibration. While improved plastic scintillation systems[28, 29164, 165] enable fast and precise eye plaque dosimetry, they are not available commercially and not easy to build and make more sense for institutions using large numbers of ^{106}Ru eye plaques. The silicon diode[1667] remains a good reliable method for central axis dosimetry and can be used for validation of other methods[12,2475, 162], however radiochromic film still is a good choice for multidimensional eye plaque dosimetry for institutions using limited numbers of ^{106}Ru eye plaques. Development of new films, like EBT3 used by Heilemann *et al*[24162] and special thin EBT1 and unlaminated EBT3 presented in this work enable full dosimetric characterization of eye plaques in a matter of days as opposed to weeks using older HD-810 and MD-55-2 film models.

In addition to the absolute dose calibration and dose uniformity, there is a question of dosimetric coverage close to the rim of the plaque. In the past BEBIG has shown in the applicator drawings that the radiation coverage ends 0.6 – 0.75mm from the rim of the plaque for most eye plaques. The most recent manufacturer's User Manual[3030] states an inactive border of 0.75 mm for most eye plaques, and there are also several types not discussed here with larger inactive areas; thus this inactive border has to be verified by measurement as part of the commissioning process. Taccini *et al*[1971] found that in the region 1 mm from the rim of the plaque, the dose decreases to

less than 40% of the uniform value. Barker *et al*[3188] report a higher than anticipated number of local tumor recurrences when using [106]Ru eye plaques and suggest adding a 3 mm margin to the tumor size when selecting the plaque, which may indicate insufficient coverage close to the rim of the plaque.

The recently published Guidelines by AAPM and GEC-ESTRO on the use of innovative brachytherapy devices and applications[3289] state that [106]Ru eye plaques have to be dosimetrically calibrated by the clinical medical physicist prior to clinical use. There are currently no primary calibration standards in the U.S. for these plaques, and thus, there is no ADCL calibration available. Therefore, [106]Ru eye plaques need to be individually commissioned dosimetrically.

This work focuses on a radiochromic film dosimetry technique, which we developed in 2001 prior to NIST calibration of [106]Ru eye plaque dosimetry[1275], in order to provide accurate dosimetric information for treatment of patients. The technique was continuously developed, refined and used by us over the last fifteen years not only for [106]Ru eye plaques, but also for ^{125}I plaques dosimetry, including a large 20 mm COMS plaque; the ^{125}I plaques dosimetry will not be discussed in this work in the interest of brevity. A small silicon diode in a water tank similar to the one used by Lax[1667] was used in the initial stages of this project for comparison with the film results as a secondary check. In addition, a cross-calibration comparison of the same [106]Ru eye plaque between our measurements and NIST was performed and found in good agreement. The results of the comparison were used by Kirov *et al*[2078] for validation of the liquid scintillation dosimetry technique.

Since the use of [106]Ru eye plaques is very limited in the U.S. and between 2007 and 2011 the manufacturer did not deliver these plaques to the U.S., full dosimetric characterization was done only for eight eye plaques, six of which belong to the CCX type, which was of special interest

at our institutions for treatment of retinoblastoma in small children. The results of dosimetric measurements of three CCX type [106]Ru eye plaques are reported here to demonstrate the technique and to publish experimental data on this type of eye plaques, since Hermida-López[33,79] attempting to compare Monte Carlo simulations to experimental results could find in the literature only our own very old results of a CCX eye plaque[20,78]. In addition brief results of a CIA type plaque are presented in order to demonstrate dosimetric data of a plaque with a cutout and point out a potential treatment problem.

2. Materials and methods

2.1. Solid Water "eye" phantom

A Solid Water "eye" phantom was constructed from Gammex 457 Solid Water™ (Gammex, Middleton, WI, Sun Nuclear Corporation) water-equivalent plastic. Solid Water, a composition developed by Constantinou[34,166] as an optimal material for calibrations of photon and electron beams is the most frequently used water equivalent solid material for in-phantom brachytherapy dosimetric measurements[25,121]. Its density of ~1.04 g/cm^3 is very close to that of water, so it has been suggested to be used for beta dosimetry[10,25,41, 121]. Solid Water is delivered as slabs and may have non-uniformities within the slabs, which can be detected with radiography. The slab used to manufacture the "eye" phantom developed in this work was radiographed prior to creating the phantom and was found to be uniform. The central part of the phantom mimics the main dimensions of a human eye, which has a surface curvature with a radius of approximately 12 mm. The typical eye dimensions are 24.2 mm transverse horizontal x 23.7 mm sagittal vertical x 22.0 – 24.8 mm axial anteroposterior[35,65]. The cross section of the phantom with a CCX [106]Ru eye plaque is shown in Figure 1. The phantom consists of a 20 mm high cylindrical body and a 10 mm high cylindrical cap with an outer diameter of 50 mm. The inside diameter of the cylindrical body is 30

mm, enabling the use of films with a maximum diameter of 30 mm. This dimension is sufficient for measuring the dose to any part of the eye and its close surroundings. The cylinder is filled by Solid Water cylindrical inserts with thicknesses of about 1 mm, 2 mm, and 5 mm. The film is sandwiched between the inserts perpendicular to the central axis of the plaque. Various combinations of inserts enable positioning of films from ~1 mm to almost 19 mm from the inner concave surface of the plaque. The space between the concave surface of the plaque and the top cylindrical insert is filled with parts shaped as segments of a hemisphere, which enable placement of smaller diameter films perpendicular to the central axis of the plaque as close as 1 mm from the plaque's surface along the central axis. Sufficiently thin and flexible films can be made to conform to the curved surface of the plaque, enabling measurements a few μm from the inner surface of the plaque, limited only by the thickness of the active layer of the film.

Several parts of the phantom, which are in direct contact with the eye plaque, are manufactured in a way which assures a tight fit without air gaps. Each type of eye plaque needs this tight fit in order to achieve precise and reproducible positioning of the eye plaque with respect to the phantom and to the film. The cylindrical cap, which is the upper part of the phantom, has an inside opening in the shape of the outside of the plaque (imprint of the plaque) and is designed to hold the plaque tightly in place. Thus the plaque position is fixed with respect to the films for the duration of the measurements.

The design of the phantom enables co-registration between the plaque and the films which allows not only measuring 2D dose distributions in the plane of the film, but reconstruction of 3D dose distributions from a set of films irradiated in planes perpendicular to the central axis of the plaque. This configuration enables accounting for dosimetric source non-uniformities during

treatment planning. In order to better understand the co-registration feature, the top view of a cylindrical insert with a CCX [106]Ru eye plaque placed within the phantom is shown in Figure 2.
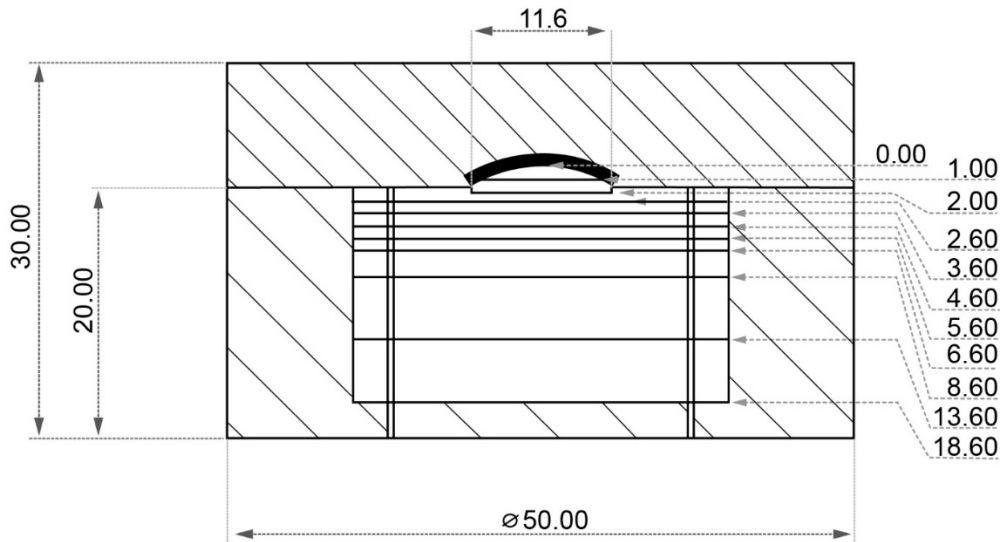
Figure 1. Cross section of the Solid Water "eye" phantom shown with a CCX [106]Ru eye plaque (all dimensions in mm).

The cylinder housing the inserts and films has two key structures (Solid Water pins) to hold the inserts in fixed positions, while the inserts and films have appropriate cutouts. This design assures that the disks and films are always placed in the same position, i.e. effectively eliminating the rotational degree of freedom of the disks and films, which is important for co-registration between the plaque and films.

Each insert has four holes located on its periphery, as can be seen in Figure 2. The holes have 1 mm diameters, are located in fixed positions with respect to the eye plaque, and are coincident for all inserts. A thin needle inserted through the holes is used to make marks on the film. Three holes are used to co-register the film and plaque. During film analysis these three marks enable creation of two perpendicular lines in the film plane (coordinate axes X and Y) which pass

through the film center. The intersection of axes X and Y coincides with the central axis Z of the plaque. The fourth hole is necessary in order to know which side of the film faced the plaque. The cylindrical inserts which are close to the eye plaque have holes or openings to accommodate the suture lugs of the plaques.
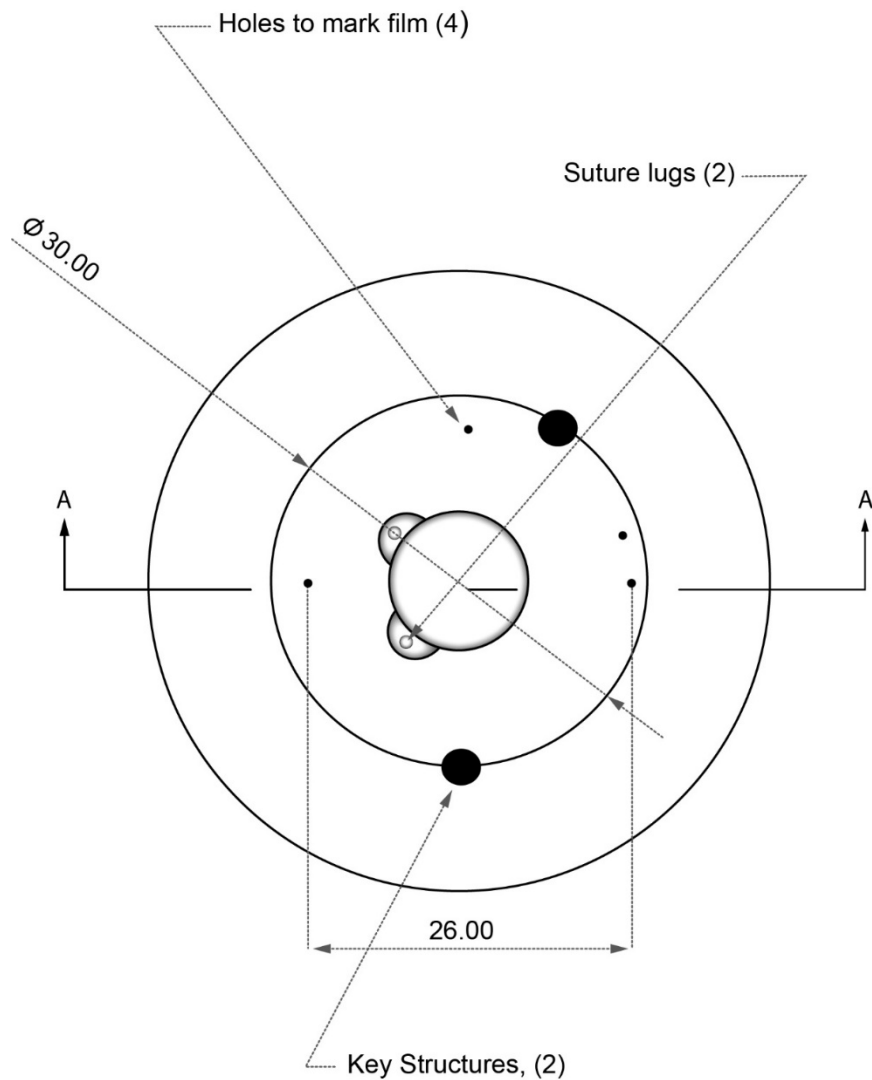
Figure 2. Top view of an insert of the "eye" phantom with a CCX [106]Ru eye plaque, inserted into the phantom, showing the key structures (Solid Water pins), and holes for marking the films (all dimensions in mm). The key structures are solid black for visibility. A – A marks the cross-section shown in Figure 1.

The disassembled Solid Water "eye" phantom and some of its various inserts are shown in Figure 3 along with a CCX [106]Ru eye plaque and an exposed unlaminated EBT3 film. The key structures can be seen inside the phantom's body, while the openings for the key structures as well as the holes for marking the films are clearly visible in the inserts and the irradiated film.
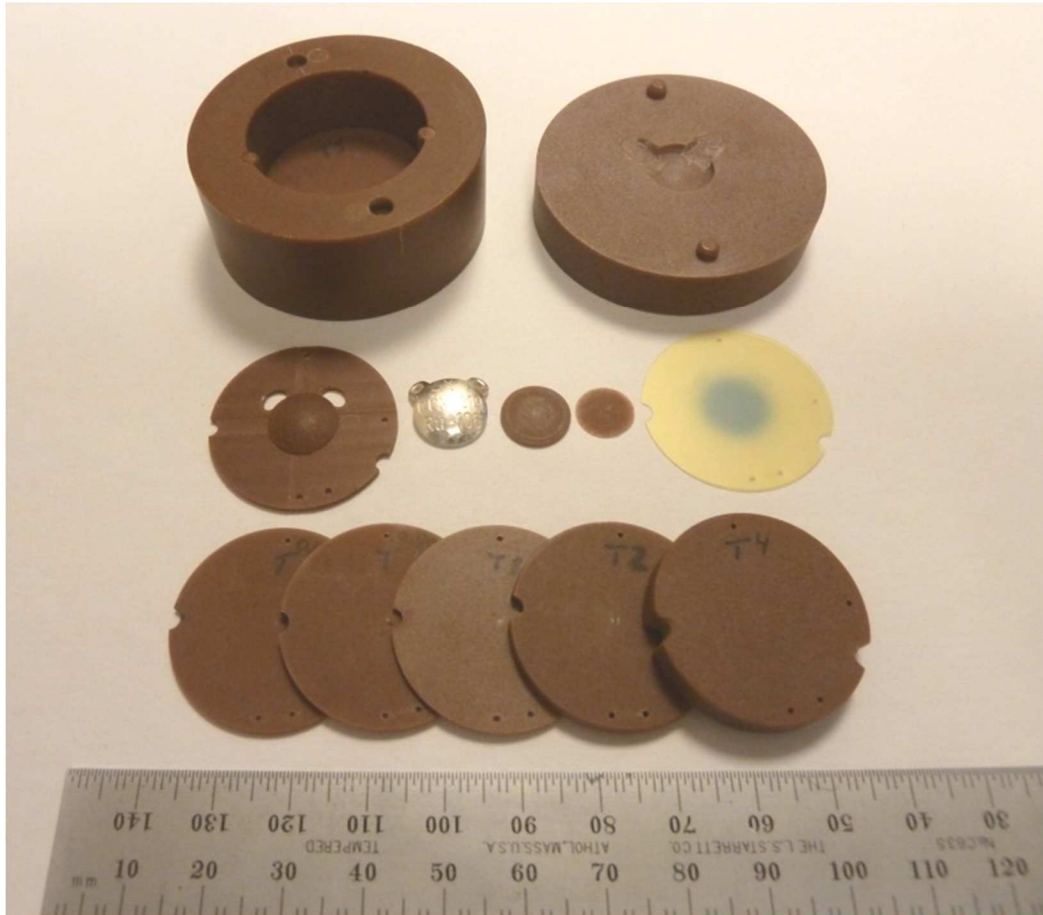
Figure 3. Solid Water "eye" phantom with its various inserts, a CCX [106]Ru eye plaque and an irradiated unlaminated EBT3 film.

While the design of the phantom enables performing measurements on any type of an eye plaque, measurements of photon sources like ^{125}I require placement of the loaded phantom into an appropriate scatter phantom, since the photon scatter contribution to the absorbed dose for ^{125}I can be as high as 38%[36][106]. For ^{106}Ru eye plaque measurements the assembled phantom with the film and eye plaque was first inserted into a 5 cm diameter cylindrical hole at the center of a 30 cm x 30 cm x 3 cm Solid Water slab which was on top of a 5 cm thick Solid Water slab and covered by another 5 cm thick Solid Water slab. The main goal of this measurement setup was to assure that the phantom with the eye plaque and film were kept together for the duration of the measurement, as well as creating consistent scatter conditions, even though the phantom alone provided sufficient scatter conditions, as was tested with and without the additional scatter phantom.

2.2. ^{106}Ru eye plaques

The phantom was used to dosimetrically characterize ^{106}Ru eye plaques belonging to CCX, CCA and CIA types. The CCX has a diameter of 11.6 mm and internal height of 1.3 mm and belongs in terms of its dimensions to the smallest plaque types manufactured by BEBIG. It is of special interest for treatment of retinoblastoma in small children. The CCA has a diameter of 15.3 mm and internal height of 2.3 mm, while the CIA designed for treatment of ciliary body melanomas[30][30] has the same dimensions as the CCA, but has a cutout in order to avoid radiation to the iris. Results of CCX 55, CCX 129, CCX 219, and partial results of CIA 156 plaques are reported in this work. The three digit number after the plaque type is its serial number.

^{106}Ru /^{106}Rh emits beta-radiation with a maximum energy of 3.541 MeV, as well as 20% 0.512 MeV, 10% 0.622 MeV, 1.6% 1.05 MeV, 0.4% 1.13 MeV, and 0.2% 1.55 MeV gamma radiation per decay[10][41]. Bremsstrahlung is also present. The main contribution to the therapeutic dose comes

from the beta radiation[3762]. The half-life of the parent isotope is 373.59 days[1041]. Each ^{106}Ru eye plaque measured in this work has two suture lugs used to attach it to the sclera.

2.3. Radiochromic film

All radiochromic films used in this work were GAFCHROMIC™ films manufactured and provided by International Specialty Products (Wayne, NJ), now Ashland (Covington, KY). The thickness and construction of the film are very important for eye plaque dosimetry and particularly dosimetry of beta emitting ^{106}Ru eye plaques with dose gradients of ~30%/mm, especially in the proximity of the concave surface of the plaque. The dosimetric measurements of the CCX 55 eye plaque were done using MD-55-2 film Lot #I1215. This was a film consisting of two active layers separated and covered by adhesive and transparent polyester layers for a total of seven layers as described by Soares *et al*[38113]. A 30 Gy dose to the film was required in order to achieve an optical density of at least 0.5, which resulted in irradiation times between a day and a week per film, depending on the film distance from the plaque's surface. The dosimetric measurements of the CIA 156 plaque were done using EBT film Lot # 34141 2x2IL. The construction of EBT film is shown in Figure 4-a. This was still a relatively thick film consisting of five layers, but required only 200 cGy for optical density of about 0.5. The construction of the EBT film enabled the closest measurement at 117 μm from the eye plaque surface, which is the middle point of the film, but this thickness and design make the film rather rigid and hard to bend to the radius of curvature necessary to measure the dose close to the surface of an eye plaque. Importantly, no other dosimeter, including TLD's, plastic scintillators, or semiconductor diodes, can measure the dose closer than about 0.5 mm - 1.0 mm from the surface of the plaque due to geometrical and mechanical limitations, forcing one to rely on extrapolated values for determination of the scleral dose. For ^{106}Ru eye plaques the central axis surface dose was reported by the manufacturer in the

plaque certificates until 2014 extrapolated from plastic scintillator measurements the closest of which was 0.6 mm from the surface. Currently, the manufacturer measures the dose rate as close as 0.48 mm from the surface and has eliminated the extrapolated surface dose from the plaque certificates, but provides it to customers upon request (private communication with BEBIG). For these reasons, International Specialty Products created for this work special thin radiochromic film, referred to here as EBT1 and shown schematically in Figure 4-b. It consists of half of the regular EBT film shown schematically in Figure 4-a. In this film the active layer is covered just by 3 μm of protective coating on one side. This film, due to the lack of the thick polyester layer is very flexible and therefore permits direct contact of the active layer of the film with the eye plaque surface for surface dose measurements. This EBT1 film Lot# 35314-4H was used for dosimetric characterization of the CCX 129 [106]Ru eye plaque.
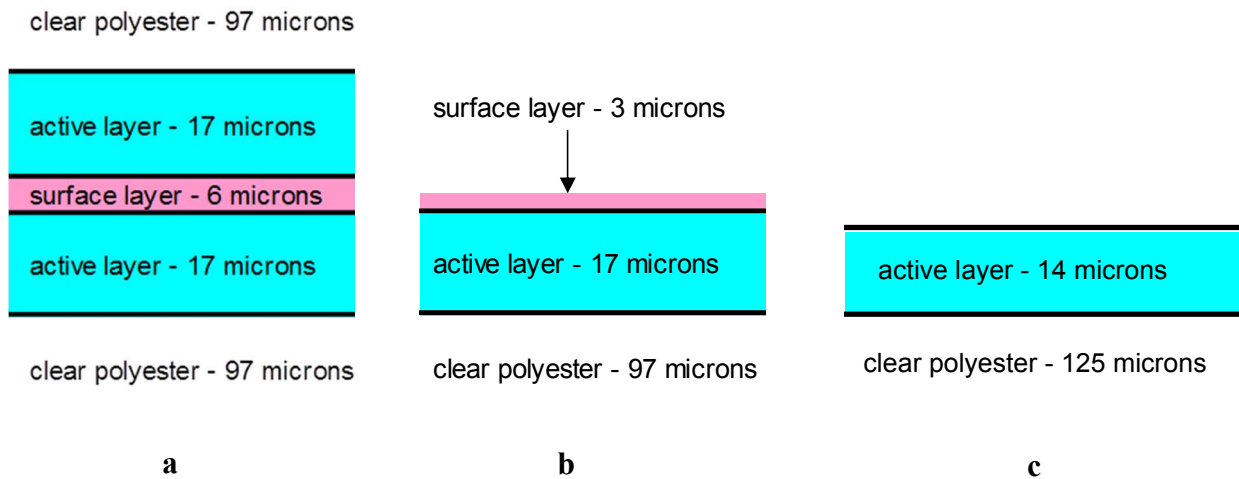
Figure 4. **a -** structure of EBT film, **b -** structure of special thin EBT1 film, **c -** structure of unlaminated EBT3 film.

The CCX 219 eye plaque was characterized using the new commercially available unlaminated EBT3 film Lot#02171601, which consists of a 125 μm thick clear polyester substrate and a 14 μm thick active layer without any protective coating as shown in Figure 4-c.

These thin films enable dosimetric measurements virtually at the surface of the eye plaques providing the doses to the outer sclera, which are an important factor in prescribing the treatment, since the sclera is considered a critical organ when prescribing to the apex of the tumor or is used by some institutions which want to deliver a minimum dose to the tumor base as the prescription point. In addition, measurements on the plaques surface also provide information on the radiation field fall-off at the rim of the plaque for proper plaque selection. The surface dose measurements also provide a good idea of the source non-uniformity, which causes dosimetrically hot and cold spots on the sclera and affect the doses delivered to the tumors and critical structures of the eye, but in this work we did not attempt covering the whole internal concave surface of the eye plaque with film, instead using planar films perpendicular to the plaques' central axis for determination of source non-uniformity, as permissible in accordance with ISO Standard 21439:2009[1041].

2.4. Preparation and handling of the appropriate sizes and shapes of films

Eye plaque dosimetry using our "eye" phantom required precise cutting of round films with diameters as small as 8.5 mm or thin strips, which could be placed on the plaques' concave surface, without separation of layers of the film and without rough edges, which could create air gaps between the films and the inserts of the phantom. A set of unique punches based on precise instrument dies custom made by Dayton Lamina Corporation (Dayton, OH) shown in Figure 5 was created by the instrument shop of Memorial Sloan-Kettering Cancer Center for this purpose. The punches enabled us to cut films of any size and shape even with the special cutouts to accommodate the key structures of the "eye" phantom without damaging parts of the film and

leaving clean flat edges. The direction of the coating was marked on each film prior to cutting, since it has to be controlled in the scanning process.

Figure 5. Special film punches.

GAFCHROMIC™ films have a certain degree of moisture content which necessitates equilibration to the environment[38][113]. From our experience, if the films are cut immediately prior to measurements, the moisture content can change the readout optical density by as much as 10% and result in non-uniform areas on the film. Thus, films used for calibration and eye plaque measurements were pre-cut at least several days prior to measurements to enable the films to equilibrate with the environment. Each cut film was kept in a separate light-tight paper envelope until irradiation and subsequent scanning.

2.5. Film calibration and scanning

For calibration of MD-55-2 film used for dosimetry of the CCX 55 plaque, 17 2 cm x 2 cm films with marked direction of coating were irradiated to doses between 20 cGy – 5000 cGy using a ^{60}Co machine as recommended by TG-55[39][98] for electron dosimetry. The TG-55[39][98]

recommendation is based on comparison of film calibrations using well- characterized ^{60}Co gamma-ray beams and ^{90}Y beta particles. The agreement between both calibrations can be explained since the dose in ^{60}Co beams in condensed media is being mainly imparted by secondary electrons with an energy spectrum similar to the beta particles of both ^{90}Sr/^{90}Y and ^{106}Ru/^{106}Rh. Any differences would be negligible. Moreover, as was shown by Monte Carlo calculations[40103], the restricted mass collision stopping power ratios and ratios of mass-energy absorption coefficients for the sensitive materials in radiochromic films relative to water are almost constant in the energy range of interest in this work between 100 KeV and 6 MeV. Therefore the film response to ^{106}Ru eye plaques as well as to calibration energies used in this work can be assumed energy independent. The films were irradiated in a 30 cm x 30 cm Solid Water phantom at 0.5 cm depth (D$_{max}$) with 10 cm backscatter. For calibration of EBT, EBT1 and unlaminated EBT3 films, a page of film was cut using a precise office paper cutter into 2 cm x 2 cm pieces, while marking at the upper left corner of each piece the coordinate of the piece on the page in form of the row#-column#. The location of the mark in the upper left corner fixed the coating direction of the film, which is important in the subsequent scanning process. For irradiation the pieces of film were randomized to dose levels using the random number generator of Microsoft Excel, thus randomizing possible non-uniformities in the page of film. For calibration of EBT film used for dosimetry of the CIA 156 plaque 22 films were irradiated to doses between 20 cGy and 440 cGy using a ^{60}Co machine. The films were irradiated at the same setup as the MD-55-2 film in a 30 cm x 30 cm Solid Water phantom at 0.5 cm depth (D$_{max}$) with 10 cm backscatter. Since the ^{60}Co machine is not available anymore, both the EBT1 and unlaminated EBT3 films were calibrated using a 6 MeV linac electron beam calibrated in terms of dose to water using TG-51[41145] protocol at the depth of 1.4 cm (D$_{max}$) with 10 cm backscatter in a 30 cm x 30 cm Solid Water phantom

similar to the beam used by Lax[16][67] for calibration of the silicon diode. To calibrate the EBT1 film batch, 19 films were irradiated in 40 cGy increments up to 600 cGy and in 100 Gy increments between 600 cGy – 1000 cGy. To calibrate the unlaminated EBT3 film batch 21 films were irradiated to doses 30 cGy – 600 cGy in 30 cGy increments.

All irradiated films along with unexposed films defining the background pixel value were scanned either 24 or 48 hours after the end of irradiation in order to let the polymerization process stabilize and have all films scanned at the same level of post-exposure growth[39][98]. The MD-55-2 Lot #I1215 films were scanned 48 hours after irradiation using an AGFA ARCUS II flatbed scanner (Agfa-Gevaert N. V., Mortsel, Belgium) with a red acetate filter[42][120] and RIT113 Film Dosimetry software (Radiological Imaging Technology, Inc., Colorado Springs, CO). The EBT films Lot # 34141 2x2IL used for dosimetry of CIA 156 plaque were scanned 24 hours after exposure using a Vidar VXR 16 Dosimetry Pro 16 bit film scanner (Vidar Systems Corporation, Herndon, VA) at 89 micron resolution and RIT113 Film Dosimetry software with films placed into clear plastic sheet protectors together with a yellow acetate filter. The red channel provides optimal response for GAFCHROMIC film[38][113], but since the RIT software was limited to monochrome (16 bit) scanning, we had to use the red acetate filter for MD-55-2 film[42][120] and the yellow acetate filter for EBT film (as recommended by the company), in order to maximize film response. The EBT1 films Lot# 35314-4H and the unlaminated EBT3 films Lot# 02171601 were scanned 24 hours after exposure using an Epson Expression 1680 flatbed scanner (Seiko Epson Corporation, Nagano, Japan) and EPSON Scan software in 48 bit RGB mode with all filters and image enhancements de-activated, followed by extraction of the red channel. The films were scanned one at a time at resolution of 254 dpi (100 microns pixel size) and saved as TIFF files.

Both calibration and eye plaque films were always placed at the center of the scanner bed. The EBT1 films were lightly attached to the scanner bed using adhesive tape at the edges of the film to avoid Newton ring artifacts. The unlaminated EBT3 films were always flat on the scanner and did not require attachment. Films were scanned in the same portrait orientation with respect to the original sheet of film marked on each film. All CCD scanners suffer from the lateral response artifact[43,44][123, 124] resulting in decreased pixel values (increased measured optical density) toward the lateral edges of the scanner bed, but since the films used in this work were small and always positioned at the same location at the center of the scanner, reader bed positioning corrections were not required[38][113].

Following scanning, and extraction of the red channel when required, the average pixel value of a 1 cm x 1 cm region of interest was measured using the film dosimetry software. Then the calibration curves in the form of pixel values vs. dose were fitted with analytical functions suggested by the curve fitting program CurveExpert Professional software by Daniel G. Hyams, Madison, AL.

2.6. Eye plaque film dosimetry and data analysis

Eye plaque films were irradiated one depth at a time, so that approximately the same dose is delivered to each film, usually around 30 Gy for MD-55-2 film, 200 cGy for EBT film, 200 – 400 cGy for EBT1 and unlaminated EBT3 films, which would produce optical density around 0.5 in the high dose area of the film. All eye plaque films were scanned at the same post exposure time as the calibration films, i.e. 48 hours for the CCX 55 plaque, and 24 hours for all other plaques.

Applying the calibration curve and conversion of the pixel values of the scanned films to dose, as well as the film analysis was done using Memorial Sloan-Kettering Cancer Center's Contour film dosimetry software package, which was customized in order to accommodate requirements of this

work. Since each film was irradiated at different dates and times, the 2D dose distributions were converted to dose rate distributions at a certain reference date and time, using the film irradiation dates and times, and ^{106}Ru decay constants.

The calibration films were exposed in Solid Water to a ^{60}Co beam or 6 MeV electrons calibrated to absorbed dose values to liquid water. The eye plaque films were irradiated in Solid Water; therefore, it is possible to assume that the measured doses are close to doses in liquid water, assuming that both phantoms, the calibration phantom and the "eye" phantom are made from the same kind of Solid Water. While we did not find publications testing the dependence on kind of Solid Water for ^{60}Co, linac and ^{106}Ru energies, Meigooni *et al*[45][135] found that certain batches of Solid Water may have 1.7% calcium content, while other batches may have 2.3% calcium content, and depending on calcium content in Solid Water, Monte Carlo calculated dose conversion factors from Solid Water to liquid water may vary by as much as 5% for ^{125}I. Therefore, exact knowledge of calcium content of the Solid Water is very important. For example, Patel et al.[46][138] performed chemical analysis of Solid Water, finding 1.6% calcium content, in contrast to the manufacturer's stated value of 2.3%. The manufacturer's reported calcium content of the non-certified Solid Water slab used to manufacture our phantom was 2.31%. To verify this, one of the inserts of our phantom was sent for chemical analysis to the same laboratory used by Patel *et al*[46][138] (Analytical Answers, Inc., Woburn, MA). Resultant gravimetric ashing and scanning electron microscopy/energy dispersive X-ray spectroscopy revealed calcium content of 2.32 ± 0.06% consistent with the manufacturer's report. Our calibration phantom consists of certified Solid Water with 2.3% calcium content as well.

2.7. Silicon diode dosimetry

In addition to the primary dosimeter it is important to have a secondary dosimetric system for independent verification of the measurements by the primary system. Lax[1667] successfully used a p-type Scanditronix silicon diode for absolute ^{106}Ru eye plaque dosimetry. A p-type silicon diode, the Scanditronix Stereotactic Field Detector (SFD) model DEB050 (Scanditronix Medical AB, Uppsala, Sweden, currently IBA Dosimetry GmbH, Schwarzenbruck, Germany) in a Scanditronix RFA200 water tank was used for ^{106}Ru eye plaque dosimetry for both, treatment planning of patients and validation of the radiochromic film dosimetry technique.

This diode detector has a 60 µm typical effective thickness of the measurement volume with a 0.6 mm ± 0.1 mm detector diameter, and a distance of 0.61 mm ± 0.15 mm displacement of the effective measurement point from the front surface of the detector. Externally, the detector is a 4.0 mm diameter cylinder which was oriented along the central axis of the eye plaque. The closest measurement point of the diode was 0.87 mm from the inner surface of the plaques due to the concave shape of the plaques and the 4.0 mm diameter of the diode both of which limited how close the diode can come to the surface of the plaque. The eye plaque was attached using Dow Corning High Vacuum grease (Dow Corning Corporation, Midland, MI) to the cap of the Solid Water "eye" phantom placed upside down, and the cap was attached using the same grease to a Lucite base positioned at the bottom of the water tank. The cap was used for this purpose since it had a customized imprint of the particular eye plaque. A special Lucite centering jig was created to assure that the diode was precisely centered on the central axis of the eye plaque and was not displaced laterally from the axis. The arrangement is shown in Figure 6. After setup the Lucite jig was removed for measurements.

For [106]Ru eye plaque dosimetry, the diode was calibrated in a 6 MV linac photon beam in the water tank. This diode dosimetric system was used for the initial [106]Ru eye plaque dosimetry cases, until it became evident that the film dosimetry system provided accurate reliable results.
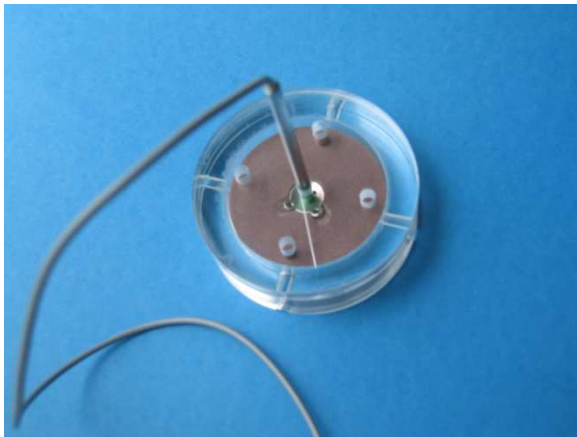
Figure 6. Lucite centering jig for the stereotactic field detector measurement setup shown with a CCX [106]Ru eye plaque in the upside down cap.

3. Results

Dosimetric measurements of CCX plaques S/N 55, 129 and 219, as well as partial results of CIA plaque S/N 156 are reported here.

Dosimetry of the CCX 55 plaque was done using MD-55 film in our Solid Water "eye" phantom, as well as with the Scanditronix Stereotactic diode in the Scanditronix RFA200 water tank. Seven films were irradiated between 1.835 mm to 7.445 mm from the inner surface of the plaque (measured from middle of the film). The use of three digits after the decimal point to define the distance from the plaques does not result from depth measurement with 1μm precision, but from adding the thickness of the phantom parts measured with a micrometer and the distance to the middle of the active layer of the film or to the middle of the film if two active layers are present,

143

calculated from the film specifications provided by the manufacturer. Three films were irradiated at 3.445 mm from the inner surface of the plaque to test reproducibility. The measured central axis dose rates of the three films agreed to within ± 5%. Diode measurements were done on the central axis every 0.5 mm between 0.87 mm and 10.87 mm from the inner surface of the plaque. Depth dose curves measured on the central axis of the plaque using either film or the diode, as well as the central axis depth dose curve provided by BEBIG, are shown in Figure 7. Both techniques – the silicon diode and the radiochromic film dosimetry are in close agreement. The ratio of the dose rate measured using the diode to the dose rate measured using film is 1.06, which is well within the uncertainties (k=2) of our measurements as reported below. The curves demonstrate a major discrepancy between our measurements and manufacturer's data. This plaque was manufactured prior to the 2002 calibration of ^{106}Ru eye plaques at the U.S. National Institute of Standards and Technology (NIST), which became the calibration standard for BEBIG. The ratios of the dose rates on the central axis of the CCX 55 plaque measured in this work and the same ratios measured at NIST for another CCX type eye plaque are shown in Table 1. The ratios measured in this work agree to within 5.5% at the closest point to the plaque and show much better agreement with the NIST measurements further from the plaque. This is considered very good agreement in beta dosimetry, where even for relative dosimetry not accounting for the calibration uncertainty of absolute dosimetry, typically the combined uncertainty (k = 1) is expected to be in the 4 - 7% range[1041].
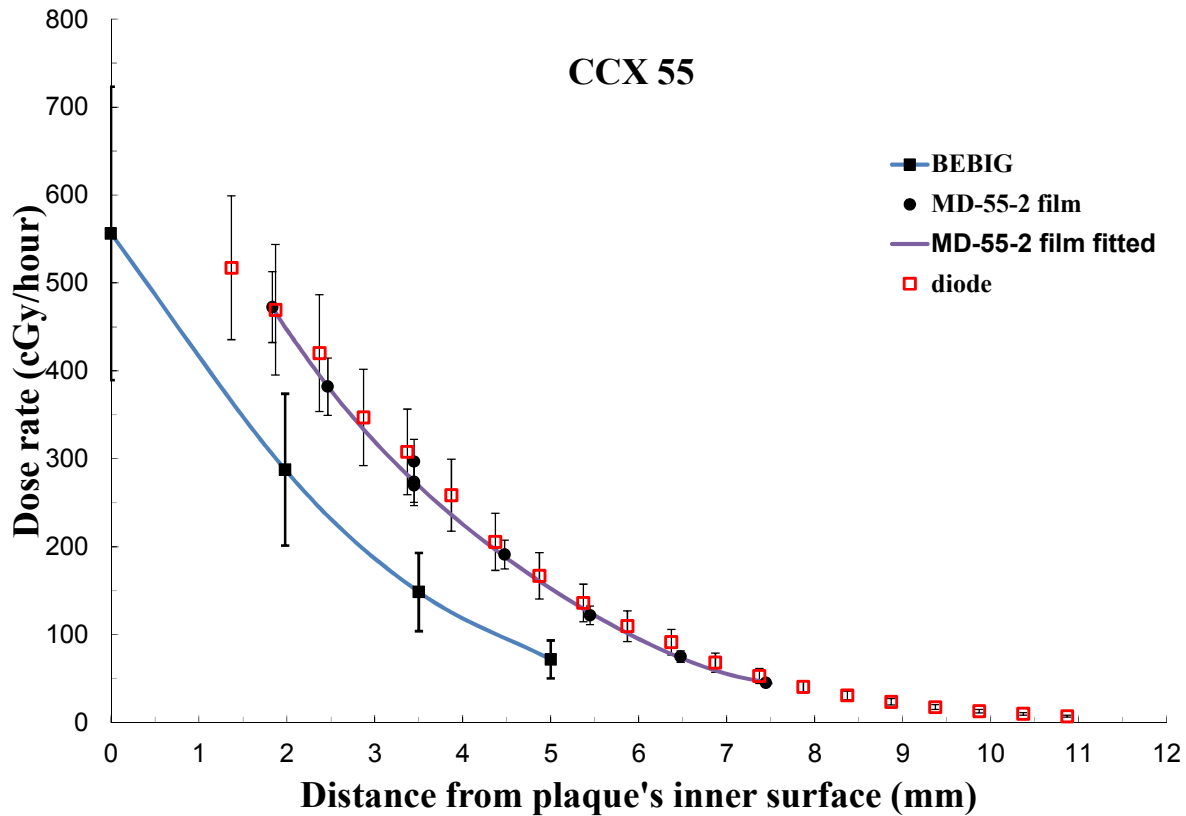
Figure 7. Dose rate along the central axis of the CCX 55 eye plaque.

Distance from plaque	2.0 mm	3.5 mm	5.0 mm
Ratio of our measurements to BEBIG's data	1.55	1.81	2.11
Ratio of NIST's measurements to BEBIG's data	1.64	1.83	2.06
Agreement of our measured ratios with NIST	-5.5%	-1.1%	2.4%

Table 1. Ratios of measurements on the central axis of the plaque to the data provided by BEBIG.

Isodose distributions measured using films at three different depths from the plaque are shown in Figures 8-a, 8-b and 8-c. Each of the films has a hot spot at the same location. The intensity of the hot spot vs. the central axis (CAX) value is ~28% for the 1.835 mm film, ~14% for the 2.465 mm film and ~4% for the 3.445 mm film.
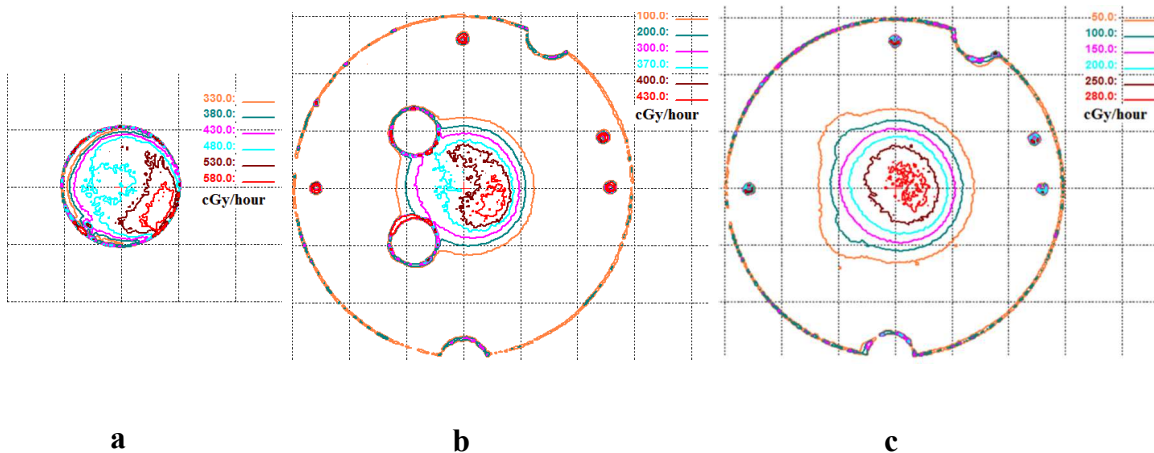
Figure 8. Dose rate in three planes perpendicular to the central axis of the CCX 55 plaque at depths **a** - 1.835 mm 28% hot spot, **b** - 2.465 mm 14% hot spot, and **c** - 3.445 mm 4% hot spot. View from the plaque. 0.5 cm between grid lines.

Dosimetric characterization up to relevant clinical depth of the CCX 129 plaque was done placing films at nine distances between 0.012 mm and 7.632 mm from the inner concave surface of the plaque. Several films at various distances were repeated in order to test reproducibility. Results on duplicate films agree within 4%. Dosimetric characterization of CCX 219 plaque was done placing films at eight distances between 0.007 mm and 6.637 mm from the inner concave surface of the plaque. Several films at various distances were repeated to test reproducibility with agreement between duplicate films within 3%.

Figures 9-a and 9-b display measured dose rate distributions of both plaques and Figures 10-a and 10-b display our measured dose rate on the central axis of both plaques as compared to the data provided by the manufacturer along with fitted curves.
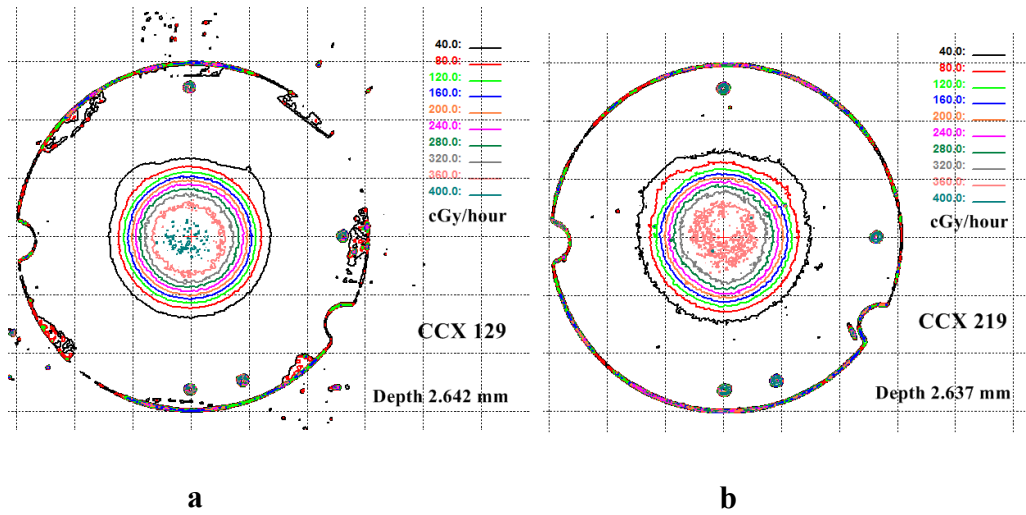
Figure 9. Measured dose rate distribution at **a** - distance 2.642 mm from the inner surface of the CCX 129 eye plaque and **b** - at distance 2.637 mm from the inner surface of the CCX 219 eye plaque. The distributions shown are a view from the plaques. The distance between grid lines is 0.5 cm.
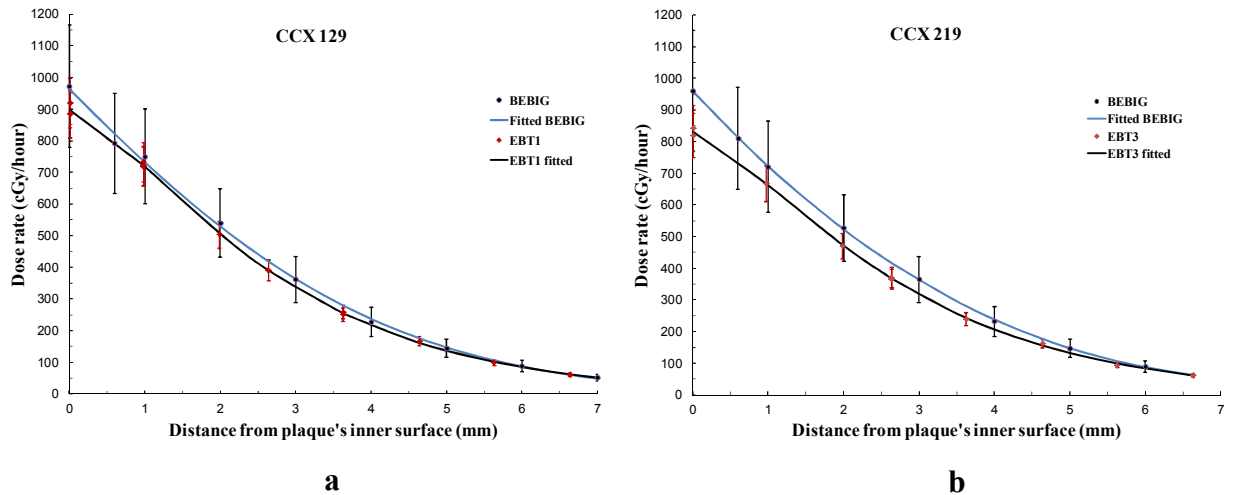
Figure 10. Measured dose rate along the central axis of **a** - the CCX 129 plaque and **b** – the CCX 219 plaque compared to the data provided by BEBIG along with fitted curves.

147

Both dose distributions look uniform and symmetric, without visible hot and cold spots, while the CCX 219 plaque shows wider coverage, which possibly results from manufacturing variations. Its diameter was found to be 11.70 mm as measured by digital Mitutoyo (Mitutoyo America, Aurora, IL) calipers vs. 11.45 mm for the CCX 129 plaque.

The measured central axis depth dose rate of the CCX 129 plaque is on the average 6% lower than the manufacturer's provided data in the first 5.62 mm from the plaque, while the dose rate of the CCX 219 plaque is on the average 11.4% lower at the same 5.62 mm distance. Further away from the plaque the measured dose rate becomes about 1% higher than the manufacturer's. Both results are well within the ±20% (k=2) dosimetric uncertainty stated by the manufacturer, which reflects among others a ±15% (k=2) uncertainty on the NIST calibrations of manufacturer's equipment, as stated in the User Manual of the eye plaques[3030]. These plaques were manufactured ten years apart and during this period the manufacturer's dosimetry system had an additional periodic re-calibration by NIST, as well as replacement of the calibrated plastic scintillator tip. Both could contribute to the dosimetric difference between the plaques, which is accounted for in the stated ±20% (k=2) dosimetric uncertainty.

In order to measure the dose rate near the surface of the plaques, 3 mm wide strips of film were attached to a hemispherical part with the inner diameter of the plaque in either of two perpendicular directions – a radial, where the film was in the middle between the suture lugs or the transverse direction. In both cases the central axis of the plaque passed through the center of the 3 mm film strip. The distance of the measurements from the inner surface of the plaque was taken as the middle of the active layer, as in all other measurements. The EBT1 measurements were 0.012 mm from the inner surface, and the unlaminated EBT3 measurements were 0.007 mm from the inner surface. In addition to directly measuring the surface dose, these measurements enable assessment

of the uniformity of the radioactive layer just under the surface of the plaque, providing a measure of the dose uniformity on the inner sclera and of the coverage in the vicinity of the rim. Obviously, this is just a sample of the total inner surface of the plaques. Profiles through two radial films are shown in Figure 11.

As it can be seen from the profiles in Figure 11, the CCX 219 plaque has wider coverage, actually as already mentioned, and its diameter is 0.25 mm larger than the diameter of the CCX 129 plaque. The CCX 219 plaque also has pronounced hot spots at the edges of the radiation field, which are also visible in the radial profile at depth 0.977 mm, not shown here, but not further away from the plaque.
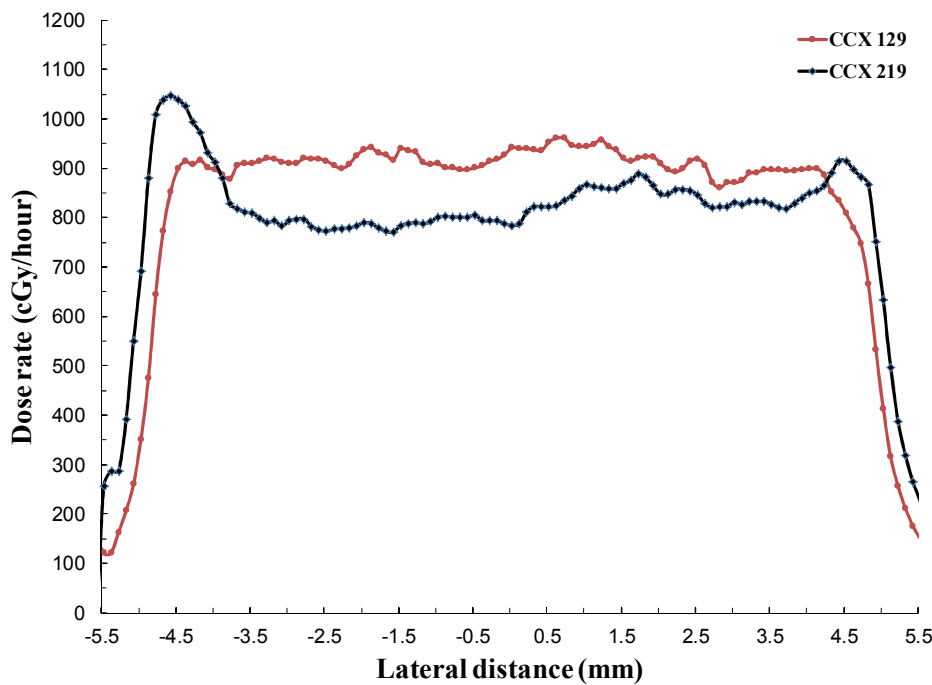
Figure 11. Profiles in the long direction through radially placed on the inner surface of the eye plaques 3 mm wide strips of film.

In order to assess the coverage of the plaques, the length of a circular sector on the inner surface of the plaque passing through the central axis of the plaque was calculated from simple geometry, knowing 12 mm, which is the inner radius of the plaque and 1.3 mm is its the internal height. This length is 11.2 mm. From the profiles in Figure 11, the "flat" area before the dose fall-off starts for the CCX 129 plaque is between -4.5 mm and 4.2 mm, for a total covered area of 8.7 mm, and for the CCX 219 plaque it is between -5.0 mm and 4.8 mm, for a total of 9.8 mm. These are lengths of full radiation coverage, excluding the penumbra. This coverage limitation should be well understood when selecting a plaque for treatment and is another reason to commission the plaques prior to clinical use, since otherwise the tumors will not be fully treated as suggested by Barker *et al*[3188] based on tumor recurrences.

Comparison of our measurements with the Monte Carlo simulations done by Hermida-López[3379] is shown in Figures 12 and 13. In Figure 12 the Monte Carlo calculated dose rate along the central axis of a CCX plaque is compared with the analytically fitted measurements of the CCX 129 and CCX 219 plaques. The three curves are normalized at the depth of 1 mm as done by Hermida-López[3379]. The CCX 129 measured point by point ratio to the Monte Carlo results is on the average 1.00, while the same ratio for the CCX 219 plaque is 1.03. It can be noticed that at the inner surface (0.0 mm depth) the Monte Carlo overestimates the measurement by 5%, while at the next point (0.5 mm depth) the Monte Carlo overestimates the measurement by 2% for both plaques.

In Figure 13 the relative lateral dose rate profiles of CCX plaques calculated by Hermida-López[3379] are compared with measured results of the CCX 129 and CCX 219 plaques.
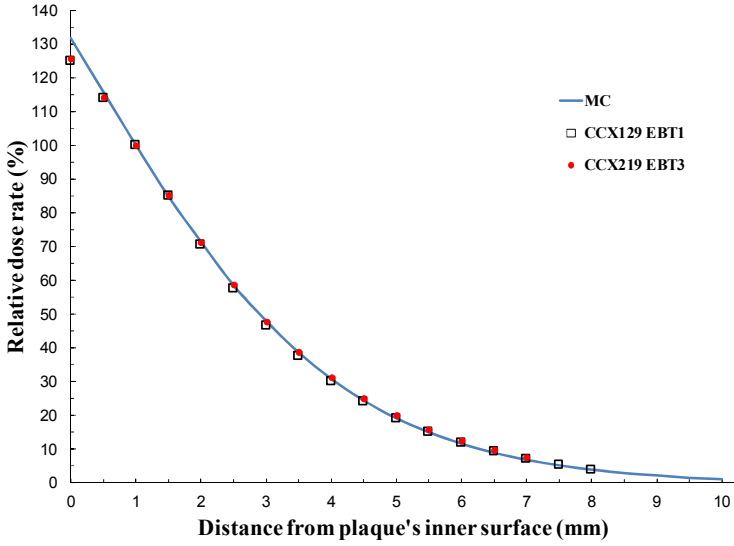
Figure 12. Relative dose rate along the central axis of CCX plaques calculated by Hermida-López[3379] compared with analytically fitted measured results of the CCX 129 and CCX 219 plaques. All curves are normalized at 1 mm depth.
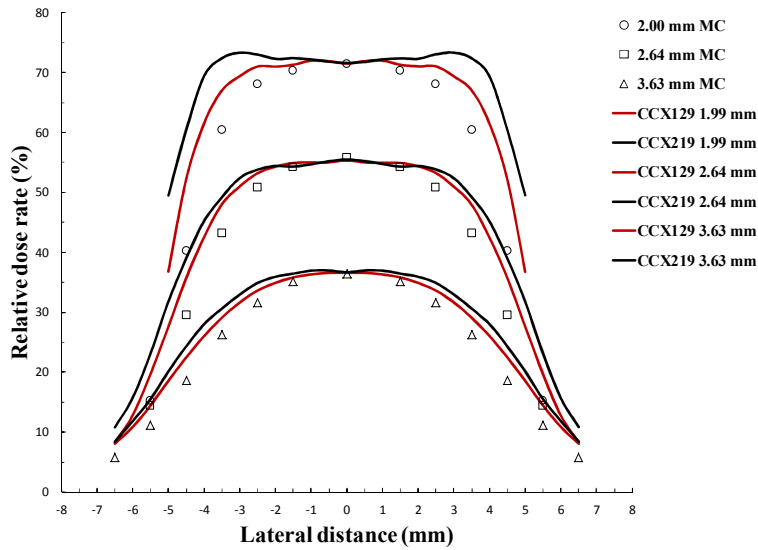
Figure 13. Relative lateral dose rate profiles of CCX plaques calculated by Hermida-López[3379] compared with measured results of the CCX 129 and CCX 219 plaques. All curves are normalized at 1 mm depth.

For this comparison, the experimental 2D dose rate distributions were smoothed using median 9 x 9 filtration prior to deriving the lateral profiles. The median filter replaces the value of each pixel with the median value of a group of pixels surrounding the particular pixel. The resultant profiles were made symmetrical by averaging between the left and right sides of the profile. The Monte Carlo calculations depths coincide with the experimental results only at depth of 2.0 mm. Therefore the lateral Monte Carlo results were interpolated using analytical fits between 2.0 mm and 3.0 mm depth and between 3.0 mm and 4.0 mm depth to enable comparison with the film measurements at depths of 2.64 mm and 3.63 mm. It can be seen from Figure 13 that the Monte Carlo calculations underestimate the width of the lateral profile. It is possible that the differences between the calculated and measured data are due to differences between the ideal plaque used for modelling and the actual plaques. Even the two plaques characterized in this work have a 0.25 mm difference in diameter, which affects the lateral profiles both on the surface and proximal to the plaque. These differences are less pronounced farther from the inner surface of the plaques.

A measured dose distribution of CIA 156 eye plaque is shown in Figure 14-a and a horizontal profile passing through the central axis of the dose distribution on Figure 14-a is shown in Figure 14-b. As can be seen in Figures 14-a and 14-b, the dose distribution of the CIA 156 eye plaque which is typical for eye plaques with a cutout has a maximum which is 23% higher than the dose at the central axis shifted about 3.0 mm laterally from the central axis. On the other hand, the data provided by the manufacturer with CIA eye plaques consists only of the dose rate on the central axis and of the surface dose rates measured at 33 points at a distance 1.0 mm from the inner concave surface. There is nothing in these data explaining or suggesting that there is a maximum shifted from the central axis, and, since most of the end users are using one-dimensional treatment planning on the central axis, part of the eye is being overdosed.
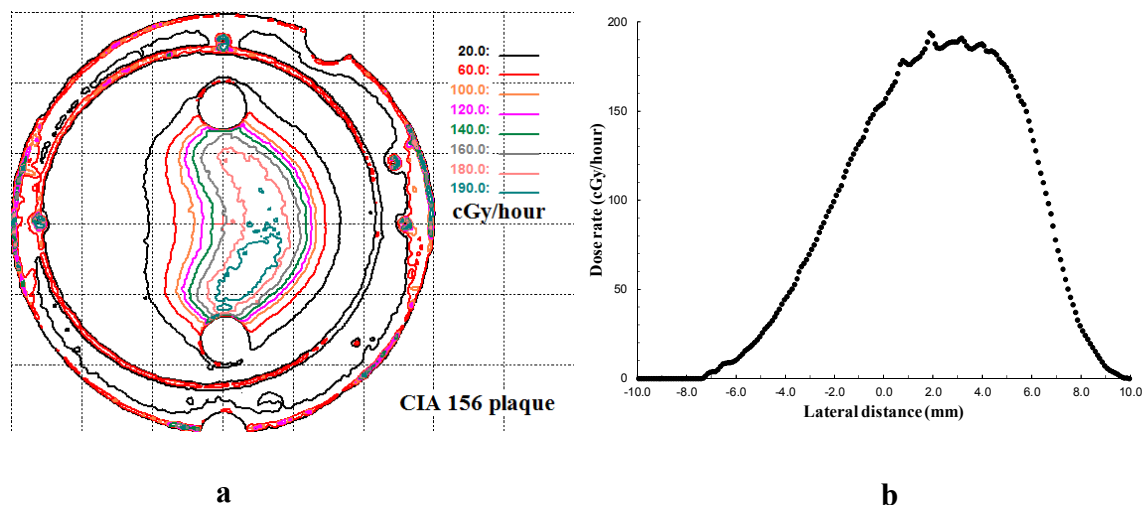
Figure 14. a - measured dose rate distribution at distance 3.505 mm from the inner surface of the CIA 156 eye plaque. The distribution shown is a view from the plaque. The distance between grid lines is 0.5 cm. **b** - horizontal profile through the central axis of the dose distribution of the CIA 156 eye plaque.

4.   Uncertainties

Estimated uncertainties of the film measurements were analyzed using guidance provided by NIST Technical Note 1297[47][167] and Mitch *et al*[48][168] Applications of uncertainty analysis to radiochromic film dosimetry in brachytherapy were discussed by Chiu-Tsao *et al*[49][141] and Soares *et al*[38][113]. Table 2 provides the estimated uncertainties for single film response, Table 3 for film calibration and Table 4 for ^{106}Ru eye plaque dosimetry using radiochromic film. Table 5 provides estimated uncertainties for ^{106}Ru eye plaque central axis dosimetry using a silicon diode.

Table 2. Estimated uncertainties in a single film response.

Component of uncertainty	Uncertainty %	Type
Typical background film uncertainty	1.0%	A
Typical irradiated film uncertainty	2.0%	A
Uncertainty due to scanner stability, reproducibility, and temperature effects	0.5%	B
Uncertainty due to lateral scanner response Correction not needed, since the films are small and always positioned at the center of the scanner bed.	0.0%	A
Combined standard uncertainty for net optical density	2.3%	

Table 3. Estimated uncertainties in film calibration.

Component of uncertainty	Uncertainty %	Type
Uncertainty in a single film response from Table 2	2.3%	A and B
Uncertainty in Linac beam calibration, including ADCL chamber calibration uncertainty 0.7%, ADCL electrometer calibration uncertainty 0.1%, setup uncertainty 0.5%	0.9%	A and B
Uncertainty in fitting parameters of the calibration curve	1.5%	B
Combined standard uncertainty for film calibration	2.9%	

Table 4. Estimated uncertainties in ^{106}Ru eye plaque dosimetry using radiochromic film.

Component of uncertainty	Uncertainty %	Type
Uncertainty in a single film response from Table 2	2.3%	A and B
Uncertainty in film calibration from Table 3	2.9%	A and B
Film non-uniformity	1.5%	A
Uncertainty in measurement depth	1.6%	A and B
Uncertainty in irradiation time	0.1%	A
Combined uncertainty	4.3%	
Combined, expanded (k=2) uncertainty	8.6%	

The uncertainties in the measurement depth for the film and diode dosimetry were assessed as the mechanical uncertainties multiplied by the dose gradient on the central axis proximal to the eye plaque, which is on the average 26%/mm in the first 3.0 mm from the inner concave surface, resulting in the dosimetric change over the mechanical uncertainty distance.

Table 5. Estimated uncertainties in ^{106}Ru eye plaque dosimetry using a silicon diode.

Component of uncertainty	Uncertainty %	Type
Uncertainty in ^{106}Ru eye plaque dosimetry using a silicon diode, as assessed by Lax[16][67]	4.5%	A and B
Uncertainty in effective measurement point position ±0.15 mm from the diode certificate	3.9%	B
Uncertainty in effective measurement point position due to water tank mechanism uncertainty	5.2%	A
Combined uncertainty	7.9%	
Combined, expanded (k=2) uncertainty	15.8%	

5. Discussion

Radiochromic film dosimetry of beta-emitting radiation sources has a long history. Soares[50,51][169, 170], Sayeg and Gregory[52][171] and Soares and McLaughlin[53][142] used early radiochromic film for surface dosimetry of ^{90}Sr/^{90}Y ophthalmic applicators. The technique using early radiochromic films was applied by Taccini *et al*[19][71] and Soares *et al*[15][73] for dosimetry of ^{106}Ru eye plaques which at that time had substantial dosimetric uncertainties and non-uniformities as described in the introduction. Taccini *et al*[19][71] used two different PMMA phantoms, one for placement of vertical films parallel to the central axis of the plaque and the other for horizontal films perpendicular to the central axis of the plaque and also used thin strips of film to measure surface doses and non-uniformity. Taccini *et al*[19][71] did not report either substantial dose disagreements with the manufacturer's data, or dosimetric non-uniformities, except of dose fall-off to less than 40% at the

1 mm region close to the rim of the plaques. Since the measurements were done during the period of known dosimetric problems of [106]Ru eye plaques, it is possible that they had a good production series of eye plaques or maybe the technique was not sufficiently sensitive. Soares *et al*[1573] compared different measurement methods of beta-emitting ophthalmic applicators including measurements in a set of Solid Water phantoms designed for placing the films perpendicular to the central axis of the plaque. They observed a serious dosimetric non-uniformity at a concave [106]Ru eye plaque. The most recent publication by Heilemann *et al*[24162] used a phantom setup similar to Taccini's *et al*[1971], a PMMA phantom enabling placing both vertical and horizontal films, but using mostly vertical films for dosimetry.

The phantom presented in this work uses horizontal films perpendicular to the central axis of the plaques, similar to the phantom used by Soares *et al*[1573], but has a few additional features helpful in clinical dosimetry, namely the rigid positioning of the eye plaque with respect to the films and the co-registration features enabling reconstruction of 3D dose matrix usable for either 2D or 3D treatment planning. Use of horizontal films enables irradiation of one film at a time, which has the advantage of selection of the "high contrast" steep dose range of the calibration curve, where the dosimetric uncertainty is less than using the decreased slope of the calibration curve at high doses, where a small change in pixel value results in a large change in dose. Using vertical films requires a large dynamic range of dose, since it has to cover the whole dose range from the surface of the eye plaque to the low doses at depth in one exposure, using the decreased slope of the calibration curve. For example Heilemann *et al*[24162] irradiated EBT3 films to doses between 15 and 18 Gy, in order to achieve "adequate dose levels even at distances of 12 mm from the plaque's surface", claiming that "no significant saturation effects were observed" and they used only the red component of the RGB image for film evaluation. The dose range of EBT3 film rated by the

manufacturer for use in the red channel is 10 Gy, and even this number is in the decreased contrast area of the calibration curve, so the uncertainty of this work for the higher dose areas in the proximity of the plaques should be fairly high. Generally using EBT3 film for dosimetry at doses above 10 Gy should be done in the green channel which enables extending the workable dose range of this film.

The unique film punches developed in the course of this work proved to be very valuable in precise cutting of films without splitting layers or damaging the edges even if cutting multilayer films.

Hot and cold spots, as well as other dosimetric non-uniformities, like the ones found at the CCX 55 eye plaque may lead to overdosing critical structures, for example the sclera, or underdosing parts of the tumor, if not accounted for. Since treatment planning for ophthalmic tumors using eye plaques is mostly one-dimensional utilizing two-dimensional ultrasound images, an in-house computer program which would use the dosimetric data from the planar films was developed at MSKCC. The program would calculate for a given eye plaque for any given depth relative to the sclera and lateral distance r, relative to the central axis, the minimum dose along an annulus of radius r. These two-dimensional reduced dose distributions would be superimposed on the ultrasound images for clinical evaluation of the minimal coverage. Similar distributions for the maximal annular dose are used to prevent overdosing critical structures adjacent to the tumor.

6. Conclusions

Radiochromic film in a Solid Water phantom is a convenient, accurate, and reproducible dosimeter for ^{106}Ru eye plaque dosimetry. Radiochromic films, especially the special single layer films, enable direct dose measurements on the inner surface of the plaques, providing precise assessment of the scleral dose, its uniformity, and of the active area of the plaques for coverage determination

and proper selection of plaques for treatment. The measured data may be used either by a 2D or 3D treatment planning system, enabling one to account for dose non-uniformities and to protect critical structures. Cutting, preparation and handling of radiochromic films play an important role in precise absolute film dosimetry. Despite improved quality and dosimetry by BEBIG, the post 2002 CCX plaques dosimetrically investigated in this work had central axis dose rates 6.0 – 11.4% lower than the manufacturer's data and hot areas in the vicinity of the rim. The relative central axis dose rates were found in good agreement with Monte Carlo calculations by Hermida-López[33][79], while the lateral disagreements between calculated and measured results could be explained by deviations of the actual plaques from expected values. The radiation coverage on the surface of one of the plaques was found to end 1.25 mm (CCX 129) from the rim vs. 0.75 mm expected from the manufacturer's specification. Each ^{106}Ru eye plaque must undergo accurate dosimetric commissioning and acceptance prior to its clinical use in the U.S. Because of the history of conflicting dosimetric results, it is important to clarify the source of the dosimetry used in the prescription protocol and it is the ultimate responsibility of the medical physicist and physician to decide what values to use for treatment delivery.

Disclosure of conflicts of interest

The authors have no relevant conflicts of interest to disclose.

ORCID iDs

Samuel Trichter id https://orcid.org/0000-0002-3909-7730

References

[1] R.J. Burri, "Eye," in *Radiation oncology management decisions,* edited by K.S.C. Chao, C.A. Perez, L.W. Brady, T. Marinetti (Lippincott Williams & Wilkins, Philadelphia, PA, 2011), pp. 193-202.

[2] H.B. Stallard, "Malignant melanoma of the choroid treated with radioactive applicators," Ann. Royal Coll. Surg. Eng. **29**, 170-182 (1961).

[3] P.K. Lommatzsch, "Results after β-irradiation (^{106}Ru/^{106}Rh) of choroidal melanomas. Twenty years' experience," Am. J. Clin. Oncol. **10**, 146-151 (1987).

[4] S. Seregard, "Long-term survival after ruthenium plaque radiotherapy for uveal melanoma. A meta-analysis of studies including 1,066 patients," Acta Ophthalmol. Scand. **77**, 414-417 (1999).

5   M. Diener-West, J.D. Earle, S.L. Fine, B.S. Hawkins, C.S. Moy, S.M. Reynolds, A.P. Schachat, B.R. Straatsma, "The COMS randomized trial of Iodine 125 brachytherapy for choroidal melanoma, III: Initial mortality findings. COMS report No. 18," Arch. Ophthalmol. **119**, 969-982 (2001).

6   L.M. Jampol, C.S. Moy, T.G. Murray, S.M. Reynolds, D.M. Albert, A.P. Schachat, K.R. Diddie, R.E. Engstrom, P.T. Finger, K.R. Hovland, L. Joffe, K.R. Olsen, C.G. Wells, "The COMS randomized trial of Iodine 125 brachytherapy for choroidal melanoma. IV. Local treatment failure and enucleation in the first 5 years after brachytherapy. COMS report No. 19," Ophthalmology **109**, 2197-2206 (2002).

7   S.-T. Chiu-Tsao, "[125]I episcleral eye plaques for treatment of intra-ocular malignancies," in *Brachytherapy Physics, AAPM 1994 Summer School Proceedings,* edited by J.F. Williamson, B.R. Thomadsen, R. Nath (Medical Physics Publishing, Madison, WI, 1995), pp. 451-483.

8   S.-T. Chiu-Tsao, "Episcleral eye plaques for treatment of intraocular malignancies and benign diseases," in *Brachytherapy Physics,* edited by B. Thomadsen, M. Rivard, W. Butler (Medical Physics Publishing, Madison, WI, 2005), pp. 673-705.

9   P.K. Lommatzsch, C. Werschnik, E. Schuster, "Long-term follow-up of Ru-106/Rh-106 brachytherapy for posterior uveal melanoma," Graefe's Arch. Clin. Exp. Ophthalmol. **238**, 129-137 (2000).

10   *ISO International Standard 21439:2009: Clinical dosimetry - beta radiation sources for brachytherapy.* (International Organization for Standardization, Geneva, Switzerland, 2009).

11   T.W. Kaulich, J. Zurheide, D. Flühs, T. Haug, F. Nüsslin, M. Bamberg, "Shortcomings of the industrial quality assurance of [106]Ru ophthalmic plaques," Strahlentherapie und Onkologie **177**, 616-627 (2001).

12   S. Trichter, H. Amols, G. Cohen, D. Lewis, T. LoSasso, M. Zaider, "Accurate dosimetry of Ru-106 ophthalmic applicators using GafChromic film in a Solid Water phantom," Med. Phys. **29**, 1349 (2002).

13   W. Binder, R. Menapace, W. Seitz, "Brachytherapie mit Ru-106-applikatoren in der Ophthalmologie," Strahlentherapie und Onkologie **166**, 639-642 (1990).

14   R. Menapace, W. Binder, A. Chiari, "Results and implications of high-resolution surface dosimetry of Ruthenium-106 eye applicators," Ophthalmologica **204**, 93-100 (1992).

15   C.G. Soares, S. Vynckier, H. Järvinen, W.G. Cross, P. Sipilä, D. Flühs, B. Schaeken, F.A. Mourtada, G.A. Baas, T.T. Williams, "Dosimetry of beta-ray ophthalmic applicators: comparison of different measurement methods," Med. Phys. **28**, 1373-1384 (2001).

16   I. Lax, "Dosimetry of [106]Ru eye applicators with a p-type silicon detector," Phys. Med. Biol. **36**, 963-972 (1991).

17   J. Davelaar, D.F. Schaling, L.A. Hennen, J.J. Broerse, "Dosimetry of ruthenium-106 eye applicators," Med. Phys. **19**, 691-694 (1992).

18   D. Flühs, M. Heintz, F. Indenkämpen, C. Wieczorek, H. Kolanoski, U. Quast, "Direct reading measurement of absorbed dose with plastic scintillators - the general concept and applications to ophthalmic plaque dosimetry," Med. Phys. **23**, 427-434 (1996).

19   G. Taccini, F. Cavagnetto, G. Coscia, S. Garelli, A. Pilot, "The determination of dose characteristics of ruthenium ophthalmic applicators using radiochromic film," Med. Phys. **24**, 2034-2037 (1997).

20   A.S. Kirov, J.Z. Piao, N.K. Mathur, T.R. Miller, S. Devic, S. Trichter, M. Zaider, C.G. Soares, T. LoSasso, "The three-dimensional scintillation dosimetry method: test for a [106]Ru eye plaque applicator," Phys. Med. Biol. **50**, 3063-3081 (2005).

21   M.F. Chan, A.Y.C. Fung, Y.-C. Hu, C.-S. Chui, H. Amols, M. Zaider, D. Abramson, "The measurement of three dimensional dose distribution of a ruthenium-106 ophthalmological applicator using magnetic resonance imaging of BANG polymer gels," J. of App. Clin. Med. Phys. **2**, 85-89 (2001).

22   R.M. Hermann, O. Pradier, K. Lauritzen, M. Ott, H. Schmidberger, C.F. Hess, "Does escalation of the apical dose change treatment outcome in β-radiation of posterior choroidal melanomas with [106]Ru plaques," Int. J. Radiation Oncology Biol. Phys. **52**, 1360-1366 (2002).

23   BEBIG, "Introduction of the new NIST-calibrated dosimetry. Introduction of the new PTB-calibrated activity measurement," (Eckert & Ziegler BEBIG GmbH, Berlin, Germany, 2002), pp. 1-8.

24   G. Heilemann, N. Nesvacil, M. Blaikner, N. Kostiukhina, D. Georg, "Multidimensional dosimetry of 106Ru eye plaques using EBT3 films and its impact on treatment planning," Med. Phys. **42**, 5798-5808 (2015).

25   H. Järvinen, W.G. Cross, C. Soares, S. Vynckier, K. Weaver, "ICRU Report 72: Dosimetry of beta rays and low-energy photons for brachytherapy with sealed sources.," Journal of the ICRU **4**, 1-175 (2004).

26   R.P. Kollaard, W.J.F. Dries, H.J. van Kleffens, A.H.L. Aalbers, J. van der Marel, J.P.A. Marijnissen, M. Piessens, D.R. Schaart, H. de Vroome, " Quality control of sealed beta sources in brachytherapy. Recommendations on detectors, measurement procedures and quality control of beta sources," Netherlands Commission on Radiation Dosimetry. Report No. 14, 2004.

27   T.W. Kaulich, J. Zurheide, T. Haug, F. Nüsslin, M. Bamberg, "Clinical quality assurance for [106]Ru ophthalmic applicators," Radiotherapy and Oncology **76**, 86-92 (2005).

28   M. Eichmann, D. Flühs, B. Spaan, "Development of a high precision dosimetry system for the measurement of surface dose rate distribution for eye applicators," Med. Phys. **36**, 4634-4643 (2009).

29   M. Eichmann, T. Krause, D. Flühs, B. Spaan, "Development of a high-precision *xyz*-measuring table for the determination of the 3D dose rate distributions of brachytherapy sources," Phys. Med. Biol. **57**, N421-N429 (2012).

30   BEBIG, "User Manual: Ru-106 Eye applicators Rev.12," (Eckert & Ziegler BEBIG GmbH, Berlin, Germany, 2016), pp. 1-19.

31   C.A. Barker, J.H. Francis, G.N. Cohen, B.P. Marr, S.L. Wolden, B. McCormick, D.H. Abramson, "[106]Ru plaque brachytherapy for uveal melanoma: Factors associated with local tumor recurrence," Brachytherapy **13**, 584-590 (2014).

32   R. Nath, M.J. Rivard, L.A. DeWerd, W.A. Dezarn, H. Thompson Heaton II, G.S. Ibbott, A.S. Meigooni, Z. Ouhib, T.W. Rusch, F.-A. Siebert, J.L.M. Venselaar, "Guidelines by the AAPM and GEC-ESTRO on the use of innovative brachytherapy devices and applications: Report of Task Group 167," Med. Phys. **43**, 3178-3205 (2016).

33   M. Hermida-López, "Calculation of dose distributions for 12 [106]Ru/[106]Rh ophthalmic applicator models with the Penelope Monte Carlo code," Med. Phys. **40**, 101705-1-101705-13 (2013).

34   C. Constantinou, F.H. Attix, B.R. Paliwal, "A solid water phantom material for radiotherapy x-ray and γ-ray beam calibrations," Med. Phys. **9**, 436-441 (1982).

35   I. Bekerman, P. Gottlieb, M. Vaiman, "Variations in eyeball diameters of the healthy adults," J. of Ophthalmology **2014**, 1-5 (2014).

36   R.G. Dale, "Some theoretical derivations relating to the tissue dosimetry of brachytherapy nuclides, with particular reference to Iodine-125," Med. Phys. **10**, 176-183 (1983).

37   M.A. Astrahan, "A patch source model for treatment planning of ruthenium ophthalmic applicators," Med. Phys. **30**, 1219-1228 (2003).

38   C.G. Soares, S. Trichter, S. Devic, "Radiochromic film," in *Clinical dosimetry measurements in radiotherapy,* edited by D.W.O. Rogers, J. Cygler (Medical Physics Publishing, Madison, WI, 2009), pp. 759-813.

39   A. Niroomand-Rad, C.R. Blackwell, B.M. Coursey, K.P. Gall, J.M. Galvin, W.L. McLaughlin, A.S. Meigooni, R. Nath, J.E. Rodgers, C.G. Soares, "Radiochromic film

dosimetry: Recommendations of AAPM Radiation Therapy Committee Task Group 55," Med. Phys. **25**, 2093-2115 (1998).

[40] D.W.O. Rogers, "Stopping-power ratios, ratios of mass-energy absorption coefficients and CSDA ranges of electrons," in *Clinical dosimetry measurements in radiotherapy,* edited by D.W.O. Rogers, J. Cygler (Medical Physics Publishing, Madison, WI, 2009), pp. 1083 - 1102.

[41] P.R. Almond, P.J. Biggs, B.M. Coursey, M.S. Huq, R. Nath, D.W.O. Rogers, "AAPM's TG-51 protocol for clinical reference dosimetry of high-energy photon and electron beams," Med. Phys. **26**, 1847-1870 (1999).

[42] D.O. Odero, G.R. Gluckman, K. Welsh, R.A. Wlodarczyk, L.E. Reinstein, "The use of an inexpensive red acetate filter to improve the sensitivity of GAFChromic dosimetry," Med. Phys. **28**, 1446-1448 (2001).

[43] S. Devic, Y.-Z. Wang, N. Tomic, E.B. Podgorsak, "Sensitivity of linear CCD array based film scanners used in film dosimetry," Med. Phys. **33**, 3993-3996 (2006).

[44] C. Fiandra, U. Ricardi, R. Ragona, S. Anglesio, F.R. Giglioli, E. Calamia, F. Lucio, "Clinical use of EBT model Gafchromic™ film in radiotherapy," Med. Phys. **33**, 4314-4319 (2006).

[45] A.S. Meigooni, S.B. Awan, N.S. Thompson, S.A. Dini, "Updated Solid Water™ to water conversion factors for ^{125}I and ^{103}Pd brachytherapy sources," Med. Phys. **33**, 3988-3992 (2006).

[46] N.S. Patel, S.-T. Chiu-Tsao, J.F. Williamson, P. Fan, T. Duckworth, D. Shasha, L.B. Harrison, "Thermoluminescent dosimetry of the Symmetra™ 125 I model 125.S06 interstitial brachytherapy seed," Med. Phys. **28**, 1761-1769 (2001).

[47] B.N. Taylor, C.E. Kuyatt, "Guidelines for evaluating and expressing the uncertainty of NIST measurement results. NIST Technical Note 1297" (National Institute of Standards and Technology, Gaithersburg, MD, 1994).

[48] M.G. Mitch, L.A. DeWerd, R. Minniti, J.F. Williamson, "Treatment of uncertainties in radiation dosimetry," in *Clinical dosimetry measurements in radiotherapy,* edited by D.W.O. Rogers, J. Cygler (Medical Physics Publishing, Madison, WI, 2009), pp. 724-757.

[49] S.-T. Chiu-Tsao, D. Medich, J. Munro III, "The use of new GAFCHROMIC® EBT film for ^{125}I seed dosimetry in Solid Water® phantom," Med. Phys. **35**, 3787-3799 (2008).

[50] C.G. Soares, "Calibration of ophthalmic applicators at NIST: A revised approach," Med. Phys. **18**, 787-793 (1991).

51   C.G. Soares, "A method for the calibration of concave $^{90}Sr+^{90}Y$ ophthalmic applicators," Phys. Med. Biol. **37**, 1005-1007 (1992).

52   J.A. Sayeg, R.C. Gregory, "A new method for characterizing beta-ray ophthalmic applicator sources," Med. Phys. **18**, 453-461 (1991).

53   C.G. Soares, W.L. McLaughlin, "Measurement of radial dose distributions around small beta particle emitters using high resolution radiochromic foil dosimetry," Radiation Protection Dosimetry **47**, 367-372 (1993).

8. Appendix 2. CCX 55 eye plaque certificate.

Ru #3

Zertifikat für umschlossene radioaktive Stoffe
Certificate for sealed radioactive sources

BEBIG
ISOTOPENTECHNIK UND
UMWELTDIAGNOSTIK
G   M   B   H

Allgemeine Angaben *general information*							
Zertifikat-Nr. *certificate no.*	Kunde *customer*					Auftrags-Nr. *order no.*	
025001	Memorial Sloan Kettering Cancer Center					110173	

Produkt-Code / Bauart *product code / model*	ISO-Klassifikation *ISO classification*	Nuklid *nuclide*	nominelle Aktivität *nominal activity*		Stück- zahl *quantity*	empfohlene Betriebsdauer [Jahre] *recommended working life [years]*
			M Bq	m Ci		
Ru6.A03	C 44343	Ru-106	7.8	0.21	1	1.5

Meß- und Prüfbericht der Strahler
Erklärungen siehe Rückseite
source test report
see backpage for more information

Serien-Nr. *serial no.*	Messung *measurement*			Dichtheitsprüfung *leakage test*		Oberflächen- kontaminationsprüfung *contamination test*		Sichtprüfung *visual test*
	Code *code*	Ergebnis (Fehler) *result (error)*	Datum *date measured*	Nr. *no.*	Datum *date passed*	Nr. *no.*	Datum *date passed*	Datum *date passed*
CCX 55	B	7.2 MBq	04.04.01			1	04.04.01	04.04.01

Bemerkungen, Anlagen
notes, annexes

Oberflächendosisleistungsverteilung, Tiefendosisleistungsverteilung
distribution of surface dose rate, distribution of depth dose rate

Dieses Zertifikat entspricht den Anforderungen nach ISO 2919
This certificate complies with the requirements of ISO 2919

Ausstellungsdatum *date of issue (dd.mm.yy)*	04.04.01	Unterschrift *signature*		Name *name*	V. Klingbeil

BEBIG GmbH · Robert-Rössle-Str. 10 · D-13125 Berlin · Tel. (+ 49 30) 94 10 84 - 0 · Fax (+ 49 30) 94 10 84 112

165

Anlage zum Zertifikat Nr. 025001
Appendix to certificate no. ....

BEBIG
ISOTOPENTECHNIK UND
UMWELTDIAGNOSTIK
G M B H

Meß-Protokoll
Protocol of Measurements

Für die radioaktiven Strahler					
For the radioactive sources					
Produkt-Code *product code*	Ru6.A03	Seriennr. *serial no.*	CCX 55	Nuklid *nuclide*	Ru-106

wurde folgende Größe durch Messung bestimmt:
the following quantity has been measured:

Meßgröße *quantity measured*	Beschreibung der Messung *description of the measurement*
Energiedosisleistung / energy dose rate	Die Energiedosisleistung der ß-Strahlung in gewebe-äquivalentem Material wurde im Wasserphantom mit einem Szintillationsdetektor (Durchmesser: 2 mm, Höhe: 2 mm) gemessen. / The energy dose rate of the ß-radiation in tissue-equivalent material has been measured with a scintillator (diameter: 2 mm, height: 2 mm) in a water phantom.

Meßergebnisse *measurement results*	Meßdatum *date of measurement*	04.04.01

Die Meßpunkte lagen auf der Zentralachse der inneren Oberfläche des Applikators an 4 verschiedenen Punkten: an der Oberfläche, in 2.0, 3.5 und 5.0 mm Tiefe. Die Ergebnisse und eine logarithmisch-lineare Regressionsfunktion sind in der folgenden Abbildung eingezeichnet. /
The measurement positions were on the central axis of the plaques inner surface at 4 different positions: at the surface, at 2.0, 3.5 and 5.0 mm depth. These results and a logarithmic-linear regression function are shown in the following figure.

Einzelergebnisse /
single results:

[mm]	[mGy/min]
0.0	116
2.0	60
3.5	31
5.0	15

Fehler / error = ± 30%

Ausstellungsdatum *date of issue (dd.mm.yy)*	04.04.01	Unterschrift *signature*	6. Klingbeil	Name *name*	V. Klingbeil

Dieses Dokument wurde per EDV erstellt. / *This document has been generated electronically.*

BEBIG GmbH • Robert-Rössle-Str. 10 • D-13125 Berlin • Tel. (+49 30) 94 10 84 - 0 • Fax (+49 30) 94 10 84 - 150   FB 008/QS. Rev. 2

166

Anlage zum Zertifikat Nr. 025001
Appendix to certificate no. ....

BEBIG
ISOTOPENTECHNIK UND
UMWELTDIAGNOSTIK
G   M   B   H

Meß-Protokoll
Protocol of Measurements

Für die radioaktiven Strahler *For the radioactive sources*						
Produkt-Code *product code*	Ru6.A03	Seriennr. *serial no.*	CCX 55	Nuklid *nuclide*	Ru-106	

wurde folgende Größe durch Messung bestimmt:
the following quantity has been measured:

Meßgröße *quantity measured*	Beschreibung der Messung *description of the measurement*
Energiedosisleistung / energy dose rate	Die Energiedosisleistung der ß-Strahlung in gewebe-äquivalentem Material wurde im Wasserphantom mit einem Szintillationsdetektor (Durchmesser: 2 mm, Höhe: 2 mm) gemessen. / The energy dose rate of the ß-radiation in tissue-equivalent material has been measured with a scintillator (diameter: 2 mm, height: 2 mm) in a water phantom.

Meßergebnisse *measurement results*	Meßdatum *date of measurement*	04.04.01

Die Meßpunkte lagen auf der inneren Oberfläche des Applikators in einem Kreis, d.h. an 9 Positionen, für kleine bzw. in 2 Kreisen, d.h. an 17 Positionen, für große Applikatoren. Die Meßergebnisse sind in % bezogen auf den Wert in der Mitte der Oberfläche in der folgenden Abbildung dargestellt. Der tatsächliche konstruktive Aufbau des Applikators wird in der Figur nur näherungsweise dargestellt. /
The measurement positions were on the plaques inner surface in 1 circle, that is 9 positions, for small plaques and in 2 circles, that is 17 positions, for large plaques. The results are given in %, related to the value in the centre.
The real construction of the plaque is shown in the figure only approximately.

Meßwert im Zentrum /
result in the centre = 100% =
116 mGy/min ± 30%

"X": Referenzpunkt /
       point of reference

11.5 mm

Ausstellungsdatum *date of issue (dd.mm.yy)*	04.04.01	Unterschrift *signature*	6. Klingbeil	Name *name*	V. Klingbeil

Dieses Dokument wurde per EDV erstellt. / *This document has been generated electronically.*

BEBIG GmbH • Robert-Rössle-Str. 10 • D-13125 Berlin • Tel. (+49 30) 94 10 84 - 0 • Fax (+49 30) 94 10 84 - 150   FB 008/QS, Rev. 2

167

9. Appendix 3. CCX 104 eye plaque certificate.
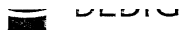
An Eckert & Ziegler Company

radioaktive Stoffe

Certificate for sealed radioactive sources

Allgemeine Angaben *general information*								
Zertifikat-Nummer *certificate number*		Kunde *customer*					Auftrags-Nummer *order number*	
010704		Memorial Sloan Kettering Cancer Center					V140424	

Produkt-Code/Bauart *product code/model*	ISO-Klassifikation *ISO classification*	Nuklid *nuclide*	nominelle Aktivität *nominal activity*		Stück-zahl *quantity*	empfohlene Betriebsdauer [Jahre] *recommended working life [years]*
			M Bq	m Ci		
Ru6.A03	C 44343	Ru-106	7.4	0.2	1	1

Mess- und Prüfbericht der Strahler
Erklärungen siehe Rückseite

source test report
see backpage for more information

Serien-Nummer *serial number*	Messung *measurement*			Dichtheitsprüfung *leakage test*		Oberflächen-kontaminationsprüfung *contamination test*		Sichtprüfung *visual test*
	Code *code*	Ergebnis (Fehler) *result (error)*	Datum *date measured*	Nr. *no.*	Datum *date passed*	Nr. *no.*	Datum *date passed*	Datum *date passed*
CCX 104 "	B	3.4 MBq	02.07.04	8 2	25.06.04 23.06.04	1	02.07.04	02.07.04

Bemerkungen, Anlagen
notes, annexes

Oberflächendosisleistungsverteilung, Tiefendosisleistungsverteilung
distribution of surface dose rate, distribution of depth dose rate

Dieses Zertifikat entspricht den Anforderungen nach ISO 2919 *This certificate complies with the requirements of ISO 2919*			
Ausstellungsdatum *date of issue (dd.mm.yy)*	02.07.04	Unterschrift *signature*	Name *name* V. Klingbeil

Mess-Protokoll
Protocol of Measurements

BEBIG

An Eckert & Ziegler Company

Für die radioaktiven Strahler *For the radioactive sources*					
Produkt-Code *product code*	Ru6.A03	Seriennr. *serial no.*	CCX 104	Nuklid *nuclide*	Ru-106

wurde folgende Größe durch Messung bestimmt:
the following quantity has been measured:

Messgröße *quantity measured*	Beschreibung der Messung *description of the measurement*
Energiedosisleistung in Wasser/ absorbed dose rate to water	Die Energiedosisleistung der ß-Strahlung in gewebe-äquivalentem Material wurde im Wasserphantom mit einem Szintillationsdetektor (Durchmesser: 1 mm, Höhe: 0.5 mm) gemessen. Die Ergebnisse sind auf den NIST-Standard (12/2001) rückführbar. / The absorbed dose rate of ß-radiation in tissue-equivalent material has been measured with a scintillator (diameter: 1 mm, height: 0.5 mm) in a water phantom. The results are traceable to NIST standard (12/2001).

Messergebnisse *measurement results*	Messdatum *date of measurement*	02.07.04

Die Messergebnisse werden in mm Abstand des Szintillatormittelpunkts von der inneren (konkaven) Oberfläche des Applikators entlang der Zentralachse angegeben und zusammen mit einer Regressionsfunktion dargestellt. Relative Angaben sind auf den Referenzpunkt (r=0.0 mm; z=2.0 mm) bezogen./ The results are stated in mm distance of the scintillator midpoint from the inner (concave) surface of the plaque along the central axis, and shown graphically on a regression function. Relative data are normalized to the reference point at (r=0.0 mm; z=2.0 mm).

Dosisleistung am Referenzpunkt r=0; z=2 / reference dose rate at r=0; z=2
42.9 mGy/min
±20% (2sigma)

Messergebnisse / measurement results:

[mm]	[mGy/min]	[%]
0.6	67.0	156
1.0	60.6	141
2.0	42.9	100
3.0	28.7	67.0
4.0	18.7	43.6
5.0	11.6	27.1
6.0	7.05	16.4
7.0	4.21	9.83
8.0	2.45	5.71
9.0	1.31	3.05
10.0	0.707	1.65

Extra-, interpolierte Daten / extra-, interpolated data:

[mm]	[mGy/min]	[%]
0.0	81.1	189
3.5	23.4	54.5

Ausstellungsdatum *date of issue (dd.mm.yy)*	02.07.04	Unterschrift *signature*		Name *name*	V. Klingbeil

169

BEBIG

An Eckert & Ziegler Company

Für die radioaktiven Strahler					
For the radioactive sources					
Produkt-Code *product code*	Ru6.A03	Seriennr. *serial no.*	CCX 104	Nuklid *nuclide*	Ru-106

wurde folgende Größe durch Messung bestimmt:
the following quantity has been measured:

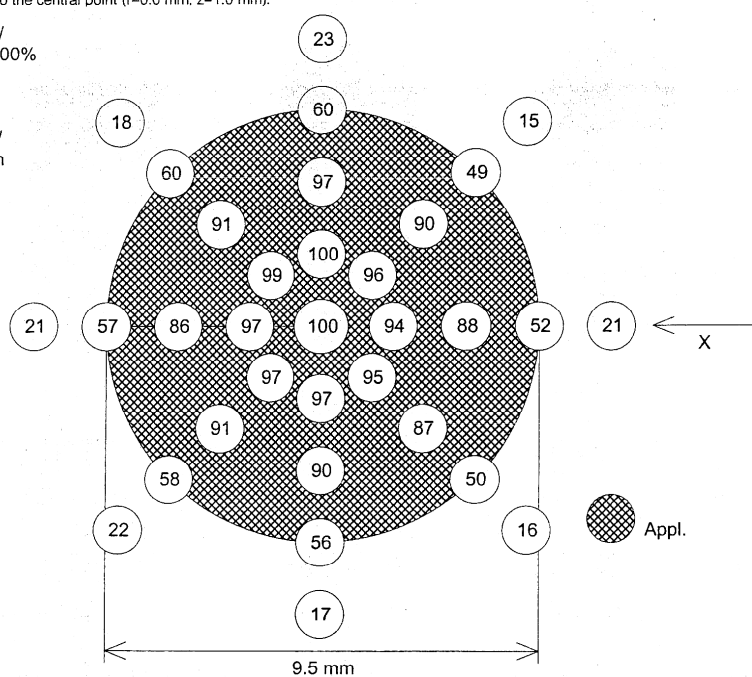| Messgröße *quantity measured*	Beschreibung der Messung *description of the measurement*
Energiedosisleistung in Wasser/ absorbed dose rate to water	Die Energiedosisleistung der ß-Strahlung in gewebe-äquivalentem Material wurde im Wasserphantom mit einem Szintillationsdetektor (Durchmesser: 1 mm, Höhe: 0.5 mm) gemessen. Die Ergebnisse sind auf den NIST-Standard (12/2001) rückführbar. / The absorbed dose rate of ß-radiation in tissue-equivalent material has been measured with a scintillator (diameter: 1 mm, height: 0.5 mm) in a water phantom. The results are traceable to NIST standard (12/2001).

Messergebnisse *measurement results*	Messdatum *date of measurement*	02.07.04

Die Messpunkte befinden sich an 33 Positionen auf einer gedachten konzentrischen Kugelfläche in 1.0 mm Abstand über der inneren Oberfläche des Applikators. Die ersten zwei Kreise mit Messpunkten liegen innerhalb der Applikatorfläche, der dritte Kreis über dem Rand der aktiven Schicht und der äußere Kreis ca. 5 mm außerhalb. Die dargestellten relativen Messdaten (in %) sind auf den Wert des Zentralpunkts (r=0.0 mm; z=1.0 mm) normiert./
The measurement points are placed at 33 positions on a concentric sphere 1.0 mm above the plaque's inner surface . The inner two circle positions are within the applicator surface, the third circle above the edge of the active layer and the outer circle is about 5 mm outside. The relative data shown in % are normalized to the central point (r=0.0 mm; z=1.0 mm).

Messwert im Zentrum /
result in the centre = 100%
60.6 mGy/min
±20% (2sigma)

"X": Referenzrichtung /
reference direction

9.5 mm

Ausstellungsdatum *date of issue (dd.mm.yy)*	02.07.04	Unterschrift *signature*	*[signature]*	Name *name*	V. Klingbeil

170

10. Appendix 4. CIA 156 eye plaque certificate.

BEBIG

An Eckert & Ziegler Company

Zertifikat für umschlossene radioaktive Stoffe

Certificate for sealed radioactive sources

Allgemeine Angaben *general information*							
Zertifikat-Nummer *certificate number*	Kunde *customer*					Auftrags-Nummer *order number*	
010904	Memorial Sloan Kettering Cancer Center					V140424	

Produkt-Code/Bauart *product code/model*	ISO-Klassifikation *ISO classification*	Nuklid *nuclide*	nominelle Aktivität *nominal activity*		Stück-zahl *quantity*	empfohlene Betriebsdauer [Jahre] *recommended working life [years]*
			M Bq	m Ci		
Ru6.A13	C 44343	Ru-106	9.99	0.27	1	1

Mess- und Prüfbericht der Strahler

Erklärungen siehe Rückseite

source test report

see backpage for more information

Serien-Nummer *serial number*	Messung *measurement*			Dichtheitsprüfung *leakage test*		Oberflächen-kontaminationsprüfung *contamination test*		Sichtprüfung *visual test*
	Code *code*	Ergebnis (Fehler) *result (error)*	Datum *date measured*	Nr. *no.*	Datum *date passed*	Nr. *no.*	Datum *date passed*	Datum *date passed*
CIA 156 "	B	6.7 MBq	02.07.04	8 2	25.06.04 23.06.04	1	02.07.04	02.07.04

Bemerkungen, Anlagen

notes, annexes

Oberflächendosisleistungsverteilung, Tiefendosisleistungsverteilung
distribution of surface dose rate, distribution of depth dose rate

Dieses Zertifikat entspricht den Anforderungen nach ISO 2919
This certificate complies with the requirements of ISO 2919

Ausstellungsdatum	Unterschrift	Name

171

Mess-Protokoll
Protocol of Measurements

BEBIG

An Eckert & Ziegler Company

Für die radioaktiven Strahler *For the radioactive sources*					
Produkt-Code *product code*	Ru6.A13	Seriennr. *serial no.*	CIA 156	Nuklid *nuclide*	Ru-106

wurde folgende Größe durch Messung bestimmt:
the following quantity has been measured:

Messgröße *quantity measured*	Beschreibung der Messung *description of the measurement*
Energiedosisleistung in Wasser/ absorbed dose rate to water	Die Energiedosisleistung der ß-Strahlung in gewebe-äquivalentem Material wurde im Wasserphantom mit einem Szintillationsdetektor (Durchmesser: 1 mm, Höhe: 0.5 mm) gemessen. Die Ergebnisse sind auf den NIST-Standard (12/2001) rückführbar. / The absorbed dose rate of ß-radiation in tissue-equivalent material has been measured with a scintillator (diameter: 1 mm, height: 0.5 mm) in a water phantom. The results are traceable to NIST standard (12/2001).

Messergebnisse *measurement results*	Messdatum *date of measurement* 02.07.04

Die Messergebnisse werden in mm Abstand des Szintillatormittelpunkts von der inneren (konkaven) Oberfläche des Applikators entlang der Zentralachse angegeben und zusammen mit einer Regressionsfunktion dargestellt. Relative Angaben sind auf den Referenzpunkt (r=0.0 mm; z=2.0 mm) bezogen./ The results are stated in mm distance of the scintillator midpoint from the inner (concave) surface of the plaque along the central axis, and shown graphically on a regression function. Relative data are normalized to the reference point at (r=0.0 mm; z=2.0 mm).

Dosisleistung am Referenzpunkt r=0; z=2 /
reference dose rate at r=0; z=2
52.8 mGy/min
±20% (2sigma)

Messergebnisse /
measurement results:

[mm]	[mGy/min]	[%]
0.6	90.6	171
1.0	78.7	149
2.0	52.8	100
3.0	35.5	67.1
4.0	24.0	45.4
5.0	15.9	30.2
6.0	10.0	18.9
7.0	6.05	11.4
8.0	3.56	6.73
9.0	2.04	3.86
10.0	1.10	2.08

Extra-, interpolierte Daten /
extra-, interpolated data:

[mm]	[mGy/min]	[%]
0.0	113	213
3.5	29.3	55.5

Mess-Protokoll
Protocol of Measurements

BEBIG

An Eckert & Ziegler Company

Für die radioaktiven Strahler *For the radioactive sources*					
Produkt-Code *product code*	Ru6.A13	Seriennr. *serial no.*	CIA 156	Nuklid *nuclide*	Ru-106

wurde folgende Größe durch Messung bestimmt:
the following quantity has been measured:

Messgröße *quantity measured*	Beschreibung der Messung *description of the measurement*
Energiedosisleistung in Wasser/ absorbed dose rate to water	Die Energiedosisleistung der ß-Strahlung in gewebe-äquivalentem Material wurde im Wasserphantom mit einem Szintillationsdetektor (Durchmesser: 1 mm, Höhe: 0.5 mm) gemessen. Die Ergebnisse sind auf den NIST-Standard (12/2001) rückführbar. / The absorbed dose rate of ß-radiation in tissue-equivalent material has been measured with a scintillator (diameter: 1 mm, height: 0.5 mm) in a water phantom. The results are traceable to NIST standard (12/2001).

Messergebnisse *measurement results*	Messdatum *date of measurement* 02.07.04

Die Messpunkte befinden sich an 33 Positionen auf einer gedachten konzentrischen Kugelfläche in 1.0 mm Abstand über der inneren Oberfläche des Applikators. Die ersten zwei Kreise mit Messpunkten liegen innerhalb der Applikatorfläche, der dritte Kreis über dem Rand der aktiven Schicht und der äußere Kreis ca. 5 mm außerhalb. Die dargestellten relativen Messdaten (in %) sind auf den Wert des Zentralpunkts (r=0.0 mm; z=1.0 mm) normiert./ The measurement points are placed at 33 positions on a concentric sphere 1.0 mm above the plaque's inner surface . The inner two circle positions are within the applicator surface, the third circle above the edge of the active layer and the outer circle is about 5 mm outside. The relative data shown in % are normalized to the central point (r=0.0 mm; z=1.0 mm).

Messwert im Zentrum /
result in the centre = 100%
78.7 mGy/min
±20% (2sigma)

"X": Referenzrichtung /
reference direction
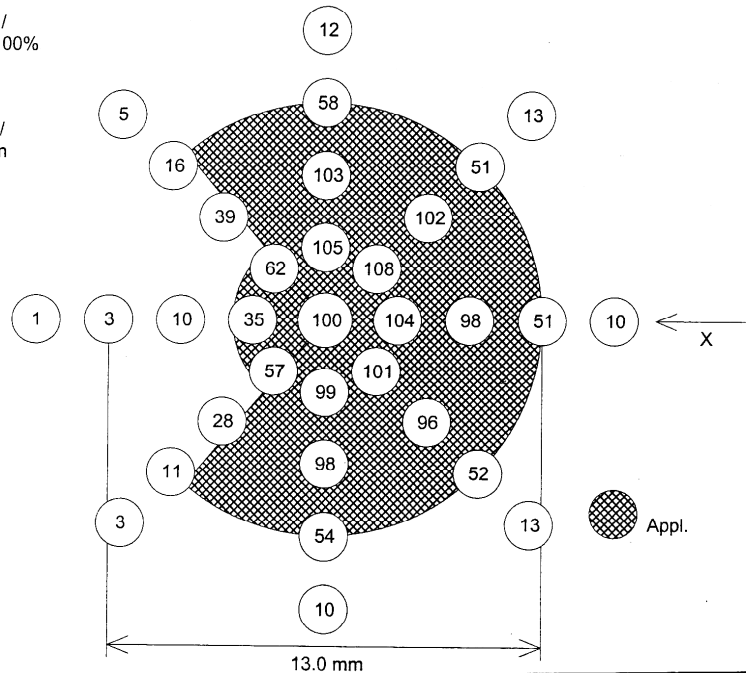
13.0 mm

Ausstellungsdatum *date of issue (dd.mm.yy)*	02.07.04	Unterschrift *signature*		Name *name*	V. Klingbeil

BEBIG GmbH · Robert-Rössle-Str. 10 · 13125 Berlin · Germany · Tel. +49-30-941084-0 · Fax +49-30-941084-112 · e-Mail: info@bebig.de

11. Dissertation references.

1   D.M. Albert, A.S. Polans, "Preface," in *Ocular Oncology*, edited by D.M. Albert, A.S. Polans (Marcel Dekker, Inc., New York, Basel, 2003), pp. v-vi.

2   R.J. Burri, "Eye," in *Radiation oncology management decisions,* edited by K.S.C. Chao, C.A. Perez, L.W. Brady, T. Marinetti (Lippincott Williams & Wilkins, Philadelphia, PA, 2011), pp. 193-202.

3   H.B. Stallard, "Malignant melanoma of the choroid treated with radioactive applicators," Ann. Royal Coll. Surg. Eng. **29**, 170-182 (1961).

4   H.B. Stallard, "Radiotherapy for malignant melanoma of the choroid," Br. J. Ophthalmol. **50**, 147-155 (1966).

5   P.K. Lommatzsch, "Results after β-irradiation (^{106}Ru/^{106}Rh) of choroidal melanomas: 20 years' experience," Br. J. Ophthalmol. **70**, 844-851 (1986).

6   P.K. Lommatzsch, "Results after β-irradiation (^{106}Ru/^{106}Rh) of choroidal melanomas. Twenty years' experience," Am. J. Clin. Oncol. **10**, 146-151 (1987).

7   P.K. Lommatzsch, C. Werschnik, E. Schuster, "Long-term follow-up of Ru-106/Rh-106 brachytherapy for posterior uveal melanoma," Graefe's Arch. Clin. Exp. Ophthalmol. **238**, 129-137 (2000).

8   M. Diener-West, J.D. Earle, S.L. Fine, B.S. Hawkins, C.S. Moy, S.M. Reynolds, A.P. Schachat, B.R. Straatsma, "The COMS randomized trial of Iodine 125 brachytherapy for choroidal melanoma, III: Initial mortality findings. COMS report No. 18," Arch. Ophthalmol. **119**, 969-982 (2001).

9   L.M. Jampol, C.S. Moy, T.G. Murray, S.M. Reynolds, D.M. Albert, A.P. Schachat, K.R. Diddie, R.E. Engstrom, P.T. Finger, K.R. Hovland, L. Joffe, K.R. Olsen, C.G. Wells, "The COMS randomized trial of Iodine 125 brachytherapy for choroidal melanoma. IV. Local treatment failure and enucleation in the first 5 years after brachytherapy. COMS report No. 19," Ophthalmology **109**, 2197-2206 (2002).

10   R. Pötter, K. Janssen, F.J. Prott, J. Widder, U. Haverkamp, H. Busse, R.P. Müller, "Ruthenium-106 eye plaque brachytherapy in the conservative treatment of uveal melanoma: evaluation of 175 patients treated with 150 Gy from 1981-1989," in *Frontiers*

of Radiation Therapy and Oncology, Vol. 30: Radiotherapy of Ocular Disease, edited by T. Wiegel, N. Bornfeld, M.H. Foerster, W. Hinkelbein (1997), pp. 143-149.

11   S. Seregard, "Long-term survival after ruthenium plaque radiotherapy for uveal melanoma. A meta-analysis of studies including 1,066 patients," Acta Ophthalmol. Scand. **77**, 414-417 (1999).

12   J.L. Hungerford, "Current trends in the treatment of ocular melanoma by radiotherapy," Clin. Experiment. Ophthalmol. **31**, 8-13 (2003).

13   R.-P. Müller, H. Busse, R. Pötter, P. Kroll, U. Haverkamp, "Results of high dose 106-ruthenium irradiation of choroidal melanomas," Int. J. Radiation Oncology Biol. Phys. **12**, 1749-1755 (1986).

14   B.E. Amendola, A.M. Markoe, J.J. Augsburger, U.L. Karlsson, M. Giblin, J.A. Shields, L.W. Brady, R. Woodleigh, "Analysis of treatment results in 36 children with retinoblastoma treated by scleral plaque irradiation," Int. J. Radiation Oncology Biol. Phys. **17**, 63-70 (1989).

15   F. Bacin, E. Albuisson, R. Rozan, D. Donnarieix, P. Verrelle, H. Dalens, "Uveal malignant melanomas treated by plaque therapy: tumor control, survival, complications," J. Fr. Ophtalmol. **14**, 383-396 (1991).

16   J.C. Hernandez, L.W. Brady, C.L. Shields, J.A. Shields, P. De Potter, "Conservative treatment of retinoblastoma. The use of plaque brachytherapy," Am. J. Clin. Oncol. **16**, 397-401 (1993).

17   S. Seregard, E. af Trampe, I. Lax, E. Kock, G. Lundell, "Results following episcleral ruthenium plaque radiotherapy for posterior uveal melanoma. The Swedish experience," Acta Ophthalmol. Scand. **75**, 11-16 (1997).

18   F. Bacin, F. Kwiatkowski, H. Dalens, R. Rozan, S. Gagyi, D. Donnarieix, J.J. Bard, J.L. Robert, "Long-term results of cobalt 60 plaque radiotherapy in the treatment of uveal melanomas," J. Fr. Ophtalmol. **21**, 333-344 (1998).

19   C.L. Shields, J.A. Shields, J. Cater, I. Othmane, A.D. Singh, B. Micaily, "Plaque radiotherapy for retinoblastoma: long-term tumor control and treatment complications in 208 tumors," Ophthalmology **108**, 2116-2121 (2001).

20   P.T. Finger, A. Berson, T. Ng, A. Szechter, "Palladium-103 plaque radiotherapy for choroidal melanoma: an 11-year study," Int. J. Radiation Oncology Biol. Phys. **54**, 1438-1445 (2002).

21   Y.M. Bartlema, J.A. Oosterhuis, J.G. Journée-de Korver, R.E. Tjho-Heslinga, K. J.E.E., "Combined plaque radiotherapy and transpupillary thermotherapy in choroidal melanoma: 5 years' experience," Br. J. Ophthalmol. **87**, 1370-1373 (2003).

22   L. Bergman, B. Nilsson, G. Lundell, M. Lundell, S. Seregard, "Ruthenium brachytherapy for uveal melanoma, 1979 - 2003. Survival and functional outcomes in the Swedish population," Ophthalmology **112**, 834-840 (2005).

23   B. Damato, I. Patel, I.R. Campbell, H.M. Mayles, R.D. Errington, "Local tumor control after [106]Ru brachytherapy of choroidal melanoma," Int. J. Radiation Oncology Biol. Phys. **63**, 385-391 (2005).

24   A.O. Schueler, D. Flühs, G. Anastassiou, C. Jurklies, M. Neuhäuser, H. Schilling, N. Bornfeld, W. Sauerwein, "β-ray brachytherapy with [106]Ru plaques for retinoblastoma," Int. J. Radiation Oncology Biol. Phys. **65**, 1212-1221 (2006).

25   H. Abouzeid, R. Moekli, M.-C. Gaillard, M. Beck-Popovic, A. Pica, L. Zographos, A. Balmer, S. Pampallona, F.L. Munier, "[106]Ruthenium brachytherapy for retinoblastoma," Int. J. Radiation Oncology Biol. Phys. **71**, 821-828 (2008).

26   P.T. Finger, K.J. Chin, G. Duvall, "Palladium-103 ophthalmic plaque radiation therapy for choroidal melanoma: 400 treated patients," Ophthalmology **116**, 790-796 (2009).

27   K.M.S. Verschueren, C.L. Creutzberg, N.E. Schalij-Delfos, M. Ketelaars, F.L.L. Klijsen, B.I. Haeseker, S.M.B. Ligtenberg, J.E.E. Keunen, C.A.M. Marijnen, "Long-term outcomes of eye-conserving treatment with Ruthenium[106] brachytherapy for choroidal melanoma," Radiotherapy and Oncology **95**, 332-338 (2010).

28   "The Collaborative Ocular Melanoma Study (COMS) Randomized Trial of Pre-enucleation Radiation of Large Choroidal Melanoma. II: Initial Mortality Findings. COMS Report No. 10," Am. J. Ophthalmol. **125**, 779-796 (1998).

29   R.L.S. Jennelle, J.L. Berry, J.W. Kim, "Uveal Melanoma," in *Adult CNS Radiation Oncology. Principles and Practice,* edited by E.L. Chang, P.D. Brown, S.S. Lo, A. Sahgal, J.H. Suh (Springer International Publishing AG, Cham, Switzerland, 2018), pp. 243 - 258.

30 BEBIG, "User Manual: Ru-106 Eye applicators Rev.12," (Eckert & Ziegler BEBIG GmbH, Berlin, Germany, 2016), pp. 1-19.

31 S.-T. Chiu-Tsao, "[125]I episcleral eye plaques for treatment of intra-ocular malignancies," in *Brachytherapy Physics, AAPM 1994 Summer School Proceedings,* edited by J.F. Williamson, B.R. Thomadsen, R. Nath (Medical Physics Publishing, Madison, WI, 1995), pp. 451-483.

32 J.A. Shields, J.J. Augsburger, L.W. Brady, J.L. Day, "Cobalt plaque therapy of posterior uveal melanomas," Ophthalmology **50**, 1201-1207 (1982).

33 B. Chan, M. Rotman, G.J. Randall, "Computerized dosimetry of ^{60}Co ophthalmic applicators," Radiology **103**, 705-707 (1972).

34 D.H. Char, L.I. Lonn, L.W. Margolis, "Complications of cobalt plaque therapy of choroidal melanomas," Am. J. Ophthalmol. **70**, 844-851 (1986).

35 G. Luxton, M.A. Astrahan, P.E. Liggett, D.L. Neblett, D.M. Cohen, Z. Petrovich, "Dosimetric calculations and measurements of gold plaque ophthalmic irradiators using Irridium-192 and Iodine-125 seeds," Int. J. Radiation Oncology Biol. Phys. **15**, 167-176 (1988).

36 G. Luxton, M.A. Astrahan, "Ophthalmic plaque brachytherapy and ^{125}I dose constants," in *Radiation Oncology Physics, Dosimetry, Treatment Planning, and Brachytherapy,* edited by J.A. Purdy (American Institute of Physics, Woodbury, NY, 1992), pp. 728-753.

37 J. Earle, R.W. Kline, D.M. Robertson, "Selection of I-125 for the Collaborative Ocular Melanoma Study," Arch. Ophthalmol. **105**, 763-764 (1987).

38 B.R. Straatsma, S.L. Fine, J.D. Earle, B.S. Hawkins, M. Diener-West, J.A. McLaughlin, The Collaborative Ocular Melanoma Study research group, "Enucleation versus plaque irradiation for choroidal melanoma," Ophthalmology **95**, 1000-1004 (1988).

39 S.-T. Chiu-Tsao, "Episcleral eye plaques for treatment of intraocular malignancies and benign diseases," in *Brachytherapy Physics,* edited by B. Thomadsen, M. Rivard, W. Butler (Medical Physics Publishing, Madison, WI, 2005), pp. 673-705.

40 S.-T. Chiu-Tsao, M.A. Astrahan, P.T. Finger, D.S. Followill, A.S. Meigooni, C.S. Melhus, F. Mourtada, M.E. Napolitano, R. Nath, M.J. Rivard, D.W.O. Rogers, R.M.

Thomson, "Dosimetry of ^{125}I and [103]Pd COMS eye plaques for intraocular tumors: Report of Task Group 129 by the AAPM and ABS," Med. Phys. **39**, 6161-6184 (2012).

41   *ISO International Standard 21439:2009: Clinical dosimetry - beta radiation sources for brachytherapy*. (International Organization for Standardization, Geneva, Switzerland, 2009).

42   S. Trichter, C.G. Soares, M. Zaider, J.K. DeWyngaert, L.A. DeWerd, N.J. Kleiman, "15 years of [106]Ru eye plaque dosimetry at Memorial Sloan-Kettering Cancer Center and Weill Cornell Medical Center using radiochromic film in a Solid Water phantom," Biomed. Phys. Eng. Express **4**, 1 - 17 (2018).

43   M. Diener-West, B.S. Hawkins, S.L. Fine, J.D. Earle, B.R. Straatsma, R.L. Mowery, "Design and methods of a clinical trial for a rare condition: The Collaborative Ocular Melanoma Study. COMS Report No. 3," Controlled Clinical Trials **14**, 362 - 391 (1993).

44   J.E. Freire, P. De Potter, L.W. Brady, W.A. Longton, "Brachytherapy in primary ocular tumors," Seminars in Surgical Oncology **13**, 167-176 (1997).

45   S. Nag, D. Wang, H. Wu, C.J. Bauer, R.B. Chambers, F.H. Davidorf, "Custom-made "Nag" eye plaques for ^{125}I brachytherapy," Int. J. Radiation Oncology Biol. Phys. **56**, 1373-1380 (2003).

46   J. Poder, S. Corde, "I-125 ROPES eye plaque dosimetry: Validation of a commercial 3D ophthalmic brachytherapy treatment planning system and independent dose calculation software with GafChromic® EBT3 films," Med. Phys. **40**, 121709-1-121709-11 (2013).

47   W. Alberti, B. Pothmann, P. Tabor, K. Muskalla, K.-P. Hermann, D. Harder, "Dosimetry and physical treatment planning for iodine eye plaque therapy," Int. J. Radiation Oncology Biol. Phys. **20**, 1087-1092 (1991).

48   M.A. Astrahan, G. Luxton, Q. Pu, Z. Petrovich, "Conformal episcleral plaque therapy," Int. J. Radiation Oncology Biol. Phys. **39**, 505-519 (1997).

49   M. Bambynek, D. Flühs, M. Heintz, H. Kolanoski, D. Wegener, U. Quast, "Fluorescence ^{125}I eye applicator," Med. Phys. **26**, 2476-2481 (1999).

[50]   M.A. Astrahan, A. Szechter, P.T. Finger, "Design and dosimetric considerations of a modified COMS plaque: The reusable "seed-guide" insert," Med. Phys. **32**, 2706-2716 (2005).

[51]   P.T. Finger, "Finger's "slotted" eye plaque for radiation therapy: treatment of juxtapapillary and circumpapillary intraocular tumors," Br. J. Ophthalmol. **91**, 891-894 (2007).

[52]   P.T. Finger, D.M. Moshfeghi, T.K. Ho, "Palladium 103 ophthalmic plaque radiotherapy," Arch. Ophthalmol. **109**, 1610 - 1613 (1991).

[53]   M.J. Rivard, B.M. Coursey, L.A. DeWerd, W.F. Hanson, M.S. Huq, G.S. Ibbott, M.G. Mitch, R. Nath, J.F. Williamson, "Update of AAPM Task Group No. 43 Report: A revised AAPM protocol for brachytherapy dose calculations," Med. Phys. **31**, 633-674 (2004).

[54]   R.M. Thomson, R.E.P. Taylor, D.W.O. Rogers, "Monte Carlo dosimetry for ^{125}I and ^{103}Pd eye plaque brachytherapy," Med. Phys. **35**, 5530-5543 (2008).

[55]   G. Luxton, M.A. Astrahan, Z. Petrovich, "Backscatter measurements from a single seed of ^{125}I for ophthalmic plaque dosimetry," Med. Phys. **15**, 397-400 (1988).

[56]   S.-T. Chiu-Tsao, L.L. Anderson, K. O'Brien, L. Stabile, J.C. Liu, "Dosimetry for ^{125}I seed (model 6711) in eye plaques," Med. Phys. **20**, 383-389 (1993).

[57]   A. de la Zerda, S.-T. Chiu-Tsao, J. Lin, L.L. Boulay, I. Kanna, J.H. Kim, H.-S. Tsao, "^{125}I eye plaque dose distribution including penumbra characteristics," Med. Phys. **23**, 407-418 (1996).

[58]   A. Wu, F. Krasin, "Film dosimetry analyses on the effect of gold shielding for Iodine-125 eye plaque therapy for choroidal melanoma," Med. Phys. **17**, 843-846 (1990).

[59]   M.A. Astrahan, "Improved treatment planning for COMS eye plaques," Int. J. Radiation Oncology Biol. Phys. **61**, 1227-1242 (2005).

[60]   M.J. Rivard, S.-T. Chiu-Tsao, P.T. Finger, A.S. Meigooni, C.S. Melhus, F. Mourtada, M.E. Napolitano, D.W.O. Rogers, R.M. Thomson, R. Nath, "Comparison of dose calculation methods for brachytherapy of intraocular tumors," Med. Phys. **38**, 306-316 (2011).

61   S. Trichter, S.-T. Chiu-Tsao, M. Zaider, A. Sabbas, F. Kulidzhanov, J. Chang, G. Cohen, D. Nori, K.S.C. Chao, "Accurate dosimetric characterization of a fully loaded 20 mm COMS I-125 eye plaque using specially designed GAFCHROMIC™ film," Med. Phys. **38**, 3791 (2011).

62   M.A. Astrahan, "A patch source model for treatment planning of ruthenium ophthalmic applicators," Med. Phys. **30**, 1219-1228 (2003).

63   M.A. Astrahan, G. Luxton, G. Jozsef, T.D. Kampp, P.E. Liggett, M.D. Sapozink, Z. Petrovich, "An interactive treatment planning system for ophthalmic plaque radiotherapy," Int. J. Radiation Oncology Biol. Phys. **18**, 679 - 687 (1990).

64   M.A. Astrahan, G. Luxton, G. Jozsef, P.E. Liggett, Z. Petrovich, "Optimization of ^{125}I ophthalmic plaque brachytherapy," Med. Phys. **17**, 1053 - 1057 (1990).

65   I. Bekerman, P. Gottlieb, M. Vaiman, "Variations in eyeball diameters of the healthy adults," J. of Ophthalmology **2014**, 1-5 (2014).

66   W. Binder, R. Menapace, W. Seitz, "Brachytherapie mit Ru-106-applikatoren in der Ophthalmologie," Strahlentherapie und Onkologie **166**, 639-642 (1990).

67   I. Lax, "Dosimetry of ^{106}Ru eye applicators with a p-type silicon detector," Phys. Med. Biol. **36**, 963-972 (1991).

68   R. Menapace, W. Binder, A. Chiari, "Results and implications of high-resolution surface dosimetry of Ruthenium-106 eye applicators," Ophthalmologica **204**, 93-100 (1992).

69   D. Flühs, M. Heintz, F. Indenkämpen, C. Wieczorek, H. Kolanoski, U. Quast, "Direct reading measurement of absorbed dose with plastic scintillators - The general concept and applications to ophthalmic plaque dosimetry," Med. Phys. **23**, 427-434 (1996).

70   D. Flühs, M. Bambynek, M. Heintz, F. Indenkämpen, H. Kolanoski, D. Wegener, W. Sauerwein, U. Quast, "Dosimetry and design of radioactive eye plaques," in *Frontiers of Radiation Therapy and Oncology, Vol. 30: Radiotherapy of Ocular Disease,* edited by T. Wiegel, N. Bornfeld, M.H. Foerster, W. Hinkelbein (1997), pp. 26-38.

71   G. Taccini, F. Cavagnetto, G. Coscia, S. Garelli, A. Pilot, "The determination of dose characteristics of ruthenium ophthalmic applicators using radiochromic film," Med. Phys. **24**, 2034-2037 (1997).

72   T.W. Kaulich, J. Zurheide, D. Flühs, T. Haug, F. Nüsslin, M. Bamberg, "Shortcomings of the industrial quality assurance of ^{106}Ru ophthalmic plaques," Strahlentherapie und Onkologie **177**, 616-627 (2001).

73   C.G. Soares, S. Vynckier, H. Järvinen, W.G. Cross, P. Sipilä, D. Flühs, B. Schaeken, F.A. Mourtada, G.A. Baas, T.T. Williams, "Dosimetry of beta-ray ophthalmic applicators: Comparison of different measurement methods," Med. Phys. **28**, 1373-1384 (2001).

74   T.W. Kaulich, J. Zurheide, T. Haug, F. Nüsslin, M. Bamberg, "Clinical quality assurance for ^{106}Ru ophthalmic applicators," Radiotherapy and Oncology **76**, 86-92 (2005).

75   S. Trichter, H. Amols, G. Cohen, D. Lewis, T. LoSasso, M. Zaider, "Accurate dosimetry of Ru-106 ophthalmic applicators using GafChromic film in a Solid Water phantom," Med. Phys. **29**, 1349 (2002).

76   S. Trichter, G.N. Cohen, T. LoSasso, B. McCormick, D. Abramson, M. Zaider, H. Amols, "Treatment planning for Ru-106 eye plaques: pitfalls and remedies," in *Proceedings of the 88th Scientific Assembly and Annual Meeting of the RSNA, Supplement to Radiology, 225(P)* (Chicago, IL, 2002), pp. 192.

77   S. Trichter, G. Cohen, M. Zaider, "Accurate dosimetry of Ru-106 eye plaques and treatment planning implications," in *Proceedings of the World Congress on Medical Physics and Biomedical Engineering* (Sydney, Australia, 2003).

78   A.S. Kirov, J.Z. Piao, N.K. Mathur, T.R. Miller, S. Devic, S. Trichter, M. Zaider, C.G. Soares, T. LoSasso, "The three-dimensional scintillation dosimetry method: test for a ^{106}Ru eye plaque applicator," Phys. Med. Biol. **50**, 3063-3081 (2005).

79   M. Hermida-López, "Calculation of dose distributions for 12 ^{106}Ru/^{106}Rh ophthalmic applicator models with the Penelope Monte Carlo code," Med. Phys. **40**, 101705-1-101705-13 (2013).

80   M. Hermida-López, L. Brualla, "Absorbed dose distributions from ophthalmic ^{106}Ru/^{106}Rh plaques measured in water with radiochromic film," Med. Phys. **45**, 1699 - 1707 (2018).

81   BEBIG, "Introduction of the new NIST-calibrated dosimetry. Introduction of the new PTB-calibrated activity measurement.," (Eckert & Ziegler BEBIG GmbH, Berlin, Germany, 2002), pp. 1-8.

82   S. Trichter, M. Zaider, A. Sabbas, F. Kulidzhanov, D. Lewis, C.G. Soares, D. Nori, "Acceptance and commissioning of [106]Ru eye plaques in accordance with the forthcoming ISO Beta Dosimetry Standard using novel GAFCHROMIC® film," in *Proceedings of the Meeting of the International Society of Ocular Oncology* (Siena, Italy, 2007).

83   S. Trichter, M. Zaider, D. Nori, A. Sabbas, F. Kulidzhanov, D. Lewis, C.G. Soares, "Clinical dosimetry of [106]Ru eye plaques in accordance with the forthcoming ISO Beta Dosimetry Standard using specially designed GAFCHROMIC® film," Int. J. Radiation Oncology Biol. Phys. **69**, S665-S666 (2007).

84   Y.C. Lee, Y. Kim, J.W.-Y. Huynh, R.J. Hamilton, "Failure modes and effects analysis for ocular brachytherapy," Brachytherapy **16**, 1265 - 1279 (2017).

85   M.S. Huq, B.A. Fraass, P.B. Dunscombe, J.P. Gibbons Jr., G.S. Ibbott, A.J. Mundt, S. Mutic, J.R. Palta, F. Rath, B.R. Thomadsen, J.F. Williamson, E.D. Yorke, "The report of Task Group 100 of the AAPM: Application of risk analysis methods to radiation therapy quality management," Med. Phys. **43**, 4209 - 4262 (2016).

86   E.P. Messmer, W. Sauerwein, T. Heinrich, W. Höpping, D. Klueter-Reckmann, N. Bornfeld, H. Sack, M. Förster, W. Havers, "New and recurrent tumor foci following local treatment as well as external beam radiation in eyes of patients with hereditary retinoblastoma," Graefe's Arch. Clin. Exp. Ophthalmol. **228**, 426-431 (1990).

87   R.M. Hermann, O. Pradier, K. Lauritzen, M. Ott, H. Schmidberger, C.F. Hess, "Does escalation of the apical dose change treatment outcome in β-radiation of posterior choroidal melanomas with [106]Ru plaques," Int. J. Radiation Oncology Biol. Phys. **52**, 1360-1366 (2002).

88   C.A. Barker, J.H. Francis, G.N. Cohen, B.P. Marr, S.L. Wolden, B. McCormick, D.H. Abramson, "[106]Ru plaque brachytherapy for uveal melanoma: Factors associated with local tumor recurrence," Brachytherapy **13**, 584-590 (2014).

89   R. Nath, M.J. Rivard, L.A. DeWerd, W.A. Dezarn, H. Thompson Heaton II, G.S. Ibbott, A.S. Meigooni, Z. Ouhib, T.W. Rusch, F.-A. Siebert, J.L.M. Venselaar, "Guidelines by the AAPM and GEC-ESTRO on the use of innovative brachytherapy devices and applications: Report of Task Group 167," Med. Phys. **43**, 3178-3205 (2016).

90   G.J. Kutcher, L. Coia, M. Gillin, W.F. Hanson, S. Leibel, R.J. Morton, J.R. Palta, J.A. Purdy, L.E. Reinstein, G.K. Svensson, M. Weller, L. Wingfield, "Comprehensive QA for

radiation oncology: Report of AAPM Radiation Therapy Committee Task Group 40," Med. Phys. **21**, 581-618 (1994).

91   D.F. Schaling, P.K. Lommatzsch, J.L. van Delft, D. de Wolff-Rouendaal, J.A. van Best, J.A. Oosterhuis, "Effect of beta-irradiation by a 106 ruthenium plaque on the rabbit eye choroid," Graefe's Arch. Clin. Exp. Ophthalmol. **227**, 194-199 (1989).

92   P.K. Lommatzsch, W. Alberti, R. Lommatzsch, F. Rohrwacher, "Radiation effects on the optic nerve observed after brachytherapy of choroidal melanomas with [106]Ru/[106]Rh plaques," Graefe's Arch. Clin. Exp. Ophthalmol. **232**, 482-487 (1994).

93   R. Jones, E. Gore, W. Mieler, K. Murray, M. Gillin, K. Albano, B. Erickson, "Posttreatment visual acuity in patients treated with episcleral plaque therapy for choroidal melanomas: dose and dose rate effect," Int. J. Radiation Oncology Biol. Phys. **52**, 989-995 (2002).

94   I. Puusaari, J. Heikkonen, T. Kivelä, "Effect of radiation dose on ocular complications after iodine brachytherapy for large uveal melanoma: empirical data and simulation of collimating plaques," Investigative Ophthalmology & Visual Science **45**, 3425-3434 (2004).

95   P.T. Finger, J.E. Reid, C.E. Iacob, "Palladium-103 eye plaque brachytherapy for primary adenocarcinoma of the ciliary body epithelium," Brachytherapy **10**, 503-507 (2011).

96   S. Nag, J.M. Quivey, J.D. Earle, D. Followill, J. Fontanesi, P.T. Finger, "The American Brachytherapy Society recommendations for brachytherapy of uveal melanomas," Int. J. Radiation Oncology Biol. Phys. **56**, 544-555 (2003).

97   S.-T. Chiu-Tsao, A. de la Zerda, J. Lin, J.H. Kim, "High-sensitivity GafChromic film dosimetry for ^{125}I seed," Med. Phys. **21**, 651-657 (1994).

98   A. Niroomand-Rad, C.R. Blackwell, B.M. Coursey, K.P. Gall, J.M. Galvin, W.L. McLaughlin, A.S. Meigooni, R. Nath, J.E. Rodgers, C.G. Soares, "Radiochromic film dosimetry: Recommendations of AAPM Radiation Therapy Committee Task Group 55," Med. Phys. **25**, 2093-2115 (1998).

99   T.D. Bohm, D.W. Pearson, R.K. Das, "Measurements and Monte Carlo calculations to determine the absolute detector response of radiochromic film for brachytherapy dosimetry," Med. Phys. **28**, 142-146 (2001).

100   S.-T. Chiu-Tsao, T. Duckworth, C. Zhang, N.S. Patel, C.-Y. Hsiung, L. Wang, J.A. Shih, L.B. Harrison, "Dose response characteristics of new models of GAFCHROMIC films: Dependence on densitometer light source and radiation energy," Med. Phys. **31**, 2501-2508 (2004).

101   S.-T. Chiu-Tsao, Y. Ho, R. Shankar, L. Wang, L.B. Harrison, "Energy dependence of response of new high sensitivity radiochromic films for megavoltage and kilovoltage radiation energies," Med. Phys. **32**, 3350-3354 (2005).

102   M.J. Butson, T. Cheung, P.K.N. Yu, "Weak energy dependence of EBT gafchromic film dose response in the 50 kVp-10MVp X-ray range," Applied Radiation and Isotopes **64**, 60-62 (2006).

103   D.W.O. Rogers, "Stopping-power ratios, ratios of mass-energy absorption coefficients and CSDA ranges of electrons," in *Clinical dosimetry measurements in radiotherapy,* edited by D.W.O. Rogers, J. Cygler (Medical Physics Publishing, Madison, WI, 2009), pp. 1083 - 1102.

104   P. Lindsay, A. Rink, M. Ruschin, D. Jaffray, "Investigation of energy dependence of EBT and EBT-2 Gafchromic film," Med. Phys. **37**, 571-576 (2010).

105   H. Bekerat, S. Devic, F. DeBlois, K. Singh, A. Sarfehnia, J. Seuntjens, S. Shih, X. Yu, D. Lewis, "Improving the energy response of external beam therapy (EBT) GafChromic™ dosimetry films at low energies (<=100 keV)," Med. Phys. **41**, 022101-1-022101-14 (2014).

106   R.G. Dale, "Some theoretical derivations relating to the tissue dosimetry of brachytherapy nuclides, with particular reference to Iodine-125," Med. Phys. **10**, 176-183 (1983).

107   C.C. Ling, M.C. Schell, E.D. Yorke, B.B. Palos, D.O. Kubiatowicz, "Two-dimensional dose distribution of ^{125}I seeds," Med. Phys. **12**, 652-655 (1985).

108   C.C. Ling, E.D. Yorke, I.J. Spiro, D. Kubiatowicz, D. Bennett, "Physical dosimetry of ^{125}I seeds of a new design for interstitial implant," Int. J. Radiation Oncology Biol. Phys. **9**, 1747-1752 (1983).

109   M. Ahmad, D.P. Fontenla, S.-T. Chiu-Tsao, C.S. Chui, J.E. Reiff, L.L. Anderson, D.Y.C. Huang, M.C. Schell, "Diode dosimetry of models 6711 and 6712 ^{125}I seeds in a water phantom," Med. Phys. **19**, 391-399 (1992).

110   S. Knutsen, R. Hafslund, O.R. Monge, H. Valen, L.P. Muren, B.L. Rekstad, J. Krohn, O. Dahl, "Dosimetric verification of a dedicated 3D treatment planning system for episcleral plaque therapy," Int. J. Radiation Oncology Biol. Phys. **51**, 1159-1166 (2001).

111   M.J. Butson, P.K.N. Yu, T. Cheung, P. Metcalfe, "Radiochromic film for medical radiation dosimetry," Material Science and Engineering R **41**, 61-120 (2003).

112   C.G. Soares, "Radiochromic film dosimetry," Radiat. Meas. **41**, S100-S116 (2007).

113   C.G. Soares, S. Trichter, S. Devic, "Radiochromic film," in *Clinical dosimetry measurements in radiotherapy,* edited by D.W.O. Rogers, J. Cygler (Medical Physics Publishing, Madison, WI, 2009), pp. 759-813.

114   S.-T. Chiu-Tsao, A. Niroomand-Rad, P. Alvarez, M. Chan, I. Das, M. Grams, G. Massillon-JL, M. Kissick, D. Lewis, C. Soares, S. Trichter, L. Van Battum, "Radiochromic film dosimetry: An update to TG-55. Report of AAPM Task Group 235," (to be published in Med. Phys., 2019).

115   B.D. Lynch, J. Kozelka, M.K. Ranade, J.G. Li, W.E. Simon, J.F. Dempsey, "Important considerations for radiochromic film dosimetry with flatbed CCD scanners and EBT GAFCHROMIC® film," Med. Phys. **33**, 4551-4556 (2006).

116   A.S. Meigooni, M.F. Sanders, G.S. Ibbott, S.R. Szeglin, "Dosimetric characteristics of an improved radiochromic film," Med. Phys. **23**, 1883-1888 (1996).

117   Y. Zhu, A.S. Kirov, V. Mishra, A.S. Meigooni, J.F. Williamson, "Quantitative evaluation of radiochromic film response for two-dimensional dosimetry," Med. Phys. **24**, 223-231 (1997).

118   A. Micke, D.F. Lewis, X. Yu, "Multichannel film dosimetry with nonuniformity correction," Med. Phys. **38**, 2523-2534 (2011).

119   I. Ali, C. Costescu, M. Vicic, J.F. Dempsey, J.F. Williamson, "Dependence of radiochromic film optical density post-exposure kinetics on dose and dose fractionation," Med. Phys. **30**, 1958-1967 (2003).

120   D.O. Odero, G.R. Gluckman, K. Welsh, R.A. Wlodarczyk, L.E. Reinstein, "The use of an inexpensive red acetate filter to improve the sensitivity of GAFChromic dosimetry," Med. Phys. **28**, 1446-1448 (2001).

[121] H. Järvinen, W.G. Cross, C. Soares, S. Vynckier, K. Weaver, "ICRU Report 72: Dosimetry of beta rays and low-energy photons for brachytherapy with sealed sources," Journal of the ICRU **4**, 1-175 (2004).

[122] J.F. Dempsey, D.A. Low, S. Mutic, J. Markman, A.S. Kirov, G.H. Nussbaum, J.F. Williamson, "Validation of a precision radiochromic film dosimetry system for quantitative two-dimensional imaging of acute exposure dose distributions," Med. Phys. **27**, 2462-2475 (2000).

[123] S. Devic, Y.-Z. Wang, N. Tomic, E.B. Podgorsak, "Sensitivity of linear CCD array based film scanners used in film dosimetry," Med. Phys. **33**, 3993-3996 (2006).

[124] C. Fiandra, U. Ricardi, R. Ragona, S. Anglesio, F.R. Giglioli, E. Calamia, F. Lucio, "Clinical use of EBT model Gafchromic™ film in radiotherapy," Med. Phys. **33**, 4314-4319 (2006).

[125] ISP, "Effects of light scattering by films on the performance of CCD scanners," (International Specialty Products, Wayne, NJ, currently Ashland, Covington, KY, 2006).

[126] L. Menegotti, A. Delana, A. Martignano, "Radiochromic film dosimetry with flatbed scanners: A fast and accurate method for dose calibration and uniformity correction with single film exposure," Med. Phys. **35**, 3078-3085 (2008).

[127] S. Saur, J. Frengen, "GafChromic EBT film dosimetry with flatbed CCD scanner: A novel background correction method and full dose uncertainty analysis," Med. Phys. **35**, 3094-3101 (2008).

[128] L.J. van Battum, D. Hoffmans, H. Piersma, S. Heukelom, "Accurate dosimetry with GafChromic™ EBT film of a 6 MV photon beam in water: What level is achievable?," Med. Phys. **35**, 704-716 (2008).

[129] H. Miras, R. Arrans, "An easy method to account for light scattering dose dependence in radiochromic films," Med. Phys. **36**, 3866-3869 (2009).

[130] S. Trichter, F. Trichter, A. Sabbas, D. Lovelock, F. Kulidzhanov, D. Nori, "Evaluation of GafChromic EBT film for IMRT QA using two different scanners," Med. Phys. **32**, 2167 (2005).

[131] L. Beaulieu, Å. Carlsson Tedgren, J.-F. Carrier, S.D. Davis, F. Mourtada, M.J. Rivard, R.M. Thomson, F. Verhaegen, T.A. Wareing, J.F. Williamson, "Report of the Task Group 186 on model-based dose calculation methods in brachytherapy beyond the TG-43 formalism: Current status and recommendations for clinical implementation.," Med. Phys. **39**, 6208 - 6236 (2012).

[132] A.S. Meigooni, J.A. Meli, R. Nath, "A comparison of solid phantoms with water for dosimetry of ^{125}I brachytherapy sources," Med. Phys. **15**, 695-701 (1988).

[133] J.F. Williamson, "Comparison of measured and calculated dose rates in water near I-125 and Ir-192 seeds," Med. Phys. **18**, 776-786 (1991).

[134] A.S. Meigooni, Z. Li, V. Mishra, J.F. Williamson, "A comparative study of dosimetric properties of Plastic Water and Solid Water in brachytherapy applications," Med. Phys. **21**, 1983-1987 (1994).

[135] A.S. Meigooni, S.B. Awan, N.S. Thompson, S.A. Dini, "Updated Solid Water™ to water conversion factors for ^{125}I and ^{103}Pd brachytherapy sources," Med. Phys. **33**, 3988-3992 (2006).

[136] R.W. Kline, "Trachsel Dental Studio, Inc. COMS ^{125}I eye plaques," (Trachsel Dental Studio, Inc., Rochester, MN, 1987), pp. 1 - 8.

[137] M.J. Rivard, W.M. Butler, L.A. DeWerd, M.S. Huq, G.S. Ibbott, A.S. Meigooni, C.S. Melhus, M.G. Mitch, R. Nath, J.F. Williamson, "Supplement to the 2004 update of the AAPM Task Group No. 43 Report," Med. Phys. **34**, 2187-2205 (2007).

[138] N.S. Patel, S.-T. Chiu-Tsao, J.F. Williamson, P. Fan, T. Duckworth, D. Shasha, L.B. Harrison, "Thermoluminescent dosimetry of the Symmetra™ 125 I model 125.S06 interstitial brachytherapy seed," Med. Phys. **28**, 1761-1769 (2001).

[139] O.A. Zeidan, S.A.L. Stephenson, S.L. Meeks, T.H. Wagner, T.R. Willoughby, P.A. Kupelian, K.M. Langen, "Characterization and use of EBT radiochromic film for IMRT dose verification," Med. Phys. **33**, 4064-4072 (2006).

[140] Y. Le, I. Ali, J.F. Dempsey, J.F. Williamson, "Prospects for quantitative two-dimensional radiochromic film dosimetry for low dose-rate brachytherapy sources," Med. Phys. **33**, 4622-4634 (2006).

[141] S.-T. Chiu-Tsao, D. Medich, J. Munro III, "The use of new GAFCHROMIC® EBT film for ^{125}I seed dosimetry in Solid Water® phantom," Med. Phys. **35**, 3787-3799 (2008).

[142] C.G. Soares, W.L. McLaughlin, "Measurement of radial dose distributions around small beta particle emitters using high resolution radiochromic foil dosimetry," Radiation Protection Dosimetry **47**, 367-372 (1993).

[143] D.M. Duggan, B.L. Johnson, "Dosimetry of the I-Plant Model 3500 iodine-125 brachytherapy source," Med. Phys. **28**, 661-670 (2001).

[144] T.P. Selvam, B. Keshavkumar, "Monte Carlo investigation of energy response of various detector materials in ^{125}I and ^{169}Yb brachytherapy dosimetry," J. of App. Clin. Med. Phys. **11**, 70-82 (2010).

[145] P.R. Almond, P.J. Biggs, B.M. Coursey, M.S. Huq, R. Nath, D.W.O. Rogers, "AAPM's TG-51 protocol for clinical reference dosimetry of high-energy photon and electron beams," Med. Phys. **26**, 1847-1870 (1999).

[146] R.J. Schulz, P.R. Almond, J.R. Cunningham, J.G. Holt, R. Loevinger, N. Suntharalingam, K.A. Wright, R. Nath, G.D. Lempert, "A protocol for the determination of absorbed dose from high-energy photon and electron beams. Task Group 21, Radiation Therapy Committee, American Association of Physicists in Medicine," Med. Phys. **10**, 741-771 (1983).

[147] D.C. Medich, J.J. Munro III, "Monte Carlo calculated TG-43 dosimetry parameters for the SeedLink™ ^{125}I brachytherapy system," Med. Phys. **30**, 2503-2508 (2003).

[148] T.E. Booth, F.B. Brown, J.S. Bull, L.J. Cox, R.A. Forster, J.T. Goorley, H.G. Hughes, R.D. Mosteller, R.E. Prael, E.C. Selcow, A. Sood, J.E. Sweeney, "MCNP – a general Monte Carlo n-particle transport code. Report No. LA-UR-03-1987, Version 5," (Los Alamos National Laboratory, Los Alamos, New Mexico, 2003).

[149] D.E. Cullen, J.H. Hubbell, L. Kissel, "EPDL97: The Evaluated Photon Data Library, '97 Version," Report No. UCRL-50400, Vol. 6, Rev. 5, (Lawrence Livermore National Library, Livermore, CA, 1997).

[150] T.D. Bohm, P.M. DeLuca, Jr., L.A. DeWerd, "Brachytherapy dosimetry of ^{125}I and ^{103}Pd sources using an updated cross section library for the MCNP Monte Carlo transport code," Med. Phys. **30**, 701-711 (2003).

151   J.J. DeMarco, R.E. Wallace, K. Boedeker, "An analysis of MCNP cross-sections and tally methods for low-energy photon emitters," Phys. Med. Biol. **47**, 1321-1332 (2002).

152   B. Reniers, F. Verhaegen, S. Vynckier, "The radial dose function of low-energy brachytherapy seeds in different solid phantoms: comparison between calculations with the EGSnrc and MCNP4C Monte Carlo codes and measurements," Phys. Med. Biol. **49**, 1569-1582 (2004).

153   Brookhaven National Laboratory Decay Radiation Database, (http://www.nndc.bnl.gov/nudat2/indx_dec.jsp, accessed November 24, 2013).

154   D.C. Medich, J.J. Munro III, "Dependence of Yb-169 absorbed dose energy correction factors on self-attenuation in source material and photon buildup in water," Med. Phys. **37**, 2135-2144 (2010).

155   D.C. Medich, M.A. Tries, J.J. Munro III, "Monte Carlo characterization of an ytterbium-169 high dose rate brachytherapy source with analysis of statistical uncertainty," Med. Phys. **33**, 163-172 (2006).

156   C.G. Soares, *Report of Calibration of BEBIG ^{106}Ru-^{106}Rh Ophthalmic Applicator Type CCX, S/N 41*. (National Institute of Standards and Technology, Gaithersburg, MD, 2001).

157   A.S. Kirov, J.Z. Piao, N. Mathur, T.R. Miller, S. Devic, S. Trichter, M. Zaider, T. LoSasso, C. Soares, "A test of the 3D scintillation dosimetry method for a Ru-106 eye plaque applicator," Med. Phys. **32**, 2002 (2005).

158   S. Trichter, M. Zaider, J. Munro, A. Sabbas, D. Nori, "Accurate dosimetric characterization of a novel ^{125}I eye plaque design," Med. Phys. **35**, 2632 (2008).

159   J.H. Hubbell, S.M. Seltzer, "Tables of x-ray mass attenuation coefficients and mass energy-absorption coefficients from 1keV to 20 MeV for elements Z=1 to 92 and 48 additional substances of dosimetric interest," (https://www.nist.gov/pml/x-ray-mass-attenuation-coefficients, July 2004 update, DOI: https://dx.doi.org/10.18434/T4D01F).

160   J. Davelaar, D.F. Schaling, L.A. Hennen, J.J. Broerse, "Dosimetry of ruthenium-106 eye applicators," Med. Phys. **19**, 691-694 (1992).

161   M.F. Chan, A.Y.C. Fung, Y.-C. Hu, C.-S. Chui, H. Amols, M. Zaider, D. Abramson, "The measurement of three dimensional dose distribution of a ruthenium-106

ophthalmological applicator using magnetic resonance imaging of BANG polymer gels," J. of App. Clin. Med. Phys. **2**, 85-89 (2001).

162   G. Heilemann, N. Nesvacil, M. Blaikner, N. Kostiukhina, D. Georg, "Multidimensional dosimetry of 106Ru eye plaques using EBT3 films and its impact on treatment planning," Med. Phys. **42**, 5798-5808 (2015).

163   R.P. Kollaard, W.J.F. Dries, H.J. van Kleffens, A.H.L. Aalbers, J. van der Marel, J.P.A. Marijnissen, M. Piessens, D.R. Schaart, H. de Vroome, " Quality control of sealed beta sources in brachytherapy. Recommendations on detectors, measurement procedures and quality control of beta sources," Netherlands Commission on Radiation Dosimetry. Report No. 14, 2004.

164   M. Eichmann, D. Flühs, B. Spaan, "Development of a high precision dosimetry system for the measurement of surface dose rate distribution for eye applicators," Med. Phys. **36**, 4634-4643 (2009).

165   M. Eichmann, T. Krause, D. Flühs, B. Spaan, "Development of a high-precision *xyz*-measuring table for the determination of the 3D dose rate distributions of brachytherapy sources," Phys. Med. Biol. **57**, N421-N429 (2012).

166   C. Constantinou, F.H. Attix, B.R. Paliwal, "A solid water phantom material for radiotherapy x-ray and γ-ray beam calibrations," Med. Phys. **9**, 436-441 (1982).

167   B.N. Taylor, C.E. Kuyatt, "Guidelines for evaluating and expressing the uncertainty of NIST measurement results. NIST Technical Note 1297" (National Institute of Standards and Technology, Gaithersburg, MD, 1994).

168   M.G. Mitch, L.A. DeWerd, R. Minniti, J.F. Williamson, "Treatment of uncertainties in radiation dosimetry," in *Clinical dosimetry measurements in radiotherapy,* edited by D.W.O. Rogers, J. Cygler (Medical Physics Publishing, Madison, WI, 2009), pp. 724-757.

169   C.G. Soares, "Calibration of ophthalmic applicators at NIST: A revised approach," Med. Phys. **18**, 787-793 (1991).

170   C.G. Soares, "A method for the calibration of concave ^{90}Sr+^{90}Y ophthalmic applicators," Phys. Med. Biol. **37**, 1005-1007 (1992).

[171] J.A. Sayeg, R.C. Gregory, "A new method for characterizing beta-ray ophthalmic applicator sources," Med. Phys. **18**, 453-461 (1991).